

Molecular Analysis of Kinetochore-Microtubule Attachment in Budding Yeast

by

Daniel R. Rines

B.S. Biochemistry
University of California – Davis, 1997

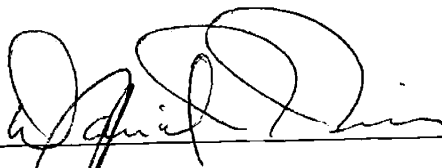
SUBMITTED TO THE DEPARTMENT OF BIOLOGY
IN PARTIAL FULFILLMENT OF THE REQUIREMENTS FOR THE DEGREE OF

DOCTOR OF PHILOSOPHY IN BIOLOGY
AT THE
MASSACHUSETTS INSTITUTE OF TECHNOLOGY

JUNE 2003

© Massachusetts Institute of Technology. All rights reserved.

Signature of Author: _____



Department of Biology
May 23, 2003

Certified by: _____

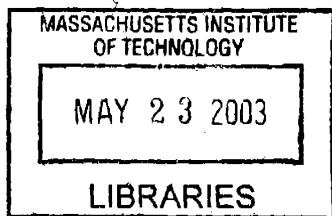


Peter K. Sorger
Associate Professor of Biology
Thesis Supervisor

Accepted by: _____



Alan Grossman
Professor of Biology
Chairman, Committee for Graduate Students



ARCHIVES



Room 14-0551
77 Massachusetts Avenue
Cambridge, MA 02139
Ph: 617.253.5668 Fax: 617.253.1690
Email: docs@mit.edu
<http://libraries.mit.edu/docs>

DISCLAIMER OF QUALITY

Due to the condition of the original material, there are unavoidable flaws in this reproduction. We have made every effort possible to provide you with the best copy available. If you are dissatisfied with this product and find it unusable, please contact Document Services as soon as possible.

Thank you.

Some pages in the original document contain color pictures or graphics that will not scan or reproduce well.

Molecular Analysis of Kinetochores- Microtubule Attachment in Budding Yeast

by

Daniel R. Rines

Submitted to the Department of Biology
on May 23, 2003, in Partial Fulfillment of the
Requirements for the Degree of Doctor of Philosophy in Biology

Abstract

Kinetochores bind to microtubules and are responsible for chromosome segregation and the accurate transmission of genetic information during cell division. Kinetochores are DNA-protein complexes that assemble on centromeric DNA sequences. In budding yeast, the kinetochores consist of approximately fifty proteins that are organized into a large multi-subunit complex. Multiple kinetochore proteins are thought to work together in establishing, sensing and maintaining the microtubule attachment. Following attachment, kinetochores act to couple microtubule force generation to chromosome movements. Microtubule associated proteins are also thought to play a key role in this process by regulating plus-end microtubule dynamics and tensile force generation. However, the actual molecular mechanism of force generation is unclear.

We have used a combination of live-cell imaging, biochemical and genetic techniques in the budding yeast, *S. cerevisiae*, to identify ten kinetochore subunits and elucidate their roles in microtubule attachment. Among these proteins are microtubule binding proteins and a molecular motor with homologues in animal cells. By analyzing the changes in chromosome positioning and dynamics in various kinetochore mutants, we show that different kinetochore proteins are required for the imposition of tension on paired sister kinetochores and for correct chromosome motion throughout the cell cycle. Utilizing 3D comparative motion analysis of the chromosomes has revealed that kinetochore proteins essential for microtubule attachment in early S-phase are not required at other points in the cell cycle. Our results suggest that different subsets of kinetochore proteins regulate the dynamic nature of microtubule growth and shrinkage for the generation of mechanical force and proper chromosome segregation.

Thesis Supervisor: Peter K. Sorger
Title: Associate Professor of Biology

Daniel R. Rines

Education

MASSACHUSETTS INSTITUTE OF TECHNOLOGY – Cambridge, MA
Ph.D. – Biology, June 2003. Department of Biology. *Thesis: Molecular Analysis of Kinetochore-Microtubule Attachment in Budding Yeast*

UNIVERSITY OF CALIFORNIA – Davis, CA
B.S. – Biochemistry, June 1997

Honors & Awards

Fellowship, 1996 Howard Hughes Medical Institute (University of California, Davis)
Summer Honors Advanced Research

Fellowship, 1995 Howard Hughes Medical Institute (University of California, Davis)
Transfer Student Fellows Program

Research Experience

1999 - 2003 Massachusetts Institute of Technology
Principal Investigator: Peter K. Sorger

1995 - 1997 University of California, Davis
Principal Investigator: Jonathan M. Scholey

Publications

Rines D.R., Dorn J, Thomann D, Danuser G, & Sorger P.K (2003) Yeast Live-Cell Fluorescence Microscopy. *Cold Spring Harbor Laboratory: Live Cell Microscopy, In press.*

Thomann D., Rines D.R, Sorger P.K, & Danuser G (2002) Automatic Fluorescent Tag Detection in 3D with Super Resolution: Application to the Analysis of Chromosome Movement. *Journal of Microscopy*, 208(Pt 1):49-64.

Rines D.R., He X., & Sorger P.K (2002) Quantitative Microscopy of Green Fluorescent Protein-Labeled Yeast. *Guide to Yeast Genetics and Molecular and Cell Biology(Part C) - Methods in Enzymology*, 351: 16-33.

He X*, Rines D.R*, Espelin C.W., & Sorger P.K; (2001) Molecular analysis of kinetochore-microtubule attachment in budding yeast. *Cell*, 106: 195-206. (* authors contributed equally)

Meyer D., Rines D.R., Kashina A., Cole D.G., & Scholey J.M (1998) Purification of novel kinesins from embryonic systems. *Methods in Enzymology*, 298: 133-54.

Professional Experience

02/98 - 08/98 Industry Consultant, Navitel Communications – Menlo Park, CA

01/96 - 02/98 Research Lab Technician, University of California – Davis, CA

10/91 - 08/93 Director of Marketing, Appsoft Inc. – Redwood Shores, CA

03/90 - 10/91 Product Marketing Manager, Adobe Systems Inc. – San Jose, CA

ACKNOWLEDGEMENTS

I owe a debt of gratitude to my advisor Peter Sorger for accepting me into his lab and creating an environment for exciting and productive research. Your intellectual guidance, technical discussions and unending encouragement have been invaluable. Your excitement and unbridled passion for kinetochores, chromosome segregation, computational sciences, applied mathematics, microscopy and biology in general are extremely contagious. Your honest critiques on my public speaking, technical writing and, more importantly, intellectual approach to scientific discovery have been instrumental to my success. I consider it a great honor to have been a member of your lab and it has been a pleasure to be one of your students.

I would also like to thank my friends and colleagues in the Sorger lab. I am especially indebted to Iain Russell for his lessons in yeast molecular biology and unending patience during the early days, to Xiangwei He for his enthusiasm and advice about kinetochore biology, to Ilya Goldberg for pulling me into the OME project, to Andrew McAnish for the constant stream of intellectual discussions, to Viji Dravium and Patrick Meraldi for opening my eyes to the world of mammalian biology and for demonstrating that animal cells are a viable experimental system, and to all the other members of the Sorger lab. You are all an outstanding collection of scientists and some of the nicest people with which I have ever had the fortune to work.

I would like to express my many thanks to our collaborators in Switzerland for providing such an excellent collection of computational tools. Dominik and Jonas are inarguably the spot tracking masters of the universe. Gaudenz your insights, mathematical intellect and computational approach to biology are not only exciting but also second to none. I look forward to our future endeavors together.

To Carl Brown and Paul Goodwin of Applied Precision, I would especially like to thank you for your instruction, patience and technical assistance with the microscope systems. Your expert lessons on deconvolution microscopy, acquisition hardware and image processing have been an important part of the discoveries presented in this dissertation.

Thank you to all the members of my defense committee for participating in my thesis defense and for taking the time out of their busy schedules to review and provide feedback. Angelika, Frank and Steve, your ideas and perspective throughout the last three years have been a great source of support and inspiration. I could not have asked for more enjoyable thesis meetings than those we have had together.

To my family and friends, I am deeply indebted to you all for your support in good times and bad. Your faith and backing has been a constant driving force in this long and sometimes arduous endeavor. I would especially like to express my gratitude to my mother and father, who instilled in me not only the courage to attempt such lofty goals but also the determination to make them come true. Your affectionate and devoted encouragement has made this undertaking a very rewarding experience and I am proud to be your son.

Lastly, I would like to thank the individuals that generously donated their precious time to read and reread copies of this manuscript. Without the help of Viji Dravium, Susan Gaudet, Emily Gillett, Peter Sorger and Jessica Tytell, this thesis would have been a complete failure.

TABLE OF CONTENTS

Abstract	2
Personal Statement	3
Acknowledgements	4
Chapter 1 Kinetochore Structure and Function	6
Chapter 2 Molecular Analysis of Kinetochore-Microtubule Attachment	50
Chapter 3 Quantitative Microscopy of Green Fluorescent Protein-Labeled Yeast	93
Chapter 4 Automatic Fluorescent Tag Detection in 3D with Super-Resolution: Application to the Analysis of Chromosome Movement	127
Chapter 5 Analyzing the Role of Kinetochore Proteins on Monopolar Chromosome Dynamics in <i>S. cerevisiae</i>	174
Chapter 6 Conclusions and Future Directions	208

CHAPTER 1

Kinetochores Structure and Function

1.1	Introduction.....	8
1.2	Building the Kinetochores: A Centromere-Microtubule Attachment Apparatus.....	12
1.2.1	Kinetochores first assemble onto centromeric DNA	13
1.2.2	Linking the MT-interacting proteins to the DNA-binding proteins.....	15
1.2.2.1	Ndc80 complex	15
1.2.2.2	Mtw1 complex	16
1.2.2.3	Ctf19 complex.....	17
1.2.2.4	Ctf3 complex.....	18
1.2.3	Microtubule-binding and polymer regulatory components	18
1.2.3.1	Dam1 complex	19
1.2.3.2	Stu2p	21
1.2.3.3	Bik1p.....	21
1.2.3.4	Motor proteins.....	22
1.2.4	Regulation of kinetochores assembly.....	22
1.3	Chromosome Motion in a Dynamic Mechanical System	24
1.3.1	Spindle organization	26
1.3.2	Monitoring chromosome motion with 3D fluorescence microscopy	29
1.3.3	Three types of defects in chromosome-microtubule interactions	29
1.3.4	Chromosome dynamics.....	30
1.3.5	Powering chromosome dynamics via regulation at microtubule plus-ends.....	31
1.3.6	Cell cycle dependent kinetochores functions	32
1.4	Microtubule Attachment Surveillance System	33
1.4.1	Centromere-microtubule attachment sensor	34
1.5	Computational Approaches to Study Kinetochores Function	35
1.5.1	Machine vision technology.....	35
1.5.2	Computational modeling.....	36
1.6	Concluding Remarks.....	37
1.7	References.....	39

1.1 Introduction

The accurate transmission of genetic information during cell division depends on the attachment of sister chromatids to microtubules (MTs) of the mitotic spindle. This attachment is mediated by kinetochores, specialized DNA binding complexes that assemble onto centromeric DNA. For chromosomes to be correctly segregated into two equal sets, it is essential that all the kinetochores establish and maintain bipolar attachment prior to the loss of cohesion between sister chromatids at the onset of anaphase (reviewed in Cheeseman et al., 2002b; Chubb et al., 2002; Rieder and Salmon, 1998; Salmon et al., 1989). Bipolar attachment occurs when one kinetochore binds to MTs emanating from one spindle pole and the sister kinetochore binds to MTs emanating from the opposite pole. In the event of incomplete attachment, the kinetochore signals to a surveillance mechanism, known as the mitotic spindle assembly checkpoint, to delay cell division until all kinetochores are correctly attached (reviewed in Amon, 1999; Gillett and Sorger, 2001).

In *S. cerevisiae*, centromeres are well-defined DNA sequences (Baker and Masison, 1990; Cai and Davis, 1990; Espelin et al., 1997; Lechner and Carbon, 1991). This small region consists of three DNA elements called CDEI, CDEII and CDEIII (Clarke and Carbon, 1980; Hegemann and Fleig, 1993), all of which are highly conserved among the 16 chromosomes (Fitzgerald-Hayes et al., 1982). In wild-type budding yeast, errors in chromosome transmission occur on the order of $\sim 10^{-5}$ per cell division. Deletion of CDEI causes about a 10-fold increase in transmission errors (Baker and Masison, 1990; Cai and Davis, 1990); deletion of CDEII or CDEIII abolish centromere function altogether (Gaudet and Fitzgerald-Hayes, 1987; Lechner and Carbon, 1991). In most other eukaryotes, however, specific DNA sequences are not known and centromeres consist of broad DNA domains

covering many kilobases (Bloom, 1993; Marschall and Clarke, 1995; Pluta et al., 1995). In fact, the mammalian core centromere is formed by hundreds of kilobases of repetitive, heterochromatic, α -satellite DNA found at the major constriction of mitotic chromosomes (reviewed in Van Hooser et al., 1999).

Kinetochores are large complexes that consist of multi-protein subunits that link centromeric DNA directly to microtubules. In budding yeast, kinetochores consist of approximately fifty proteins organized into a multi-layer structure where the very core kinetochore proteins are directly recruited to centromere sequences (reviewed in Shimoda and Solomon, 2002; McAinsh A, Tytell J and Sorger PK, 2003 *in press*). Individual kinetochore proteins function as part of subcomplexes that are thought to play collaborative roles in establishing, sensing, and maintaining the kinetochore-MT attachment. Failures in kinetochore function during mitosis can often lead to unequal partitioning of the genetic material and increased rates of chromosome missegregation.

MTs function as important mechanical and structural components. As highly dynamic polymers, MTs make frequent changes between stages of growth and shrinkage (Inoue and Salmon, 1995; Mitchison and Kirschner, 1984a). MTs assemble via the GTP-dependent polymerization of $\alpha\beta$ -tubulin heterodimers into linear protofilaments arranged to form hollow fibers (Amos and Klug, 1974; Weisenberg and Deery, 1976). The asymmetry of tubulin heterodimers creates an intrinsic MT polarity, with a relatively stable end (called the minus-end) and a more dynamic end (called the plus-end) often exhibiting transitions between growth and shrinkage, termed “dynamic instability” (Allen and Borisy, 1974; Fan et al., 1996; Mitchison and Kirschner, 1984b). This instability not only provides them with the unique ability to ‘search-for-and-capture’ kinetochores (Inoue, 1997; Kirschner and

Mitchison, 1986), but also supplies the energy necessary for force generation via depolymerization (Desai and Mitchison, 1997).

During mitosis duplicated chromatids are physically pulled into daughter cells by the MTs of the mitotic spindle. The spindle consists of a bipolar array of MTs with each minus-end anchored to a microtubule organizing center (MTOC or centrosome), also called a spindle pole body (SPB) in yeast. Budding yeast maintains a simple bipolar spindle and undergoes a closed mitosis in which the SPBs remain embedded in the nuclear envelope throughout the cell cycle. Budding yeast contain two classes of intranuclear MTs: those that bind to kinetochores (k-MTs) and those that project into the spindle midzone to overlap with MTs from the other pole (p-MTs). Each of the 16 centromeres in *S. cerevisiae* binds to a single MT so that the mature yeast spindle contains 32 k-MTs and 5–8 p-MTs (O'Toole et al., 1999).

Chromosome segregation involves a complex series of movements back and forth along the MTs of the mitotic spindle. In mammalian prometaphase and metaphase, pairs of sister chromatids move first in one direction and then in the opposite direction, a behavior known as “directional instability” (Rieder and Salmon, 1998). Studies suggest that when bipolar attachment is eventually established, the extreme plus-ends of MTs become embedded in kinetochores, but chromosome motion remains highly dynamic. Bipolar MT fibers will eventually shorten in opposite directions. These depolymerizing fibers generate opposing forces on paired sisters and centromeric DNA is physically stretched apart (Shelby et al., 1996). In yeast and humans, the glue-like proteins (cohesins) located between sister chromatids partially resist this pulling force and centromeric DNA regions experience periods of transient separations prior to the onset of anaphase while opposing forces fluctuate

(Goshima and Yanagida, 2000; He et al., 2000; Shelby et al., 1996). Some microtubule associated proteins (MAPs) are found to interact with the kinetochore and play a role in regulating plus-end MT dynamics and tensile force generation (Desai and Mitchison, 1995; Desai and Mitchison, 1997; Walczak et al., 2002). This suggests that not only is chromosome motion powered largely by the interaction of kinetochores with MTs but may be directly coupled to MT polymerization and depolymerization at the plus-end.

The genetically tractable budding yeast, *S. cerevisiae*, has proven an exceptional model system and an attractive organism for studying kinetochore function. The role of the kinetochore in yeast and mammals exhibits a high degree of conservation (reviewed in Kitagawa and Hieter, 2001). Unlike higher organisms, however, each budding yeast kinetochore binds to only a single MT, making it a relatively simple system for studying kinetochore-MT attachment (O'Toole et al., 1999). Previously, the small size of yeast made it difficult to use for *in vivo* microscopy and thus direct observation of chromosome motion was more accessible in higher eukaryotes (Li and Nicklas, 1995; Nicklas, 1997; Skibbens et al., 1993; Waters et al., 1996). A critical advance in yeast biology was the development of fluorescent chromosome tagging in which an array of operator binding sites is integrated at a unique location in the genome of cells expressing repressor-GFP fusion proteins (Ciosk et al., 1998; Straight et al., 1996). Combining sophisticated computer vision algorithms and three-dimensional (3D) imaging techniques with genetics has overcome the size limitation in yeast and permitted single chromosome motion studies (He et al., 2000; He et al., 2001; Pearson et al., 2001; Rines et al., 2002; Thomann et al., 2002). This powerful combination of yeast genetics and microscopy now allow us to examine the degree to which evolutionarily distinct organisms share dynamics of chromosome motion.

In this chapter I begin by first focusing on the gross structure of the yeast kinetochore, working from the innermost complexes out toward the MT interacting components; second on microscopy-based assays for *in vivo* chromosome dynamics with special emphasis on the establishment and maintenance of attachment; third on the mitotic surveillance system's responsibilities in monitoring complete attachment and signaling for mitotic progression; and finally, I conclude with a brief discussion on how technological developments in imaging and computational biology will continue to extend our understanding of kinetochore function in the future.

1.2 Building the Kinetochore: A Centromere-Microtubule Attachment Apparatus

The yeast kinetochore appears to assemble in multiple layers such that inner DNA binding proteins support and recruit successive outer layers of proteins. The main components of the kinetochore can be subdivided into DNA sequence elements (*cis* acting determinants) and protein-DNA or protein-protein interacting components (*trans* acting determinants). The structure of the yeast kinetochore is thought to be organized into a three-layer system. The innermost, or core-layer, consists of protein-DNA binding complexes that form directly at centromeric regions. The middle, or linker-layer, consists of subcomplexes that glue the DNA binding components to the MT interacting proteins and to cell cycle regulatory proteins. The outer layer consists of microtubule associated proteins (MAPs) that bind directly to the MT protofilaments to regulate polymer dynamics at the plus-end of k-MTs. Together the complexes work in harmony to create a strong kinetochore-MT linkage.

The individual subcomplexes are reviewed in the following sections based on kinetochore architecture and physical characterization (organization adapted from McAinsh A, Tytell J and Sorger PK, 2003 *in press*). Table 1-1 provides a listing of all subcomplexes and the protein components based on multi-layer organization for convenience.

Table 1-1. Kinetochore components.

Core Kinetochore Complexes
CBF3: Ndc10p, Cep3p, Ctf13p, Skp1p CBF1: Cbf1p CSE4: Cse4p
Linker Kinetochore Complexes
NDC80: Ndc80p, Spc24p, Spc25p, Nuf2p MTW1: Mtw1p, Dsn1p, Nnf1p, Nsl1p CTF19: Ctf19p, Mcm21p, Okp1p, Amel1p CTF3: Ctf3p, Mcm22p, Mcm16p
Outer Kinetochore Complexes
DAM1: Dam1p, Ask1p, Duo1p, Dad1p, Dad2p, Dad3p, Dad4p, Spc19p, Spc34p STU2: Stu2p BIK1: Bik1p MOTORS: Kip1p, Kip3p, Cin8p

1.2.1 Kinetochores first assemble onto centromeric DNA

The assembly of *S. cerevisiae* kinetochores appears to begin with the binding of a four-protein complex, CBF3 (Centromere Binding Factor), to the essential CDEIII-region (25 bp) of centromeric DNA (Espelin et al., 1997; Russell et al., 1999). All four subunits of CBF3 are encoded by essential genes (NDC10, CEP3, CTF13 and SKP1). Temperature sensitive mutations in any one of these subunits abolish CDEIII binding activity of the

complex and give rise to greatly elevated rates of chromosome loss under restrictive conditions. CDEII is a 75-80 bp sequence lying between CDEI and III composed of A/T rich DNA (90%). Recent evidence suggests that mutations in CDEII sequences cause chromosome loss rates to increase to $\sim 10^{-2}$ per cell division (C. Espelin, unpublished data). Ndc10p is the only known protein shown to directly interact with CDEII *in vitro*, and other proteins have been suggested to be CDEII-interactors *in vivo* (K. Simons, C. Espelin and P.K. Sorger, 2003 *submitted*). The last *cis*-acting element, CDEI, contains an 8 bp imperfect palindromic sequence which recruits a helix-loop-helix protein, centromere-binding factor 1 (Cbf1p—also known as Cp1, Cpfl or Cep1). Deletion of the CDEI element increases chromosome loss rate approximately 10-fold, suggesting that it is not essential for viability but still important for optimal chromosome segregation frequency (Baker and Masison, 1990; Cai and Davis, 1990).

In addition to CBF3, a DNA binding protein, Cse4p, is encoded by an essential gene with more than 60% identity to yeast histone H3 and to the mammalian centromere protein CENP-A (Stoler et al., 1995). The temperature sensitive mutant *cse4-1* demonstrates elevated rates of chromosome nondisjunction when combined with point mutants in CDEII and causes a mitotic cell cycle arrest at restrictive temperatures. The N-terminus of Cse4p contains a specialized domain that appears to interact with outer kinetochore components (Chen et al., 2000; Keith et al., 1999; Ortiz et al., 1999). Recent evidence has further characterized kinetochore assembly order and demonstrated that Cse4p requires Ndc10p (Measday et al., 2002). Less is known about the order of assembly of human core-kinetochore components. CENP-A, like Cse4p, is a histone H3 variant, and experiments suggest that it is also a centromeric nucleosome component (Vafa and Sullivan, 1997; Warburton et al., 1997). To

date, no homologues of Ndc10p have been found in higher organisms (Cep3 and Ctf13 homologues are also unknown); however, other DNA binding proteins such as CENP-B have demonstrated binding to α -satellite DNA as a homo-dimer (Masumoto et al., 1989; Yoda et al., 1992).

1.2.2 Linking the MT-interacting proteins to the DNA-binding proteins

The second layer in the kinetochore-MT attachment site involves multiple subcomplexes that appear to function as the glue between the DNA- and MT-binding components. As mentioned earlier, the number of proteins known to assemble on or around CBF3 has grown rapidly over the last five years and now exceeds 50 proteins in yeast including both essential and non-essential genes (reviewed in Shimoda and Solomon, 2002; McAinsh A, Tytell J and Sorger PK, 2003 *in press*). Many of these proteins interact as discrete substructures to form an intricate network of connections between the core-kinetochore components, the MT binding proteins and the spindle assembly checkpoint. Biophysical studies are just now beginning to characterize the physical intra- and inter-subcomplex interactions (Wigges and Kilmartin, 2001; Cheeseman et al., 2002a; Hanke et al., 2002; Li et al., 2002; DeWulf P, McAinsh A & Sorger PK, *submitted* 2003).

1.2.2.1 Ndc80 complex

The Ndc80 complex consists of Spc24p, Spc25p, Nuf2p and Ndc80p, all of which are essential proteins and have been localized to kinetochores by fluorescent microscopy (He et al., 2001; Wigge and Kilmartin, 2001; Janke et al., 2002). Biochemical purifications from budding yeast extracts have shown that the four members form a tight complex (Wigge and Kilmartin, 2001). Chemical cross-linking and Chromatin-ImmunoPrecipitation (ChIP) of epitope-tagged versions of the Ndc80 complex demonstrated that centromere specific DNA

sequences were pulled-down in a CBF3 dependent manner (He et al., Wigge and Kilmarting, 2001; Janke et al., 2002). From a functional standpoint, the Ndc80 complex appears to be required for linking several MT interacting proteins, including Dam1p, Stu2p, Cin8p and Kip1p, to centromeric DNA sequences as assayed using the same chemical cross-linking methods (He et al., 2001; Janke et al., 2002; Tytell & Sorger, *in preparation*). Temperature sensitive mutations in components of the Ndc80 complex result in the complete detachment of chromosomes from the spindle during mitosis (He et al., 2001; Wigge and Kilmartin, 2001; Janke et al., 2002). Additional support for the significance of this complex is the evolutionary conservation of *hsHEC1*, a human homologue of Ndc80p, a protein found to be over-expressed in certain forms of cancer (Chen et al., 1997). Besides being found in *S. pombe* and *Xenopus*, a Nuf2p homologue was identified in humans based on sequence comparison from the expressed sequence tagged (EST) database.

1.2.2.2 Mtw1 complex

The Mtw1 complex contains at least four proteins including Mtw1p, a protein initially identified as a homologue of the *S. pombe* Mis12⁺ kinetochore protein (Goshima and Yanagida, 2000). Three independent groups, including our own lab have shown that Mtw1p interacts with a number of other kinetochore proteins (Cheeseman et al., 2002a; Euskirchen, 2002; DeWulf P, McAinsh A & Sorger PK, *in preparation*); however, results differ on the exact size and composition of the complex. Based on the more stringent affinity purification and on two-hybrid analysis, Dsn1p, Nnf1p and Nsl1p form a stable complex with Mtw1p (Euskirchen, 2002; DeWulf P, McAinsh A & Sorger PK, *in preparation*). All four components in this complex are essential for viability. Mtw1p is also required for proper chromosome segregation and has been localized to the kinetochore using ChIP and

microscopy in a CBF3 dependent manner (Goshima and Yanagida, 2000). The temperature sensitive mutation *mtw1-1* demonstrates partial loss of chromosome attachment at the restrictive temperature *in vivo* when assayed using a single fluorescent chromosome tag (Rines, unpublished results). Nnf1p has recently been shown to be a nuclear protein involved in mitotic spindle stability and the temperature sensitive mutant *nnf1-17* is synthetically lethal with *mtw1-1* (Euskirchen, 2002). Further characterization of this complex, including the other two essential members, has yet to be reported.

1.2.2.3 Ctf19 complex

The Ctf19 complex is in close association with the Mtw1 complex and contains Ctf19p, Mcm21p, Okp1p and Ame1p (Cheeseman et al., 2002a; Ortiz et al., 1999; DeWulf P, McAinsh A & Sorger PK, *submitted* 2003). Deletions of the *CTF19* or *MCM21* genes increase the rates of chromosome loss yet are non-essential (Ortiz et al., 1999; Spencer et al., 1990); however, Okp1p and Ame1p are required for viability. CTF19 was originally identified in a synthetic dosage lethality (SDL) screen using overexpression of the CTF13 gene product. Mutations in the *ctf19* gene caused severe chromosome missegregation based on colony sectoring assays (Hyland et al., 1999). In addition to Ctf19p, all the members of this complex have also been shown to interact with centromeric DNA sequences in a CBF3 dependent manner using epitope-tagged proteins and ChIP (Hyland et al., 1999; Ortiz et al., 1999). Okp1p exhibits homology to CENP-F, a human protein that associates with the centromere (Choo, 1997). All the members of the Ctf19 complex have been localized to the kinetochore throughout the cell cycle and have been proposed to play a structural role in linking Cse4p, Mif2p, Cbf1p to the CBF3 complex (Ortiz et al., 1999). Based on recent evidence from our lab, several members of the Ctf19 complex also depend on Ndc80p for

their interaction with centromeric DNA in ChIP assays (DeWulf P, McAinsh A & Sorger PK, *submitted* 2003); thus the Ctf19p/Mcm21p/Okp1p/Ame1p linkage between Cbf1p, Cse4p and CBF3 may not be direct. Ame1p is an uncharacterized member of the complex and may interact directly with MTs based on information submitted to the *Saccharomyces Genome Database* (SGD: genome-www.stanford.edu/Saccharomyces). Unfortunately, no published report is currently available. The Ctf19 complex has previously been labeled an ‘outer-kinetochore complex’ (Ortiz et al., 1999); I am reserving this designation, however, for those complexes or proteins that have been shown to possess domains that interact directly with MTs.

1.2.2.4 Ctf3 complex

The Ctf3 complex is currently not well defined, but immunoprecipitation experiments suggest that it contains at least three subunits, Ctf3p, Mcm22p and Mcm16p, all of which are non-essential and localize to kinetochores exclusively and in a Ctf19p dependent manner (Measday et al., 2002). Ctf3p has been conserved through evolution and the *S. pombe* homologue of Ctf3p, Mis6⁺ is required for the recruitment of the fission yeast Cse4p histone (Cnp1⁺) to centromeric DNA (Takahashi et al., 2000). However, the opposite is found in budding yeast and humans where Ctf3p/hMis6 requires Cse4p/CENP-A for CEN association (Measday et al., 2002). The current thinking is that the Ctf3 complex may be involved in some aspect of centromeric chromatin assembly.

1.2.3 Microtubule-binding and polymer regulatory components

The last group of components to be reviewed as kinetochore-MT attachment assembly members are the ‘outer-kinetochore factors’ (e.g., subcomplexes possessing MAPs and molecular motors). Kinetochore are thought to be directly bound to MTs via MAPs.

Motor proteins such as kinesin and dynein are well characterized mechano-chemical molecules that bind to MTs and use the energy from ATP hydrolysis for force generation and directed motility; both kinesin and dynein function in a 'hand over hand' mechanism pulling their cargo as they move along the length of the polymer (reviewed in Vale and Milligan, 2000). In addition to the motors, other proteins interact with the MT protofilaments to regulate polymer dynamics, to cross-link multiple MTs or to act as anchors tethering cellular organelles to the cytoskeleton. The key elements necessary for forming the kinetochore-MT attachment remain largely unknown despite the fact that several MAPs interact with the kinetochore.

1.2.3.1 *Dam1* complex

The *Dam1* complex binds to MTs *in vitro* and contains nine subunits including *Dam1p* (*Duo1p* and *Mps1p* interacting factor) an essential protein required for spindle function (Hofmann et al., 1998; Jones et al., 1999). The *DAM1* gene was originally identified in a screen for mutants that enhanced the defects of mutations in *MPS1* (Jones et al., 1999), a kinase involved in SPB duplication and the spindle checkpoint (Weiss and Winey, 1996; Winey et al., 1991). Immunofluorescence experiments using an epitope-tagged version of *Dam1p* demonstrate localization to kinetochores and MTs and suggest that *Dam1p* may play a role in linking chromosomes directly to the spindle. In support of this, electron micrographs show that *dam1* mutations result in bent, broken and hyper-elongated spindles (Cheeseman et al., 2001; Hofmann et al., 1998), and *in vitro* studies suggest that *Dam1p* can bind directly to MTs. The temperature sensitive mutant *dam1-1* causes a checkpoint dependent metaphase arrest with 2C DNA content at the restrictive temperature of 37°C (Jones et al., 1999).

Two-hybrid analysis and co-immunoprecipitation studies indicate that Dam1p interacts physically with at least eight other proteins: Ask1p, Duo1p, Dad1p, Dad2p, Dad3p, Dad4p, Spc19p and Spc34p (Cheeseman et al., 2002a; Cheeseman et al., 2001; Hofmann et al., 1998; Ito et al., 2001; Janke et al., 2002; Li et al., 2002). Duo1p (Death Upon Over-production) was previously isolated because its over-expression caused defects in mitosis and a mitotic arrest. Duo1p was localized by immunofluorescence, immunoelectron microscopy, and tagging with green fluorescent protein (GFP), to the intranuclear spindle MTs. Under restrictive conditions, temperature sensitive *duo1* mutants arrest with a short spindle which is dependent on the mitotic checkpoint (Hofmann et al., 1998). The *DAD* genes (Duo1p and Dam1p interacting) were isolated from several two-hybrid studies and from co-immunoprecipitation experiments (Cheeseman et al., 2002a; Ito et al., 2001). However, little is currently known about their role at the kinetochore. Ask1p is an essential protein and appears to play a role in spindle stability and possibly in MT binding. The temperature sensitive mutant, *ask1-1*, demonstrates a high degree of nondisjunction and a mitotic arrest that is dependent on the spindle assembly checkpoint gene *MAD2* (Li et al., 2002). In addition, the stable association of Ask1p to the kinetochore appears to depend on the presence of MTs (Li et al., 2002). Spc34p and Spc19p were originally identified as components of the SPB (Wigge et al., 1998). Recent evidence based on GFP-tagged localization and co-immunoprecipitation results suggest that they are instead components of the outer-kinetochore (Cheeseman et al., 2002a; He et al., 2001; Janke et al., 2002; Li et al., 2002; DeWulf P, McAinsh A & Sorger PK, *submitted* 2003). Currently, little is known about the role of Spc19p. However, Spc34p is thought to play a role in the maturation and strengthening of kinetochore-MT attachment. Under restrictive conditions chromosomes in,

spc34 cells exhibit single mitotic pole (monopolar) interactions. However, in a recent set of experiments, *spc34-3* cells lacking cohesin segregated individual sister chromatids more or less equally between the two spindle poles (Janke et al., 2002). This data implies that both sets of sister kinetochores in *spc34* cells can separately capture MTs but cannot form MT links strong enough to counteract the pulling forces generated by bipolar attachment.

1.2.3.2 *Stu2p*

Stu2p is a conserved MAP with homologues identified in *Xenopus* (XMAP215), *Drosophila* (MSPs), *S. pombe* (Dis1⁺), *C. elegans* (ZYG-9) and humans (*ch-TOG1*). *Stu2p* was originally identified as an essential MT binding protein in yeast that localizes to the mitotic spindle, kinetochores, SPBs and cell cortex (He et al., 2001; Wang and Huffaker, 1997). The TOG/XMAP215 family of proteins has a direct effect on MT dynamics (Gard and Kirschner, 1987; Tournebize et al., 2000). XMAP215 promotes the polymerization of pure tubulin *in vitro* by increasing the growth rate and stimulating an increase in the rescue rate (Vasquez et al., 1994). Conversely, *Stu2p* acts to induce catastrophes by destabilizing rather than stabilizing MTs *in vitro* by sterically blocking tubulin addition to the MT plus-end (Van Breugel, Dreschel & Hyman, *personal communication*). These findings are consistent with data showing MTs are less dynamic in *stu2* mutants compared to wild-type cells (Kosco et al., 2001) and suggest that kinetochores in *stu2* cells have a reduced ability to polymerize MTs.

1.2.3.3 *Bik1p*

Bik1p is a plus-end MT binding protein and is thought to be an orthologue of the human protein CLIP170 (Berlin et al., 1990). The *Bik1p* protein colocalizes with tubulin, kinetochores and cortical attachment sites (Berlin et al., 1990; He et al., 2001). *BIK1Δ* cells

are synthetically lethal with mutations in α - and β -tubulin suggesting a direct interaction with the MT polymer lattice (Berlin et al., 1990). Recent experiments have also shown that Bik1p is required for the viability of polyploid cells and may contribute to the maintenance of tension on sister chromatids prior to the onset of anaphase (Lin et al., 2001).

1.2.3.4 Motor proteins

The kinesin related proteins (KRPs) Kip1p, Kip3p and Cin8p are motor proteins that have recently been shown to interact with the budding yeast kinetochore using GFP-tagged localization and ChIP against centromeric DNA (He et al., 2001; Tytell, JD and Sorger, PK, *submitted* 2003). Cin8p and Kip1p function in spindle stability (Goldstein and Philp, 1999). Kip3p is a member of the MCAK/XKCM1/KinI family of kinesins that play a role in mitotic-spindle assembly *in vitro* and acts to decrease catastrophe rate (Walczak et al., 2002). Recent experiments suggest that Cin8p and Kip1p may be required to cluster kinetochores during metaphase and thereby increasing the fidelity of chromosome segregation. Still, mutations in Cin8p, Kip1p or Kip3p motors alone or in various combinations, do not appear to have a significant effect on chromosome movement in live-cell assays (Tytell, JD and Sorger, PK, *submitted* 2003). Mammalian cells injected with antibodies against CENP-E, a plus-end directed kinesin, failed to congress chromosomes during prometaphase (Schaar et al., 1997).

1.2.4 Regulation of kinetochore assembly

Currently, it is thought that there are two regulated stages of kinetochore-MT assembly. The binding of core CBF3 components onto centromeric DNA sequences, which in turn recruit the remaining proteins in the kinetochore, and the kinetochore-MT attachment.

CBF3 loading onto CDEIII is regulated in a Skp1p and Sgt1p dependent manner (Kaplan et al., 1997; Kitagawa et al., 1999). Skp1p, regulates the DNA binding activity of the

other CBF3 components by controlling the phosphorylation of Ctf13p. The activity of Skp1p depends on the presence of an additional protein, Sgt1p (Kitagawa et al., 1999). Two mutant alleles of Skp1p, *skp1-3* or *skp1-4*, cause cells to arrest prior to G2 or prior to DNA replication, respectively (Connelly and Hieter, 1996). These independent events suggest that the Skp1p/Sgt1p activity is important not only for mitotic progression but also for initiating DNA replication. Both Skp1p and Sgt1p are highly conserved and homologues have been identified in humans, unlike the other members of the CBF3 complex (Bai et al., 1996). In fact, the human SGT1 gene can rescue the yeast *sgt1* null mutant, demonstrating that its function is highly conserved as well (Kitagawa et al., 1999). Nonetheless, the lack of other CBF3 homologues in higher organisms suggests that throughout evolution the core-kinetochore components have not all been conserved even though the overall function of the kinetochore has remained constant.

The Ipl1p and Sli15p complex are required for symmetric chromosome segregation and may regulate proper bipolar attachment by promoting turnover of kinetochore-MT attachments (Tanaka et al., 2002). Ipl1p is the founding member of the Aurora kinase family (Chan and Botstein, 1993) and Sli15p is thought to be the *S. cerevisiae* orthologue of the human INCENP proteins (Kim et al., 1999). The Ipl1p/Sli15p complex relocates from the kinetochore to the spindle midzone at the metaphase to anaphase transition (Buvelot et al., 2003). Many of the Ipl1p targets also colocalize to the spindle mid-zone during the metaphase-anaphase transition and may regulate both kinetochore- and interpolar-MTs plus ends. In addition, Ipl1p and Sli15p have been suggested to play a role in regulating proper kinetochore-MT attachment by destabilizing attachments in the absence of tension (Cheeseman et al., 2002a; Tanaka et al., 2002). Thus it could also be argued that Ipl1p

dependent binding is not a part of kinetochore assembly *per se* and instead only a post-assembly correction mechanism.

Our understanding of how the linker complexes and MT-binding components interact is still incomplete and needs to be elucidated further. We can imagine at least two possible scenarios: the linker-components such as the Ndc80 complex first recruit the MAPs and then form an interaction with the MT. Alternatively, the MAPs first bind to the MT and wait until the pre-assembled linker-kinetochore components interact with the pre-bound kinetochore MAPs. Since several kinetochore protein targets of Ipl1p have been identified, including Ndc10p (Biggins et al., 1999), Cse4p (Hsu et al., 2000), and Dam1p (Cheeseman et al., 2002a), it is possible that Ipl1p activity may play a role in regulating both assembly and attachment but this remains to be characterized better.

1.3 Chromosome Motion in a Dynamic Mechanical System

The spindle is a dynamic mechanical system that generates forces on paired chromatids to position and separate them into daughter cells during cell division. Determining how the force-generating mechanisms function in a coordinated manner to achieve chromosome segregation depends on evaluating the effects of the spindle and kinetochore components on directional instability. Moreover, many of the kinetic properties are influenced by the strength or type of kinetochore-MT attachment. For instance, velocity and acceleration are different when paired chromatids are only connected to MTs from a single pole (monopolar) as opposed to when they are attached to MTs from both poles (bipolar). To accurately record kinetic information, changes in position must be measured quantitatively so that velocity and acceleration can be derived. Ultimately, calculating

mechanical forces will also require complex force-balance equations that depend on chromosome mass and external forces such as viscosity. As a first step to understanding the spindle mechanics, however, chromosome motion tracking studies in wild-type and mutant backgrounds can be compared. Data gained from genetic disruptions will point to the roles individual components play in establishing, maintaining and regulating the kinetochore-MT attachment.

In higher organisms, cells transitioning from interphase to mitosis demonstrate an increase in the MT catastrophe frequency that results in an approximately ten-fold increase in MT turnover (Belmont et al., 1990; Mitchison et al., 1986; Verde et al., 1992). Two MAPs have been shown to promote catastrophe in mitosis: *Xenopus* XKCM1 and human MCAK (both Kip3p homologues) disrupt the interaction of tubulin subunits with the plus-ends of MTs (Desai et al., 1999; Walczak et al., 1996). However, XKCM1 exhibits similar activity levels in both interphase and mitosis; it has thus been proposed that the mitotic change in MT dynamics instead occurs by down-regulation of other MAPs that promote MT stability by increasing polymerization rates, suppressing catastrophe, and promoting rescue (Pryer et al., 1992; Tournebize et al., 2000). The resulting shift towards increased catastrophe and MT turnover creates dense arrays of shorter, more dynamic MTs that are highly effective in the capture of kinetochores (Hayden et al., 1990; Holy and Leibler, 1994).

In the following sections I discuss how the spindle is thought to be organized throughout the cell cycle, the status of the kinetochore-MT attachment as determined by motion studies with *in vivo* single chromosome tagging, and the cell cycle dependent changes on chromosome dynamics.

1.3.1 Spindle organization

Unlike vertebrate cells, yeast undergo a closed mitosis, in which the nuclear envelope never breaks down (reviewed in Winey and O'Toole, 2001). The SPBs nucleate all MTs and remain embedded in the nuclear membrane throughout the cell cycle. In G1, a short linear array of MTs emanates from the unduplicated SPB. In late G1/early S-phase, the spindle pole body is duplicated; the duplicated SPBs, each with a complete set of MTs, remain side-by-side, connected by a bridge structure (Adams and Kilmartin, 2000). Then, at mid/late S-phase, while the DNA is being duplicated and the replicated sister chromatids are linked via cohesins (Guacci et al., 1997), the SPBs rapidly separate to give rise to the mitotic spindle (Figure 1-1).

The process of chromosome segregation occurs in a series of ordered steps that are cell cycle dependent. In metaphase, sister chromatids must achieve a state of bipolar attachment, with each sister attached to a k-MT emanating from the opposing pole (Amon, 1999; Hoyt, 2001). Once all pairs of sisters have achieved bipolar attachment, anaphase is triggered and sister chromatid cohesion is then dissolved (Uhlmann et al., 1999). During anaphase, the kinetochores are pulled towards the poles (anaphase A) and the spindle elongates (anaphase B), bringing one SPB and set of chromatids into the daughter cell while the other remains in the mother. During telophase, spindle disassembly and cytokinesis occur, returning the cells to a G1-state in which each cell has one SPB and one set of chromosomes (Bardin et al., 2000).

Unlike mammalian cells, budding yeast kinetochores do not dissolve the kinetochore-MT attachment they had during the previous cell cycle once they pass into G1 (Gasser, 2002; Jin et al., 1998; Jin et al., 2000). Based on localization studies, centromeres in budding yeast

are known to cluster to a region near the SPB throughout interphase. Recently, Jin *et al.* used fluorescence *in situ* hybridization (FISH) and indirect immunofluorescence to show that centromeric clustering is reduced in the presence of the MT poison nocodazole and in a mutant which disrupts kinetochore structure (Jin *et al.*, 2000). This interesting phenomenon allows us to study regulation of MTs dynamics by kinetochore-MAPs using temperature sensitive mutations. Combining mutant kinetochore-MAPs with fluorescently labeled chromosomes (see below) and 3D time-lapse microscopy to record *in vivo* chromosome dynamics during G1 cells, we have recently determined that strains lacking Stu2p function exhibit shortened MT structures and that *dam1* deficient cells exhibit lengthened MTs structures as compared to wild-type cells (Rines, *et. al.*, *unpublished results – see Chapter 5*) This data suggests that Stu2p may promote MT growth *in vivo*. While, Dam1p may function to upregulate MT catastrophe rates *in vivo* and increase force generation via depolymerization. Without a bipolar spindle, the role of MAPs can be elucidated more easily in the absence of opposing forces on chromatids.

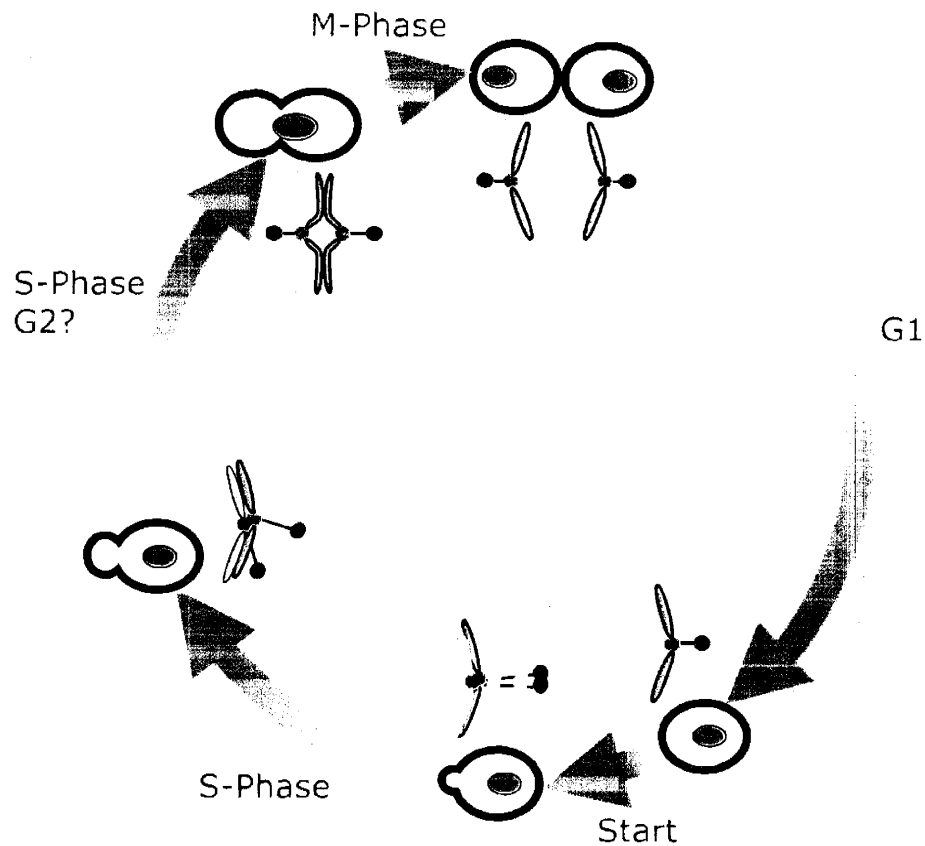


Figure 1-1. Changes in spindle orientation throughout the cell cycle.

The state of kinetochore-MT attachment is represented with respect to the budding yeast cell cycle. At 'start' G1 chromosomes are still attached to the short array of MTs coming the single SPB. During SPB duplication and DNA replication, the kinetochore-MT attachment is disrupted briefly. During late S-phase, SPBs separate and kinetochores establish bipolar attachment. Tension increases as the microtubules pull on the kinetochores and paired sister chromatids are stretched in metaphase. Once all kinetochores are bipolarly attached, the cohesion between sisters is dissolved and the chromatids are pulled into the daughter cell.

1.3.2 Monitoring chromosome motion with 3D fluorescence microscopy

Detailed analysis of chromosome dynamics in budding yeast has become possible only through the development of methods to tag chromosomes with GFP (Straight et al., 1996). To study chromosome segregation in living cells several labs including our own have fluorescently tagged a single chromosome at specific positions along the length of the arms (Ciosk et al., 1998; He et al., 2000; Lin et al., 2001; Pearson et al., 2001; Straight et al., 1996). The tag consists of an array of tetracycline operators (TetO) sequences integrated along the length of any chromosome arm. For studies involving kinetochore motion, the array is usually integrated 2 kb from the centromere. In addition to the array of operators, cells express GFP-tagged tetracycline repressor (TetR-GFP) protein integrated elsewhere in the genome (Ciosk et al., 1998; Straight et al., 1996). The combination of the operators and operator-binding protein results in a single fluorescent spot closely colocalized with the kinetochore prior to chromosome segregation or two spots once sister centromeric regions are pulled apart. As a spindle reference marker, cells also contain a protein known to localize to the central SPB plaque, Spc42p (Wigge et al., 1998), tagged either with GFP or CFP. The combination of these fluorescence tags makes it possible to monitor the position of a single chromosome relative to the spindle axis. In fact, when imaged on a 3D fluorescent system, quantitative *in vivo* chromosome motion studies can be used to determine the position of kinetochores within ~50 nm in the X/Y-plane and ~250 nm in the Z-direction (Rines et al., 2002; Thomann et al., 2002; Rines, D.R. and Sorger, P.K., 2003 *submitted*).

1.3.3 Three types of defects in chromosome-microtubule interactions

By mapping the time-dependent kinetic data into a cylindrical coordinate system centered on the axis of the spindle, defects in chromosome-MT attachment can be

categorized into distinct functional classes (He et al., 2001). Although different alleles of mutant proteins may exhibit varying degrees of any functional class, the disruptions in attachment tend to fall into the following three subclasses: (1) complete loss of chromosome-MT attachment, (2) monopolar chromosome-MT attachment, or (3) non-functional bipolar attachment having decreased MT force generation.

1.3.4 Chromosome dynamics

Live-cell time-lapse imaging of individual GFP-tagged chromosomes has provided some of the first evidence that different kinetochore proteins play different roles in MT attachment and force generation (He et al., 2001; Lin et al., 2001). Analysis of metaphase cells shows that chromosomes oscillate back and forth across the spindle, and, once bipolar attachment is achieved, sufficient force is generated at the kinetochore to transiently separate sister chromatids (Goshima and Yanagida, 2000; Tanaka et al., 2000; He et al., 2000). When these wild-type chromosome dynamics were compared to the dynamics observed in various mutant kinetochore proteins, several defects in chromosome movement were observed. Mutations that disrupt kinetochore assembly (such as *ndc10-1* and *ndc80-1*) cause a complete loss of attachment. Mutations in other kinetochore proteins, however, leave some aspects of MT attachment intact. For example, in *stu2-277* cells, chromosomes appear to achieve bipolar attachment but peak velocities are three to four times lower than in wild-type cells. In *dam1-11* and *ipl1-321* cells, chromosomes remain closely associated with one SPB, suggesting that bipolar attachment is never established (He et al., 2001).

While these initial studies have provided important insight, they have limitations. First, their descriptions of chromosome motion are largely qualitative. This qualitative understanding allows detection of only gross defects in chromosome movement. Still, the

complexity and redundancy of the kinetochore and spindle apparatus suggest that molecular dissection of chromosome-MT attachment and force generation will require the ability to recognize and quantify much subtler defects in chromosome movement. Second, our recent chromosome motion studies (see Chapter 5) suggest that chromosome velocities can reach up to 0.20 $\mu\text{m}/\text{sec}$ and point out that our initial studies using 30 second time points were too slow for accurate kinetic determination (He et al., 2001). Pearson and colleagues subsequently monitored metaphase and anaphase chromosome dynamics with sampling rates of less than 1 second (Pearson et al., 2001). However, they achieved these high rates by imaging only one plane and, therefore, did not accurately measure three-dimensional distances. Much of their work was also done using Nuf2p as a SPB marker. Nuf2p has since been identified as a kinetochore not SPB component (He et al., 2001). Finally, previous work on kinetochore mediated chromosome dynamics has focused primarily on metaphase and anaphase chromosome dynamics. Although there have been studies of interphase chromosome dynamics, these investigations have generally focused on the MT-independent motion of the chromosome arms (Gasser, 2002; Heun et al., 2001; Marshall et al., 1997); but centromeres cluster around SPBs even in G1 cells (Jin et al., 1998; Jin et al., 2000) and may maintain close association with the SPBs throughout the cell cycle. Understanding kinetochore-MT attachment and chromosome dynamics at the early stages of the cell cycle will be essential to gain a complete understanding of how attachment and force generation are achieved and how kinetochore architecture is regulated.

1.3.5 Powering chromosome dynamics via regulation at microtubule plus-ends

Eukaryotic cells use two primary mechanisms to generate the force required to move chromosomes: the ATP-dependent sliding of motor proteins along MTs; and the GTP-

dependent growth and shrinkage of MTs, regulated by microtubule associated proteins (MAPs) and kinesin related motor proteins (KRPs) (McIntosh et al., 2002). These forces can be generated at the plus ends of k-MTs embedded in the kinetochore, at the minus-ends of MTs at the SPBs (microtubule flux), or through the interaction of p-MTs with chromosome arms (polar ejection force) (Rieder and Salmon, 1994; Waters et al., 1996). The relative importance of these different mechanisms appears to vary considerably in different cell types. In budding yeast, neither MT flux nor polar ejection force has been observed (Maddox et al., 2000; O'Toole et al., 1999); thus the interface between the kinetochore and the plus-end of MTs is likely to be the primary locus of force generation. However, we still know very little about how kinetochores bind to MTs or how the forces required for chromosome movement are generated.

1.3.6 Cell cycle dependent kinetochore functions

In prometaphase, chromosomes bind to the sides of MTs and move rapidly towards a pole (Alexander and Rieder, 1991; Rieder and Alexander, 1990). When bipolarity is established, the extreme plus ends of MTs become embedded in kinetochores. Bipolarly attached chromosomes undergo oscillatory movements throughout metaphase (Skibbens et al., 1993), and kinetochores are thought to regulate MT dynamics (Hyman and Mitchison, 1990). However, the proteins that mediate the attachment of kinetochores to MTs and the process that regulates MT dynamics are not well understood.

In G1 cells, we have observed that the average distance between the SPB and chromosome tag is 0.7 μm . However, in early S-phase, the SPB-to-centromere distance shortens considerably, suggesting that there is a cell cycle dependent change in MT dynamics and force generation (unpublished data). To investigate the molecular basis of this change in

chromosome positioning and dynamics, we have analyzed the effects of various conditional mutants in kinetochore proteins. 3D computer modeling and comparative motion analysis of the chromosomes have revealed that kinetochore proteins essential for attachment in early S-phase are not required at other points in the cell cycle. In particular, we have found that mutations in the known MT binding kinetochore proteins do not have an effect on attachment in G1. Our results suggest that different subsets of kinetochore proteins mediate attachment and regulate chromosome dynamics during the different stages of the cell cycle (see Chapter 5).

1.4 Microtubule Attachment Surveillance System

A surveillance mechanism known as the spindle assembly checkpoint monitors errors in formation of the mitotic spindle apparatus and arrests cells in metaphase (Amon, 1999; Burke, 2000). Sister separation occurs at the metaphase to anaphase transition, an irreversible step during cell division that is closely regulated. In the event of incomplete attachment by any of the sisters, separation of all sister chromatids is delayed by the spindle checkpoint to provide time for bipolar attachment to be established; once complete, sister chromatid cohesion is then dissolved and chromatids begin their anaphase movement toward the spindle poles.

After DNA replication, sister chromatids are tightly linked to one another via the DNA “cohesin” protein Scc1p (Mcd1p) (Michaelis et al., 1997). The tight association between both sisters is thought to play an important role in establishing chromosome ‘bi-orientation’ (bipolar attachment) during metaphase (Tanaka et al., 2000). Once all sisters have established bipolar attachment, the Esp1p cleaves Scc1p and thereby facilitates

chromosome segregation and anaphase movements via loss of arm cohesion (Ciosk et al., 1998). However, this activity is normally blocked prior to the onset of anaphase by a member of the checkpoint, Map2p (Li et al., 1997), and is thought to occur via Mad2p binding directly to Cdc20p.

MAD and *BUB* genes were originally identified through genetic screens in budding yeast and are important components of the surveillance mechanism (Hoyt et al., 1991; Li and Murray, 1991). Wild-type cells normally arrest in the presence of MT destabilizing drugs, such as benomyl and nocodazole, which induce spindle damage and inhibit the formation of stable kinetochore-MT attachments. Loss of any single checkpoint gene disables a cell's ability to block the metaphase to anaphase transition in response to spindle damage.

1.4.1 Centromere-microtubule attachment sensor

Functional kinetochores are required to transduce 'wait' signals to the surveillance mechanism. In the absence of a functional kinetochore, as seen in *ndc10-1* cells placed under restrictive conditions, centromere-MT establishment is unsuccessful and cells fail to arrest at the metaphase-anaphase transition (Goh and Kilmartin, 1993), suggesting that components involved in signaling to the checkpoint interact with kinetochores in a CBF3 dependent manner. Furthermore, it has also been demonstrated that components of the Ndc80 complex play an important role in error checking. The loss of *SPC24* or *SPC25* function inactivates the spindle assembly checkpoint (He et al., 2001; Janke et al., 2002), and points to the Ndc80 complex in the recruitment of spindle checkpoint proteins to the kinetochore.

Studies in higher eukaryotes have also shown that even a single unattached chromosome is sufficient to engage the spindle checkpoint. Our lab has recently determined that the yeast Bub1p and Bub3p proteins associate with all kinetochores until the onset of

metaphase, when they are eventually displaced. Mad2p in contrast, is recruited only to unattached kinetochores following MT depolymerization by destabilizing drugs or following kinetochore disruption (Gillett E.S, Espelin C.W and Sorger P.K, *submitted*). Collectively, these data suggest that the surveillance signals emanate from kinetochores; and that kinetochores may function as attachment sensors.

1.5 Computational Approaches to Study Kinetochore Function

The development of machine vision techniques for data analysis began over 30 years ago and has been exploited in many fields including robotics, biomedicine, meteorological and environmental survey, surveillance, and manufacturing. Computational models have also been an important part of chemistry, physics and mechanical engineering for just as long. However, applications to *in vivo* biological studies have been long in coming. It is difficult to speculate on the reasons for their delay but may be due to the low signal to noise ratios of most *in vivo* imaging or the lack of data available for developing *in silico* models.

1.5.1 Machine vision technology

In cell biology the analysis of microscopy data is traditionally performed manually and on a qualitative level, the advent of new imaging and visualization techniques as well as electronic imaging devices has changed this dramatically. For example, with the introduction of GFP it became possible to label specific proteins in live cells with fluorescent markers and to observe their dynamics over extended periods. The development of sensitive, high-resolution digital cameras connected to computer systems rendered the recording of the cellular dynamics possible which is essential for a quantitative analysis and data interpretation. Frequently though, large amounts of data are acquired with very high

information content and consequently the bottleneck in these cases is not the experiment, but the extraction and analysis of useful information. An accurate and complete manual analysis is cumbersome or in many cases infeasible. With the help of highly automated machine vision techniques and image analysis it will soon be possible to tackle these challenges.

As part of the studies presented in this thesis, I have used improved microscopy techniques to gain a more detailed and quantitative understanding of chromosome dynamics, not only in metaphase and anaphase, but throughout the cell cycle. Initial techniques were based on relatively slow and required a manual data entry (spot localization). Through advancements in imaging technology (e.g., faster cameras) and our own efforts (e.g., automated spot detection) methods now allow us to sample chromosome motion at 2-5 second intervals while imaging the entire yeast nucleus to ensure that true 3D distances are measured (see Chapter 4). When combined with molecular genetics in yeast (see Chapter 3), automated spot detection makes it possible to rapidly acquire and analyze the chromosome dynamics at resolutions better than diffraction limited resolution of a normal epifluorescent light microscope (refer to Chapter 4 for more information on Super-Resolution). In fact, we are currently using this approach to understand the role of kinetochore-MAPs on MT dynamic instability and chromosome motion throughout the cell cycle (see Chapter 5).

1.5.2 Computational modeling

The kinetochore is an integral part of a multi-component mechanical system. To uncover the tensile capabilities of this dynamic system will require the development of mathematical and computational models that successfully factor in redundant MT regulatory machinery and cell cycle dependencies. In fact, we are currently continuing to characterize yeast chromosome movement throughout the cell cycle in sufficient detail that accurate rates

of acceleration can be measured, forces deduced, and a mechanical model of the process developed. We believe that development of such quantitative, mechanistic models of spindle and chromosome dynamics will be instrumental in uncovering the molecular details of attachment and force generation at the kinetochore.

Several groups have employed computational models to explain complex phenomenon involving structural rearrangements of cellular components. Some of the initial mathematical modeling in cell biology attempted to explain dynamic instability based on the GTP-cap model using monte carlo simulations (Chen and Hill, 1985). Using approximations for association constants and rates of GTP-hydrolysis, Bayley and Martin were able to reproduce patterns of MT length changes similar to those observed *in vivo* and *in vitro* (Bayley et al., 1989a; Bayley et al., 1989b). Using a combination of time-lapse 3D imaging and stochastic modeling they have also demonstrated that global chromosome positions are heritable through the cell cycle in mammalian cells (Gerlich et al., 2003). Force-balance modeling has recently been used to understand the role of multiple MT motors in mitotic spindle elongation and force production in *Drosophila* (Cytrynbaum et al., 2003). These new areas of research are just now beginning to mature and suggest at many exciting possibilities.

1.6 Concluding Remarks

Ultimately, the success of genetic transmission depends in part on the proper assembly of kinetochore components onto centromeric DNA regions, maturation of MT attachment, management of the mitotic checkpoint, and regulation of opposing tensile forces before anaphase onset. Original studies of yeast kinetochore biology suggested that the kinetochore was a simple organelle consisting of not much more than a centromeric DNA

sequence, a basic centromere binding complex (e.g., CBF3) and a kinesin-like motor (Hyman et al., 1992). Upon further biochemical and genetic studies, the picture of the yeast kinetochore evolved considerably (Sorger et al., 1994). Recent evidence suggests that the kinetochore is a highly intricate organelle with many subcomplexes (Cheeseman et al., 2002a; Cheeseman et al., 2001; He et al., 2001; Janke et al., 2002; Wigge and Kilmartin, 2001). To this day, however, the minimal number of components needed to maintain kinetochore-MT attachment remains elusive. Future breakthroughs will depend on *fin vivo* studies, biochemical purifications and biophysical characterization of the individual subcomplexes, better imaging technologies and the development of mechanical models to explain the sophisticated nature of the mitotic spindle.

Currently, the anti-microtubule drug, taxol, is used in the treatment of several forms of cancer. Taxol functions by stabilizing polymerized MTs. By combining information already gained about kinetochore function with machine vision techniques, computational models, genetic and biochemical studies, future research can focus on discovering other therapeutic agents for the treatment of human disease. Using automated chromosome tracking tools with large scale recombinant chemical libraries, it may be possible to identify compounds from automated screens that may modulate aspects of chromosome segregation.

1.7 References

- Adams, I. R., and Kilmartin, J. V. (2000). Spindle pole body duplication: a model for centrosome duplication? *Trends Cell Biol* 10, 329-335.
- Alexander, S. P., and Rieder, C. L. (1991). Chromosome motion during attachment to the vertebrate spindle: initial saltatory-like behavior of chromosomes and quantitative analysis of force production by nascent kinetochore fibers. *J Cell Biol* 113, 805-815.
- Allen, C., and Borisy, G. G. (1974). Structural polarity and directional growth of microtubules of *Chlamydomonas* flagella. *J Mol Biol* 90, 381-402.
- Amon, A. (1999). The spindle checkpoint. *Curr Opin Genet Dev* 9, 69-75.
- Amos, L., and Klug, A. (1974). Arrangement of subunits in flagellar microtubules. *J Cell Sci* 14, 523-549.
- Bai, C., Sen, P., Hofmann, K., Ma, L., Goebel, M., Harper, J. W., and Elledge, S. J. (1996). SKP1 connects cell cycle regulators to the ubiquitin proteolysis machinery through a novel motif, the F-box. *Cell* 86, 263-274.
- Baker, R. E., and Masison, D. C. (1990). Isolation of the gene encoding the *Saccharomyces cerevisiae* centromere-binding protein CP1. *Mol Cell Biol* 10, 2458-2467.
- Bardin, A. J., Visintin, R., and Amon, A. (2000). A mechanism for coupling exit from mitosis to partitioning of the nucleus. *Cell* 102, 21-31.
- Bayley, P., Schilstra, M., and Martin, S. (1989a). A lateral cap model of microtubule dynamic instability. *FEBS Lett* 259, 181-184.
- Bayley, P. M., Schilstra, M. J., and Martin, S. R. (1989b). A simple formulation of microtubule dynamics: quantitative implications of the dynamic instability of microtubule populations in vivo and in vitro. *J Cell Sci* 93 (Pt 2), 241-254.
- Belmont, L. D., Hyman, A. A., Sawin, K. E., and Mitchison, T. J. (1990). Real-time visualization of cell cycle-dependent changes in microtubule dynamics in cytoplasmic extracts. *Cell* 62, 579-589.
- Berlin, V., Styles, C. A., and Fink, G. R. (1990). BIK1, a protein required for microtubule function during mating and mitosis in *Saccharomyces cerevisiae*, colocalizes with tubulin. *J Cell Biol* 111, 2573-2586.
- Biggins, S., Severin, F. F., Bhalla, N., Sassoon, I., Hyman, A. A., and Murray, A. W. (1999). The conserved protein kinase Ip11 regulates microtubule binding to kinetochores in budding yeast. *Genes Dev* 13, 532-544.

- Bloom, K. (1993). The centromere frontier: kinetochore components, microtubule-based motility, and the CEN-value paradox. *Cell* 73, 621-624.
- Burke, D. J. (2000). Complexity in the spindle checkpoint. *Curr Opin Genet Dev* 10, 26-31.
- Buvelot, S., Tatsutani, S. Y., Vermaak, D., and Biggins, S. (2003). The budding yeast Ipl1/Aurora protein kinase regulates mitotic spindle disassembly. *J Cell Biol* 160, 329-339.
- Cai, M., and Davis, R. W. (1990). Yeast centromere binding protein CBF1, of the helix-loop-helix protein family, is required for chromosome stability and methionine prototrophy. *Cell* 61, 437-446.
- Chan, C. S., and Botstein, D. (1993). Isolation and characterization of chromosome-gain and increase-in-ploidy mutants in yeast. *Genetics* 135, 677-691.
- Cheeseman, I. M., Anderson, S., Jwa, M., Green, E. M., Kang, J., Yates, J. R., 3rd, Chan, C. S., Drubin, D. G., and Barnes, G. (2002a). Phospho-regulation of kinetochore-microtubule attachments by the Aurora kinase Ipl1p. *Cell* 111, 163-172.
- Cheeseman, I. M., Drubin, D. G., and Barnes, G. (2002b). Simple centromere, complex kinetochore: linking spindle microtubules and centromeric DNA in budding yeast. *J Cell Biol* 157, 199-203.
- Cheeseman, I. M., Enquist-Newman, M., Muller-Reichert, T., Drubin, D. G., and Barnes, G. (2001). Mitotic spindle integrity and kinetochore function linked by the Duo1p/Dam1p complex. *J Cell Biol* 152, 197-212.
- Chen, Y., Baker, R. E., Keith, K. C., Harris, K., Stoler, S., and Fitzgerald-Hayes, M. (2000). The N terminus of the centromere H3-like protein Cse4p performs an essential function distinct from that of the histone fold domain. *Mol Cell Biol* 20, 7037-7048.
- Chen, Y., Riley, D. J., Chen, P. L., and Lee, W. H. (1997). HEC, a novel nuclear protein rich in leucine heptad repeats specifically involved in mitosis. *Mol Cell Biol* 17, 6049-6056.
- Chen, Y. D., and Hill, T. L. (1985). Monte Carlo study of the GTP cap in a five-start helix model of a microtubule. *Proc Natl Acad Sci U S A* 82, 1131-1135.
- Choo, K. H. (1997). Centromere DNA dynamics: latent centromeres and neocentromere formation. *Am J Hum Genet* 61, 1225-1233.
- Chubb, J. R., Boyle, S., Perry, P., and Bickmore, W. A. (2002). Chromatin motion is constrained by association with nuclear compartments in human cells. *Curr Biol* 12, 439-445.
- Ciosk, R., Zachariae, W., Michaelis, C., Shevchenko, A., Mann, M., and Nasmyth, K. (1998). An ESP1/PDS1 complex regulates loss of sister chromatid cohesion at the metaphase to anaphase transition in yeast. *Cell* 93, 1067-1076.

- Clarke, L., and Carbon, J. (1980). Isolation of a yeast centromere and construction of functional small circular chromosomes. *Nature* 287, 504-509.
- Connelly, C., and Hieter, P. (1996). Budding yeast SKP1 encodes an evolutionarily conserved kinetochore protein required for cell cycle progression. *Cell* 86, 275-285.
- Cytrynbaum, E. N., Scholey, J. M., and Mogilner, A. (2003). A force balance model of early spindle pole separation in *Drosophila* embryos. *Biophys J* 84, 757-769.
- Desai, A., and Mitchison, T. J. (1995). A new role for motor proteins as couplers to depolymerizing microtubules. *J Cell Biol* 128, 1-4.
- Desai, A., and Mitchison, T. J. (1997). Microtubule polymerization dynamics. *Annu Rev Cell Dev Biol* 13, 83-117.
- Desai, A., Verma, S., Mitchison, T. J., and Walczak, C. E. (1999). Kin I kinesins are microtubule-destabilizing enzymes. *Cell* 96, 69-78.
- Espelin, C. W., Kaplan, K. B., and Sorger, P. K. (1997). Probing the architecture of a simple kinetochore using DNA-protein crosslinking. *J Cell Biol* 139, 1383-1396.
- Euskirchen, G. M. (2002). Nnf1p, Dsn1p, Mtw1p, and Nsl1p: a new group of proteins important for chromosome segregation in *Saccharomyces cerevisiae*. *Eukaryot Cell* 1, 229-240.
- Fan, J., Griffiths, A. D., Lockhart, A., Cross, R. A., and Amos, L. A. (1996). Microtubule minus ends can be labelled with a phage display antibody specific to alpha-tubulin. *J Mol Biol* 259, 325-330.
- Fitzgerald-Hayes, M., Clarke, L., and Carbon, J. (1982). Nucleotide sequence comparisons and functional analysis of yeast centromere DNAs. *Cell* 29, 235-244.
- Gard, D. L., and Kirschner, M. W. (1987). A microtubule-associated protein from *Xenopus* eggs that specifically promotes assembly at the plus-end. *J Cell Biol* 105, 2203-2215.
- Gasser, S. M. (2002). Visualizing chromatin dynamics in interphase nuclei. *Science* 296, 1412-1416.
- Gaudet, A., and Fitzgerald-Hayes, M. (1987). Alterations in the adenine-plus-thymine-rich region of CEN3 affect centromere function in *Saccharomyces cerevisiae*. *Mol Cell Biol* 7, 68-75.
- Gerlich, D., Beaudouin, J., Kalbfuss, B., Daigle, N., Eils, R., and Ellenberg, J. (2003). Global chromosome positions are transmitted through mitosis in mammalian cells. *Cell* 112, 751-764.

- Gillett, E. S., and Sorger, P. K. (2001). Tracing the pathway of spindle assembly checkpoint signaling. *Dev Cell* 1, 162-164.
- Goh, P. Y., and Kilmartin, J. V. (1993). NDC10: a gene involved in chromosome segregation in *Saccharomyces cerevisiae*. *J Cell Biol* 121, 503-512.
- Goldstein, L. S., and Philp, A. V. (1999). The road less traveled: emerging principles of kinesin motor utilization. *Annu Rev Cell Dev Biol* 15, 141-183.
- Goshima, G., and Yanagida, M. (2000). Establishing biorientation occurs with precocious separation of the sister kinetochores, but not the arms, in the early spindle of budding yeast. *Cell* 100, 619-633.
- Guacci, V., Koshland, D., and Strunnikov, A. (1997). A direct link between sister chromatid cohesion and chromosome condensation revealed through the analysis of MCD1 in *S. cerevisiae*. *Cell* 91, 47-57.
- Hayden, J. H., Bowser, S. S., and Rieder, C. L. (1990). Kinetochores capture astral microtubules during chromosome attachment to the mitotic spindle: direct visualization in live newt lung cells. *J Cell Biol* 111, 1039-1045.
- He, X., Asthana, S., and Sorger, P. K. (2000). Transient sister chromatid separation and elastic deformation of chromosomes during mitosis in budding yeast. *Cell* 101, 763-775.
- He, X., Rines, D. R., Espelin, C. W., and Sorger, P. K. (2001). Molecular analysis of kinetochore-microtubule attachment in budding yeast. *Cell* 106, 195-206.
- Hegemann, J. H., and Fleig, U. N. (1993). The centromere of budding yeast. *Bioessays* 15, 451-460.
- Heun, P., Laroche, T., Shimada, K., Furrer, P., and Gasser, S. M. (2001). Chromosome dynamics in the yeast interphase nucleus. *Science* 294, 2181-2186.
- Hofmann, C., Cheeseman, I. M., Goode, B. L., McDonald, K. L., Barnes, G., and Drubin, D. G. (1998). *Saccharomyces cerevisiae* Duo1p and Dam1p, novel proteins involved in mitotic spindle function. *J Cell Biol* 143, 1029-1040.
- Holy, T. E., and Leibler, S. (1994). Dynamic instability of microtubules as an efficient way to search in space. *Proc Natl Acad Sci U S A* 91, 5682-5685.
- Hoyt, M. A. (2001). A new view of the spindle checkpoint. *J Cell Biol* 154, 909-911.
- Hoyt, M. A., Totis, L., and Roberts, B. T. (1991). *S. cerevisiae* genes required for cell cycle arrest in response to loss of microtubule function. *Cell* 66, 507-517.

- Hsu, J. Y., Sun, Z. W., Li, X., Reuben, M., Tatchell, K., Bishop, D. K., Grushcow, J. M., Brame, C. J., Caldwell, J. A., Hunt, D. F., *et al.* (2000). Mitotic phosphorylation of histone H3 is governed by Ipl1/aurora kinase and Glc7/PP1 phosphatase in budding yeast and nematodes. *Cell* 102, 279-291.
- Hyland, K. M., Kingsbury, J., Koshland, D., and Hieter, P. (1999). Ctf19p: A novel kinetochore protein in *Saccharomyces cerevisiae* and a potential link between the kinetochore and mitotic spindle. *J Cell Biol* 145, 15-28.
- Hyman, A. A., Middleton, K., Centola, M., Mitchison, T. J., and Carbon, J. (1992). Microtubule-motor activity of a yeast centromere-binding protein complex. *Nature* 359, 533-536.
- Hyman, A. A., and Mitchison, T. J. (1990). Modulation of microtubule stability by kinetochores in vitro. *J Cell Biol* 110, 1607-1616.
- Inoue, S. (1997). The role of microtubule assembly dynamics in mitotic force generation and functional organization of living cells. *J Struct Biol* 118, 87-93.
- Inoue, S., and Salmon, E. D. (1995). Force generation by microtubule assembly/disassembly in mitosis and related movements. *Mol Biol Cell* 6, 1619-1640.
- Ito, T., Chiba, T., Ozawa, R., Yoshida, M., Hattori, M., and Sakaki, Y. (2001). A comprehensive two-hybrid analysis to explore the yeast protein interactome. *Proc Natl Acad Sci U S A* 98, 4569-4574.
- Janke, C., Ortiz, J., Tanaka, T. U., Lechner, J., and Schiebel, E. (2002). Four new subunits of the Dam1-Duo1 complex reveal novel functions in sister kinetochore biorientation. *Embo J* 21, 181-193.
- Jin, Q., Trelles-Sticken, E., Scherthan, H., and Loidl, J. (1998). Yeast nuclei display prominent centromere clustering that is reduced in nondividing cells and in meiotic prophase. *J Cell Biol* 141, 21-29.
- Jin, Q. W., Fuchs, J., and Loidl, J. (2000). Centromere clustering is a major determinant of yeast interphase nuclear organization. *J Cell Sci* 113 (Pt 11), 1903-1912.
- Jones, M. H., Bachant, J. B., Castillo, A. R., Giddings, T. H., Jr., and Winey, M. (1999). Yeast Dam1p is required to maintain spindle integrity during mitosis and interacts with the Mps1p kinase. *Mol Biol Cell* 10, 2377-2391.
- Kaplan, K. B., Hyman, A. A., and Sorger, P. K. (1997). Regulating the yeast kinetochore by ubiquitin-dependent degradation and Skp1p-mediated phosphorylation. *Cell* 91, 491-500.

- Keith, K. C., Baker, R. E., Chen, Y., Harris, K., Stoler, S., and Fitzgerald-Hayes, M. (1999). Analysis of primary structural determinants that distinguish the centromere-specific function of histone variant Cse4p from histone H3. *Mol Cell Biol* 19, 6130-6139.
- Kim, J. H., Kang, J. S., and Chan, C. S. (1999). Sli15 associates with the ip11 protein kinase to promote proper chromosome segregation in *Saccharomyces cerevisiae*. *J Cell Biol* 145, 1381-1394.
- Kirschner, M. W., and Mitchison, T. (1986). Microtubule dynamics. *Nature* 324, 621.
- Kitagawa, K., and Hieter, P. (2001). Evolutionary conservation between budding yeast and human kinetochores. *Nat Rev Mol Cell Biol* 2, 678-687.
- Kitagawa, K., Skowyra, D., Elledge, S. J., Harper, J. W., and Hieter, P. (1999). SGT1 encodes an essential component of the yeast kinetochore assembly pathway and a novel subunit of the SCF ubiquitin ligase complex. *Mol Cell* 4, 21-33.
- Kosco, K. A., Pearson, C. G., Maddox, P. S., Wang, P. J., Adams, I. R., Salmon, E. D., Bloom, K., and Huffaker, T. C. (2001). Control of microtubule dynamics by Stu2p is essential for spindle orientation and metaphase chromosome alignment in yeast. *Mol Biol Cell* 12, 2870-2880.
- Lechner, J., and Carbon, J. (1991). A 240 kd multisubunit protein complex, CBF3, is a major component of the budding yeast centromere. *Cell* 64, 717-725.
- Li, R., and Murray, A. W. (1991). Feedback control of mitosis in budding yeast. *Cell* 66, 519-531.
- Li, X., and Nicklas, R. B. (1995). Mitotic forces control a cell-cycle checkpoint. *Nature* 373, 630-632.
- Li, Y., Bachant, J., Alcasabas, A. A., Wang, Y., Qin, J., and Elledge, S. J. (2002). The mitotic spindle is required for loading of the DASH complex onto the kinetochore. *Genes Dev* 16, 183-197.
- Li, Y., Gorbea, C., Mahaffey, D., Rechsteiner, M., and Benezra, R. (1997). MAD2 associates with the cyclosome/anaphase-promoting complex and inhibits its activity. *Proc Natl Acad Sci USA* 94, 12431-12436.
- Lin, H., de Carvalho, P., Kho, D., Tai, C. Y., Pierre, P., Fink, G. R., and Pellman, D. (2001). Polyploids require Bik1 for kinetochore-microtubule attachment. *J Cell Biol* 155, 1173-1184.
- Maddox, P. S., Bloom, K. S., and Salmon, E. D. (2000). The polarity and dynamics of microtubule assembly in the budding yeast *Saccharomyces cerevisiae*. *Nat Cell Biol* 2, 36-41.

- Marschall, L. G., and Clarke, L. (1995). A novel cis-acting centromeric DNA element affects *S. pombe* centromeric chromatin structure at a distance. *J Cell Biol* 128, 445-454.
- Marshall, W. F., Straight, A., Marko, J. F., Swedlow, J., Dernburg, A., Belmont, A., Murray, A. W., Agard, D. A., and Sedat, J. W. (1997). Interphase chromosomes undergo constrained diffusional motion in living cells. *Curr Biol* 7, 930-939.
- Masumoto, H., Masukata, H., Muro, Y., Nozaki, N., and Okazaki, T. (1989). A human centromere antigen (CENP-B) interacts with a short specific sequence in alphoid DNA, a human centromeric satellite. *J Cell Biol* 109, 1963-1973.
- McAinsh, A., Tytell, J. and Sorger, P.K. (2003). Structure, function and regulation of budding yeast kinetochores. *Annu Rev Cell Biol*, In press.
- McIntosh, J. R., Grishchuk, E. L., and West, R. R. (2002). Chromosome-microtubule interactions during mitosis. *Annu Rev Cell Dev Biol* 18, 193-219.
- Measday, V., Hailey, D. W., Pot, I., Givan, S. A., Hyland, K. M., Cagney, G., Fields, S., Davis, T. N., and Hieter, P. (2002). Ctf3p, the Mis6 budding yeast homolog, interacts with Mcm22p and Mcm16p at the yeast outer kinetochore. *Genes Dev* 16, 101-113.
- Michaelis, C., Ciosk, R., and Nasmyth, K. (1997). Cohesins: chromosomal proteins that prevent premature separation of sister chromatids. *Cell* 91, 35-45.
- Mitchison, T., Evans, L., Schulze, E., and Kirschner, M. (1986). Sites of microtubule assembly and disassembly in the mitotic spindle. *Cell* 45, 515-527.
- Mitchison, T., and Kirschner, M. (1984a). Dynamic instability of microtubule growth. *Nature* 312, 237-242.
- Mitchison, T., and Kirschner, M. (1984b). Microtubule assembly nucleated by isolated centrosomes. *Nature* 312, 232-237.
- Nicklas, R. B. (1997). How cells get the right chromosomes. *Science* 275, 632-637.
- Ortiz, J., Stemmann, O., Rank, S., and Lechner, J. (1999). A putative protein complex consisting of Ctf19, Mcm21, and Okp1 represents a missing link in the budding yeast kinetochore. *Genes Dev* 13, 1140-1155.
- O'Toole, E. T., Winey, M., and McIntosh, J. R. (1999). High-voltage electron tomography of spindle pole bodies and early mitotic spindles in the yeast *Saccharomyces cerevisiae*. *Mol Biol Cell* 10, 2017-2031.
- Pearson, C. G., Maddox, P. S., Salmon, E. D., and Bloom, K. (2001). Budding yeast chromosome structure and dynamics during mitosis. *J Cell Biol* 152, 1255-1266.

- Pluta, A. F., Mackay, A. M., Ainsztein, A. M., Goldberg, I. G., and Earnshaw, W. C. (1995). The centromere: hub of chromosomal activities. *Science* 270, 1591-1594.
- Pryer, N. K., Walker, R. A., Skeen, V. P., Bourns, B. D., Soboeiro, M. F., and Salmon, E. D. (1992). Brain microtubule-associated proteins modulate microtubule dynamic instability in vitro. Real-time observations using video microscopy. *J Cell Sci* 103 (Pt 4), 965-976.
- Rieder, C. L., and Alexander, S. P. (1990). Kinetochores are transported poleward along a single astral microtubule during chromosome attachment to the spindle in newt lung cells. *J Cell Biol* 110, 81-95.
- Rieder, C. L., and Salmon, E. D. (1994). Motile kinetochores and polar ejection forces dictate chromosome position on the vertebrate mitotic spindle. *J Cell Biol* 124, 223-233.
- Rieder, C. L., and Salmon, E. D. (1998). The vertebrate cell kinetochore and its roles during mitosis. *Trends Cell Biol* 8, 310-318.
- Rines, D. R., He, X., and Sorger, P. K. (2002). Quantitative microscopy of green fluorescent protein-labeled yeast. *Methods Enzymol* 351, 16-34.
- Russell, I. D., Grancell, A. S., and Sorger, P. K. (1999). The unstable F-box protein p58-Ctf13 forms the structural core of the CBF3 kinetochore complex. *J Cell Biol* 145, 933-950.
- Salmon, T., Walker, R. A., and Pryer, N. K. (1989). Video-enhanced differential interference contrast light microscopy. *Biotechniques* 7, 624-633.
- Schaar, B. T., Chan, G. K., Maddox, P., Salmon, E. D., and Yen, T. J. (1997). CENP-E function at kinetochores is essential for chromosome alignment. *J Cell Biol* 139, 1373-1382.
- Shelby, R. D., Hahn, K. M., and Sullivan, K. F. (1996). Dynamic elastic behavior of alpha-satellite DNA domains visualized in situ in living human cells. *J Cell Biol* 135, 545-557.
- Shimoda, S. L., and Solomon, F. (2002). Integrating functions at the kinetochore. *Cell* 109, 9-12.
- Skibbens, R. V., Skeen, V. P., and Salmon, E. D. (1993). Directional instability of kinetochore motility during chromosome congression and segregation in mitotic newt lung cells: a push-pull mechanism. *J Cell Biol* 122, 859-875.
- Sorger, P. K., Severin, F. F., and Hyman, A. A. (1994). Factors required for the binding of reassembled yeast kinetochores to microtubules in vitro. *J Cell Biol* 127, 995-1008.
- Spencer, F., Gerring, S. L., Connelly, C., and Hieter, P. (1990). Mitotic chromosome transmission fidelity mutants in *Saccharomyces cerevisiae*. *Genetics* 124, 237-249.

Stoler, S., Keith, K. C., Curnick, K. E., and Fitzgerald-Hayes, M. (1995). A mutation in CSE4, an essential gene encoding a novel chromatin-associated protein in yeast, causes chromosome nondisjunction and cell cycle arrest at mitosis. *Genes Dev* 9, 573-586.

Straight, A. F., Belmont, A. S., Robinett, C. C., and Murray, A. W. (1996). GFP tagging of budding yeast chromosomes reveals that protein-protein interactions can mediate sister chromatid cohesion. *Curr Biol* 6, 1599-1608.

Takahashi, K., Chen, E. S., and Yanagida, M. (2000). Requirement of Mis6 centromere connector for localizing a CENP-A-like protein in fission yeast. *Science* 288, 2215-2219.

Tanaka, T., Fuchs, J., Loidl, J., and Nasmyth, K. (2000). Cohesin ensures bipolar attachment of microtubules to sister centromeres and resists their precocious separation. *Nat Cell Biol* 2, 492-499.

Tanaka, T. U., Rachidi, N., Janke, C., Pereira, G., Galova, M., Schiebel, E., Stark, M. J., and Nasmyth, K. (2002). Evidence that the Ipl1-Sli15 (Aurora kinase-INCENP) complex promotes chromosome bi-orientation by altering kinetochore-spindle pole connections. *Cell* 108, 317-329.

Thomann, D., Rines, D. R., Sorger, P. K., and Danuser, G. (2002). Automatic fluorescent tag detection in 3D with super-resolution: application to the analysis of chromosome movement. *J Microsc* 208, 49-64.

Tournebize, R., Popov, A., Kinoshita, K., Ashford, A. J., Rybina, S., Pozniakovsky, A., Mayer, T. U., Walczak, C. E., Karsenti, E., and Hyman, A. A. (2000). Control of microtubule dynamics by the antagonistic activities of XMAP215 and XKCM1 in *Xenopus* egg extracts. *Nat Cell Biol* 2, 13-19.

Uhlmann, F., Lottspeich, F., and Nasmyth, K. (1999). Sister-chromatid separation at anaphase onset is promoted by cleavage of the cohesin subunit Scc1. *Nature* 400, 37-42.

Vafa, O., and Sullivan, K. F. (1997). Chromatin containing CENP-A and alpha-satellite DNA is a major component of the inner kinetochore plate. *Curr Biol* 7, 897-900.

Vale, R. D., and Milligan, R. A. (2000). The way things move: looking under the hood of molecular motor proteins. *Science* 288, 88-95.

Van Hooser, A. A., Mancini, M. A., Allis, C. D., Sullivan, K. F., and Brinkley, B. R. (1999). The mammalian centromere: structural domains and the attenuation of chromatin modeling. *Faseb J* 13 Suppl 2, S216-220.

Vasquez, R. J., Gard, D. L., and Cassimeris, L. (1994). XMAP from *Xenopus* eggs promotes rapid plus end assembly of microtubules and rapid microtubule polymer turnover. *J Cell Biol* 127, 985-993.

- Verde, F., Dogterom, M., Stelzer, E., Karsenti, E., and Leibler, S. (1992). Control of microtubule dynamics and length by cyclin A- and cyclin B-dependent kinases in *Xenopus* egg extracts. *J Cell Biol* 118, 1097-1108.
- Visintin, R., Prinz, S., and Amon, A. (1997). CDC20 and CDH1: a family of substrate-specific activators of APC-dependent proteolysis. *Science* 278, 460-463.
- Walczak, C. E., Gan, E. C., Desai, A., Mitchison, T. J., and Kline-Smith, S. L. (2002). The microtubule-destabilizing kinesin XKCM1 is required for chromosome positioning during spindle assembly. *Curr Biol* 12, 1885-1889.
- Walczak, C. E., Mitchison, T. J., and Desai, A. (1996). XKCM1: a *Xenopus* kinesin-related protein that regulates microtubule dynamics during mitotic spindle assembly. *Cell* 84, 37-47.
- Wang, P. J., and Huffaker, T. C. (1997). Stu2p: A microtubule-binding protein that is an essential component of the yeast spindle pole body. *J Cell Biol* 139, 1271-1280.
- Warburton, P. E., Cooke, C. A., Bourassa, S., Vafa, O., Sullivan, B. A., Stetten, G., Gimelli, G., Warburton, D., Tyler-Smith, C., Sullivan, K. F., *et al.* (1997). Immunolocalization of CENP-A suggests a distinct nucleosome structure at the inner kinetochore plate of active centromeres. *Curr Biol* 7, 901-904.
- Waters, J. C., Skibbens, R. V., and Salmon, E. D. (1996). Oscillating mitotic newt lung cell kinetochores are, on average, under tension and rarely push. *J Cell Sci* 109 (Pt 12), 2823-2831.
- Weisenberg, R. C., and Deery, W. J. (1976). Role of nucleotide hydrolysis in microtubule assembly. *Nature* 263, 792-793.
- Weiss, E., and Winey, M. (1996). The *Saccharomyces cerevisiae* spindle pole body duplication gene MPS1 is part of a mitotic checkpoint. *J Cell Biol* 132, 111-123.
- Wigge, P. A., Jensen, O. N., Holmes, S., Soues, S., Mann, M., and Kilmartin, J. V. (1998). Analysis of the *Saccharomyces* spindle pole by matrix-assisted laser desorption/ionization (MALDI) mass spectrometry. *J Cell Biol* 141, 967-977.
- Wigge, P. A., and Kilmartin, J. V. (2001). The Ndc80p complex from *Saccharomyces cerevisiae* contains conserved centromere components and has a function in chromosome segregation. *J Cell Biol* 152, 349-360.
- Winey, M., Goetsch, L., Baum, P., and Byers, B. (1991). MPS1 and MPS2: novel yeast genes defining distinct steps of spindle pole body duplication. *J Cell Biol* 114, 745-754.
- Winey, M., and O'Toole, E. T. (2001). The spindle cycle in budding yeast. *Nat Cell Biol* 3, E23-27.

Yoda, K., Kitagawa, K., Masumoto, H., Muro, Y., and Okazaki, T. (1992). A human centromere protein, CENP-B, has a DNA binding domain containing four potential alpha helices at the NH2 terminus, which is separable from dimerizing activity. *J Cell Biol* 119, 1413-1427.

CHAPTER 2

The following chapter is adapted, with permission, from He et al., 2001. This work was done in collaboration with Xiangwei He and Christopher Espelin. Xiangwei performed the colocalization and ChIP analysis shown in Figure 2-1 and 2-2. Xiangwei also performed the mutant ChIP analysis in Figure 2-6. Christopher Espelin performed the CEN specific ChIP mapping experiments shown in Figure 2-3.

He, X., ¹ Rines, D. R., ¹ Espelin, C. W., and Sorger, P. K. (2001). Molecular analysis of kinetochore-microtubule attachment in budding yeast. *Cell* 106, 195-206. (1) These authors contributed equally to this work.

Molecular Analysis of Kinetochores- Microtubule Attachment in Budding Yeast

2.1	Abstract.....	52
2.2	Introduction.....	52
2.3	Results.....	55
2.3.1	Proteins Localized Primarily to Kinetochores	58
2.3.2	Proteins Bound to Kinetochores and to the Mitotic Spindle	62
2.3.3	Proteins Bound to Kinetochores and a Variety of Microtubule-Based Structures ..	63
2.3.4	Mapping Chromosome Association to Centromeric DNA.....	66
2.3.5	Mutations in Kinetochores Reduce Transient Sisters Separation	69
2.3.6	Live Cell Analysis Reveals Three Types of Defect in Chromosome Movement...	73
2.3.7	A Multilayer Structure at the Yeast Kinetochores	79
2.4	Discussion.....	81
2.4.1	Kinetochores-Associated Microtubule Binding Proteins.....	82
2.4.2	General Implications for Kinetochores-Microtubule Attachment.....	84
2.5	Experimental Procedures	87
2.5.1	Yeast Strains and Manipulations	87
2.5.2	Microscopy and Image Analysis.....	87
2.6	References.....	88

2.1 Abstract

The complex series of movements that mediates chromosome segregation during mitosis is dependent on the attachment of microtubules to kinetochores, DNA-protein complexes that assemble on centromeric DNA. We describe the use of live-cell imaging and chromatin immunoprecipitation in *S. cerevisiae* to identify ten kinetochore subunits, among which are yeast homologs of microtubule binding proteins in animal cells. By analyzing conditional mutations in several of these proteins, we show that they are required for the imposition of tension on paired sister kinetochores and for correct chromosome movement. The proteins include both molecular motors and microtubule associated proteins (MAPs), implying that motors and MAPs function together in binding chromosomes to spindle microtubules.

2.2 Introduction

The segregation of replicated sister chromatids into two equal sets at mitosis involves a complex series of movements mediated by kinetochores, DNA-protein complexes that assemble on centromeric DNA. Following microtubule attachment early in mitosis, paired sister chromatids exhibit directional instability and undergo oscillatory movements back and forth along spindle microtubules (Skibbens et al., 1993). Sister separation is delayed by a mitotic checkpoint comprising MAD and BUB genes that is silenced only when all pairs of chromatids have achieved bivalent attachment. Sister cohesion is then dissolved and chromatids begin their anaphase movement toward the spindle poles.

As structures that link centromeres to spindle fibers, kinetochores have both DNA and microtubule binding activities. The unusual compactness of *S. cerevisiae* centromeres (approximately 175 bp) has facilitated biochemical and genetic analysis of kinetochore-

associated DNA binding proteins. These include CBF3 and the specialized H3 histone Cse4p (Stoler et al., 1995). The assembly of kinetochores in *S. cerevisiae* appears to begin with the binding of CBF3, a four-protein complex, to the essential CDEIII region of centromeric DNA. Cells carrying temperature sensitive mutations in CBF3 subunits (Ndc10p, Cep3p, Ctf13p, or Skp1p) experience greatly elevated chromosome loss under semipermissive conditions (Hyman and Sorger, 1995). Several additional proteins have been identified that bind to yeast centromeres in a CBF3-dependent fashion (Hyland et al., 1999; Meluh et al., 1998; Ortiz et al., 1999; Stoler et al., 1995; Zheng et al., 1999). However, none of these proteins have been implicated directly in the attachment of chromosomes to microtubules or in the generation of force.

Historically, an important question about chromosome-microtubule attachment has been the identity of the kinetochore-associated motors. In animal cells, the kinesin-related motor proteins (KRPs) CENPE and MCAK have been shown to function in kinetochore-dependent chromosome movement, as has dynein (for review, see Rieder and Salmon, 1998); in yeast, it is not known which among the six KRP and dynein motors are kinetochore bound. Moreover, experiments in several organisms have shown that both the ATP-dependent sliding of motor proteins along microtubules and the GTP-dependent depolymerization of microtubule fibers are capable of generating sufficient force to move chromosomes (Hunter and Wordeman, 2000). Thus, nonmotor microtubule associated proteins (MAPs) may function to link kinetochores and microtubule plus ends during periods of polymer growth and shrinkage. The goal of a molecular analysis of yeast kinetochores is therefore to provide answers to the following general questions (1) how many different proteins are involved in chromosome-microtubule attachment and what are the relative roles of motors and MAPs,

(2) do these proteins function only at kinetochores or also in other cellular structures, and (3) do different proteins mediate different aspects of the complex pattern of metaphase and anaphase chromosome movement?

The identification of microtubule binding proteins in yeast kinetochores has been hindered by the absence of an assay to monitor chromosome-microtubule attachment. However, we and others have recently shown that force-generating processes at *S. cerevisiae* kinetochores impose sufficient tension on paired chromatids during metaphase to transiently separate centromeric chromatin toward opposite ends of the spindle (Goshima and Yanagida, 2000; He et al., 2000; Tanaka et al., 2000). Transient separations can pull sisters up to 1 μm apart for several minutes (a large movement relative to the 1.5 to 2 μm yeast spindle) and involve toward-the-pole separating forces and opposing cohesive forces. We reasoned that, by exploiting the phenomenon of transient sister separation to measure and analyze forces exerted on centromeres in wild-type and mutant yeast strains, a molecular analysis of microtubule attachment would be possible. In this paper, we identify as kinetochore components ten *S. cerevisiae* proteins previously thought to be involved in other mitotic processes. Some of these proteins, or their mammalian orthologs, are motors or microtubule binding proteins and mutations in several of these newly-identified kinetochore subunits impair force generation and chromosome movement in vivo. These data lead us to conclude that we have identified some of the proteins involved directly in the formation of microtubule attachment sites.

2.3 Results

We have previously reported that kinetochore proteins in *S. cerevisiae* localize during metaphase to two lobes that lie on either side of the spindle midzone (He et al., 2000). The separation between these lobes is typically about half the separation between spindle pole bodies (SPBs). The distribution of kinetochore proteins changes subtly on a time scale of seconds concomitant with fluctuations in the extent of overlap among the 32 centromeres in a mitotic haploid cell. Because the bilobed distribution of kinetochores was unexpected, we reasoned that it should be possible to identify additional kinetochore proteins based on this distinctive pattern and that some of these proteins might have been misidentified previously as spindle components. Of twenty or so spindle proteins whose functions were not well understood but for which some localization data were available, we found a total of ten (Table 1-1) that probably constitute structural kinetochore components and one kinase that appears to regulate kinetochore function.

Table 1-1. Summary of the kinetochore proteins analyzed in this study

Protein ^a	Localization ^b					ChIP		Alleles Used in This Study	Homologues	Interactions ^{a,c,d}	Reported Functions ^d
	Kinetochores	Nuclear-MTs	SPB	Cortical-Tip	Cyto-MTs	In WT	In <i>ndc10-1</i>				
Ndc80p (E)	+	-	-	-	-	+	-	<i>ndc80-1</i>	HEC1	2H: <i>SPC24</i> , <i>SPC19</i>	Chromosome segregation
Nuf2p (E)	+	-	-	-	-	+	-	<i>nuf2-61; -457</i>	Nuf2R	2H: <i>CIN8</i> , <i>NDC80</i> , <i>SPC19</i>	Chromosome segregation
Spc24p (E)	+	-	-	-	-	+	-	none	<i>S.pombe</i> C336.08	2H: <i>SPC25</i>	Chromosome segregation
Spc25p (E)	+	-	-	-	-	+	-	none	N/A	2H: <i>SPC24</i>	Chromosome segregation
Dam1p (E)	+	-	-	-	-	+	-	<i>dam1-1; -9; -11</i>	N/A	2H: Ndc80, <i>SPC34</i> SL: <i>cin8Δ</i>	Microtubule binding; Spindle integrity
Spc19p (E)	+	+	-	-	-	+	-	none	N/A	2H: <i>SPC34</i> , <i>NDC80</i>	Unknown
Spc34p (E)	+	+	-	-	-	+	-	none	N/A	2H: <i>SPC19</i>	Unknown
Stu2p (E)	+	+	+	+	-	+	-	<i>stu2-276; -27; -278; -279</i>	XMAP215	N/A	Microtubule binding
Bik1p (NE)	+	+	-	+	+	+	-	<i>bik1Δ:His3</i>	CLIP-170	2H: <i>STU2</i> SL: <i>cin8Δ</i>	Spindle elongation
Cin8p (NE)	+	+	-	-	-	+	-	<i>cin8Δ:His3</i>	BimC kinesins	SL: <i>bik1Δ</i> SL: <i>dam1-1</i>	Spindle assembly and elongation; Chromosome segregation
Ipl1p (E)	+	+	-	-	-	-	-	<i>ipl1-2, -321</i>	Aurora-like kinases	SL: <i>cin8Δ</i>	Histone phosphorylation; Regulation of kinetochore-microtubule binding

^aAbbreviations: E, Essential; NE, Non-essential; 2H, Two Hybrid; SL, Synthetic Lethality; SP, Suppression.

^bCellular localization shown by this study.

^cOnly interactions among proteins listed in this table are shown. Extensive genetic and biochemical interactions among Ndc80p, Nuf2p, Spc24p, Spc25p have also been demonstrated (Janke et al., 2001; Wigge and Kilmartin, 2001) and are not shown.

^dReferences for interactions and reported functions are listed at the YPD database (Costanzo et al., 2000) and for 2-hybrid analysis in (Ito et al., 2001; Newman et al., 2000).

To determine the localization of candidate kinetochore proteins, they were tagged with GFP at their extreme C termini and introduced into cells in the place of the wild-type gene using homologous recombination. The positions of the SPBs were determined by replacing the integral SPB protein Spc42p with a fusion to cyan fluorescent protein (Spc42p-CFP; Donaldson and Kilmartin, 1996; He et al., 2000). Time lapse and fixed-cell fluorescence microscopy were performed in two colors to visualize both GFP fusion proteins and spindle poles using optical sectioning microscopy followed by iterative deconvolution (on an Applied Precision DeltaVision Microscope). Cell cycle state in asynchronous cultures and synchrony-release experiments were determined by examining nuclear morphology and spindle length. All GFP (or CFP) fusions tested, including those involving essential genes (Table 1-1), supported wild-type rates of growth. To demonstrate that various proteins were indeed localized to kinetochores, we examined the CBF3-dependence of their localization. GFP fusion proteins and Spc42p-CFP were introduced into *ndc10-1* cells and analyzed at 37°C, conditions that inactivate CBF3 and therefore disrupt kinetochore structure (Goh and Kilmartin, 1993).

As an independent assay for centromere association, we asked whether GFP-tagged proteins were bound to centromeric DNA in vivo as judged by formaldehyde crosslinking and chromatin immunoprecipitation (ChIP). Wild-type and *ndc10-1* cells carrying different GFP-tagged proteins were treated with formaldehyde, cells were lysed, and DNA sheared by sonication to an average of 200–500 bp. Immune complexes were isolated using anti-GFP antibodies and the fraction of coprecipitating DNA determined by PCR using primers specific for *CENIV* and a negative control *URA3* sequence.

2.3.1 *Proteins Localized Primarily to Kinetochores*

The first proteins we examined were Ndc80p, Spc24p, Spc25p, and Nuf2p. Ndc80p, Spc24p, and Spc25p were originally identified by MALDI-based microsequencing as proteins that cofractionate with yeast spindle pole bodies (SPBs) and localize, by immunofluorescence, to the nuclear face of the SPB central plaque and to microtubules (Wigge et al., 1998). Nuf2p has been reported to be an SPB component based on its bilobed localization, but the small separation between the lobes seemed to us typical of a kinetochore protein (Osborne et al., 1994). When fixed and live cells were examined by 3D deconvolution microscopy, Ndc80p-GFP, Spc24p-GFP, Spc25p-GFP, and Nuf2p-GFP were seen during metaphase to localize to two lobes on either side of the spindle midzone to move toward the poles during anaphase (Figures 2-1A through 2-1F and data not shown). In cells that lack functional CBF3 (*ndc10-1* cells at 37°C) the bilobed pattern was abolished and replaced by dim, uniform nuclear fluorescence (Figures 2-1C and 2-1F). The fluctuating bilobed distribution of Ndc80p-GFP, Spc24p-GFP, Spc25p-GFP, and Nuf2p-GFP was indistinguishable from that of Slk19p-GFP and Mtw1p-GFP, two bona fide kinetochore proteins that we and others have analyzed in some detail (Goshima and Yanagida, 2000; He et al., 2000; Zeng et al., 1999).

When assayed by ChIP, Ndc80p-GFP, Spc24p-GFP, Spc25p-GFP, and Nuf2p-GFP exhibited strong *NDC10*-dependent association to *CENIV* DNA but only background association with a negative control *URA3* fragment (Figures 2-1P and 2-1Q). ChIP has previously been used to localize Cse4p, Mif2p, Slk19p, and other proteins to kinetochores (Meluh and Koshland, 1997; Meluh et al., 1998; Zeng et al., 1999), but we were concerned about possible nonspecific binding of spindle proteins to CEN DNA. As negative controls, we therefore performed ChIP with three nonkinetochore spindle proteins fused to GFP:

Tub1p, which encodes α -tubulin, Tub4p, which encodes the SPB-localized γ -tubulin, and Spc42p, a component of the SPB central plaque. None of these proteins associated to any significant extent with centromeric DNA, confirming the specificity of the ChIP reaction (Figure 2-1R).

These findings confirm very recent reports that Ndc80p, Spc24p, Spc25p, and Nuf2p are components of an evolutionarily conserved multiprotein complex that associates with kinetochores in several eukaryotic organisms (Janke et al., 2001; Wigge et al., 1998). Careful examination of images of Ndc80p-GFP, Spc24p-GFP, Spc25p-GFP, and Nuf2p-GFP at different stages of the cell cycle with and without Spc42p-CFP to control for fluorescence bleedthrough showed only the bilobed localization typical of kinetochores and no association with spindle poles, spindle microtubules, or other nuclear structures (Figures 2-1A and 2-1F; data not shown). We have found that Dam1p, a microtubule binding protein previously shown to be involved in spindle (Hofmann et al., 1998; Jones et al., 1999) and kinetochore function (Cheeseman et al., 2001) is a fifth protein that associates with *CEN*-DNA in a *NDC10*-dependent fashion and that exhibits a localization in metaphase essentially identical to that of Ndc80p (data not shown). Overall, we conclude that Ndc80p, Nuf2p, Spc24p, Spc25p, and Dam1p associate with centromeres during mitosis in a CBF3-dependent manner and that kinetochores may be the only cellular structures with a significant level of these proteins as judged by GFP-tagging.

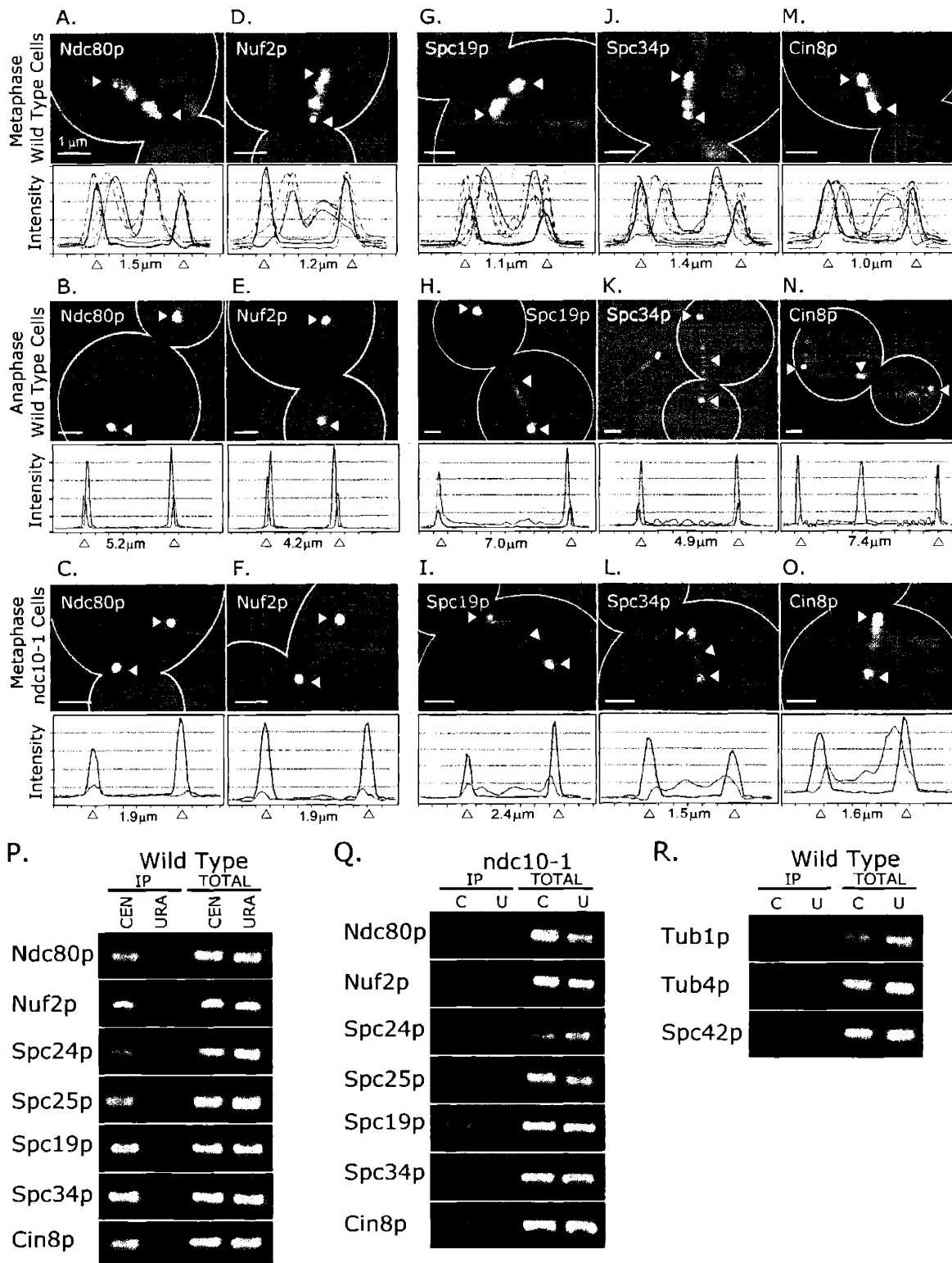


Figure 2-1. Analysis of Proteins Localized to Kinetochores, or to Kinetochores and Spindle Microtubules

Yellow arrows mark SPBs and white arrows spindle microtubules. (A, D, G, J, and M) Typical images from metaphase wild type cells carrying Spc42p-CFP (in red) and Ndc80p-GFP, Nuf2p-GFP, Spc19p-GFP, Spc34p-GFP, or Cin8p-GFP (in green). Images represent projections of 3D image stacks containing ten to twenty 0.2 μm sections. The graph shows the distributions of CFP and GFP signal intensities along the spindle axis (in arbitrary units) in several cells. The bold line is derived from the image shown after correction for bleed-through from the CFP to the GFP channel (see Experimental Procedures). (B, E, H, K, and N) Typical images from anaphase wild-type cells or (C, F, I, L, and O) metaphase *ndc10-1* cells. (P and Q) Crosslinking of proteins tagged with GFP to *CENIV* DNA in wild-type or *ndc10-1* cells at 37°C as assayed by chromatin immunoprecipitation (ChIP). DNA in immune complexes (IP) was amplified with primers specific for *CENIV* (CEN lanes) or, as a negative control, *URA3* (URA lanes) and compared to the amount of DNA in whole-cell lysates (TOTAL). (R) ChIP assays with control proteins not found at kinetochores. TUB1 encodes α -tubulin, TUB4, γ -tubulin, and SPC42, an integral component of the SPB.

2.3.2 Proteins Bound to Kinetochores and to the Mitotic Spindle

Next, we examined three proteins that appeared, from careful examination of published images, to be at least partially localized to two nuclear lobes: Spc19p and Spc34p, proteins that copurify biochemically with SPBs (Wigge et al., 1998) and Cin8p, one of the six kinesin-like proteins in budding yeast (Hoyt et al., 1992; Roof et al., 1992). GFP fusions of all three proteins showed some *NDC10*-dependent kinetochore localization (Figure 2-1) and specific binding to centromeric DNA by ChIP (Figures 2-1P and 2-1Q). However, in contrast to Ndc80p, Nuf2p, Spc24p, Spc25p, and Dam1p discussed above, Spc19p, Spc34p, and Cin8p also localized to other microtubule-based structures in the cell.

In wild-type cells, Spc19p, Spc34p, and Cin8p were broadly similar in being localized to two kinetochore-like lobes as well as along the microtubules of the mitotic spindle (Figures 2-1G through 2-1O). In anaphase, all three proteins retained their spindle localization while also concentrating at spindle poles, where centromeres are clustered. As described previously, Cin8p also has the interesting property of localizing to the spindle midbody late in anaphase (Figure 2-1N; Hoyt et al., 1992). In *ndc10-1* cells, the bilobed components of Spc19p and Spc34p localization were abolished, whereas localization to spindle microtubules remained. Cin8p-GFP largely shifted to one pole or the other. The *NDC10*-dependence of localization is seen most clearly in intensity-distance plots that integrate the GFP and CFP signals along the spindle axis (see Figures 2-1J and 2-1L in particular). In interpreting the plots and images, it should be noted that spindles in *ndc10-1* cells are about 25% longer than in wild-type cells, reflecting the loss of kinetochore-dependent pulling forces that shorten the spindle. In conclusion, although the localization patterns of Spc19p, Spc34p, and Cin8p are more complex than those of the five proteins

discussed in the previous section, imaging and ChIP are consistent with the idea that a fraction of Spc19p, Spc34p, and Cin8p is associated with kinetochores in metaphase yeast cells. Kinetochores association appears to be CBF3-dependent, whereas binding to spindle microtubules is CBF3-independent.

2.3.3 Proteins Bound to Kinetochores and a Variety of Microtubule-Based Structures

Next, we examined two microtubule binding proteins that are found in both the cytoplasm and the nucleus: Bik1p and Stu2p. Bik1p is homologous to the plus-end microtubule binding protein mammalian CLIP170 (Berlin et al., 1990) and Stu2p is a microtubule binding protein similar in sequence to *Xenopus* XMAP215 (Wang and Huffaker, 1997) and human TOGp (Spittle et al., 2000). Bik1p-GFP exhibited a complex localization to kinetochore-like lobes, to spindle microtubules, and to distinct spots in the cytoplasm that correspond to cortical attachment sites (Berlin et al., 1990), and only part of the localization appeared to be disrupted in *ndc10-1* cells at 37°C (Figures 2-2A and 2-2C). Cortical capture sites are structures in the plasma membrane that bind the plus ends of microtubules that emanate from SPBs and function to orient the nucleus in the mother-bud neck late in metaphase (for review see Bloom, 2000). The localization of Bik1p to both kinetochores and cortical attachment sites is consistent with data that CLIP-170 binds selectively to the plus ends of microtubules. Stu2p-GFP was found in a pattern broadly similar to that of Bik1p and again, only a subset of the nuclear Stu2p-GFP appeared sensitive to *ndc10-1* inactivation (Figures 2-2D through 2-2F). To determine whether the bright spots of Stu2p-GFP along the periphery of the cell might be cortical capture sites, we generated cells carrying α -tubulin-GFP (Tub1p-GFP) and Stu2p-CFP. In both metaphase and anaphase cells, cytoplasmic foci of Stu2p-CFP clearly lay at the extreme ends of cytoplasmic microtubule bundles, strongly

suggesting that the foci were indeed cortical capture sites. Consistent with this localization, Stu2p and the well-characterized cortical site protein Kar9p have recently been shown to interact by two-hybrid analysis (Miller et al., 2000). By ChIP, both Bik1p and Stu2p exhibited *NDC10*-dependent binding to centromeric DNA (Figure 2-2J). From these data, we conclude that Bik1p and Stu2p are proteins that associate with a variety of microtubule-based structures including kinetochores and cortical capture sites, both of which bind to microtubule plus ends.

The final protein we examined was Ipl1p, an Aurora kinase that has been proposed to function in yeast kinetochore assembly (Biggins et al., 1999; Sassoon et al., 1999). It has previously been observed that Nuf2p is mislocalized in *ipl1-2* cells, a finding interpreted to reflect a role for Ipl1p in SPB formation (Kim et al., 1999). However, since Nuf2p is actually localized to kinetochores and not SPBs as previously assumed, we wondered whether Ipl1p might be a regulator of kinetochores. With Ipl1p-GFP, we observed a pattern consistent with kinetochore localization as well as with spindle binding, and a subset of the localization was *NDC10*-dependent but CEN-association was not detected by ChIP. The ChIP assay is a stringent criterion for kinetochore association and some kinetochore proteins may simply be too distant from DNA to be successfully crosslinked by formaldehyde. Our inclusion of Ipl1p in this analysis is justified by its clear role in chromosome movement (see below).

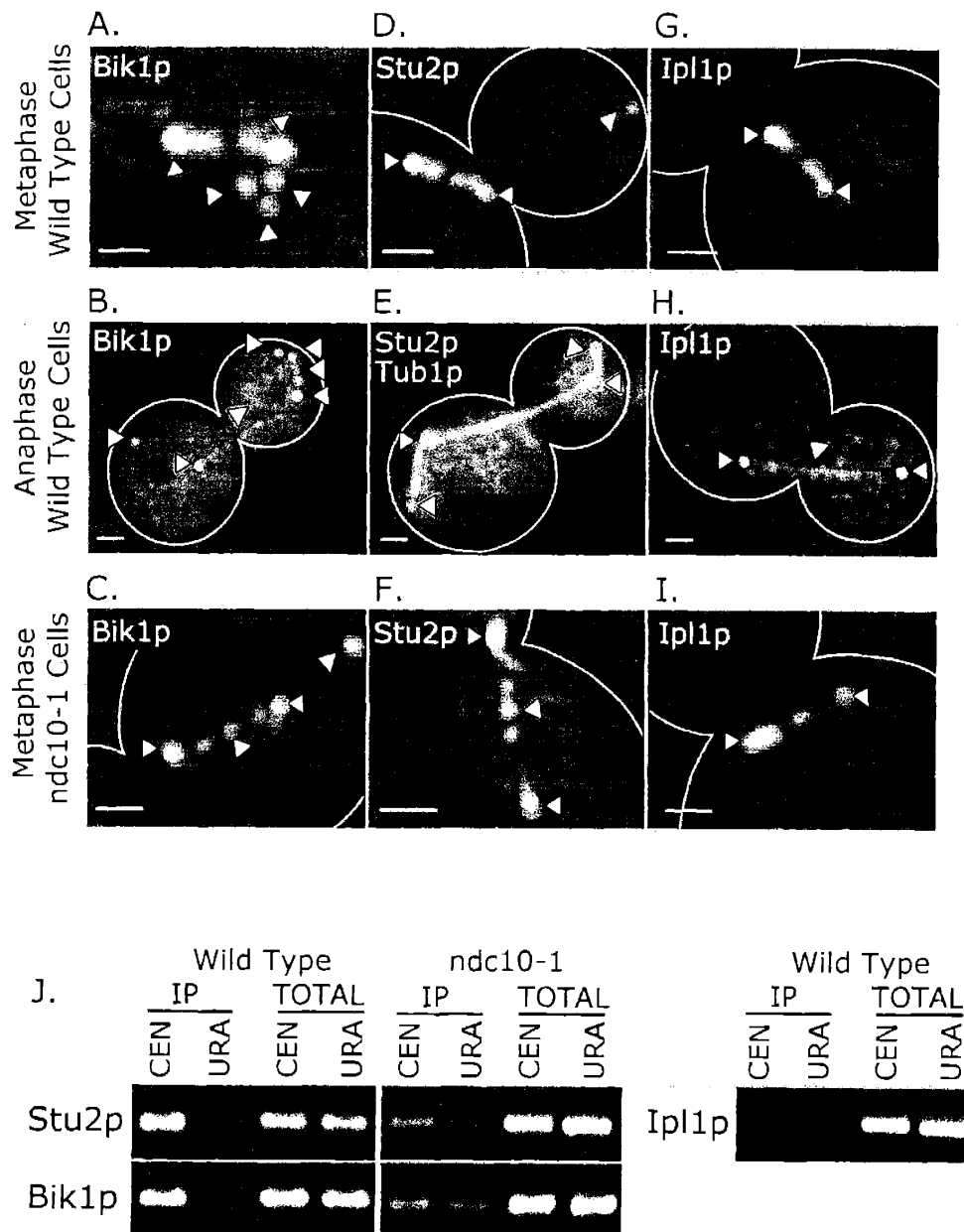


Figure 2-2. Analysis of Proteins Localized to Kinetochores and to Other Microtubule-Based Structures

(A–I) Imaging of Bik1p, Stu2p, and Ipl1p as described in Figure 2-1. Yellow arrows mark SPBs, white arrows mark spindle microtubules, and pink arrows mark cortical capture sites. Note that in (E), the fluorophores have been changed so that Stu2p is fused to CFP (in red) and α -tubulin to Tub1p to GFP (in green). (J) Crosslinking of Bik1p, Stu2p, and Ipl1p to *CENIV* DNA as assayed by ChIP as described in Figure 2-1.

2.3.4 Mapping Chromosome Association to Centromeric DNA

We have previously proposed that centromeric chromatin in budding yeast spans nearly 20 kb of DNA centered on the centromere. This centromeric chromatin appears to be involved in the large-scale stretching that occurs during transient sister separation. It seemed possible that proteins we had localized to centromeres might be associated not with kinetochores themselves, but rather with an extended chromatin domain. This seemed particularly likely for Ndc80p, whose human homolog, Hec1, has been shown to complement an *NDC80* disruption in single copy and to interact biochemically and genetically with the Smc1p and Smc2p subunits of yeast cohesin and condensin (Zheng et al., 1999). In mitotic *S. cerevisiae* cells, cohesin is found both at centromeres and at discrete sites along chromosome arms, whereas condensin is ubiquitously distributed along chromatin (Freeman et al., 2000; Megee et al., 1999; Tanaka et al., 1999). To map the sequences to which Ndc80p binds, we used ChIP to quantitate its association to five successive 200 bp fragments of chromosomal DNA that span *CENIII*. We also examined Ndc80p binding to an 18 kb region on the arm of chromosome V that has previously been shown to contain a cohesin binding site (Tanaka et al., 1999). We observed that Ndc80p was present at high levels on the 200 bp fragment centered on *CENIII*, at much lower levels on sequences to the left and right of the centromere, and at only background levels at sites along chromosome V arms (Figures 2-3A and 2-3B). The concentration of Ndc80p at centromeres was, if anything, tighter than that of Mif2p (Meluh and Koshland, 1997), the centromere-bound homolog of mammalian CENP-C, and clearly distinct from the broad distribution of Scc1p, a cohesin subunit (Megee et al., 1999; Tanaka et al., 1999). We therefore conclude that Ndc80p is tightly concentrated at centromeres and does not have the broader distribution along chromosomes characteristic of

cohesin and condensin. Similar CEN-specific crosslinking was observed for Spc19p, Spc34p, Cin8p, Bik1p, and Stu2p (Figure 2-3C), confirming our conclusion that all of these proteins are specifically associated with kinetochores.

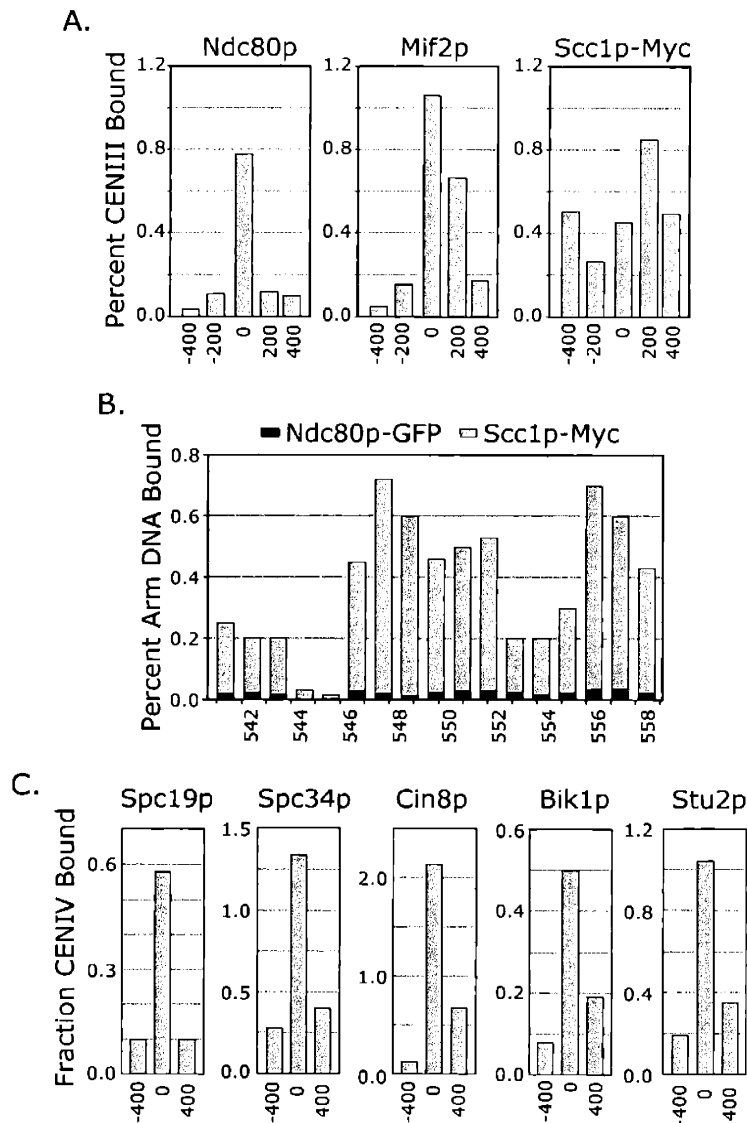


Figure 2-3. Quantitative Crosslinking Analysis by ChIP

(A) Quantitative ChIP analysis of the binding of Ndc80p, Mif2p, and Scc1p to *CENIII* and flanking DNA. The horizontal axis denotes the position of 200 bp fragments, relative to the center of *CENIII*, and the vertical axis the fraction of total DNA present in immune complexes as determined by PCR from serial dilution. Ndc80p was immunoprecipitated with anti-GFP polyclonal antiserum, Mif2p with rabbit polyclonal antiserum, and Scc1-Myc₁₂ with anti-Myc polyclonal antibodies.

(B) Quantitative ChIP analysis of Ndc80p and Scc1p crosslinking to sites along the arm of chromosome V (Tanaka et al., 1999). Numbers on the horizontal axis refer to the position, in kilobases, from the left telomere as indicated at the Stanford Genome Database.

(C) Quantitative ChIP analysis of Spc19p, Spc34p, Cin8p, Bik1p, and Stu2p binding to *CENIII* and flanking DNA as described in (A).

2.3.5 Mutations in Kinetochores Reduce Transient Sisters Separation

To establish a function for proteins localized to kinetochores, we examined the extent of transient sister chromatid separation. We reasoned that mutations in proteins required for chromosome-microtubule attachment should interfere with the imposition of tension on sister centromeres and thereby decrease the frequency or extent to which sisters separate in metaphase. Nine of the eleven proteins we had localized to kinetochores are essential for vegetative growth but temperature sensitive mutants were available for only four (Table 1-1). Among the five genes without conditional mutations, it seemed most important to examine *Stu2p*, because it has a higher cell homolog (XMAP215) whose function is at least partially understood (Tournebise et al., 2000). We therefore generated 19 temperature sensitive alleles in the *STU2* gene using PCR mutagenesis and plasmid shuffling (see Experimental Procedures), and selected for further analysis alleles that arrested within one cell cycle of temperature upshift.

Centromeric DNA was visualized by integrating a TetO array 2 kb from CEN IV (construct -2ChIV of He et al., 2000) in cells expressing TetR-GFP and a Spc42p-GFP. This generates cells in which both *CENIV*-proximal chromatin and spindle poles are marked with small green dots, permitting rapid single-color imaging. To quantitate sister separation in wild-type and mutant strains, they were synchronized at START using α -factor and then released into prewarmed medium at 37°C for 75–90 min prior to fixation and imaging. When the extent of synchrony was assessed morphologically, more than 90% of cells were observed to have entered prometaphase and assembled bipolar spindles, and fewer than 5% were in anaphase. As positive and negative controls, we showed that the fraction of wild-type cells with separated sisters was 50%–60%, whereas in *ndc10-1* cells it was less than 1%

(Figure 2-4A; He et al., 2000). In *ndc80-1*, *dam1-1*, *nuf2-61*, and *stu2-277* cells, the extent of transient sister separation was 10- to 20-fold lower than in wild-type cells, while in *ipl1-321* cells it was 4- to 5-fold lower (in about 15% of *ipl1-321* cells, centromeres appeared hyperstretched, with the TetO/TetR-GFP tag extended the full length of the spindle). Both *bik1Δ* and *cin8Δ* cells (which were assayed at 25°C, a temperature at which wild-type cells had fewer transient separations) exhibited a normal frequency of transient separation (Figure 2-4B). In conclusion, these data show that Ndc80p, Nuf2p, Dam1p, Stu2p, and Ipl1p are required for transient sister chromatid separation, and thus, probably, for the imposition of normal tension on sister chromatids.

The proteins in this study fall into two classes: those that are found primarily at kinetochores (as judged by imaging GFP fusion proteins) and those that localize to both kinetochores and other microtubule-based structures in mitotic cells. To determine whether this distinction is also reflected in the functions of the proteins, we asked whether mutations that reduce tension across sister kinetochores also impair the migration of the nucleus into the mother-bud junction, an essential step in mitosis mediated by the interaction of cytoplasmic microtubules with cortical attachment sites. We observed that whereas nuclear migration was substantially perturbed in *stu2-276* cells, it appeared normal in *ndc10-1*, *ndc80-1*, *dam1-1*, *ipl1-321I*, and *nuf2-61* mutants (Figure 2-4C; normal nuclear migration is observed in *bik1Δ* cells, a consequence of functional redundancy in proteins required for cortical attachment; Bloom, 2000). We conclude that kinetochore function is not required for nuclear migration and that the requirement for Stu2p probably reflects its localization to cortical capture sites. Additional nonkinetochore functions for proteins analyzed in this paper are summarized in Table 1-1.

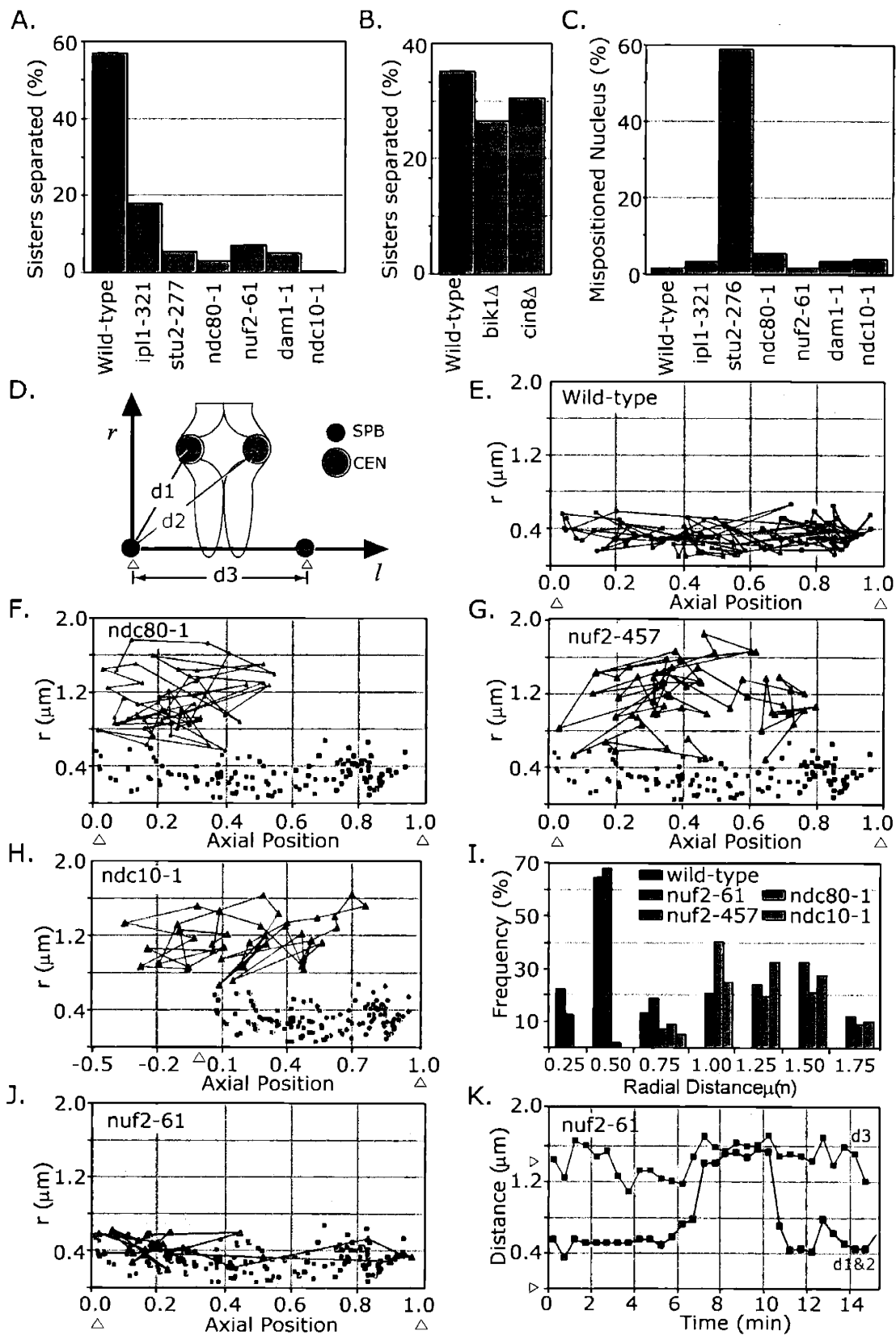


Figure 2-4. Effects of Mutations in Kinetochore Proteins on Transient Sister Separation, Nuclear Positioning Migration, and Chromosome Movement

(A) Mutations in essential kinetochore proteins reduce transient sister separation. Cells carrying Spc42p-GFP, the centromere-proximal -2ChIV chromosome tag (He et al., 2000), and the indicated temperature sensitive mutations were synchronized at START with α -factor at 25°C, and then released into prewarmed medium at the restrictive temperature of 37°C for 75 min prior to fixation and analysis. The fraction of metaphase cells ($n \approx 100$), as judged by nuclear morphology, with separated sister chromosome tags was then scored.

(B) Analysis of transient sister separation in wild-type, *bik1 Δ ::HIS3*, and *cin8 Δ ::HIS3* cells performed at 25°C, as described in (A).

(C) Analysis of nuclear positioning prior to anaphase. Preanaphase cells in which the nucleus had not migrated to the bud-proximal hemisphere of the mother cell were scored as mispositioned (Korinek et al., 2000). Note that the *STU2* allele used in this analysis was different from that in (A). We have observed partial separation of *STU2* function in these alleles, with *stu2-277*; *279* having the greatest defect in transient sister separation and *stu2-276* having the greatest defect in nuclear positioning (by comparison 10% of *stu2-276* cells were transiently separated in a synchrony-release experiment).

(D) Schematic of the -2ChIV GFP chromosome tag and Spc42p-GFP spindle pole tag, showing the spindle-centered polar reference system (with r and l coordinates) and three key parameters: d_1 , the distance from the reference spindle pole to the center of one chromatid tag; d_2 , the distance to the sister chromatids tag; and d_3 , the SPB-SPB distance.

(E) Scatter plot of the positions of the -2ChIV chromosome tag over 15 min in a time-lapse movie of a wild-type cell. The vertical axis is the absolute radial position (r) and the horizontal axis the relative axial position (l/d_3). Dots represent the position of the tag at each time point; black and purple denote the independent paths of the two sisters during periods of transient sister separation.

(F, G, and H) Scatter plots of chromosome movement in *ndc80-1*, *nuf2-457*, and *ndc10-1* cells compared to the wild-type movement in (E) (black and purple dots). Negative values of l arise when the CEN tag drifts so far from the SPBs that it is “behind” them. The phenotype of *ndc10-1* and *ndc80-1* cells are very homogeneous, but 15%–20% of *nuf2-457* cells exhibited behavior similar to that shown in (J) and (K). Synchrony-release experiments established that these cells are ones in which bipolar microtubule attachments had formed prior to temperature upshift.

(I) Distribution of radial distances (r) between the chromosome tag and the spindle axis in wild-type, *nuf2-61*, *-457*, *ndc10-1*, and *ndc80-1* cells. The data from sections (E–H) and (J) were used to calculate values for r , which were then grouped in bins of 0.25 μm to generate a frequency distribution. Scatter (J) and distance (K) plots for *nuf2-61* cells at 37°C. Because no transient separation occurs, $d_1 = d_2$ (red line). Spindle length (d_3) is shown in black.

2.3.6 Live Cell Analysis Reveals Three Types of Defect in Chromosome Movement

In principle, different kinetochore defects, ranging from complete failures of assembly to more subtle problems with force generation could reduce transient sister separation. To investigate the defects in *ndc80*, *nuf2*, *stu2*, *dam11*, and *ipl1* mutants, cells carrying GFP-tagged chromatids and SPBs were filmed at 37°C and the motion of centromeres determined relative to the spindle axis by manual and automated analysis of deconvolved 3D image stacks (Figures 2-4D and 2-4E; He et al., 2000). In wild-type cells, metaphase chromosome movement is characterized by several superimposed motions along the spindle axis: rapid oscillations 10%–20% of spindle length of 0.2–0.5 μm , long duration oscillations 30%–60% of spindle length of up to 1.0 μm , and transient sister separations in which the two chromatids move independently for periods of 2–10 min (He et al., 2000). In neither *ndc10-1*, *ndc80-1* (Figure 2-4F and 2-4H, green and orange lines, respectively), or *nuf2-457* cells (Figure 2-4G, blue lines; see figure legend for additional details) were any of these behaviors observed during metaphase and chromosomes remained exclusively in the mother cell at anaphase. Furthermore, whereas chromosomes stayed within 0.40 μm of the spindle axis in wild-type cells, in *ndc10-1*, *ndc80-1*, and *nuf2-457* cells, they appeared to detach completely from the spindle and were typically 1.0–1.5 μm from the spindle axis, the maximum distance possible in 2.5 to 3.0 μm nucleus (Figure 2-4I). We conclude that loss-of-function mutants in *NDC80* and *NUF2*, like mutations in *CBF3* genes, cause chromosomes to detach from spindle microtubules and move randomly within the mother cell.

In *ndc80-1*, *nuf2-457*, and *ndc10-1* cells, spindles undergo anaphase B elongation on approximately the same schedule as wild-type cells (data not shown), consistent with the conclusion by Janke et al. (2001) that the Ndc80p-Nuf2p complex is required for the mitotic

checkpoint. We were therefore surprised to observe that at 37°C, *nuf2-61* cells arrested homogeneously at the metaphase-anaphase transition in a Mad1-dependent fashion (data not shown), implying that the *nuf2-61* lesion engages the mitotic checkpoint (see also Janke et al., 2001). When *nuf2-61* cells were examined by live-cell microscopy, chromosomes were observed to associate with one pole for 5 to 10 min and then suddenly jump to the other pole, binding to it for 5 to 10 min before jumping again (Figures 2-4J and 2-4K, red lines). In some cells, we observed up to four shifts between the poles in a 30 min period. During these jumps, chromosomes remained as close to the spindle axis as in wild-type cells, supporting the notion that they were bound to microtubules, albeit aberrantly (Figure 2-4I). Our interpretation of these findings is that whereas microtubule attachment sites are unable to assemble in *nuf2-457* cells, the attachments that form in *nuf2-61* mutants are metastable. In the complete absence of kinetochore-microtubule attachment, no checkpoint signal is generated whereas metastable kinetochore-microtubule attachments do signal the checkpoint and arrest cells at metaphase (see Discussion).

Next, we analyzed chromosome segregation in *stu2*, *dam1*, and *ipl1* cells. Because we were interested in gene-specific differences in phenotype rather than allele-dependent variation, multiple temperature sensitive mutants were examined for each gene. To identify loss-of-function mutants, alleles were ranked in severity based on the extent of transient sister separation, as judged using fixed-cell assays (as described in Figure 2-4A). With many alleles, we observed a significant level of transient sister separation (approximately 20%–40% of chromatids were split), presumably representing a hypomorphic phenotype, but for each gene we were able to select two strong mutants.

In *dam1-1* and *dam 1-11* cells, we observed close association of tagged chromosomes with a single spindle pole (Figures 2-5A through 2-5D). During this monopolar association, the chromosomes were found within 0.2 spindle diameters of the pole, but continued to oscillate rapidly (with an apparent velocity up to 1 $\mu\text{m}/\text{min}$). An even more dramatic monopolar association was observed in *ipl1-321* and *ipl1-2* cells, in which chromosomes remaining within approximately 0.1 spindle diameters of the pole (Figures 2-5E through 2-5H). This monopolar association was clearly distinct from the spindle detachment observed in *ndc10-1*, *ndc80-1*, or *nuf2-457* cells, and in none of the several dozen movies of *dam1* and *ipl1* cells were chromosomes further from the spindle axis than in wild-type cells (0.4–0.5 μm). Yet a third phenotype was observed in *stu2-277* and *stu2-279* cells (Figures 2-5I through 2-5L). Chromosomes in *stu2* mutants moved to the middle of the spindle (congression), where they oscillated back and forth along the spindle axis (see especially Figure 2-5I), apparently having achieved bipolar attachment and remaining at a wild-type radius from the spindle axis, but they covered a total distance 2- to 3-fold less than in wild-type cells and exhibited peak velocities at least 3- to 4-fold lower (0.3–0.4 $\mu\text{m}/\text{min}$). This pattern of movement is consistent with diminished force generation at bivalently attached chromatid pairs.

In summary, live-cell analysis of chromosome dynamics in strains carrying mutant kinetochore proteins reveals at least three classes of defects: a complete failure of chromosome-microtubule attachment (in *ndc80*, *nuf2*, and *ndc10* cells), attachment to a single pole with a failure to undergo congression (in *dam1* and *ipl1* cells), and bivalent microtubule attachment with reduced rates of movement and reduced tension across sister centromeres (in *stu2* cells). The existence of distinct mutant phenotypes suggests that

Ndc80p, Stu2p, Dam1p, Ipl1p, and Nuf2p have different functions in kinetochore-microtubule attachment.

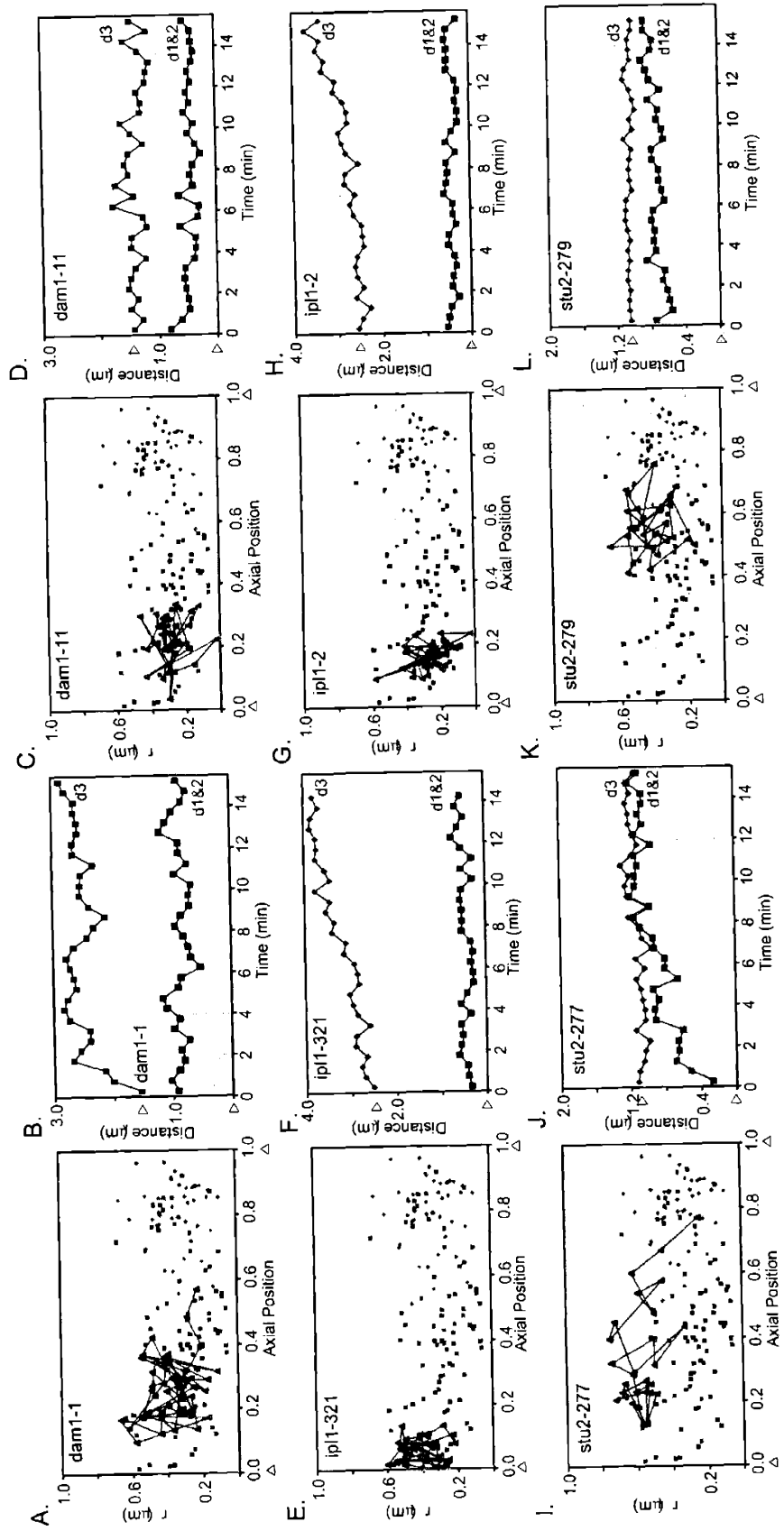


Figure 2-5. Distinct Defects in Chromosome Movement Are Observed in Cells Carrying Mutations in Different Kinetochores Proteins

(A, C, E, G, I, and K) Scatter plots showing the radial (r) and relative axial positions ($l/d3$) of a -2ChIV chromosome tag over a 15 min period of metaphase in various strains at 37°C (see Figure 2-4D for an explanation of the coordinates). The blue and purple dots show wild-type positions.

(B, D, F, H, J, and L) Distance plots transforming the data to show distance between the sister chromatids and a reference SPB (red line; because no transient separation occurs, $d1 = d2$) and the SPB-SPB distance ($d3$; black line). Multiple movies (3–6) were examined for each strain and the behaviors shown here are typical. The penetrance of the *ipl1-321* allele was only about 80% however, and some cells exhibited a sustained hyperstretching of the chromosome tag. The sampling rates used to collect this data are too low to permit the accurate measurement of rapid movements, but we have estimated the rates of long wavelength motions by smoothing the curves and then calculating a first derivative. On this basis, we find that centromeres in *stu2-277; 279* cells move at least 3- to 4-fold slower than in wild type cells.

2.3.7 A Multilayer Structure at the Yeast Kinetochores

Among the chromosome segregation defects described in this paper, those caused by *ndc10-1*, *ndc80-1*, and *nuf2-457* are much more severe than any others. The severe phenotype of *ndc10-1*, is thought to arise because no kinetochore components, not even error-detecting checkpoint proteins, can associate with centromeric DNA in the absence of CBF3 (Gardner et al., 2001; Goh and Kilmartin, 1993). To explore the role of Ndc80p in kinetochore assembly, we used ChIP to determine interdependencies among various kinetochore subunits. As described above, the association of Ndc80p with kinetochores was dependent on functional CBF3 (Figure 2-6A), but the reciprocal was not true: both the Ndc10p (Figure 2-6B) and Cep3p (data not shown) CBF3 proteins were centromere bound in *ndc80-1* cells at 37°C. However Nuf2p (Figure 2-6C) and Stu2p (Figure 2-6D) required both *NDC10* and *NDC80* function for kinetochore association. The association of the cohesin subunit Scc1p with centromeres requires *NDC10* (Tanaka et al., 1999), but Ndc80p and Scc1p bind independently to DNA (Figures 2-6E and 2-6F). Thus, the assembly of *S. cerevisiae* kinetochores appears to involve a hierarchy of dependencies: CBF3 at the first level, Ndc80p at the second, and Stu2p at the third. We conclude that the severity of the *ndc80* phenotype probably reflects a requirement for Ndc80p in the association of several other proteins with centromeres.

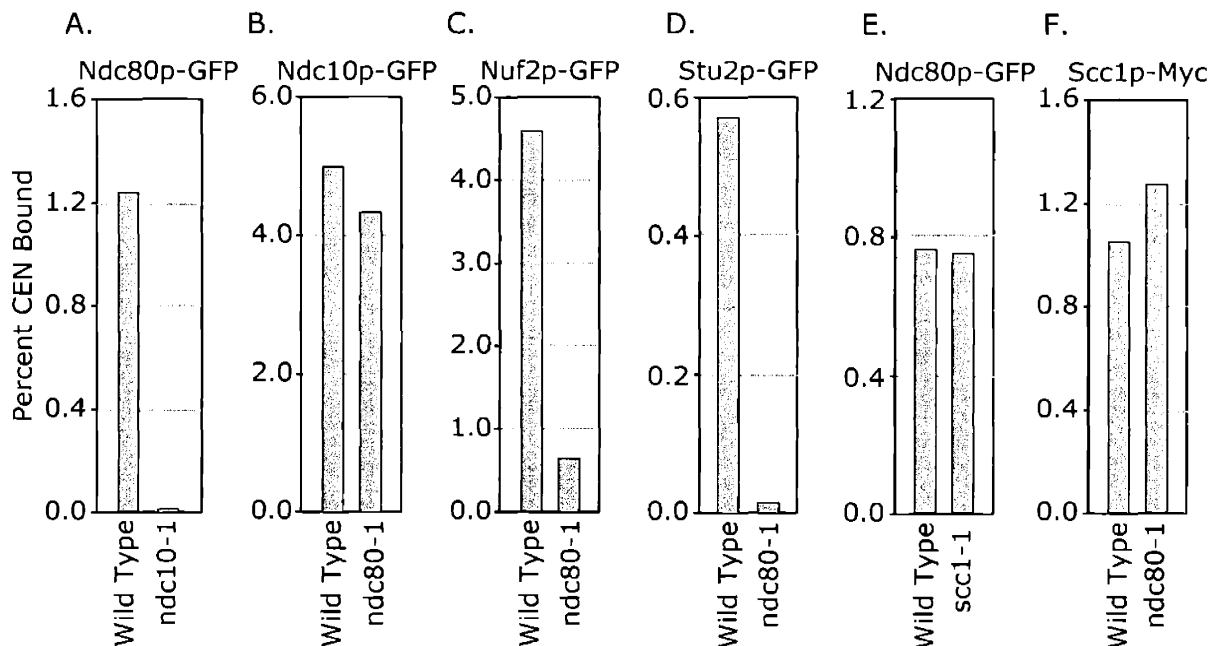


Figure 2-6. Hierarchy of Dependencies in the Association of Kinetochores with Centromeric DNA

Quantitative ChIP was used to determine the effects of various mutations on the extent to which GFP-tagged protein crosslinked to *CENIII* DNA. Cells were grown at 25°C to mid-log phase and shifted to 37°C for 2.5 hr prior to analysis. The amount of the *CENIII* DNA in immune complexes (IP) is shown as the percentage of the DNA in the lysate (see Figure 2-3). Absolute differences in the amount of DNA precipitated between panels are not considered to be meaningful.

2.4 Discussion

We have used three criteria to identify kinetochore proteins: (1) CBF3-dependent localization to the yeast “metaphase plate,” a bilobed distribution that fluctuates over time as kinetochores move back and forth along the spindle axis, (2) CBF3-dependent association with centromeric DNA, as judged by chromatin immunoprecipitation, and (3) functional involvement in kinetochore-microtubule attachment, as judged by disruption of the normal pattern of transient sister separation and chromosome movement. By these criteria, we find that ten previously described spindle proteins of uncertain function are associated with *S. cerevisiae* kinetochores and an eleventh appears to be a kinetochore regulator. Among these kinetochore proteins are several that bind to microtubules, or have animal cell homologs that are microtubule binding. Mutations in these proteins disrupt chromosome movement and appear to reduce or eliminate the tension that is normally imposed on sister centromeres. We hypothesize that the proteins are involved directly in the formation of microtubule attachment sites.

The mitotic spindle is a large multicomponent machine with long-range physical interactions among kinetochores, microtubules, and spindle poles. It is therefore important to inquire into the physical basis by which proteins might become associated with *CEN* DNA. We can imagine three possibilities. First, centromere association might be highly indirect, involving distant interactions mediated by microtubules. This seems unlikely because neither α -tubulin, γ -tubulin, nor the spindle pole component Spc42p detectably coprecipitated with *CEN* DNA by ChIP, and the available evidence suggests that ChIP is a reliable and highly selective cross-linking method (Meluh and Broach, 1999). Moreover, in cases in which *CEN* binding by ChIP is backed up by colocalization and functional data, our confidence in

kinetochore association seems justified. Second, centromere association might involve binding directly to DNA, as in the case of CBF3, or binding to CBF3 in a multilayer kinetochore structure (Ortiz et al., 1999). In this case, a protein should be found associated with kinetochores independent of whether the kinetochores are linked to microtubules. Third, a protein that binds to microtubules might show centromere association through the attachment of microtubule plus ends to kinetochores. The human APC tumor suppresser protein, for example, localizes to kinetochores as a consequence of its binding to microtubule ends (Kaplan et al., 2001). Both of these latter possibilities are consistent with a protein's functioning in aspects of chromosome-microtubule attachment, but we have not yet distinguished between them experimentally.

2.4.1 Kinetochore-Associated Microtubule Binding Proteins

Among the eleven proteins discussed in this paper, four—Stu2p, Bik1p, Dam1p, and Cin8p—have been shown previously to bind microtubules and mutations in two of these—Stu2p and Dam1p—abolish the tension normally imposed on sister kinetochores. In principle, mutations that affect transient sister separation could act by diminishing the microtubule-mediated forces that pull centromeres apart or by increasing the cohesive forces that hold sister kinetochores together. Although our data do not conclusively distinguish between these possibilities, the abnormal chromosome movements we have observed seem most consistent with a failure to establish and maintain microtubule attachment, and not with an increase in sister cohesion. We speculate that the failure of deletions in the nonessential *CIN8* and *BIK1* genes to impair kinetochore-microtubule attachment is a consequence of functional redundancy. Previously reported redundancy in *CIN8* and *KIP1* during spindle

assembly (Hoyt et al., 1992) and *BIK1* and *KAR9* during nuclear positioning (Miller and Rose, 1998) support this conclusion.

The higher cell homologs of Stu2p, XMAP215 in *Xenopus* and TOGp in humans, have been shown to bind to and modulate the dynamic behavior of microtubules (Gard and Kirschner, 1987; Tournebize et al., 2000; Vasquez et al., 1994). Kinetochore-associated Stu2p might therefore be expected to contribute to chromosome movement by altering the stability of microtubule plus ends. A similar function has been proposed for Dis1, an *S. pombe* homolog of Stu2p that is required for correct chromosome movement and transient sister separation in fission yeast (Nabeshima et al., 1998). The human homolog of Bik1p, CLIP-170, localizes to microtubule plus ends, including those at kinetochores (Dujardin et al., 1998), and has also been postulated to regulate microtubule dynamics (Diamantopoulos et al., 1999). The *S. pombe* CLIP-170 homolog, Tip1p, functions to prevent catastrophic depolymerization of microtubule plus ends, thereby promoting their capture at the cell cortex (Brunner and Nurse, 2000). We might therefore expect that Bik1p participates in plus-end microtubule capture at *S. cerevisiae* kinetochores. Yeast Dam1p has been shown to bind to microtubules, but its biochemical analysis has just begun (Hofmann et al., 1998), and, Dam1p has no obvious homologs in higher cells.

The observation that Cin8p localizes to yeast kinetochores is surprising. Cin8p is one of four kinesin-like proteins in yeast with a nuclear function, but it is most similar to the BimC class of motors thought to slide microtubules relative to each other (for review, see Hildebrandt and Hoyt, 2000). This is not an activity expected of a kinetochore protein although a plus-end-directed motor could generate a force that separates spindle poles, a well characterized activity of Cin8p (Gheber et al., 1999; Hoyt et al., 1992). Assuming that the

association of Cin8p with kinetochores is not adventitious, then its function must be redundant with that of other proteins. We have looked for kinetochore association by the Kip1-3 motors using GFP-tagging and ChIP and have preliminary data that Kip3p, at least, may also localize to kinetochores. We must now undertake a careful analysis of chromosome dynamics and transient separation in cells lacking combinations of two, three, and four motor proteins.

2.4.2 General Implications for Kinetochore-Microtubule Attachment

Four implications of general significance for kinetochore biology can be drawn from the data in this paper. First, multiple proteins appear to be involved in the attachment of kinetochores to microtubules, including both motor proteins and MAPs, and these proteins play at least partially overlapping roles. Mutations in *NDC10*, *NUF2*, and *NDC80* cause a complete disruption of chromosome-microtubule attachment, apparently because they disrupt kinetochore assembly. In contrast, mutations in *STU2*, *IPL1*, and *DAM1* interfere with chromosome movement but kinetochores retain some microtubule attachment. It therefore seems likely that multiple microtubule binding proteins contribute simultaneously to the formation of a fully functional attachment site.

Second, the formation of kinetochores with at least some microtubule binding activity, however aberrant, is required for mitotic checkpoint function. The genetic interaction between structural components of the kinetochore and the mitotic checkpoint is complex. Some mutations in kinetochore proteins, such as *ndc10* (Goh and Kilmartin, 1993; Tavormina and Burke, 1998) and *spc24* and *ndc80* (Janke et al., 2001; Wigge et al., 1998), are as effective as *mad2Δ* in disrupting checkpoint function. Other mutations however, appear to cause a checkpoint-dependent arrest, including *ctf13* (Doheny et al., 1993) and

cep3 (Strunnikov et al., 1995). This difference cannot be explained simply by postulating different biochemical functions for checkpoint-disrupting and checkpoint-engaging mutations: Ndc10p, Ctf13p, and Cep3p are all required for the DNA binding activity of CBF3. However, our data on *nuf2-61* and *nuf2-457* provide strong support for the hypothesis that it is the extent of kinetochore disruption that determines whether the checkpoint will function. When chromosome attachment is completely disrupted, as seen in *nuf2-457* cells, the checkpoint is abolished. However, when metastable attachments are generated, as in *nuf2-61* cells, the checkpoint is engaged. Similarly, the partially defective attachments generated in *dam1* and *stu2* cells arrest cells in a checkpoint-dependent fashion. These data fit well with the idea that kinetochores are the source of a checkpoint signal that acts to monitor the formation of fully functional microtubule attachment sites (Gardner et al., 2001).

Third, mutations in different proteins give rise to different defects in chromosome movement, including a complete loss of attachment (in *ndc10*, *ndc80*, and *nuf2*), slow movement of chromatids that have apparently achieved bivalent attachment (in *stu2*), and close association with a single pole, presumably reflecting monopolar microtubule attachment (*dam1* and *ipl1*). This latter phenotype could arise either from a failure to duplicate kinetochores following DNA replication, or from a failure to develop microtubule attachments strong enough to oppose the splitting forces exerted on sisters during metaphase. A likely interpretation of these three phenotypic classes is that different proteins mediate different aspects of microtubule attachment and chromosome movement.

Fourth, many proteins involved in kinetochore-microtubule attachment also localize to other microtubule-based structures and appear to have more than one function in the cell. For example, Stu2p and Bik1p appear to function at both kinetochores and at cortical capture

sites (and probably also at SPBs; Wang and Huffaker, 1997). Membrane-associated cortical capture sites bind cytoplasmic microtubules that emanate from the SPB and function to orient the nucleus into the mother-bud neck, a precondition for transporting chromosomes into the daughter during anaphase B (for review, see Bloom, 2000). The important similarity between cortical capture sites and kinetochores is that both bind to the plus ends of dynamic microtubules.

In conclusion, the data in this paper suggest that yeast kinetochores contain several functional layers comprising DNA binding proteins such as CBF3, linker proteins such as Ndc80p, and microtubule binding components such as Stu2p, Dam1p, Cin8p, and Bik1p. The DNA binding and linker proteins seem to be highly specific to kinetochores, whereas several of the microtubule binding proteins have other functions in the cell. Although additional kinetochore subunits undoubtedly remain to be identified in yeast, our data have implications for the fundamental question of whether it is motor or nonmotor proteins that play the primary role in microtubule attachment. Our findings clearly point to a critical role for nonmotor MAPs in chromosome-microtubule binding and force generation.

2.5 Experimental Procedures

2.5.1 Yeast Strains and Manipulations

All yeast strains used in this study were haploid and derived from W303 or S228C. Chromosomes and spindle poles were tagged with GFP as described (He et al., 2000). Proteins were tagged with GFP as follows: a 400–1000 bp C-terminal gene fragment was amplified with PCR and EGFP linked at the C terminus in the integrating vector pRS306. The endogenous gene was replaced with the tagged form in one-step gene replacement and correct integrants confirmed by PCR. Nineteen *stu2* ts mutants were generated by mutagenizing the *STU2* ORF in vitro using error-prone PCR, replacing *STU2* in the genomes with the library of mutagenized clones and then complementing the ts phenotype with wild-type *STU2* on a plasmid. Sequencing revealed the presence of multiple mutations in each ts allele. ChIP experiments were performed using standard methods (Meluh and Broach, 1999), and quantitation of PCR products by serial dilution. Anti-GFP polyclonal antibodies were from Clontech, anti-myc polyclonal antibodies from Santa Cruz Biotechnology, and anti-Mif2 polyclonal antibodies produced in house.

2.5.2 Microscopy and Image Analysis

Live cell imaging was performed using a Deltavision optical sectioning microscope on a Nikon TE200 base and Roper RTE camera essentially as described in He et al., 2000. A custom-built heated stage and a Bioptechs lens heater with feedback control were used to maintain the temperature at 37°C (details are available upon request). Dual-color fixed cell images of cells carrying both CFP and GFP fusion proteins were collected using a Photometrics CH350 camera and Chroma 86002 JP4 (CFP) and 41018 (GFP) filters. The intensity plots in Figures 2-1 and 2-2 were corrected for 30% bleedthrough.

2.6 References

- Berlin, V., Styles, C. A., and Fink, G. R. (1990). BIK1, a protein required for microtubule function during mating and mitosis in *Saccharomyces cerevisiae*, colocalizes with tubulin. *J Cell Biol* 111, 2573-2586.
- Biggins, S., Severin, F. F., Bhalla, N., Sassoan, I., Hyman, A. A., and Murray, A. W. (1999). The conserved protein kinase Ipl1 regulates microtubule binding to kinetochores in budding yeast. *Genes Dev* 13, 532-544.
- Bloom, K. (2000). It's a kar9ochore to capture microtubules. *Nat Cell Biol* 2, E96-98.
- Brunner, D., and Nurse, P. (2000). CLIP170-like tip1p spatially organizes microtubular dynamics in fission yeast. *Cell* 102, 695-704.
- Cheeseman, I. M., Enquist-Newman, M., Muller-Reichert, T., Drubin, D. G., and Barnes, G. (2001). Mitotic spindle integrity and kinetochore function linked by the Duo1p/Dam1p complex. *J Cell Biol* 152, 197-212.
- Diamantopoulos, G. S., Perez, F., Goodson, H. V., Batelier, G., Melki, R., Kreis, T. E., and Rickard, J. E. (1999). Dynamic localization of CLIP-170 to microtubule plus ends is coupled to microtubule assembly. *J Cell Biol* 144, 99-112.
- Doheny, K. F., Sorger, P. K., Hyman, A. A., Tugendreich, S., Spencer, F., and Hieter, P. (1993). Identification of essential components of the *S. cerevisiae* kinetochore. *Cell* 73, 761-774.
- Donaldson, A. D., and Kilmartin, J. V. (1996). Spc42p: a phosphorylated component of the *S. cerevisiae* spindle pole body (SPB) with an essential function during SPB duplication. *J Cell Biol* 132, 887-901.
- Dujardin, D., Wacker, U. I., Moreau, A., Schroer, T. A., Rickard, J. E., and De Mey, J. R. (1998). Evidence for a role of CLIP-170 in the establishment of metaphase chromosome alignment. *J Cell Biol* 141, 849-862.
- Freeman, L., Aragon-Alcaide, L., and Strunnikov, A. (2000). The condensin complex governs chromosome condensation and mitotic transmission of rDNA. *J Cell Biol* 149, 811-824.

Gard, D. L., and Kirschner, M. W. (1987). A microtubule-associated protein from *Xenopus* eggs that specifically promotes assembly at the plus-end. *J Cell Biol* 105, 2203-2215.

Gardner, R. D., Poddar, A., Yellman, C., Tavormina, P. A., Monteagudo, M. C., and Burke, D. J. (2001). The spindle checkpoint of the yeast *Saccharomyces cerevisiae* requires kinetochore function and maps to the CBF3 domain. *Genetics* 157, 1493-1502.

Gheber, L., Kuo, S. C., and Hoyt, M. A. (1999). Motile properties of the kinesin-related Cin8p spindle motor extracted from *Saccharomyces cerevisiae* cells. *J Biol Chem* 274, 9564-9572.

Goh, P. Y., and Kilmartin, J. V. (1993). NDC10: a gene involved in chromosome segregation in *Saccharomyces cerevisiae*. *J Cell Biol* 121, 503-512.

Goshima, G., and Yanagida, M. (2000). Establishing biorientation occurs with precocious separation of the sister kinetochores, but not the arms, in the early spindle of budding yeast. *Cell* 100, 619-633.

He, X., Asthana, S., and Sorger, P. K. (2000). Transient sister chromatid separation and elastic deformation of chromosomes during mitosis in budding yeast. *Cell* 101, 763-775.

Hildebrandt, E. R., and Hoyt, M. A. (2000). Mitotic motors in *Saccharomyces cerevisiae*. *Biochim Biophys Acta* 1496, 99-116.

Hofmann, C., Cheeseman, I. M., Goode, B. L., McDonald, K. L., Barnes, G., and Drubin, D. G. (1998). *Saccharomyces cerevisiae* Duo1p and Dam1p, novel proteins involved in mitotic spindle function. *J Cell Biol* 143, 1029-1040.

Hoyt, M. A., He, L., Loo, K. K., and Saunders, W. S. (1992). Two *Saccharomyces cerevisiae* kinesin-related gene products required for mitotic spindle assembly. *J Cell Biol* 118, 109-120.

Hunter, A. W., and Wordeman, L. (2000). How motor proteins influence microtubule polymerization dynamics. *J Cell Sci* 113 Pt 24, 4379-4389.

Hyland, K. M., Kingsbury, J., Koshland, D., and Hieter, P. (1999). Ctf19p: A novel kinetochore protein in *Saccharomyces cerevisiae* and a potential link between the kinetochore and mitotic spindle. *J Cell Biol* 145, 15-28.

Hyman, A. A., and Sorger, P. K. (1995). Structure and function of kinetochores in budding yeast. *Annu Rev Cell Dev Biol* 11, 471-495.

Janke, C., Ortiz, J., Lechner, J., Shevchenko, A., Magiera, M. M., Schramm, C., and Schiebel, E. (2001). The budding yeast proteins Spc24p and Spc25p interact with Ndc80p and Nuf2p at the kinetochore and are important for kinetochore clustering and checkpoint control. *Embo J* 20, 777-791.

Jones, M. H., Bachant, J. B., Castillo, A. R., Giddings, T. H., Jr., and Winey, M. (1999). Yeast Dam1p is required to maintain spindle integrity during mitosis and interacts with the Mps1p kinase. *Mol Biol Cell* 10, 2377-2391.

Kaplan, K. B., Burds, A. A., Swedlow, J. R., Bekir, S. S., Sorger, P. K., and Nathke, I. S. (2001). A role for the Adenomatous Polyposis Coli protein in chromosome segregation. *Nat Cell Biol* 3, 429-432.

Kim, J. H., Kang, J. S., and Chan, C. S. (1999). Sli15 associates with the ip11 protein kinase to promote proper chromosome segregation in *Saccharomyces cerevisiae*. *J Cell Biol* 145, 1381-1394.

Megee, P. C., Mistrot, C., Guacci, V., and Koshland, D. (1999). The centromeric sister chromatid cohesion site directs Mcd1p binding to adjacent sequences. *Mol Cell* 4, 445-450.

Meluh, P. B., and Broach, J. R. (1999). Immunological analysis of yeast chromatin. *Methods Enzymol* 304, 414-430.

Meluh, P. B., and Koshland, D. (1997). Budding yeast centromere composition and assembly as revealed by in vivo cross-linking. *Genes Dev* 11, 3401-3412.

Meluh, P. B., Yang, P., Glowczewski, L., Koshland, D., and Smith, M. M. (1998). Cse4p is a component of the core centromere of *Saccharomyces cerevisiae*. *Cell* 94, 607-613.

Miller, R. K., Cheng, S. C., and Rose, M. D. (2000). Bim1p/Yeb1p mediates the Kar9p-dependent cortical attachment of cytoplasmic microtubules. *Mol Biol Cell* 11, 2949-2959.

Miller, R. K., and Rose, M. D. (1998). Kar9p is a novel cortical protein required for cytoplasmic microtubule orientation in yeast. *J Cell Biol* 140, 377-390.

Nabeshima, K., Nakagawa, T., Straight, A. F., Murray, A., Chikashige, Y., Yamashita, Y. M., Hiraoka, Y., and Yanagida, M. (1998). Dynamics of centromeres during metaphase-anaphase transition in fission yeast: Dis1 is implicated in force balance in metaphase bipolar spindle. *Mol Biol Cell* 9, 3211-3225.

Ortiz, J., Stemmann, O., Rank, S., and Lechner, J. (1999). A putative protein complex consisting of Ctf19, Mcm21, and Okp1 represents a missing link in the budding yeast kinetochore. *Genes Dev* 13, 1140-1155.

Osborne, M. A., Schlenstedt, G., Jinks, T., and Silver, P. A. (1994). Nuf2, a spindle pole body-associated protein required for nuclear division in yeast. *J Cell Biol* 125, 853-866.

Rieder, C. L., and Salmon, E. D. (1998). The vertebrate cell kinetochore and its roles during mitosis. *Trends Cell Biol* 8, 310-318.

Roof, D. M., Meluh, P. B., and Rose, M. D. (1992). Kinesin-related proteins required for assembly of the mitotic spindle. *J Cell Biol* 118, 95-108.

Sassoon, I., Severin, F. F., Andrews, P. D., Taba, M. R., Kaplan, K. B., Ashford, A. J., Stark, M. J., Sorger, P. K., and Hyman, A. A. (1999). Regulation of *Saccharomyces cerevisiae* kinetochores by the type 1 phosphatase Glc7p. *Genes Dev* 13, 545-555.

Skibbens, R. V., Skeen, V. P., and Salmon, E. D. (1993). Directional instability of kinetochore motility during chromosome congression and segregation in mitotic newt lung cells: a push-pull mechanism. *J Cell Biol* 122, 859-875.

Spittle, C., Charrasse, S., Larroque, C., and Cassimeris, L. (2000). The interaction of TOGp with microtubules and tubulin. *J Biol Chem* 275, 20748-20753.

Stoler, S., Keith, K. C., Curnick, K. E., and Fitzgerald-Hayes, M. (1995). A mutation in CSE4, an essential gene encoding a novel chromatin-associated protein in yeast, causes chromosome nondisjunction and cell cycle arrest at mitosis. *Genes Dev* 9, 573-586.

Strunnikov, A. V., Kingsbury, J., and Koshland, D. (1995). CEP3 encodes a centromere protein of *Saccharomyces cerevisiae*. *J Cell Biol* 128, 749-760.

Tanaka, T., Cosma, M. P., Wirth, K., and Nasmyth, K. (1999). Identification of cohesin association sites at centromeres and along chromosome arms. *Cell* 98, 847-858.

Tanaka, T., Fuchs, J., Loidl, J., and Nasmyth, K. (2000). Cohesin ensures bipolar attachment of microtubules to sister centromeres and resists their precocious separation. *Nat Cell Biol* 2, 492-499.

Tavormina, P. A., and Burke, D. J. (1998). Cell cycle arrest in *cdc20* mutants of *Saccharomyces cerevisiae* is independent of Ndc10p and kinetochore function but requires a subset of spindle checkpoint genes. *Genetics* 148, 1701-1713.

Tournebise, R., Popov, A., Kinoshita, K., Ashford, A. J., Rybina, S., Pozniakovsky, A., Mayer, T. U., Walczak, C. E., Karsenti, E., and Hyman, A. A. (2000). Control of microtubule dynamics by the antagonistic activities of XMAP215 and XKCM1 in *Xenopus* egg extracts. *Nat Cell Biol* 2, 13-19.

Vasquez, R. J., Gard, D. L., and Cassimeris, L. (1994). XMAP from *Xenopus* eggs promotes rapid plus end assembly of microtubules and rapid microtubule polymer turnover. *J Cell Biol* 127, 985-993.

Wang, P. J., and Huffaker, T. C. (1997). Stu2p: A microtubule-binding protein that is an essential component of the yeast spindle pole body. *J Cell Biol* 139, 1271-1280.

Wigge, P. A., Jensen, O. N., Holmes, S., Soues, S., Mann, M., and Kilmartin, J. V. (1998). Analysis of the *Saccharomyces* spindle pole by matrix-assisted laser desorption/ionization (MALDI) mass spectrometry. *J Cell Biol* 141, 967-977.

Zeng, X., Kahana, J. A., Silver, P. A., Morphew, M. K., McIntosh, J. R., Fitch, I. T., Carbon, J., and Saunders, W. S. (1999). Slk19p is a centromere protein that functions to stabilize mitotic spindles. *J Cell Biol* 146, 415-425.

Zheng, Y. Z., Roseman, R. R., and Carlson, W. R. (1999). Time course study of the chromosome-type breakage-fusion-bridge cycle in maize. *Genetics* 153, 1435-1444.

CHAPTER 3

The following chapter is adapted, with permission, from Rines et al., 2002. The methods described in this chapter were developed in collaboration with Xiangwei He, Paul Goodwin of Applied Precision, and Dominic Hoepfner of the Phillipsen Lab. Paul Goodwin performed the microscopy for the point spread functions shown in Figure 3-1, and 3-4. Dominic Hoepfner initially developed the agarose pad mounting technique discussed in Section 3.3.

Rines, D. R., He, X., and Sorger, P. K. (2002). Quantitative microscopy of green fluorescent protein-labeled yeast. *Methods Enzymol* 351, 16-34.

Quantitative Microscopy of GFP-labeled Yeast

3.1	Introduction.....	95
3.2	Deconvolution in Fluorescence Microscopy	96
3.3	Preparing the biological sample.....	100
3.3.1	Growth conditions.....	100
3.3.2	Mounting cells for microscopy	101
3.3.2.1	Preparing slides with agar pads for live-cell microscopy	101
3.3.2.2	Mounting cells on agar pads	102
3.3.2.3	Mounting live cells without agar pads	103
3.3.3	Fixing cells with paraformaldehyde and mounting	104
3.4	Optimizing Microscope Optics	105
3.4.1	Selecting Filters.	105
3.4.2	Kohler v. critical illumination	109
3.4.3	Selecting cover glass.....	109
3.4.4	Temperature control.....	110
3.4.5	Minimizing spherical aberration through oil matching.	112
3.5	Acquiring Images.....	114
3.5.1	Camera settings.....	114
3.5.2	Viewing and printing the image.....	116
3.6	An Example of Imaging GFP-labeled Yeast	117
3.7	Future Developments in High Performance Microscopy	122
3.8	Web Resources.....	123
3.9	References.....	124

3.1 Introduction

With the development of methods to tag proteins using green fluorescent protein (GFP) (Chalfie et al., 1994), fluorescence microscopy has become increasingly important for characterizing of protein functions in yeast. In this chapter, we describe the use of three-dimensional deconvolution microscopy to perform fixed and live-cell analysis of cells carrying GFP-tagged proteins. Despite our focus on high-performance imaging, the methods we describe are applicable to a wide range of experiments using conventional wide-field microscopes.

The goal of fluorescence microscopy is to determine the position and time-dependent distributions of one or more proteins within the cell. Such an analysis is often referred to as five-dimensional, having three spatial, one time, and one wavelength dimension. A microscope image is only two-dimensional, however, and three-dimensional images must be reconstructed from a stack of 2D image planes, each acquired at different focal planes. A major problem that arises in reconstructing 3D representations from image stacks is that each 2D image contains not only in-focus light but also from out-of-focus light from objects that lie above and below the focal plane (Swedlow, 1997). This occurs because light becomes smeared, particularly along the vertical axis (parallel to the path of illumination), when it passes through microscope lenses. Two methods have been developed to address the problem of out-of-focus light. In confocal microscopy, scanning point source illumination (typically a laser) combined with a pin-hole at the photodetector is used to ensure the collection of in-focus light. In contrast, deconvolution microscopy applies a computational correction to a stack of 2D images to correct for the smearing imposed by the microscope optics. The 2D stack is composed of wide-field images in which the entire focal plane is

illuminated and the emitted light captured on a camera. Comparing the performances of confocal and deconvolution microscopy is complicated by the fact that the instruments are quite different. Confocal microscopes use lasers to scan the sample, illuminating each point successively, and photomultiplier tubes (PMTs) to digitize the emitted light pixel by pixel. Deconvolution microscopes use wide-field illumination from mercury or xenon burners (lamps) and CCD (charge coupled device) cameras to record images. Iterative deconvolution algorithms generally perform better than confocal microscopy when the sample is thin, the magnification high (objectives over 20X and 0.85NA) and the amount of light scattering small (Goodwin, 1996). Deconvolution microscopy has higher spatial resolution, greater sensitivity and causes less photodamage to samples than confocal microscopy. Yeast cells represent a near-optimal sample for deconvolution microscopy, and in this chapter focus on wide-field methods.

3.2 Deconvolution in Fluorescence Microscopy

The extent to which microscope optics smear the light emitted by an object is described by the point spread function (PSF). This blurring is intrinsic to optical systems, occurs in both confocal and wide-field microscopes, and is greatest along the Z-axis (perpendicular to the plane of the slide). The PSF can be determined by examining the distribution of blurred light emitted from a point source object, a small bead, for example, when the objective is focused through the object (Figure 3-1A). Almost all of the smearing in a modern microscope occurs in the objective lens, and a PSF must be experimentally determined for each objective.

Blurring can then be computationally corrected by deconvolving the stack of 2D images with the PSF (see Ref. 2). The result is an accurate 3D representation of the object. In applying deconvolution methods, it is important to distinguish between constrained iterative

deconvolution (Gold, 1964; Jansson, 1970; Swedlow, 1997), in which the quality of the data is fundamentally improved, and nearest-neighbors deconvolution, which is little more than a filtering method. For high quality work, constrained iterative deconvolution must be performed, usually using commercial packages from Applied Precision (SoftWoRx; www.api.com), Intelligent Imaging Innovations (SlideBook; www.intelligent-imaging.com), or AutoQuant (AutoDeblur; www.autoquant.com) to name a few. It is also important to note that careful sample preparation and acquisition are essential for good results. Deconvolution is designed to correct computationally for a well-understood smearing effect imposed by microscope optics, not to make poor quality data look good.

Three characteristics distinguish good and bad quality images. The first is optical distortion. With modern apochromat objectives, the field of view is typically very flat and the biggest concern is spherical aberration, a problem that can be controlled optimizing the immersion oil. In multicolor imaging, one must also worry about shifts in the position of objects from one channel to the next (Dunn and Maxfield, 1998; Kozubek and Matula, 2000). If this chromatic aberration is large, something is probably wrong with the objective. Small shifts are observed even with very good objectives however, and can be dealt with computationally. A second characteristic of good images is accuracy in intensity. Modern scientific grade CCD cameras typically have a dynamic range of 10^3 to 10^4 (12 bit depth), low thermal noise, and the capacity for quantitative recording from biological structures (Hiraoka et al., 1987). The key to recording intensities accurately is to correct for out-of-focus light (by deconvolution, for example) and to select recording conditions that maximize the signal-to-noise ratio (SNR). A third characteristic of a good image or image series (e.g., a movie) is high spatial and temporal resolution. The most commonly used definition of

spatial resolution is the Rayleigh limit, the minimum separation for two point sources such that their intensity distributions overlap approximately at their half-maximal values (Figure 3-1B). Using a DeltaVision microscope and the methods described in this chapter, we can achieve a Rayleigh resolution of 225 nm in X-Y and 400 nm in Z. It should be noted, however, that objects as close as 150 nm can easily be discriminated and changes in position as small as 5-10 nm can be resolved when objects are tracked from one time point to the next (Figure 3-1C) (Bobroff, 1986; Danuser et al., 2000). In time-lapse studies, temporal resolution is also an issue, and a good rule of thumb is that periodic motion must be sampled at a minimum of twice its highest frequency (the Nyquist limit; Figure 3-1D, E).

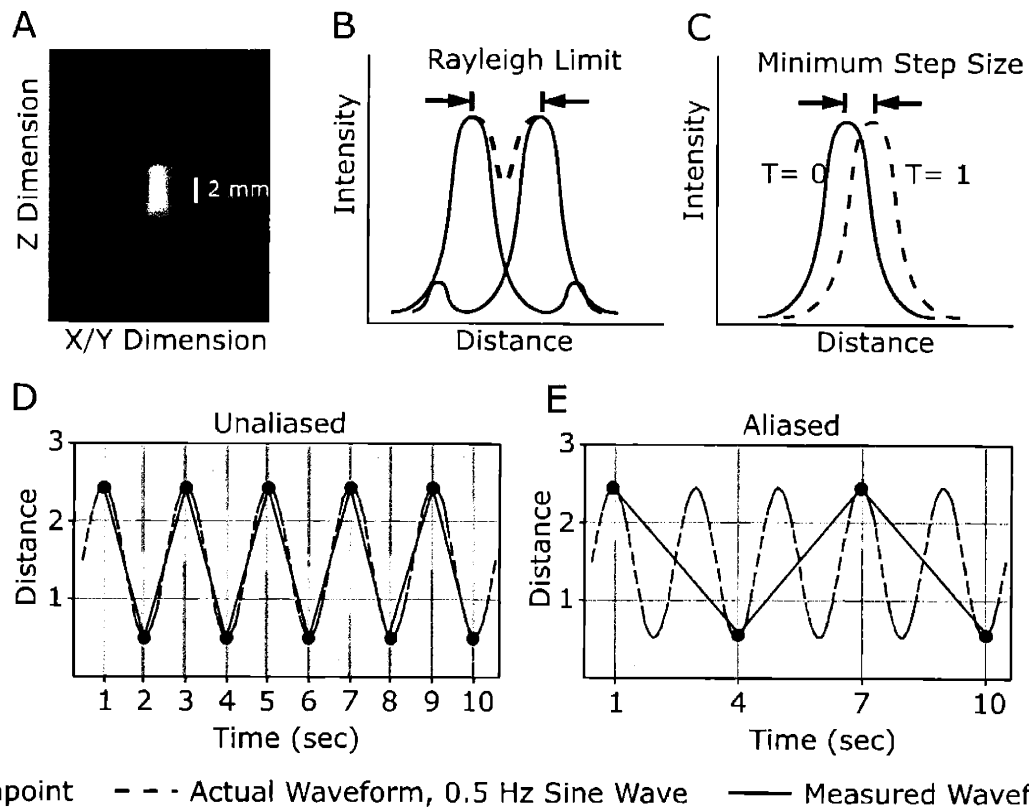


Figure 3-1. Image formation and resolution in an optical microscope

(A) Point spread function. Cross-sectional view of a sub-resolution bead. A stack of images is obtained by incrementally moving the focus through the fluorescent bead (along Z) while collecting 2D (X-Y) images at each step. The collection of 2D images is rotated 90° so and a single cross-sectional plane through the center of the Z-stack is shown. The conical pattern of light above and below the bead shows the smearing effect imposed by the objective lens and represents the point spread function (PSF) **(B) The Rayleigh limit.** Cross-section along the X or Y axis of the emitted light from two point source objects (this distribution is approximated by a Bessel function). The Rayleigh criteria determines the minimum distance between the two objects at which they can be distinguished. More precisely, it is the point at which the first trough in the intensity distribution of one object is coincident with the intensity peak of the second object. For two equal intensity objects, this occurs at about 42% of their maximal intensity (Bracegirdle, 1998). **(C) Minimum step size.** Even if a bead is displaced in a time series by less than the Rayleigh limit, its motion can still be detected. Under optimal conditions the minimum step size that can be measured is on the order of 10 nm. **(D, E) Nyquist criteria in a time series.** Plots representing the sinusoidal movement of an object relative to a fixed point over time with a frequency of 0.5 Hz. In panel (D), data is collected every second and the frequency correctly determined (even if the waveform is not known). In contrast, when samples are taken every three seconds (panel E) the frequency is incorrectly determined. The possibility of aliasing makes it important to collect datapoints at a minimum of twice the highest frequency of the motion.

3.3 Preparing the biological sample

Strain construction. A first step in obtaining good images is to use a bright label. A large number of GFP variants have been isolated and new ones are reported all the time (reviewed in Ref. 11). Currently, the brightest GFP molecule is enhanced GFP (EGFP) and its variants, with an excitation peak at 488 nm and an emission peak at 508 nm (Heim and Tsien, 1996). Cyan (CFP), yellow (YFP), and blue (BFP) derivatives can also be used in yeast. The CFP-YFP combination has the noteworthy property of forming a FRET (fluorescence energy resonance transfer) pair (Miyawaki et al., 1997). In FRET, the light emitted by one fluorophore has the potential to excite a nearby second fluorophore so that the physical proximity of the two fluorophores can be studied. Typically, we fuse GFP to the extreme C-termini of proteins by one-step integration into the genome, thereby replacing the endogenous gene with a tagged version. In at least 20 of the 25 essential genes we have examined, functional C-terminal fusions could be generated (He et al., 2001).

3.3.1 *Growth conditions.*

Autofluorescence is a significant problem with yeast, particularly with strains that are ade^- . An intermediate in adenine biosynthesis, phosphoribosylaminoimidazole (Stotz and Linder, 1990) accumulates to high levels in ade^- cells (Ishiguro, 1989) and is highly fluorescent in GFP channels. Autofluorescence can be minimized in both ade^- and ADE^+ strains by growing them in SD media supplemented with essential amino acids, 20 $\mu\text{g/ml}$ adenine and a carbon source. Cultures must be maintained below 5×10^6 cells per ml for 4–10 generations and the medium should be refreshed prior to imaging.

3.3.2 Mounting cells for microscopy.

Two methods are available for mounting cells, depending on the length of time that they are to be kept growing. For short duration observations of live cells (1 hour or less) and fixed samples, cells are suspended in a small amount of medium, the medium is applied directly to a microscope slide and a cover glass is pressed in placed and sealed with petroleum jelly. Mounting substrates (such as poly-L-lysine) are not necessary because surface tension is enough to exert a slight positive pressure on the sample and hold the cells in place. For long duration observations, cells are maintained on a pad of 1.2% agarose formed in a slide with a shallow depression. The use of an agarose pad is especially important for time-lapse experiments that run for several generations. However, the pad-free method is simpler, suitable for fixed cells, and also optically superior.

3.3.2.1 Preparing slides with agar pads for live-cell microscopy

1. Prepare a solution of 1.2% (w/v) agarose in SD medium supplemented with a complete mixture of essential amino acids (Bio 101; www.bio101.com), 20 µg/ml of additional adenine, and a carbon source. Make sure that the agarose is completely melted.
2. Add approximately 200 µl of melted agarose to a slide fabricated with a shallow hemispherical depression (VWR: 48324-001) and prewarmed to 60°C. Quickly cover the agarose-filled depression with a regular microscopy slide (the “top-slide”) by placing the top-slide at one end of the depression-slide and moving the top-slide over the agarose while pressing down with your thumbs. It is essential that no air pockets are trapped in the agarose during this process and that the agarose forms a smooth and very flat bed above the well. Hold the top-slide tightly over the depression slide for 2 min while the agarose hardens. Leave the top-slide in place until the cell culture is ready for mounting.

With a little practice this method will become routine. We have found it to be more reliable than the competing method of cutting out small agarose blocks and transplanting them into slides.

3. Prepare a 22 x 22 mm, No. 1.5 (0.16 - 0.19 mm), cover glass (VWR: 48367-106) for mounting by first cleaning any dust particles from the cover glass using a precision wipe (Kimwipe) and hand blower (e.g. Bergeon Blower 3B-750 from www.watchmakertools.com). Cleaning is important because dust and other particles prevent a tight seal between the cover glass and the agarose pad. Never use Dustoff or similar compressed gas products because they usually contain small, highly fluorescent particles.
4. Apply a very fine band of pure petroleum jelly (Vaseline) to the extreme edge of the cover glass. This should be done to all four sides by adding a small amount of jelly with a pipette tip to one corner and running a finger lightly along the edge to distribute the jelly evenly. The jelly prevents rapid evaporation of the media and creates a better seal when the cover glass is applied to the depression slide. Be careful not to get any jelly on the microscope objectives.

3.3.2.2 *Mounting cells on agar pads*

1. Transfer 1 - 2 ml of log-phase cell culture to an eppendorf tube and spin at highest speed (14,000 rpm, ~20,000 x g) for 1 min to pellet the cells.
2. Remove the supernatant from the eppendorf tube and resuspend the cells in 0.05 – 0.10 ml of fresh media. The volume used to suspend the cells depends on the size of the cell pellet in the previous step. For 1×10^7 cells, use 0.75 ml. After removing the top-slide

from the depression-slide and exposing the agarose bed (this is done by sliding the top-slide toward one end of the depression-slide to release the seal between the two slides), transfer 2.2 μ l of cell culture to the agarose and gently place the cover glass over the cell culture. To create a tight seal, apply a very light amount of pressure at the extreme edges of the cover glass. Care should be taken because pressing too hard can damage or crush the cells between the cover glass and microscope slide.

3. If necessary, spot a little nail polish at the four corners of the cover glass (this is only required for extended time courses of greater than 4 - 5 hours since small bubbles are generated by the yeast and cause the cover glass to pull away from the agarose bed).

3.3.2.3 Mounting live cells without agar pads

For short duration observations, cells are mounted directly between a slide and cover glass.

The use of a depression-slide is not required.

1. Transfer 1 - 2 ml of log-phase cell culture to an eppendorf tube and spin at highest speed (14,000 rpm, \sim 20,000 x g) for 1 min to pellet the cells.
2. Remove the supernatant from the eppendorf tube and resuspend the cells in 0.05 – 0.10 ml of fresh media.
3. Mount washed cells by spotting 2.2 μ l on a dust-free slide and then pressing the cover glass firmly in place. Surface tension holds the cover glass in place fairly well, but it helps to seal it in place using nail polish. The sample is good for about an hour until carbon dioxide production causes the cover slip to bow outward.

3.3.3 Fixing cells with paraformaldehyde and mounting

Proteins tagged with GFP and its variants can also be localized in cells fixed with paraformaldehyde. Imaging fixed cells is advantageous when performing colocalization with dim signals and does not require the use of a depression-slide. Additionally, since GFP is less sensitive to photobleaching than other chemical fluorophores, the use of anti-fade or glycerol based mounting media is usually not required.

1. To 0.875 ml of fresh culture, add 0.125 ml of EM grade 16% aqueous paraformaldehyde (Electron Microscopy Sciences No: 15710; www.emsdiasum.com/ems) for a final concentration of 2% w/v and mix by inversion for 10 min at 25°C.
2. Pellet cells in an Eppendorf centrifuge for 2 min at highest speed (20,000 x g).
3. Remove the supernatant and resuspend the cell pellet in 1.0 ml of 0.1 M K-PO₄, pH 6.6. Wash the cell pellet for 10 min at 25°C to remove excess formaldehyde before re-pelleting cells again and resuspending in 0.05 – 0.10 ml of K-PO₄ buffer (volume varies with cell density).
4. To image the cellular DNA, DAPI (4,6-diamidino-2-phenylindole) (Palmer et al., 1989) is added to a final concentration of 3 µg/ml into the K-PO₄ buffer and incubated for 30 seconds. Excess DAPI is then washed out by performing three additional rounds of centrifugation and resuspension in K-PO₄ buffer.
5. Mount 2.2 µl of washed cells on a dust-free slide as described above.

3.4 Optimizing Microscope Optics

Obtaining high quality images involves optimizing the optics of the microscope, illumination conditions and camera settings. We do not discuss the selection of objectives and cameras, referring the reader to the chapter by Kron, 2002 found in the same text as this original article, and instead concentrate on user-adjustable settings and conditions.

3.4.1 *Selecting Filters.*

In an Epifluorescence microscope, the excitation and emission wavelengths are selected by three optical elements: an excitation filter, a beamsplitter and an emission filter (see Davidson and Abramowitz, 2001, www.microscopy.fsu.edu, for a detailed discussion of microscope optics and architecture). Broad spectrum light from the mercury or xenon burner (lamp) passes through the excitation filter and is reflected by the beamsplitter into the objective so that it illuminates the sample via the objective. Light emitted by the sample is collected by the objective and passes through the beamsplitter and then the emission filter before being recorded by the camera (Figure 3-2A). This optical path relies on a special property of beamsplitters: they reflect light shorter than a characteristic wavelength but are transparent to longer wavelengths. Dichroic beamsplitters (or dichroic mirrors) discriminate between wavelengths at one transition whereas polychroic beamsplitters by more than one. Longpass and shortpass filters are described by a number denoting the wavelength in nanometers at which the filter cuts on or off (more precisely, the wavelength for 50% transmission). Bandpass filters are described by the wavelength of peak emission (the center wavelength) and the bandwidth (the full width at half maximum transmission) (e.g., 520/20). These features are most easily understood with reference to a plot of filter performance (Figure 3-2B).

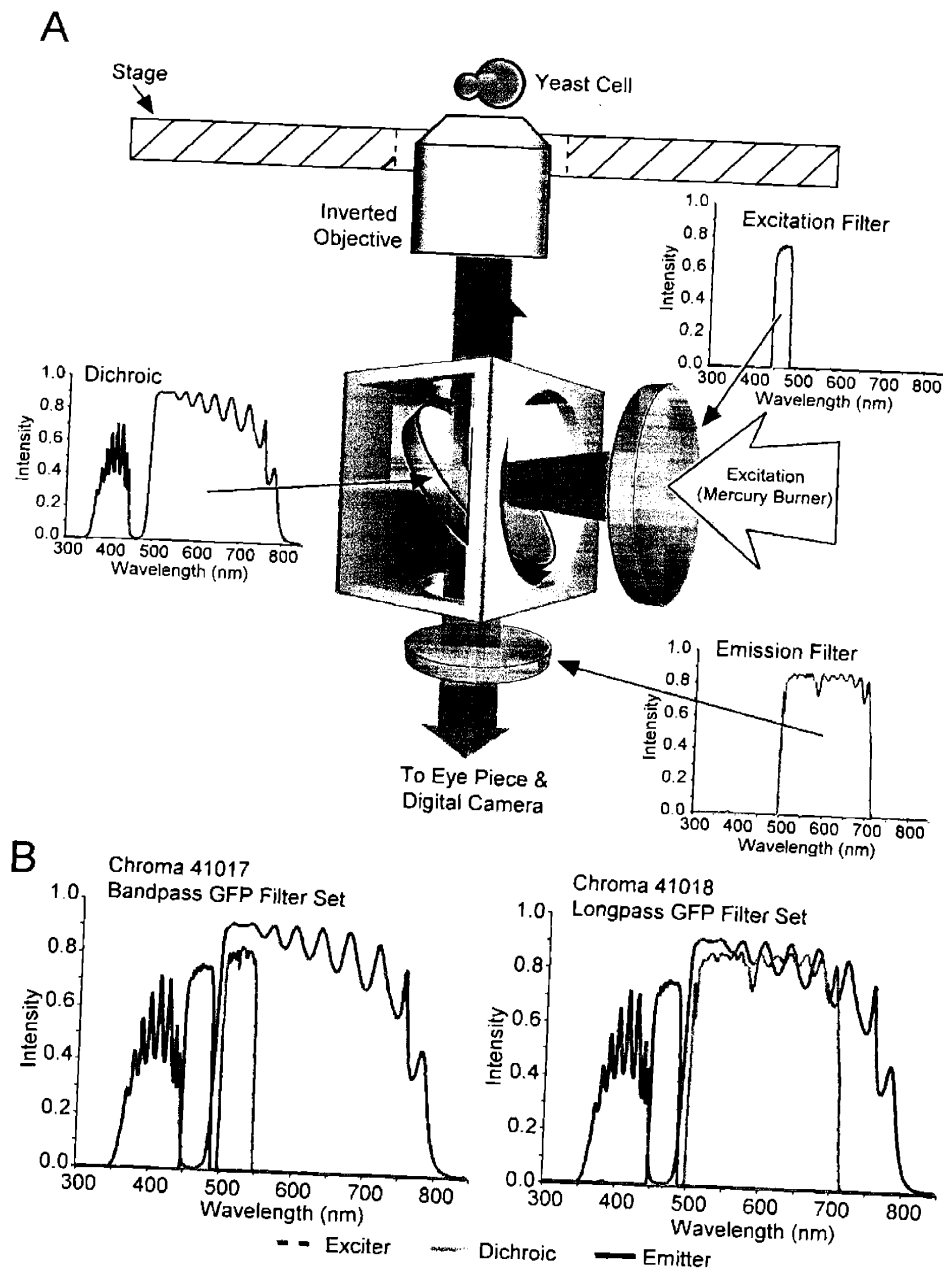


Figure 3-2. Filtering elements in an epifluorescent microscope.

(A) A typical filter cube showing the positions and spectral properties of the excitation filter, beamsplitter and emission filter. Light from the mercury or xenon burner (lamp) enters the microscope from right. Only those photons between 450 – 500 nm pass through the excitation filter before being reflected by the angled beamsplitter up through the objective lens and to the yeast cell. The excitation causes the GFP molecule in the yeast to emit photons at 508 nm which are then collected by the objective and focused down through the beamsplitter and onto the emission filter. Only photons above 508 nm pass through the emission filter and reach the eye piece and CCD camera. (B) Graphs representing Chroma's bandpass and longpass filter sets. The 41018 filter set is also illustrated in A.

Filter manufacturers such as Omega Optical (www.omegafilters.com) and Chroma (www.chroma.com) combine these elements into sets (sometimes called filter cubes) suitable for various applications (Table 3-1). With each set the goal is to achieve the maximum signal strength, particularly in the emission channel, while minimizing interference from autofluorescence and, in multispectral images, from other fluorophores. However, a tradeoff is made between sensitivity and selectivity with every set. Because the optimal choice is dictated by the application, companies such as Chroma sell many different EGFP filter sets, each with a different combination of elements. By examining the characteristics of each element in these sets it is possible to make a good guess about which will work best for a particular application although some empirical experimentation is often required as well.

For single-color recording from cells carrying EGFP, we use Chroma filter set 41018 whose 500LP longpass emission filter provides good sensitivity (Figure 3-2B). When autofluorescence is a problem, particularly with *ade⁻* strains, the use of the 41017 set with a bandpass emission filter is helpful (Table 3-1). With appropriate filters, dual-color recording of CFP and EGFP can be accomplished with relatively little bleedthrough and with good signal strength. If you are examining proteins present in a cell at different amounts, the less abundant one should be tagged with EGFP since it is considerably brighter (Heim et al., 1995; Heim et al., 1994). An alternative approach to dual color imaging is to use CFP and YFP with the Chroma 86002 filter set (which contains two emission and excitation filters). The signal from YFP is considerably less intense than EGFP but bleedthrough into the CFP channel is negligible. It should also be noted that CFP and YFP can be used as a FRET pair with the Chroma 86002 set (Miyawaki et al., 1997). Chroma provides an excellent

downloadable guide to these filter sets and additional information on fluorescent proteins can be found in Patterson et al., 2001.

Table 3-1. Selected Filter Sets for Epifluorescence Microscopy with GFP Molecules

Fluorophores	Excitation	Beamsplitter	Emission	Manufacturer/ Catalog No.	Notes
EGFP (Bandpass)	HQ470/40x	Q495LP	HQ525/50m	Chroma/41017	Wide emission range for highest intensity
EGFP (Longpass)	HQ470/40x	Q495LP	HQ500LP	Chroma/41018	Higher selectivity in cases of autofluorescence problems
EGFP and YFP	S460/20x	86001bs ^b	S500/22m	Chroma/86001	For EGFP
	S523/20x	86001bs ^b	S568/50m		For EYFP
YFP and CFP	S500/20x	86002bs ^c	S535/30m	Chroma/86002	For EYFP
	S436/10x	86002bs ^c	S470/30m		For ECFP
BFP and EGFP	S380/30x	86003bs	S445/40m	Chroma/86003	For BFP
	S485/40m	86003bs	S535/50m		For EGFP
BFP and GFP	XF1048	XF2041	XF3054	Omega/XF50	Designed for simultaneous imaging of BFP and GFP
CFP and YFP	XF1078	XF2065	XF3099	Omega/XF135	Multi-band set allowing simultaneous visualization of CFP and YFP

Notes:

^a The prefix and suffix letters indicate special features of the filters. HQ denotes a high efficiency filter, LP is long pass, S is single band, x is excitation, m is emission, bs is beamsplitter, XF is standard fluorescence.

^b JP3 – Multi-band (polychroic) Beamsplitter for EGFP and EYFP

^c JP4 – Multi-band (polychroic) Beamsplitter for ECFP and EYFP

^d Chroma provides an excellent downloadable guide to these filter sets.

^e Information on fluorescent proteins can be found in Patterson et al., 2001.

As discussed below, phototoxicity is often a problem in live-cell analysis and any unwanted light that leaks through the excitation filter (particularly in the UV range) should

be blocked. We typically add a HQ500LP longpass emission filter and an infra-red blocking filter in series with the excitation filter. This can be accomplished by inserting filters in the cube, the excitation filter wheel, or the auxiliary positions in the epifluorescence module, depending on the arrangement of your microscope. We have also noticed that, over time, filters develop small imperfections and pinhole defects. For critical live-cell work, filters should be replaced after about six months of heavy use.

3.4.2 Kohler v. critical illumination.

Normally microscopes are aligned so that the light source is focused at the condenser aperture to produce an even and unfocused source of light in the specimen plane (Kohler illumination; see Kron, 2002). However, with small objects, such as yeast, in which the entire field does not need to be illuminated, it can be advantageous to focus the light source on the image plane (critical illumination). By using critical illumination, the partial confocal effect of the microscope is maximized and the resolution in Z increased (Swedlow, 1997). Critical illumination produces unacceptably uneven light with standard collector lenses, but works well if a fiber optic scrambler is used to direct the light into the microscope from the burner, as in a DeltaVision microscope.

3.4.3 Selecting cover glass.

The cover glass is a component of a microscope's optical train and objectives are typically designed to work with a particular thickness of cover glass, usually number 1.5 (0.16 – 0.19 mm thick). For the most precise work, it is a good idea to measure the thickness of the cover glass and to use only those within ± 0.02 mm of nominal dimension. A Mititoyo micrometer suitable for this purpose can be purchased inexpensively from www.msdirect.com.

3.4.4 Temperature control.

For many live cell microscope experiments, particularly those involving temperature sensitive alleles, it is necessary to maintain cells at elevated temperatures. In our experience, it is necessary to heat both the agarose depression slide with a stage heater and the objective with an objective heater (Figure 3-3A, B). A commercial stage heater with resistive heating and a temperature controller can be purchased from Instec (www.instec.com). Alternatively, a simple stage heater can be fabricated by drilling channels in a brass block and then circulating warm water from a heated bath through the block. Because the objective and slide are coupled thermally via the immersion oil, the objective acts as a heat sink and causes unwanted local cooling. To avoid this, a heating element (available from Bioptechs Inc., www.bioptechs.com) is mounted to the objective and maintains the objective at the same temperature as the stage heater. The temperature of the sample is monitored using a subminiature RTD probe mounted on the slide adjacent to the sample (available from Omega; www.omega.com).

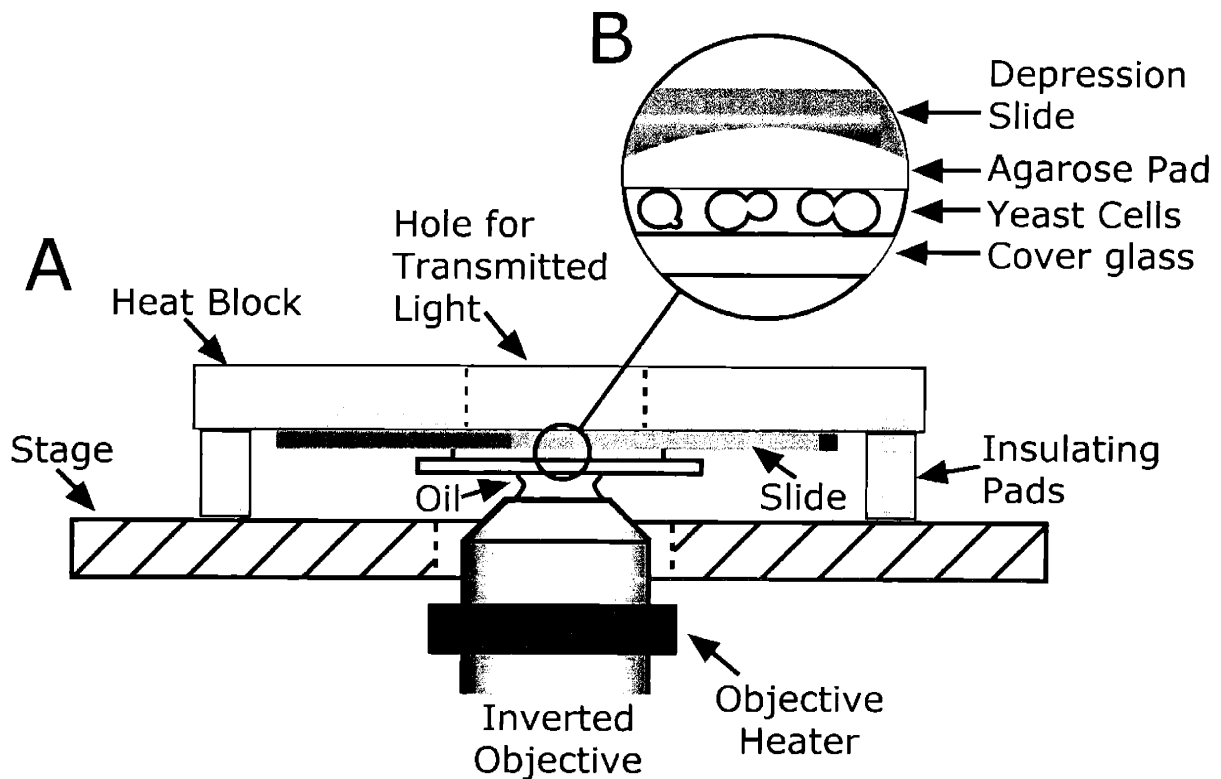


Figure 3-3. Schematic of the temperature control apparatus.

(A) Elevated temperatures are maintained by a heat block and objective heater. Yeast cells are first mounted on an agarose pad formed in a “depression-slide” that has a small hemispherical depression. (B) The yeast cells are held tightly between the agarose and cover glass without damage. Although we have depicted an inverted microscope configuration, this system can work equally well with an upright microscope. The slide is held on the underside of a stage heater by metal clips. A small amount of immersion oil is added to the cover glass and objective. Both the slide and heat block are then placed above the objective lens. Remember to check that the objective is not adjusted too high, since the weight of the heat block on the objective can damage the yeast cells or even crack the cover glass. The objective heater is adjusted to the same temperature as the stage heater and acts to prevent the objective from cooling the sample.

3.4.5 Minimizing spherical aberration through oil matching.

Spherical aberration causes light from the sample to be focused at different positions depending on where the light passes through the objective (Figure 3-4A). Thus, spherical aberration diminishes the quality of the image and causes a substantial loss of data. Spherical aberration can be minimized, however, through the choice of appropriate immersion oils. (These can be obtained in convenient kits or individual bottles with refractive values between 1.500 – 1.534 in increments of 0.002 from Applied Precision, Inc; www.api.com.) By changing the refractive index of the immersion oil, it is possible to correct for differences in the mounting media, the thickness of the cover glass and, most importantly, the temperature. The choice of mounting oil is based on an analysis of the 3D PSF under different conditions. Image a point source, such as a fluorescent bead (0.1 μm beads in the TetraSpeck Fluorescent Sampler Kit, Molecular Probes, Inc; part number T-7284, www.molecularprobes.com and mounted to poly-L-lysine coated slides) or small bright object in a cell (we routinely use GFP-tagged spindle pole bodies) by acquiring a stack of forty Z-sections spaced 0.25 μm apart. To examine the PSF, rotate the image stack 90° so that the slices are viewed edge-on and then move through the Z-X planes until the bead is in view (Figure 3-4B). Compare the cone of light above and below the brightest point. A symmetrical pair of cones indicates optimal conditions and asymmetric cones indicate the presence of spherical aberration (Hiraoka et al., 1990; Swedlow, 1997). Adjust the immersion oil until the PSF is symmetric. Once optimal conditions have been determined they should remain constant for a given objective, mounting medium and temperature, but be prepared to make adjustments when a new batch of cover slips is used.

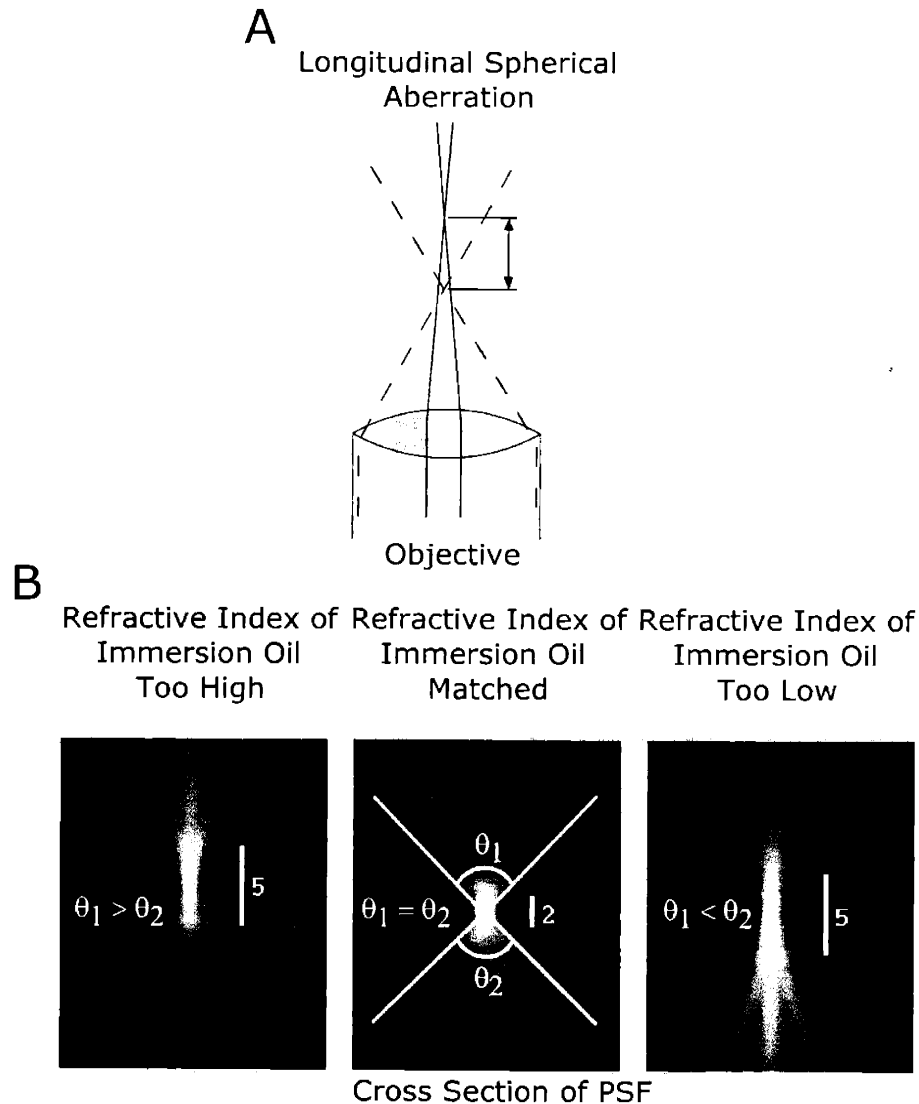


Figure 3-4. The effects of spherical aberration on the point spread function.

(A) Spherical aberration occurs when the rays of light collected from the outer edges of the lens (dashed lines) and those collected from the central portions (solid lines) do not focus to the same longitudinal position. The amount of aberration is affected by refraction at the interfaces between the immersion oil and the cover glass and between the cover glass and the mounting media. It is important to match these indices. (B) Cross sections of PSFs (from sub-resolution beads) obtained with refractive oils having index values that are too high, matched, and too low. The angle or cone of light above and below the fluorescent bead is represented by θ_1 and θ_2 , respectively. When the values of θ_1 and θ_2 are equal, the amount of spherical aberration is minimized. When the refractive index of the immersion oil is incorrectly matched to the conditions, the values of θ_1 and θ_2 are not equal, and the fluorescent signal is greatly lengthened (images kindly provided by Paul Goodwin of Applied Precision Inc).

3.5 Acquiring Images

In live-cell microscopy, photobleaching and phototoxicity impose a tradeoff between the exposure time of each image and the total number of images that can be acquired.

Photobleaching, which is also a problem with fixed cell samples, is readily apparent as a reduction in signal strength (Cubitt et al., 1995; Patterson et al., 1997; Swaminathan et al., 1997). Phototoxicity can be judged by mounting cells on agarose pads, exposing them to various amounts of light and then following their growth over several generations. If the goal of the experiment is accurate observation over a limited time period, we use longer exposures and brighter illumination (the amount of illumination can be varied using neutral density filters or an adjustable intensity burner). On the other hand, if the goal is long duration observation or high temporal resolution, we reduce exposure time to the shortest period in which an interpretable image can be acquired.

3.5.1 *Camera settings.*

The speed, size, and resolution of the image must also be weighed when programming the camera. The fastest high-sensitivity CCD cameras are capable of 4-6 full frames per second but 1-2 per second is more typical. However, the frame rate can be increased by reducing the image size. Epifluorescence microscopes are usually equipped with a “megapixel” camera whose CCD contains a photosensitive array of about 1024 x 1024 pixels. Even with a 100× objective, a yeast cell fills only a small part of the image (about 128 x 128 pixels). The camera can be programmed to record data only from a sub-region of the CCD, in some cases as small as 64 x 64 pixels, increasing the speed several-fold (to as much as 10 – 12 frames per second, although fixed delays in the camera hardware prevent a linear increase in speed as the frame size is reduced) and reducing the size of the dramatically. This latter

consideration is important since a full-frame 3D movie can require as much as a gigabyte of hard disk storage.

A second way to increase frame rate and decrease file size is to use on-chip binning. During the acquisition period, each pixel in a CCD converts incident photons into photoelectrons and stores them in a 'potential' well. During the subsequent readout period, the photoelectrons are shifted through the array until they reach a digitizer (an analog to digital converter or ADC) where they are converted into a digital signal. Binning refers to a process whereby the CCD chip adds together the photoelectrons that have accumulated in several adjacent pixels prior to digitizing them. A binned image can be read out more quickly than an unbinned image because ADC speed is usually rate limiting in data acquisition, and the binned image has a higher signal-to-noise ratio (see Roper Scientific at www.roperscientific.com for more detailed information). These advantages do, however, come at the cost of lower resolution.

The lower limit for a useful exposure is determined by the signal-to-noise ratio (SNR) of the image. This noise has several sources but can be summarized as arising either from the CCD itself—read noise—or from random fluctuations in the number of photons that are counted—shot noise (dark current is negligible in cooled CCDs). Read noise is essentially constant with variations in signal intensity whereas shot noise varies with the square root of the signal strength. Thus, very low intensity signals are read noise limited and stronger signals are shot noise limited. Even with a perfect CCD, the SNR that can be obtained by counting 100 photoelectrons is about 3-fold better than with 10 photoelectrons. If CCD noise is $10e^-$ (a realistic value) then the stronger signal will have an SNR at least 8-fold higher.

The goal is usually to work at an intensity range in which shot noise rather than read noise predominates. Image SNR is then bound by physical and not electronic limitations.

3.5.2 Viewing and printing the image.

In general, GFP-tagged yeast cells are not very bright and exposures are often in the lower region of the camera's dynamic range. 12-bit CCD cameras have 16-times the dynamic range of CRT (cathode ray tube) screens, and low intensity images therefore appear to be very faint when viewed on-screen even though they are well within the acceptable range for the CCD. Thus, it is very important that the digital image be adjusted correctly for viewing. If the signal on the CCD ranges from 8 to 128 digital units (DU), this will appear on the monitor as less than 3% of maximum intensity (e.g., virtually black). The range in the digital image, 8 to 128 in this case, must be adjusted to fit the monitor's gray scale range of 0-256. Usually, this is accomplished via a histogram tool in the image acquisition software. The result is an on-screen image with a broad dynamic range. We mention this point since it is our observation that many inexperienced microscopists overexpose their images, usually on the basis of its initial appearance on a monitor. Obviously, the noise floor limits the extent with which low intensity images can be enhanced.

A frequently encountered difficulty with multispectral images is producing a satisfactory printed copy for publication. In converting an image from an on-screen display to print, one must contend with the problem of gamut conversion. CRT screens are based on a red-green-blue (RGB) color space whereas printed images conform to a cyan-magenta-yellow-black (CMYK) color space. The gamut conversion maps the RGB color values to CMYK color values, but not all RGB colors can be mapped onto CMYK color space. These colors are replaced by approximations, most of which appear very muddy. This is a

particular problem with the bright primary colors typical of fluorescent images. Images also look quite different on Macintosh, PC, and Unix systems. This arises because the default brightness, or gamma, of monitors differs with platform but can be fixed by manually adjusting the gamma.

Gamut conversion from RGB to CMYK is a complex topic with many solutions (see “Color Management in Photoshop,” www.adobe.com, for more information), but a simple approach is to export each wavelength in the microscope image as a separate gray-scale TIFF file. The individual TIFF files from one image are imported into a desktop publishing or image manipulation program, such as Adobe Photoshop (www.adobe.com), as individual layers, allowing them to be manipulated and colorized independently. The key to this process is to choose CMYK colors for colorization and not RGB colors. We find that bright aqua, dark green, and orange-red are usually the most satisfactory choices. Done correctly, gamut conversion generates an image that can be printed correctly. However, if the monitor is not calibrated to the color printer, the image that appears on screen will still differ from the image that is printed. This calibration is accomplished through a color management system (CMS, see www.color.org).

3.6 An Example of Imaging GFP-labeled Yeast

Our analysis of kinetochore function and chromosome dynamics provides an example of applying the methods described above (Goshima and Yanagida, 2000; He et al., 2000; He et al., 2001; Michaelis et al., 1997; Straight et al., 1997). Kinetochores are DNA-protein complexes that assemble on centromeric DNA and mediate the attachment of chromosomes to the microtubules of the mitotic spindle (Hyman and Sorger, 1995). We study the

recruitment of proteins to kinetochores by tagging them with GFP (Figure 3-5A – C) (Donaldson and Kilmartin, 1996). To study the effects of inactivating kinetochore proteins on chromosome movement, mutant alleles are introduced into cells carrying the tetracycline repressor fused to GFP (TetR-GFP) and a tetracycline operator (TetO) array integrated at one location in the genome (Michaelis et al., 1997; Straight et al., 1997). These cells also contain a GFP-tagged spindle pole protein so that both the chromosome and the spindle poles are marked by bright fluorescent dots (Figure 3-5D, E).

To characterize a kinetochore protein, we first localize it in paraformaldehyde fixed cells. One-step integration is used to create C-terminal fusions between the kinetochore protein and EGFP and between the spindle pole body (SPB) protein Spc42p and CFP (Donaldson and Kilmartin, 1996). Kinetochores can then be localized relative to the spindle axis. Imaging is performed on an Applied Precision DeltaVision microscope with a Nikon TE300 base, a 1.4NA 100X objective, a Princeton Instrument's MicroMAX camera (Roper RTE/CCD-1300Y) and some of the filters described in Table 3-1. Z-slices are spaced by 0.15 μm and acquired without binning from a 256 x 256 pixel region of the camera (Figure 3-5A). Typical exposures are 1-2 sec. The raw image is then deconvolved using eight iterations. Under these conditions, kinetochore and spindle staining can be distinguished quite clearly (Figure 3-5B, C).

Chromosome dynamics are routinely examined in live cells in which both the chromosomes and SPBs are labeled with GFP. We acquire twelve to eighteen 50 msec 128 x 128 unbinned Z-slices, separated by 0.20 μm . The extremely short exposures prevent cellular damage due to photobleaching, making it possible to collect as many as one hundred 3D data-sets with as little as 3 seconds between each set. Deconvolution is then performed

(Figure 3-5E), allowing the centroids of the spots to be determined accurately (He et al., 2000; He et al., 2001). Unfortunately, live cell analysis at two wavelengths is problematic with most wide field microscopes. Switching the filter wheel from the first to the second excitation wavelength requires approximately one second. Under optimum conditions, if one switches wavelengths at each Z slice, overall acquisition time for a 15-slice image stack increases to 15 seconds as compared to approximately 2 – 3 seconds for one color. In our experiments, fluorescent structures move substantially in this time frame and colocalization of multi-color organelles is highly unreliable (He et al., 2000). One way to reduce the acquisition time is to acquire the EGFP image stack first and the CFP stack subsequently. In this case, however, displacement is observed from one channel to the next and colocalization is very difficult. No easy solution to this problem exists for wide-field microscopy (in contrast, a confocal microscope acquires all channels simultaneously using multiple PMTs). Two recent developments are very fast solid-state wavelength switchers and methods to record two wavelengths simultaneously (see Optical Insights at www.optical-insights.com). At the moment, most of our live-cell analysis is performed with cells in which several structures are labeled with EF-GFP and we exploit differences in their time-dependent motions to discriminate among them.

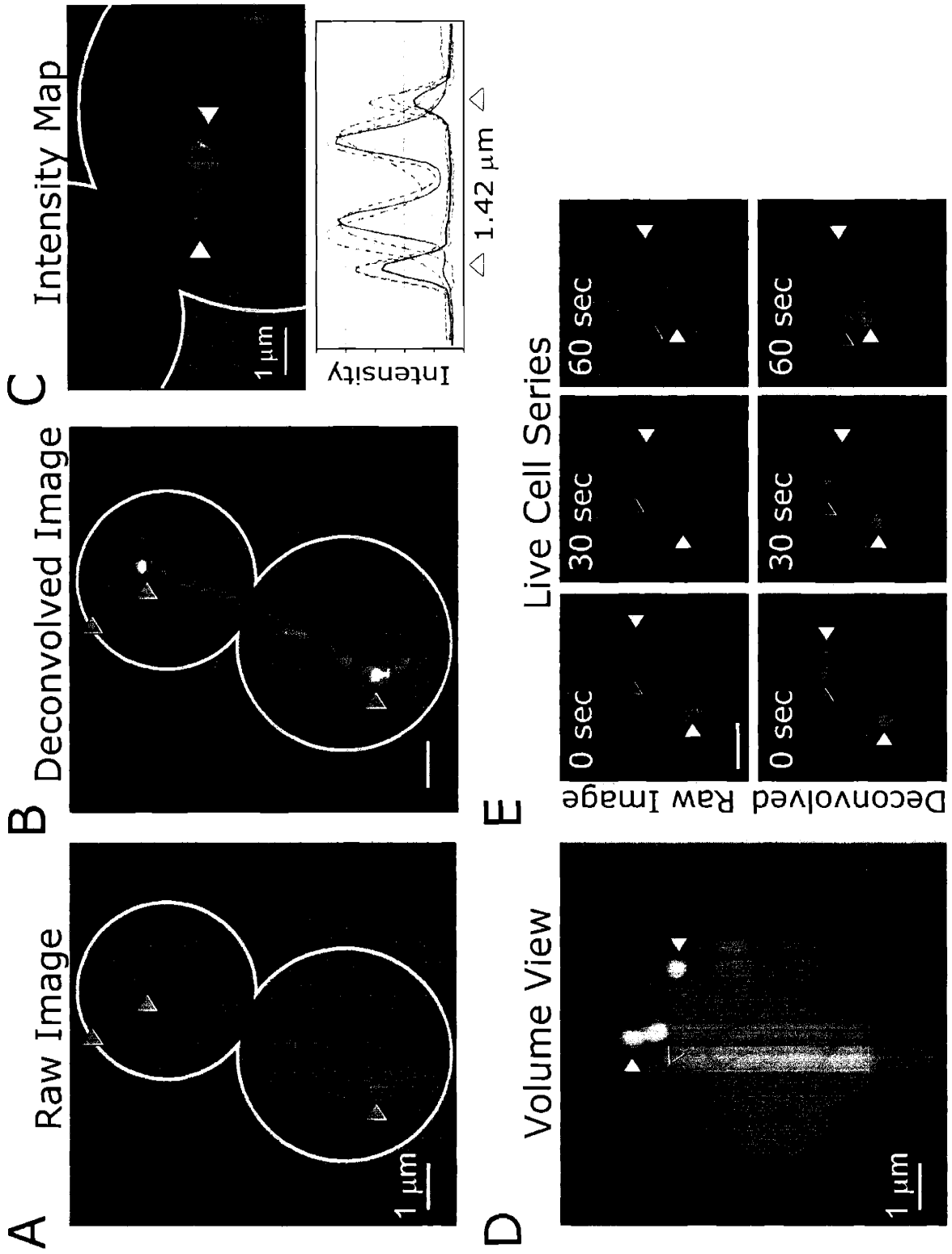


Figure 3-5. Live and fixed cell examples of imaging kinetochore proteins.

(A, B) Localization of the microtubule binding protein, Stu2p (in red), and alpha-tubulin, Tub1p (in green). Both proteins were fused to variants of GFP. Panel A is a maximum intensity projection of an unprocessed image stack while panel B shows the same image after constrained iterative deconvolution (SoftWoRx; www.api.com). The original image was collected as a stack of twenty, 0.15 μm sections with 2.0 sec exposures for GFP and 2.5 sec for CFP. The light blue arrows indicate the position of the kinetochores and cortical attachment site. **(C)** Image showing the localization of a kinetochore protein, Ndc80p (in green), and a spindle pole body protein, Spc42p (in red). The cell was fixed using paraformaldehyde and processed as described above. The graph shows the distributions of Ndc80p-GFP and Spc42p-CFP signal intensities along the spindle axis. **(D)** Image of a cell fixed in paraformaldehyde in which the green dots represent the position of the spindle pole bodies (yellow arrows) and a chromosome tagged (red arrow) with the TetO/TetR-GFP system. The DNA is shown in blue. **(E)** Live cell imaging of a yeast strain containing GFP tags similar to those shown in part D. The top image series shows a maximum intensity projection of the raw data while the bottom shows the same dataset after iterative deconvolution. The original time series was collected as a stack of sixteen sections, 0.25 μm thick, each section was exposed for 50 msec, and time points were taken every 30 seconds.

3.7 Future Developments in High Performance Microscopy

Over the next few years we can expect high quality imaging software to improve and iterative deconvolution to become routine on inexpensive workstations. Cameras can increase about 30% in sensitivity before they hit a theoretical limit but there is potential for increasing speed up to 10-fold and for significantly reducing read noise. One exciting development would be the commercial release of wide-field microscopes specialized for multi-wavelength live-cell microscopy. These microscopes would be designed with digital imaging in mind and could collect images at two or three wavelengths simultaneously. Finally, we believe that the development of new image analysis software will be essential to unlock the full potential of microscope images. This software will be modular and highly configurable by the user. Using such software, it will be possible to analyze and track very dim objects with a precision and speed far greater than is possible using current manual methods.

3.8 Web Resources

Chroma Filters, www.chroma.com:

An excellent resource for information on microscope filter sets and GFP imaging.

Molecular Expressions Website, www.microscopy.fsu.edu:

A must-see site with a wide range of information on optical microscopy. Includes a large number of animations on basic microscope concepts.

Nikon Microscopy U, www.microscopyu.com:

A commercial site with several good animations.

Omega Filters, www.omegafilters.com:

One of the two major filter manufacturers. Contains information of filter spectra.

Roper Scientific, www.roperscientific.com:

Contains a good library of articles on cameras and their use.

Zeiss, www.zeiss.com:

The microscope section contains some helpful guides on microscope alignment and use.

3.9 References

- Bobroff, N. (1986). Position measurement with a resolution and noise-limited instrument. *Rev Sci Instrum* 57, 1152-1157.
- Bracegirdle, S. B. a. B. (1998). Introduction to Light Microscopy, Vol 42 (New York, Springer-Verlag New York Inc.).
- Chalfie, M., Tu, Y., Euskirchen, G., Ward, W. W., and Prasher, D. C. (1994). Green fluorescent protein as a marker for gene expression. *Science* 263, 802-805.
- Cubitt, A. B., Heim, R., Adams, S. R., Boyd, A. E., Gross, L. A., and Tsien, R. Y. (1995). Understanding, improving and using green fluorescent proteins. *Trends Biochem Sci* 20, 448-455.
- Danuser, G., Tran, P., and Salmon, E. (2000). Tracking differential interference contrast diffraction line images with nonometre sensitivity. *J Microscopy* 198, 34-53.
- Davidson, M. W., and Abramowitz, M. (2001). Optical Microscopy (The Florida State University & Olympus America Inc.).
- Donaldson, A. D., and Kilmartin, J. V. (1996). Spc42p: a phosphorylated component of the *S. cerevisiae* spindle pole body (SPB) with an essential function during SPB duplication. *J Cell Biol* 132, 887-901.
- Dunn, K., and Maxfield, F. R. (1998). Ratio imaging instrumentation. *Methods Cell Biol* 56, 217-236.
- Gold, R. (1964). Report No. ANL-6984 (Chicago, Argonne National Laboratory).
- Goodwin, P. C. (1996). Wide-Field Deconvolution vs. Confocal Microscopy of Living Cells. *Scanning* 18, 144-145.
- Goshima, G., and Yanagida, M. (2000). Establishing biorientation occurs with precocious separation of the sister kinetochores, but not the arms, in the early spindle of budding yeast. *Cell* 100, 619-633.
- He, X., Asthana, S., and Sorger, P. K. (2000). Transient sister chromatid separation and elastic deformation of chromosomes during mitosis in budding yeast. *Cell* 101, 763-775.
- He, X., Rines, D. R., Espelin, C. W., and Sorger, P. K. (2001). Molecular analysis of kinetochore-microtubule attachment in budding yeast. *Cell* 106, 195-206.
- Heim, R., Cubitt, A. B., and Tsien, R. Y. (1995). Improved green fluorescence. *Nature* 373, 663-664.

Heim, R., Prasher, D. C., and Tsien, R. Y. (1994). Wavelength mutations and posttranslational autooxidation of green fluorescent protein. *Proc Natl Acad Sci U S A* 91, 12501-12504.

Heim, R., and Tsien, R. Y. (1996). Engineering green fluorescent protein for improved brightness, longer wavelengths and fluorescence resonance energy transfer. *Curr Biol* 6, 178-182.

Hiraoka, Y., Sedat, J. W., and Agard, D. A. (1987). The use of a charge-coupled device for quantitative optical microscopy of biological structures. *Science* 238, 36-41.

Hiraoka, Y., Sedat, J. W., and Agard, D. A. (1990). Determination of three-dimensional imaging properties of a light microscope system. Partial confocal behavior in epifluorescence microscopy. *Biophys J* 57, 325-333.

Hyman, A. A., and Sorger, P. K. (1995). Structure and function of kinetochores in budding yeast. *Annu Rev Cell Dev Biol* 11, 471-495.

Ishiguro, J. (1989). An abnormal cell division cycle in an AIR carboxylase-deficient mutant of the fission yeast *Schizosaccharomyces pombe*. *Curr Genet* 15, 71-74.

Jansson, P. A., Hunt, R.H., and Plyler, E.K. (1970). *J Opt Soc Am* 60, 596-599.

Kozubek, M., and Matula, P. (2000). An efficient algorithm for measurement and correction of chromatic aberrations in fluorescence microscopy. *J Microsc* 200 Pt 3, 206-217.

Kron, S. J. (2002). Digital time-lapse microscopy of yeast cell growth. *Methods Enzymol* 351, 3-15.

Michaelis, C., Ciosk, R., and Nasmyth, K. (1997). Cohesins: chromosomal proteins that prevent premature separation of sister chromatids. *Cell* 91, 35-45.

Miyawaki, A., Llopis, J., Heim, R., McCaffery, J. M., Adams, J. A., Ikura, M., and Tsien, R. Y. (1997). Fluorescent indicators for Ca²⁺ based on green fluorescent proteins and calmodulin. *Nature* 388, 882-887.

Palmer, R. E., Koval, M., and Koshland, D. (1989). The dynamics of chromosome movement in the budding yeast *Saccharomyces cerevisiae*. *J Cell Biol* 109, 3355-3366.

Patterson, G., Day, R. N., and Piston, D. (2001). Fluorescent protein spectra. *J Cell Sci* 114, 837-838.

Patterson, G. H., Knobel, S. M., Sharif, W. D., Kain, S. R., and Piston, D. W. (1997). Use of the green fluorescent protein and its mutants in quantitative fluorescence microscopy. *Biophys J* 73, 2782-2790.

Stotz, A., and Linder, P. (1990). The ADE2 gene from *Saccharomyces cerevisiae*: sequence and new vectors. *Gene* 95, 91-98.

Straight, A. F., Marshall, W. F., Sedat, J. W., and Murray, A. W. (1997). Mitosis in living budding yeast: anaphase A but no metaphase plate. *Science* 277, 574-578.

Swaminathan, R., Hoang, C. P., and Verkman, A. S. (1997). Photobleaching recovery and anisotropy decay of green fluorescent protein GFP-S65T in solution and cells: cytoplasmic viscosity probed by green fluorescent protein translational and rotational diffusion. *Biophys J* 72, 1900-1907.

Swedlow, J. R., Sedat, J.W., Agard, D.A., ed. (1997). *Deconvolution in Optical Microscopy*, 2nd edn (Academic Press).

CHAPTER 4

The following chapter is adapted, with permission, from Thomann et al., 2002. This work was done in collaboration with Dominik Thomann and Gaudez Danuser. Dominik Thomann developed all algorithms, theoretical modeling, software and spot detection methods as illustrated in Figures 4-2, 4-3, 4-4, 4-5, 4-6 and 4-7.

Thomann, D., Rines, D. R., Sorger, P. K., and Danuser, G. (2002). Automatic fluorescent tag detection in 3D with super-resolution: application to the analysis of chromosome movement. *J Microsc* 208, 49-64.

Automatic Fluorescent Tag Detection in 3D with Super-Resolution: Application to the Analysis of Chromosome Movement

4.1	Summary	129
4.2	Introduction.....	130
4.3	Materials and Methods.....	136
4.4	Algorithm for 3DSpot Detection with Super-Resolution	139
4.4.1	A practical 3D model for the point spread function	139
4.4.2	Noise reduction by matched filtering.....	143
4.4.3	Spot detection.....	144
4.4.4	Separation of overlapping spots.....	147
4.4.5	Classification of spots	150
4.4.6	Motion analysis.....	150
4.5	Results.....	152
4.5.1	Performance on biological data	152
4.5.2	Performance on synthetic data	162
4.5.2.1	Resolution of tag separation.....	162
4.5.2.2	Accuracy in point localization	165
4.6	Discussion	167
4.6.1	Biological Applications	167
4.6.2	Performance of the Algorithm	168
4.7	Acknowledgements.....	171
4.8	References.....	172

4.1 Summary

In this paper, we describe an algorithmic framework for the automatic detection of diffraction-limited fluorescent spots in 3D optical images at a separation below the Rayleigh limit, that is, with super-resolution. We demonstrate the potential of super-resolution detection by tracking fluorescently tagged chromosomes during mitosis in budding yeast. Our biological objective is to identify and analyze the proteins responsible for the generation of tensile force during chromosome segregation. Dynamic measurements in living cells are made possible by GFP-tagging chromosomes and spindle pole bodies to generate cells carrying four fluorescent spots, and observe the motion of the spots over time using 3D-fluorescence microscopy. The central problem in spot detection arises with the partial or complete overlap of spots when tagged objects are separated by distances below the resolution of the optics. To detect multiple spots under these conditions, a set of candidate mixture models is built, and the best candidate is selected from the set based on χ^2 -statistics of the residuals in least-square fits of the models to the image data.

Even with images having an SNR as low as 5 to 10, we are able to increase the resolution two-fold below the Rayleigh limit. In images with an SNR of 5 to 10, the accuracy with which isolated tags can be localized is less than 5 nanometers. For two tags separated by less than the Rayleigh limit, the localization accuracy is found to be between 10-20nm, depending on the effective point-to-point distance. This indicates the intimate relationship between resolution and localization accuracy.

4.2 Introduction

One of the most powerful approaches to study cell biological processes has evolved in the form of dynamic analysis of sub-cellular structures such as organelles, vesicles, and the cytoskeleton by localizing and tracking labeled proteins using light microscopy. The development of techniques in which target proteins are fused to Green Fluorescent Protein (GFP) makes it straightforward to label specific macro-molecular structures in vivo. Optical microscopes and digital imaging have advanced to the point where the recording of time-lapse series of 3D images at multiple wavelengths from living cells (frequently referred to as 5D imaging) has become routine in many labs. However, the methods for analyzing these images and for the extraction of accurate quantitative data of the localization and dynamics of biological structures are much less developed. This is particularly true in the case of structures that are small relative to the resolving power of optical microscopes and appear in images as diffraction-limited spots. Manual analysis is usually inappropriate in this situation.

Several methods have been reported for automated detection and localization of spots (Table 4-1). Most of these papers address the problem only in two dimensions and neglect the case of partially overlapping spots. This situation occurs whenever fluorescent markers are positioned at distances below the diffraction limit. The only paper listed in Table 4-1 that deals with overlapping spots is the one by (Netten et al., 1997). They apply a non-linear Laplace filter and thresholding to detect two overlapping spots, but since they are only interested in the number of present spots they do not localize the spots individually.

Table 4-1. Overview of the literature on spot detection and tracking.

Most of the articles deal with 2D data only and with non-overlapping spots.

Paper:	Dimension	Overlap	Application	Type
Netten, <i>et al.</i> (1997):	2	yes	FISH Counting only	D
Ghosh & Webb(1994)	2	no	SPM	D,L,T
Cheezum, <i>et al.</i> (2001)	2	no	Theoretical	T
Kubitscheck, <i>et al.</i> (2000)	2	no	SPM	D,L
Bornfleth, <i>et al.</i> (1999) Bornfleth, <i>et al.</i> (1998)	3	no	SF	D,L,T
Goulian & Simon(2000)	2	no	SP	D,T
Thompson, <i>et al.</i> (2002)	2	no	Theoretical	D,L

Legend: D=Detection, L=Localization, T=Tracking, SPM= Single Protein Molecule, SF= Subchromosomal foci.

Most of the other methods listed in Table 4-1 rely on conventional linear image filtering techniques and some type of maximum search strategy, in which the position of a spot is associated with a peak in the filter response field. Cheezum et al., 2001 and Thompson et al., 2002 examined the fitting of a 2D-Gaussian to the sub-resolution feature in order to improve the localization. Although these approaches give good results in localization accuracy and precision they are usually limited to well-separated spots. This limitation is a significant because in many biological systems it is necessary to detect and localize structures that are separated by less than the resolution limit of the optics. Santos and Young, 2000 were, to our knowledge, the first who suggested using multiple Gaussians to improve the resolution. However, their study is limited to the 2D case and deals with synthetic data only. The only references in Table 4-1 addressing 3D spot detection are those by Bornfleth et al., 1998 and Bornfleth et al., 1999. In contrast to the approach presented in this article, they do not apply a PSF-model in the detection and localization procedure, but perform

sophisticated image segmentation by a region-growing algorithm that includes prior knowledge from measured PSFs. This bears the advantage that they can handle spots representing images of sub-resolution tags as well as spots associated with larger structures at the same time. However, a region growing approach inherently fails in the segmentation of two or more spots that are located at less than 1-2 times the Rayleigh distance apart, dependent on the SNR. The position estimation is accomplished by centroid calculation, which works fine for symmetric spots, but is significantly biased in case of asymmetry associated with asymmetric tag distribution in non-subresolution objects, aberrations or partial fusion of multiple spots.

For noise free images the distance of resolution for equally bright, fluorescent tags is given by the Rayleigh distances (Inoue, 1995):

$$\begin{aligned} d_{xy}^R &= 0.61 \frac{\lambda}{NA} \\ d_z^R &= 2 \frac{\lambda n}{NA^2} \end{aligned} \quad \text{(Equation 4-1)}$$

The two distances correspond to the first root of the point-spread function (PSF) in the lateral and axial direction, respectively. Also, note that the distances are inversely proportional to the cutoff frequency of the optical transfer function (OTF). According to Equation 4-1, the resolution depends on the emission wavelength λ , the numerical aperture NA of the objective lens and the refractive index n of the sample medium. For all calculations in this paper, we choose $\lambda=525$, $NA=1.4$, $n=1.33$ as these were the parameters of our microscope setup (see Materials and Methods).

For many years microscopists have attempted to overcome the limits expressed in Equation 4-1 using one of two different but complementary sets of resolution-extending

methods. The first category extends resolution by narrowing the main lobe of the PSF or by increasing the bandpass of the OTF. Representative PSF engineering methods include the confocal microscope, which uses a pinhole to narrow the PSF essentially in axial direction, or the more recently developed multi-photon microscopy and stimulated emission and depletion (STED) microscopy (Klar et al., 2000), which use non-linear optical effects in fluorescence excitation and emission to narrow the PSF. Other methods, such as 4Pi microscopy or fluorescence excitation with structured illumination can be better understood in the framework of OTF bandpass extension. For a comprehensive review of these optical approaches we refer to Gustafsson, 1999. The second category of methods does not change the optical characteristics of the microscope but attempts to recover spatial frequencies beyond the OTF cut-off using post- acquisition computational analysis. Since they do not increase but break the optical band-pass of the microscope, we refer to such techniques as super-resolution methods.

The key to achieving super-resolution is the incorporation of prior knowledge, which constrains the search space in object reconstruction and permits the extrapolation of object-space frequencies beyond the cut-off of the OTF (Pask, 1975). Prior knowledge can be introduced at the level of the raw signal, as for example with the non-negativity constraint frequently applied to iterative deconvolution of fluorescence image stacks (Carrington et al., 1995), or on the higher, more symbolic level of visual information, where geometric and dynamic models of the observed specimen are included (Danuser, 2001).

In this paper we demonstrate the potential of super-resolution for a biological application: The tracking of chromosomes during mitosis in the budding yeast *S. cerevisiae*. Mitotic chromosome segregation is the process by which replicated sister chromatids are

divided equally into two physically separated sets around which daughter cells form. Sister chromatids are created by DNA replication and bind to the microtubules of the mitotic spindle, a complex contractile engine comprised of several classes of microtubules and various motor proteins (Sharp et al., 2000). Chromatids bind to microtubules in pairs via kinetochores, multi-protein complexes that assemble on centromeric DNA. An essential step in mitosis is linking one set of sisters to microtubules emanating from one spindle pole and the other set of sisters to microtubules emanating from the opposite pole to achieve a state of bipolar attachment. The process of establishing and maintaining bipolar attachment involves the oscillatory movement of sister chromatid pairs back and forth along the spindle microtubules. When bipolar attachment is achieved during metaphase, sufficient tension is imposed on sister chromatids that the chromatin stretches and the sisters separate at their centromeres but not along their arms as shown in Figure 4-1 (Goshima and Yanagida, 2000; He et al., 2000; Tanaka et al., 2000 in yeast and Sullivan, 2001 in humans). The metaphase dynamics of sister centromeres in budding yeast involves transient separation by as much as 0.8 μm on a spindle ca. 2 μm long, whereas anaphase involves the dissolution of sister linkage and the sustained movement of chromatids towards the poles.

Our long-term goal is to characterize the movement of yeast chromosomes in sufficient detail in wild-type and mutant cells such that rates of acceleration can be measured, forces deduced and a mechanical model of the process developed. Ultimately this mechanical model will be combined with molecular genetics to determine the roles of various kinetochore proteins in force generation. Real-time analysis of chromosome movement in yeast is made possible by labeling individual chromosomes with GFP (see Materials and

Methods). The challenge is to track GFP tags with high precision and at different degrees of separation in 3D movies comprising 1000 or more 2D optical slices.

As a first step in our long-term program, we report the development of a fully automated tool for chromosome and spindle pole body (SBP) detection that incorporates super-resolution techniques. The prior knowledge necessary to formulate the constraints for super-resolution detection is the assumption that each spot visible in the 3D image represents the band-limited projection of a finite number of sub-resolution GFP tags. In other words, spots are comprised of a finite number of superimposed PSFs. We find that this weak constraint suffices to improve the resolution between a factor of two and three relative to the classical limit (Equation 4-1). In the future, we intend to use more sophisticated constraints based on a mechanical model of mitotic spindle dynamics. The better our mechanical model, the stronger the constraints and the greater the power of the super-resolution tracking. This illustrates the close and fundamental interaction between data analysis and biological modeling in the development of optimized analytic routines.

The rest of the paper is organized as follows: In the following section we describe the materials and methods for 3D live cell imaging. The section “Algorithm for 3D Spot Detection with Super-Resolution” starts with mathematical preliminaries concerning the PSF and explains the spot detection algorithm in detail. In the “Results” section, we first present results on biological data and then assess the theoretical limits and performance of the algorithm using synthetic data. In the “Discussion”, we summarize and discuss the main findings of our work and give an outlook on future extensions.

4.3 Materials and Methods

Our analysis of chromosome dynamics in yeast is based on the construction of strains in which chromosomes can be tracked relative to the spindle axis (He et al., 2000; He et al., 2001). The combined tracking of chromosomes and the spindle poles is essential to distinguish between chromosome movements driven by kinetochores and motion induced by the rapid movement of the nucleus under the influence of astral microtubules. Additional motion can arise from drift in the microscope stage and whole-cell relocations in the buffer due to volume variation of the mounting gel. All of these kinetochore independent motions are eliminated by using a spindle-centered reference frame.

Chromosomes are tagged with GFP by integrating a tandem array of 100-250 tetracycline (TET) operator sequences ($p306tetO_2 \times 224$) at a unique site in the genome and then expressing a fusion between the DNA-binding TET repressor (TetR) and GFP. A typical array spans 11 kb of DNA, or about 3.5 μm of linear B-form DNA, but in mitotic yeast cells the DNA is compacted approximately 200-fold. When chromosomes are not under tension, chromosome tags are estimated to span about 25 nm and appear as diffraction limited spots as shown in Figure 4-1. When chromosomes stretch they can become deformed into linear structures as much as 750 nm long. In this paper, we make the assumption that chromosome tags are well represented by diffraction-limited spots, as indicated in Figure 4-1, for both relaxed chromosomes and chromosomes under tension. We consider the issue of tag deformation as an exceptional case and will propose a solution to this problem in the Discussion.

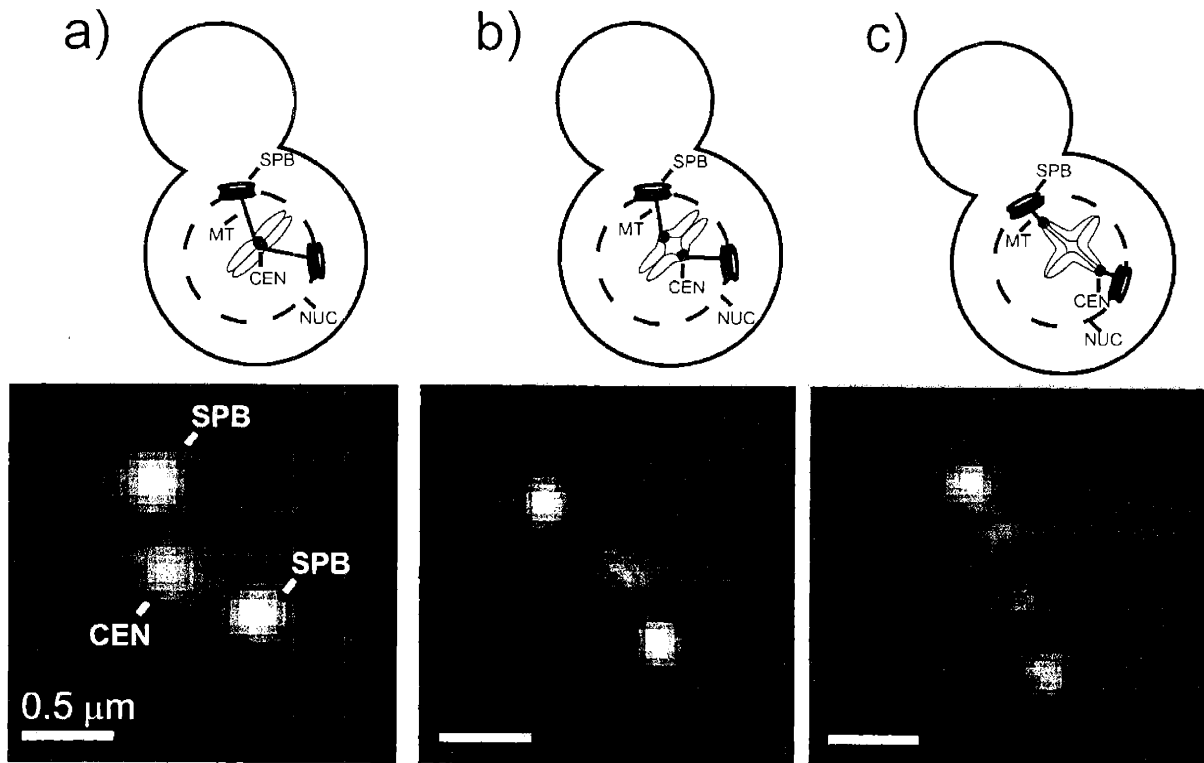


Figure 4-1. Mitosis in budding yeast

Top row: Schematic of the mitotic spindle in budding yeast.

Bottom row: Two-dimensional projection (maximum intensity projection) of 3D image data illustrating the states above. The data of this process has been acquired using a Delta Vision optical section microscope, equipped with 100× 1.4NA objective and Roper RTE camera.

a) Microtubules connect to the chromosomes through kinetochores. Black dots represent GFP tags embedded in the chromatids near centromeric DNA (CEN) and in the two spindle pole bodies (SPB). b) Once bipolar attachment is established, the spindle exerts opposing tensile forces that pull the centromeres apart reversibly. However, for most of the time points, the kinetochores tags cannot be separated visibly. c) Eventually, enough force is developed within the spindle to cause the sister centromeres to be visibly resolved, although the signal has become weak since the number of fluorophores are now physically cut in half and due to some amount of photo-bleaching.

TET operator arrays were inserted approximately 2kb (representing 5-10nm of compacted chromatin) from the CEN-IV. Thus, the chromosome tags allow proper visualization of the location of the kinetochores. The location of the mitotic spindle is determined by marking the spindle pole bodies (SPBs) with a GFP-fusion to an integral pole protein, Spc42p. Spc42p is present at ca. 1000 copies per SPB and is a component of the crystalline central plaque. EM reveals that this central plaque has dimensions of ca. 0.2 μm and it is therefore accurately represented as a point source in fluorescence images (Bullitt et al., 1997).

Live cell imaging was performed using a Deltavision optical sectioning microscope on a Nikon TE200 base with a 100X/1.4NA objective and Roper RTE camera (Applied Precision, Inc.; Issaquah, WA). 3-D image stacks consisting of 16-20 optical slices separated by 0.2 μm with exposures ranging from 0.10-0.05 seconds we recorded every 0.5 to 30 sec to generate 3D movies. These short exposures were necessary to capture the high dynamics of the spindle; to minimize photo-bleaching so that movies could be recorded over 30 to 40 minutes; and to avoid photo-damage, thereby keeping the sample viable for long periods. Critical illumination was used, giving a spatial resolution of about 0.23 μm parallel to the image plane and 0.71 μm in Z (by Raleigh criteria). Fluorescent filters used for live cell imaging were EGFP Chroma 41017 and Endow GFP Bandpass Set.

All *S. cerevisiae* strains used in this study were haploid and derived from S288C (*MATa*; *trp1-1*; *leu2-3,12*; *his3-11, 15*; *ura3-52*, *ADE+*). Live cell mounts were created by applying cells, suspended in a small amount of medium, directly to a microscope slide. A cover glass was applied and sealed in place with petroleum as described in Rines et al., 2002.

4.4 Algorithm for 3DSpot Detection with Super-Resolution

In the following, we describe an algorithm for 3D tag detection with super-resolution. This system can detect and localize multiple overlapping spot signals. The algorithm runs frame-by-frame, and the detection is therefore independent of the history of spot detection in previous frames. In future work, we will employ the detector described here only for the initialization of a time-propagating tracker that utilizes mathematical and mechanical models of movement to determine tag displacements between consecutive frames.

4.4.1 A practical 3D model for the point spread function

Because both the kinetochore and SPB tags (in their undeformed states) are sub-resolution features their images can be approximated by the PSF of the microscope. The theoretical PSF in the focal plane of an aberration free microscope, normalized to unit intensity, is given by a Bessel function of the first kind:

$$PSF(r) = \left(\frac{2J_1(ar)}{r} \right)^2 \quad \text{(Equation 4-2)}$$

$$a = \frac{2\pi NA}{\lambda}$$

It has been demonstrated that the PSF is well approximated by a Gaussian distribution (Santos and Young, 2000) for the 2D case. To validate a Gaussian approximation in 3D we compared it to the PSF model described by Gibson and Lanni, 1991. We first fitted the Gibson-model to the experimental intensity distribution of a single and isolated GFP spot. Then, we fitted a 3D Gaussian to the same data. Using the fitting residuals we calculated the χ^2 statistics for both models, yielding $\chi^2_{\text{Gibson}} = 6.01$ and $\chi^2_{\text{Gauss}} = 7.0$ in units of image grayvalues. A comparison of the two residual statistics with a Fisher significance test suggests that, given the relatively low SNR of our image data, the Gibson & Lanni model

improves the simple 3D Gaussian model for the PSF with a probability of only 30%. Figure 4-2 displays the raw data (a); the Gibson & Lanni model (b); and the Gaussian model in XZ-sections. The residuals for the Gibson & Lanni model are presented in (d) in central XZ-, YZ- and XY-sections, and in (e) for the Gaussian model. As the numerical values of the χ^2 statistics suggest, the residuals of the two models are in the same range and they look approximately random, which means that they largely reflect fitting errors due to noise. A minor exception of this conclusion has to be made for the residuals of the Gaussian model in Figure 4-2e. They exhibit a small systematic residual near the center, indicating a weak systematic error of the model. This can be explained by the fact that in our current fitting of the Gaussian we introduce only the center position and the amplitude as free parameters while keeping the parameter σ fixed (see below). In the presence of small spherical aberration, which essentially affects the axial (Z) direction, this leads to a slight imperfection in representing the image of a sub-resolution feature with a 3D Gaussian. Nevertheless, as discussed below, all the statistical tests employed for the extraction of mixture models are applied on a confidence level between 95% and 99%. Therefore, the difference of 30% between the two tested models is practically irrelevant. We chose the 3D Gaussian as our PSF model despite its minor imperfection. This choice is mainly motivated by computational considerations. The forward calculation of the Gibson model with a given set of parameters takes several seconds on a 1.2GHz AMD computer. Unfortunately, the procedure cannot be parallelized. As the fitting of the model is a non-linear and thus iterative optimization process, the computation time for localizing one sub-resolution tag increases prohibitively. Matters get even worse when fitting mixture models of several PSFs (see below).

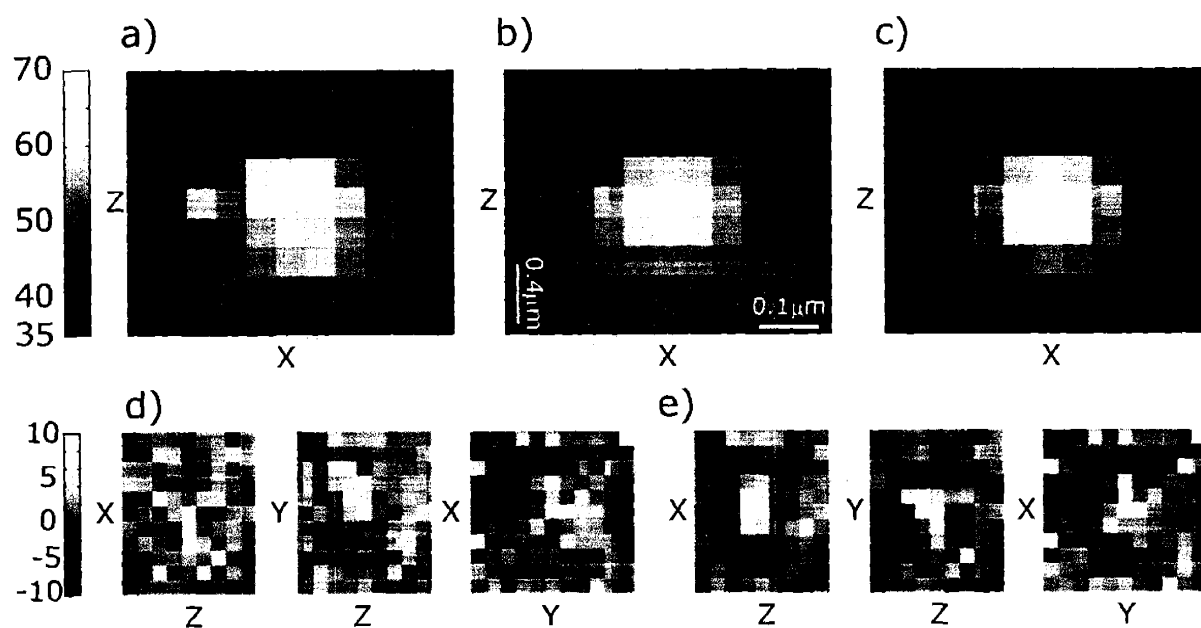


Figure 4-2. Comparison of the PSF and Gaussian models

Comparison of a complex PSF model (Gibson and Lanni, 1991) and the more simple Gaussian approximation fitted to the image of a sub-resolution GFP tag.

The top row shows the central XZ-plane of a) the raw data; b) the fit of the Gibson model; c) the fit of the Gaussian model. The bottom row shows the central planes of the fitting residual of d) the Gibson model; e) the Gaussian model. Confer text for a detailed analysis of the residuals.

An additional simplification of the Gaussian PSF model is the absence of a zero-crossing. We choose the parameter σ_{XY} – the lateral radius for which the intensity of the approximated PSF drops to $1/e=0.37$ times the peak intensity – as the value that provides an optimal least squares fit of the Gaussian to an aberration-free PSF model relying on Bessel functions. In this case the Gaussian decreases to about 1% of the maximum intensity at the position of the first root of the Bessel function. The exact percentage depends on λ and the NA . Notice that this low intensity value sufficiently approximates the exact root of the Bessel function, the latter also representing the Rayleigh limit. We write the parameter σ_{XY} of the Gaussian as

$$\begin{aligned} PSF(r_0 = 0.61 \cdot \frac{\lambda}{NA}) &= 0, \\ g(r_0) = \exp(-\frac{r_0^2}{2 \cdot \sigma_{XY}^2}) &= 0.0163 && \text{(Equation 4-3)} \\ \sigma_{XY}(\lambda, NA) &\approx 0.21 \cdot \frac{\lambda}{NA} \end{aligned}$$

This parameter is then held fixed during the fitting of Gaussian PSFs to spot images. Using Equation 4-1, a similar calculation can be made for the axial direction:

$$\sigma_z(\lambda, NA, n) \approx 0.66 \cdot \frac{\lambda n}{NA^2}.$$

Consequently, for a given set of physical parameters (λ , NA , n) the ratio between σ_{XY} and σ_z is fixed. By mapping the continuous object space into the pixelated image space an additional ratio is introduced accounting for unequal sampling in lateral and axial directions (representing the typically fine spacing of pixels in the CCD camera and the coarser spacing of Z-steps between optical slices). This second ratio is determined by the lateral to axial side length of an image voxel (P_{XY}/P_z).

For the remainder of this paper, we define the parameter $\sigma := \sigma_{XY}$ in [μm] and relate to it:

$$\sigma_z \approx 0.3 \frac{NA}{n} \cdot \sigma.$$

The relationships between object space (in μm) and image space (in voxels) that follow from these equations are summarized in Table 4-2.

Table 4-2. Image space versus object space

Relationship between the image space and the object space and between the parameter $\sigma_{[.]}$ used for PSF approximation. A Greek letter denotes that the value is expressed in the image space, i.e. in pixels as units. P_{xy} , P_z are the lateral and the axial pixel size respectively.

Object space [μm]	P_{xy} , P_z	$\sigma := \sigma_{XY} \approx 0.21 \cdot \frac{\lambda}{NA}$ $\sigma_z \approx 0.66 \cdot \frac{\lambda n}{NA^2}$	$\sigma_z \approx 3.1 \frac{n}{NA} \cdot \sigma$	$\frac{d_{XY}^R}{\sigma_{XY}} \approx 2.9,$ $\frac{d_z^R}{\sigma_z} \approx 3$
Image space [Pixels]	1	$\sigma_{\xi\eta} = \frac{\sigma_{XY}}{P_{XY}}$ $\sigma_\zeta = \frac{\sigma_z}{P_z}$	$\sigma_\zeta \approx 3.1 \frac{P_{XY} \cdot n}{P_z \cdot NA} \cdot \sigma_{\xi\eta}$	

4.4.2 Noise reduction by matched filtering

The requirement of short exposure times for each optical slice so that the sample is not subjected to excessive photo-damage results in data with typically an SNR ≈ 15 or less (see “Materials and Methods”). Consequently, the reliable detection of fluorescent spots is a challenging task. The algorithm has to distinguish between true spots and intensity maxima arising from background noise. To suppress early on as many noise-related local maxima as

possible, we filter the raw intensity data I_r with a 3D Gaussian kernel $G(\xi, \sigma)$ with the parameter vector $\sigma = (\sigma_{\xi\eta}, \sigma_{\xi\zeta}, \sigma_{\eta\zeta})$ defined in the image coordinates $\xi = (\xi, \eta, \zeta)$ (see Figure 4-3a). The parameters are matched to the optics according to Table 4-2 and Equation 4-3 with

$$\int G(\xi, \sigma) d\xi = 1.$$

The convolution of the raw intensity data with this kernel results in an intensity volume $I_f(\xi)$ that exhibits high responses at the position of potential spots, but contains, compared to the raw image, fewer noise-induced local maxima. Notice that the Gaussian filter kernel has the characteristics of amplifying low frequency features at the expense of high frequency information and hence of spatial resolution.

4.4.3 Spot detection

A 3D local maxima detection is performed on the noise-filtered image I_f to generate a set L of features representing the positions of potential spots:

$$L \triangleq \left\{ \xi \in I_f(\xi) \mid I_f(\xi) > I_f(\xi + \mathbf{t}), \forall t_i \in \{-1, 0, 1\}, \mathbf{t} \neq \mathbf{0} \right\}.$$

Because the SNR of the images is low, noise is often recognized as a feature. Thus, the set L typically contains many more candidate features than true spots present in the image. A partitioning of L into true spots and the many noise-induced local maxima applying a simple threshold is not appropriate because of low SNR. Instead, structural information has to be employed, where the distinction is made based on differential geometric considerations in \mathbb{R}^3 . For every local maximum $\mathbf{l}_i \in L$ we calculate the mean intensity \bar{I}_i of a $5\sigma \times 5\sigma \times 5\sigma$ volume surrounding the local maximum position ξ and the curvature κ_i of the intensity distribution in this point (Figure 4-3b). Note that κ_i is not the curvature of a 2D surface but of a 3D intensity

distribution. The curvature is given by the determinant of the Hessian matrix H of the intensity $I_f(\xi)$.

$$H(\xi) = \nabla \cdot \nabla^T I_f(\xi)$$

$$\kappa_i(\xi) = \det(H(\xi))$$

Based on these two numbers, we define a spot classification response

$$s_i = \bar{I}_i \cdot \kappa_i. \quad (\text{Equation 4-4})$$

This value turns out to be very sensitive in discriminating between features associated with true spots and artifactual features associated with background noise. After matched filtering noise-induced local maxima typically exhibit a random distribution of intensity changes in all directions leading to a low local curvature κ . In contrast, true spots are characterized by a combination of convex intensity distribution in all directions plus a relatively high mean intensity. Thus, while the mean intensity alone is not sufficient to separate noise-induced local maxima from true spots, a combined selection based on the concurrence of high intensity and correct curvature is very effective.

We run a statistical analysis of the data $s_j \forall \mathbf{i}_j \in L$. We generate a cumulative histogram and select a threshold, s_t , at the position where the slope of the histogram significantly flattens. Figure 4-3c displays an example of such a histogram. In the case displayed, all classification responses except those associated with the three significant spots cluster around $s \approx 0$, resulting in an almost infinitely steep slope. It is straightforward in such data to automatically define s_t and partition L accordingly into a set of noise-induced local maxima, L_N , and a set of tag-induced local maxima, L_T .

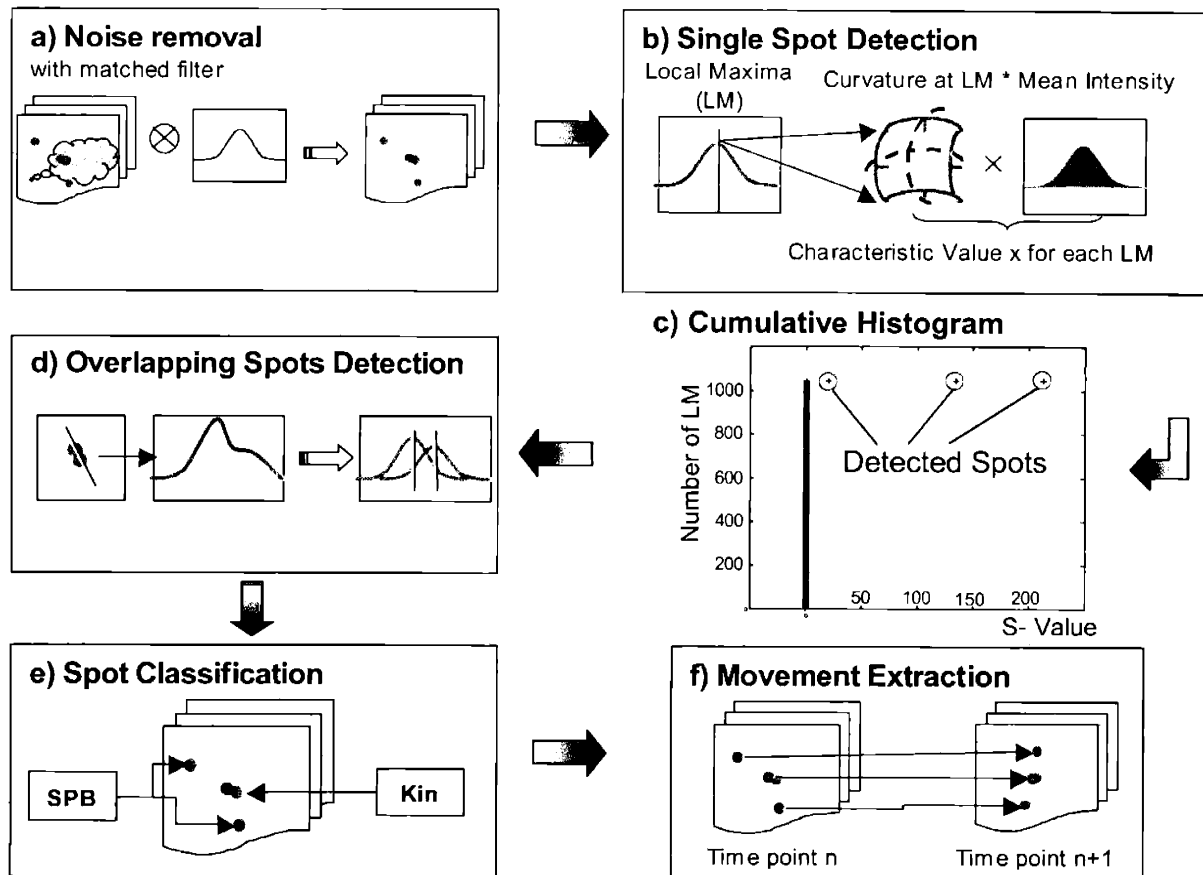


Figure 4-3. Outline of the algorithm

a) Noise reduction with a matched Gaussian filter, where the parameter σ is selected to match the width of a single GFP spot. b) Spot candidate detection by a local maxima operator. The significance of a local maximum is determined by the spot classification response s defined in Equation 4-4. It is a measure for the concurrence of high local mean intensity and a convex intensity distribution. c) Cumulative histogram of the spot classification response s over all local maxima found in one frame of a typical set of biological image data. The large separation between true spots and local maxima induced by background noise indicates that the spot classification response is a sensitive measure for robust spot selection. d) Detection of multiple overlapping spots. A single local maximum detected with the histogram analysis in c) may arise from a superposition of several spots. To find the actual number of underlying spots we fit a mixture model consisting of multiple kernels to each local maximum. With an F-Test of the χ^2 statistics of the residuals the number of contributing kernels is determined. e) In each frame, the detected spots are classified into spindle pole body (SPB) and kinetochore (Kin) spots. The SPB spots are simply selected by the longest point-to-point distance. f) Spot tracking between consecutive time-points is achieved by a minimum search of a correspondence score, where the score for one spot correspondence configuration consist of the sum of a weighted minimal distance criterion between corresponding spots. The computer generated results of steps e) and f) can be verified and manually adjusted, if necessary, using a specialized graphical user interface.

4.4.4 Separation of overlapping spots

When two tags are separated by a distance smaller than the optical resolution limit, the superposition of their images gives rise to a single local maximum only (Figure 4-3d). As explained in the section titled “Noise reduction by matched filtering,” suppressing noise by filtering decreases the resolution limit further. We address the problem of unresolved tags using a module for multiple spot detection. The idea is to build a candidate set of mixture models, where the best candidate model is selected based on a goodness-of-fit criterion. The mixture model consists of a superposition of n kernel functions and is formulated, in the case of diffraction-limited spots, as a superposition of n Gaussians, each one representing a version of the PSF shifted in space and with variable intensity

$$M(\xi, \mathbf{a}, b, \mathbf{c}, n) = \sum_{i=1}^n a_i \cdot \exp\left(-\frac{1}{2}(\xi - \mathbf{c}_i)^T \Sigma^{-1} (\xi - \mathbf{c}_i)\right) + b \quad \text{(Equation 4-5)}$$

$$\Sigma = \text{diag}(\sigma_{\xi\eta}, \sigma_{\xi\eta}, \sigma_{\zeta})$$

The free parameters of the model are the number n of Gaussians, the center positions \mathbf{c}_i of each Gaussian, the amplitudes a_i of the Gaussians and a common background value b . A number of techniques have been reported for fitting such mixture models to real data and for simultaneously determining the number n of underlying kernels. The primary challenge is to trade the goodness of fit against the degrees of freedom of the model: the larger n , the better is the fit to real data, but the higher is the probability of introducing insignificant kernels. In our analysis of tagged chromosomes and SPBs, insignificant kernels are prohibitive as they define the parameters of a non-existing tag. A recent approach to this problem is motivated by mutual information theory and starts with a large number n of kernels (Yang and Zwolinski, 2001). Each kernel is tested for its statistical dependency on the other kernels.

Kernels that are statistically independent are judged to make a significant contribution to the full model and are retained. In contrast, kernels with strong mutual dependence are eliminated from the mixture model. Our approach to finding an optimum mixture model is quite different from that of Yang and Zwolinski, 2001 in that it involves a bottom-up scheme. We start with a low number of already validated kernels and ask whether additional kernels are significant. Since our images contain four or fewer objects a small number of underlying kernels suffices for the formulation of a mixture model. Moreover, a bottom-up approach minimizes the inclusion of insignificant kernels. We fit a candidate model of the order n to the raw data and calculate the residuals R_n and the corresponding $\chi_{r_n}^2$ statistics:

$$R_n(\xi) = M(\xi) - I_r(\xi)$$

$$\chi_{r_n}^2 = \frac{\sum_{x,y,z} R_n(\xi)^2}{r_n} \quad \text{(Equation 4-6)}$$

The degree of freedom r_n is defined as $r_n = N - p_n$, where N is the number of voxels supporting the fit and $p_n = 4n + 1$ denotes the number of parameters. We formulate a statistical test

$$H_0 : \chi_{r_n}^2 = \chi_{r_{n+1}}^2$$

$$H_A : \chi_{r_n}^2 > \chi_{r_{n+1}}^2 \quad \text{(Equation 4-7)}$$

$$T = \frac{\chi_{r_n}^2}{\chi_{r_{n+1}}^2} \propto F$$

to decide whether it is necessary to represent the data with $n+1$ kernels or if n kernels suffice (Bevington and Robinson, 1992). The test statistics T is Fisher distributed and we typically test on a confidence level $\alpha=95\%$. In practice, we perform these tests as follows: from L_T we build clusters of local maxima where each member in the cluster has a minimal distance of 9σ to all non-member local maxima in L_T . The distance of 9σ guarantees that intensities of any non-member in L_T do not influence the mixed model fit of the cluster.

The number $m \geq l$ of cluster members defines a starting value for n . Notice that the fitting problem is highly non-linear. The initial set of parameters, the center coordinates of the kernels and the amplitude are derived from the position and intensities of the associated local maxima. For the fitting we use the MATLAB non-linear least square module *lsqnonlin*. This module implements a large-scale algorithm, which is based on the interior-reflective Newtonian method (Coleman and Li, 1994; Coleman and Li, 1996). After fitting an n -order model, the procedure is repeated on an $n+1$ order model. In a random sequence, we assign to every one of the m original cluster members a candidate partner spot that may have been lost in the previous noise filtering and local maximum search steps. For initial coordinates, we simply use the same values for the original and the partner spot and set the initial amplitudes equal. Applying the test procedure (Equation 4-7), we determine if the number of cluster members has to be incremented by one new kernel. If so, this additional kernel is included in all the partner search tests for the remaining spots in the cluster. The procedure is repeated for all clusters found in L_T , mapping the set L_T of local maxima into a new set S_T of detectable tags. The size of S_T is equal or larger than the size of L_T .

The method described above stands in contrast to the mutual information theory approach, in which a few significant kernels have to be extracted from a large number of insignificant kernels. Without formal proof, we suggest that for data with a small number of overlapping spots and low SNR, the bottom-up approach is more stable. In particular, our strategy allows us to initialize $n+1$ order fits with almost perfect initial guesses from an n order fit, and only one weak starting parameter set for the new kernel needs to be introduced. In top-down approaches, initializations for many unknown and potentially non-significant kernels have to be made. Depending on the quality of these parameter initializations, the

mixed model fits can drift badly and the inclusion of non-significant kernels can damage a model containing highly significant kernels. This problem of estimation drift gets more prominent when the SNR of the data is low.

4.4.5 Classification of spots

We classify the features in S_T and associate them with particular objects in the data: GFP-tagged kinetochores and SPBs (Figure 4-3e). While the algorithmic steps described above are generally applicable to any kind of spot detection, the procedures for classifying spots are specific to the biological system and involve the application of prior knowledge. Because the trajectories of kinetochores and SPBs are highly characteristic, it is our impression that human-assisted spot finding makes considerable use of time-dependent information.

However, our current spot finding algorithm works frame by frame and it is not yet possible to incorporate time-dependence in the analysis. We have, therefore, relied on a geometric argument to classify SPBs and kinetochores. In general, chromosomes lie inside the spindle poles and the longest point-to-point distance among four GFP spots is the spindle axis.

Shorter distances are the SPB-kinetochore and kinetochore-kinetochore distances. This simple approximation appears to be quite reliable in wild-type cells, but is not as reliable with mutant cells in which the spindle is often shorter due to an imbalance in mitotic forces.

In this case, the system requires operator support in classifying spots. In the future, we intend to develop more sophisticated approaches to automated spot classification.

4.4.6 Motion analysis

To track spots from one frame to the next, we have implemented an algorithm which selects a weighted minimal distance of all spots in two consecutive time points. A list of all possible correspondences of spots in time point t to spots in time point $t+1$ is generated. The sum of

weighted squared distances is computed for each configuration of correspondences and the configuration with the minimal score is selected. For an unequal number of spots in subsequent time points the software distinguishes between two cases: With three and four spots present the correspondence mapper assumes the fusion or separation of kinetochores and the scores are calculated including all possible fusions or separations of spots. In all other cases only the spindle pole tags are mapped. The weight matrix favors spot correspondences within a typical range of displacement distances and is introduced to decrease the effect of outliers or falsely detected spots. The score weight for a spot i mapped from time-point t into a spot j in time-point $t+1$ is calculated according to the following equation:

$$w_{ij} = e^{-\frac{|a_i - a_j|^2}{\sigma_a^2}} e^{-\frac{|c_i - c_j|^2}{\sigma_d^2}} \quad (\text{Equation 4-8})$$

The parameter σ_a is an estimate of the expected variation in spot intensity, e.g. due to bleaching, the parameter σ_d the expected range of displacements. In future work, we will replace this procedure with a proper differential tracking of spot configurations between consecutive frames. This will allow us to directly extract trajectories and is expected to further increase the resolution (see the “Discussion” section).

Since the spindle can move and rotate during the acquisition, we transform the coordinates from a microscope-centered Cartesian frame into a spindle-centered Cartesian frame in which the chromosome movements relative to the SPBs are easier to analyze. Because this transformation relies on a correct assignment of SPB and kinetochore tags, we have to eliminate possible errors in the above described classification scheme. Currently, we use a specialized graphical user interface where the classification and the mapping of the spots can be verified and interactively adjusted, if necessary.

4.5 Results

4.5.1 Performance on biological data

We first present results from the analysis of biological data and then focus on the performance of the algorithm using synthetic images. The algorithm is designed to work robustly on large data sets with minimal demand for parameter adjustment between movies. We did not tweak the parameters for the performance tests, but instead ran the software on synthetic data under the same conditions as on real imagery.

Initially, the software reads a definition file with optical parameters and the pixel sizes. From this, the parameter σ is calculated and the PSF is formulated according to Equation 4-3. The corresponding parameters ($\sigma_{\xi\eta}, \sigma_{\zeta}$) in the image space are derived from the relations listed in Table 4-2. In addition to the PSF definition, the operator has to set two parameters manually:

1. The threshold $t_s = \frac{1}{s_{t+1} - s_t}$ for distinction between local maxima associated with true

and artifactual spots (see Spot detection). The quantity s_t represents the spot classification response (Equation 4-4) of the first spot in the cumulative histogram considered significant and s_{t+1} denotes the response of the next higher ranked spot. This means that the algorithm determines the index t of the spot in the cumulative histogram for which the slope falls below the operator-defined threshold t_s . As mentioned before, the parameter s_t represents a very sensitive characterization of local maxima in terms of their probability of being a true spot. In the histogram true spots do not cluster with the large majority of false spots, resulting in a characteristic decrease of the histogram slope by a factor 100 or more (Figure 4-3c). Therefore, the software is very tolerant to non-optimal settings of this slope threshold.

2. The confidence parameter α used for the statistical testing of mixture models (see the section titled “Separation of overlapping spots”).

The detection of isolated spots poses no problem for the algorithm even in the case of low SNR. This is illustrated in Figure 4-4a. In this frame the cell is still in metaphase, the sister chromatids are closely linked and hence the two kinetochore GFP tags are imaged into a single spot. Figure 4-4b shows a frame where the sister chromatids are separated. Here the power of a super-resolution scheme becomes evident. Thanks to the fitting of mixture models, the software detects two overlapping spots with high positional accuracy.

Figure 4-4c displays the detection result in a time point where the chromatids are pulled towards the SPBs. In this state the four fluorescent spots are all isolated.

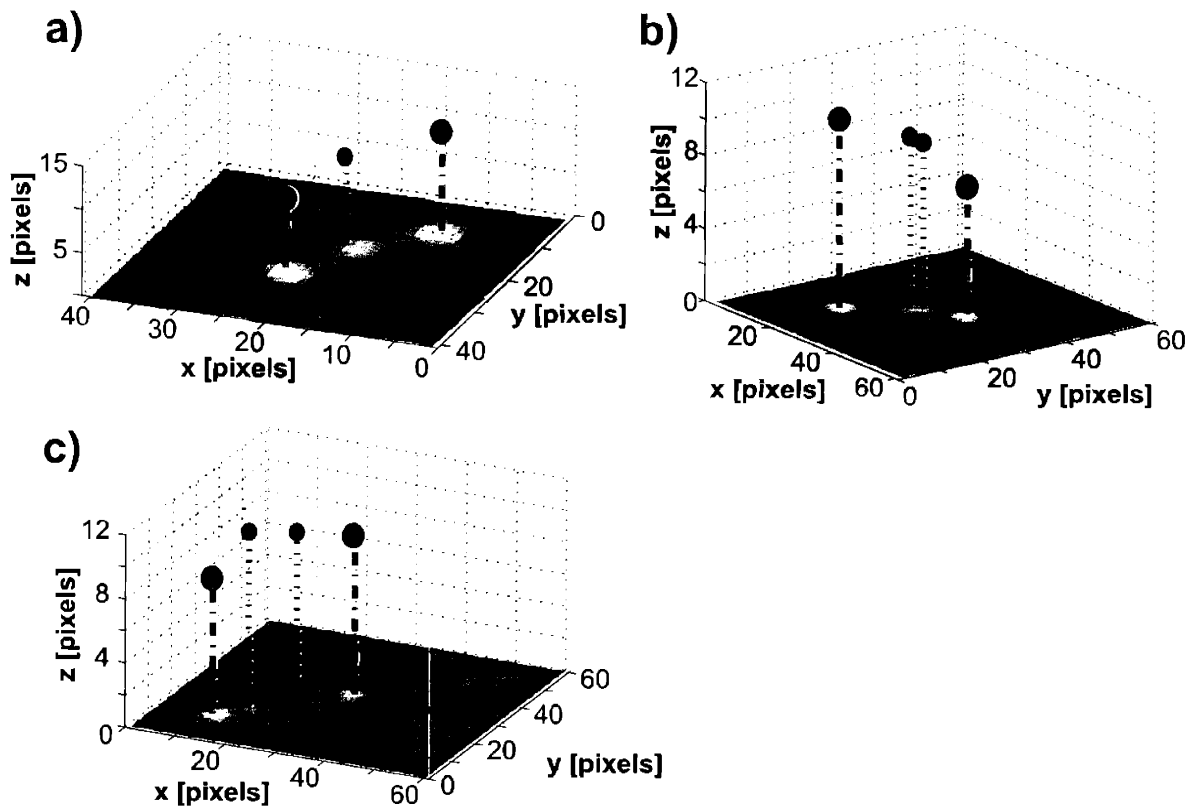


Figure 4-4. Results of the spot detection algorithm during yeast mitosis.

a) Cell in metaphase: The two SPB spots are isolated and give a strong signal. The sister chromatids are attached to each other giving rise to an image of the two kinetochore tags as in a single spot. b) Super-resolution detection of two kinetochore spots. Thanks to the fitting of mixture models, the software detects two kinetochore tags with high positional accuracy although the associated spots overlap. c) The chromatids are separated and pulled towards the SPB. In this state, the four fluorescent tags are all separated by more than the Rayleigh distance and well visible in the image as isolated spots.

Typically, the image sequences we have analyzed last more than 30 minutes. Acquiring image stacks every 30 seconds over this extended time period is accompanied by photo-bleaching, leading to a significant decrease of SNR. Thus, towards the end of the movies the detection of spots becomes problematic even though the spots may be well separated. The influence of bleaching on SNR and spot detectability is illustrated in Figure 4-5. The graphs show the number of spots detected (black line) in comparison to the mean SNR of all spots (blue line) and the SNR of the weakest spot (red line) in each frame. Figure 4-5a presents the result from a movie with 100 frames over 50 minutes of data acquisition. The graph in Figure 4-5b displays the same analysis for a movie with only 60 frames, i.e. 30 minutes of data acquisition. Both movies start with four detected spots and a mean SNR of 10. In the example in Figure 4-5a bleaching is very prominent. After 40 frames the mean SNR drops to 5 and the weakest spots are detected at an SNR level of about 3. Once this low level is reached, the algorithm breaks down and only 1 or 2 spots are detected for which the SNR is above 4. Presumably, they originate from the SPB tags, which contain more fluorophores than the kinetochore tags. In the example in Figure 4-5b the SNR is much more stable. Over the period of 60 frames, the mean value drops from 10 to 8 allowing the algorithm to detect either 3 or 4 spots for most of the frames. The SNR of the weakest spot never falls below 4. Notice that in two frames, five spots are detected. The inset in the graph displays the maximum projection of the second of these frames. With regular contrast settings, the kinetochore tags are barely visible by eye. Yet, the software extracts one kinetochore tag position near SPB1 and two kinetochore positions closer to SPB2. We know that this is biologically not possible (see Figure 4-5b). There are two reasons for such outliers: i) The algorithm may split one spot into two spots depending on the confidence level

of the statistical test (Equation 4-7). For biological data, we set this level to about 90%, with an error of the first kind of 10%. Notice that for the used statistical test, the error of the second kind, i.e. the error that artifactually split spots are classified as significant, is the same as the error of the first kind. Thus, we can decrease the frequency with which outliers are generated by increasing the confidence level, but this can be accomplished only at the risk of losing significant splits that are detected under the present settings. ii) Chromosome tags are known to get stretched mechanically during metaphase (Goshima and Yanagida, 2000; He et al., 2000; Sullivan, 2001). This leads to objects whose images do not match the PSF kernels in the mixture model. Obviously, for stretched tags the mixture model tends to prefer two kernels instead of one. This problem will be addressed in a future version of the software, where spots will be tracked differentially with mapping models that not only account for tag translocation and brightness variation between consecutive frames, but also for mechanical deformation.

Table 4-3 summarizes the results of three representative movies we have analyzed in detail. The left column specifies the number of frames contained by the movie. These values are divided in column 2 into percentages of frames with 0, 1, 2 or more spots detected. Only the third movie contains 2 frames with 5 spots and thus obvious outlier data (see Figure 4-5b). From this, we conclude that our parameter settings are sufficiently conservative that only few outliers are generated. When all movies are considered, the majority of the frames contain either three or four spots. The large number of frames in which we find only three tagged objects rather than the four present in cells suggests that despite mixture model fitting many of the kinetochore tags still cannot be resolved. Nevertheless, the benefit of the mixture model fits becomes evident from the results in columns 3 to 5. Column 3 specifies

the percentage of spots extracted with mixture model fits. For most of the movies about 25% of the detectable spots can only be found with a mixture model. And even in the second movie, where most of the frames contain only 3 spots, 15% of all spots are only detectable because of the mixture model approach. Columns 4 and 5 indicate the improvement due to mixture model fitting in geometric terms. The mean over all frames of the minimal distance between isolated points not requiring a mixture model fit amounts to $0.4 - 0.7 \mu\text{m}$, the shortest distance found in a whole movie to $0.3 - 0.4 \mu\text{m}$. Mixture model fitting systematically decreases these numbers. The mean minimal distance between mixture model spots lies between $0.3 - 0.45 \mu\text{m}$. Notice that while these values are still larger than the lateral Rayleigh distance, they are below the axial limit of resolution. We did not split the statistics into axial and vertical components. The essential result is given by the absolutely minimal distance found per movie. For the first movie this is 250 nm, right at the lateral Rayleigh limit of our optics, while for the two other movies in the table the value drops to 130 nm, a factor 2 below the Rayleigh limit. Notice that this estimate of a super-resolution factor represents a lower bound, as some of the measured distance vectors have a significant axial component.

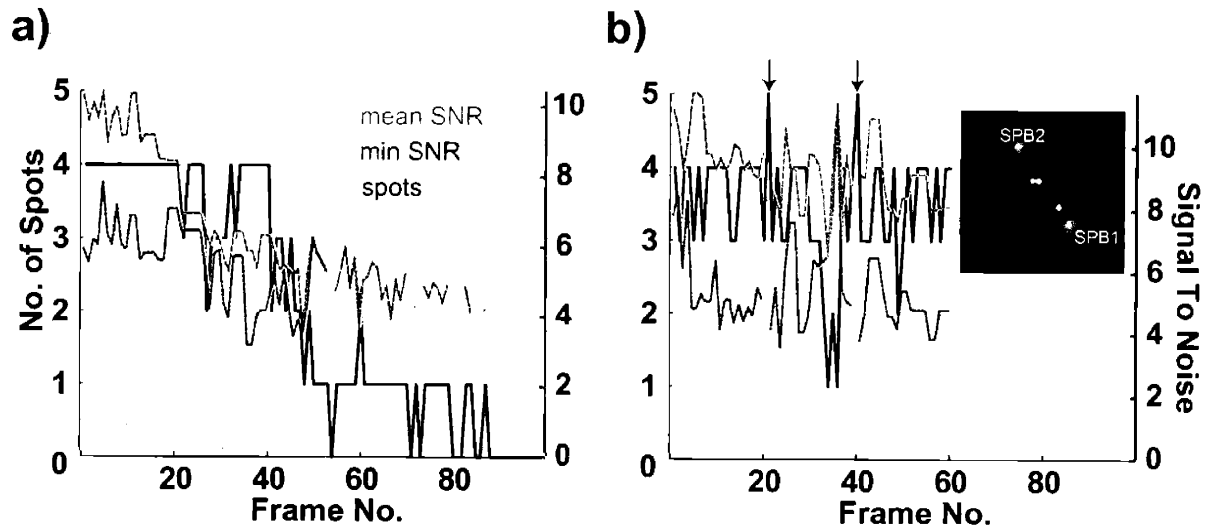


Figure 4-5. Effects of photobleaching on SNR and detection

The influence of bleaching on SNR and spot detectability is shown for two movies. The graphs show the number of detected spots (black line) in comparison to the average SNR of all spots (blue line) and the SNR of the weakest spot (red line). a) The long light exposure in this 100 frame movie leads to strong bleaching. Below an SNR of about 4 the spot detection algorithm breaks down. The one or two spots remaining after frame 50 originate from SPB-tags, which usually are stronger than the kinetochore tags, even when the latter are superimposed. b) This movie is more stable in terms of SNR. The average SNR remains around 8 and the SNR of the weakest spot never falls below 4, allowing the software to detect 3 or 4 spots in almost all frames. Two outlier frames are observed (arrows), where 5 spots are detected. The inset displays the maximum projection of the second of these frames. A detailed interpretation of this effect is given in the text.

Table 4-3. Statistical analyses of three biological data sets.

The left column specifies the number of frames contained by the movie, which are divided in column 2 into percentages of frames with 0, 1, 2 etc. spots detected. The 3rd column indicates the percentage of spots detected by the mixture model fit. Columns 4 and 5 contain the mean over all frames and the minimum of the shortest tag-to-tag distance per frame. The statistics is done separately for isolated spots not requiring a mixture model fit (d_{nm}) and between spots extracted in mixture models (d_{mm}). The numbers indicate the improvement in resolution due to mixture model fitting.

Total # of frames	# of spots per frame	% of total number of frames	% mixture model spots of total	Mean d_{nm} , Min d_{nm} distance of isolated spots [μm]	Mean d_{mm} , Min d_{mm} distance of mixture model spots ($n>1$) [μm]
100	0	21	25	0.70	0.47
	1	30			
	2	7			
	3	9			
	4	33			
	5	0			
60	0	0	15	0.56	0.44
	1	0			
	2	0			
	3	95			
	4	5			
	5	0			
60	0	0	28	0.42	0.32
	1	3			
	2	5			
	3	37			
	4	52			
	5	3			

From the estimated tag positions in each frame, kinetochore and SPB trajectories can be reconstructed (see the “Motion analysis” section). In Figure 4-6a spot trajectories of a

small part from a typical movie are displayed. The kinetochore trajectories split and rejoin several times during this period (cf. arrows for an example). For one of the time-points where kinetochores split, Figure 4-6b shows the spot configuration and the image stack projection to emphasize the need of super-resolution to recover such data. Notice that the rejoining of the kinetochore spots does not necessarily imply a physical rejoining of the tags. It only means that they are separated by a distance below the limit of detectability of our algorithm. The measured spot displacements are due to four factors: i) drifts of the microscope stage; ii) whole-cell relocations in the buffer due to volume variation of the mounting gel; iii) spindle movements relative to the cell cortex driven by microtubules and cortical motors; iv) kinetochore movements relative to the SPBs. Only type (iv) movements are driven by kinetochores. To visualize the kinetochore-dependent motion, we transform the trajectories from the microscope-centered Cartesian frame into a reference frame with one fixed SPB and the SPB-SPB axis defining the x' -axis. For any time point, the y' axis spans the plane defined by the SPB-SPB axis in the very first frame and momentary SPB-SPB axis. The z' axis is then chosen to form a right-handed coordinate frame. Figure 4-6c displays the trajectories of a transformed movie. For this movie, the two kinetochores perform a joined dance, relatively stable at half the distance between the two SPBs. Also, vertically, they always stay above the axis, an arrangement that appears to be typical of metaphase. Throughout the movie the SPBs move apart at a constant rate, another characteristic of metaphase (Figure 4-6d). The SPB-SPB distance estimates contain one outlier, which has been eliminated from the trend analysis of spindle growth. As shown in the next section, the accuracy with which well-isolated spots can be localized reaches 10 nm in movies such as this one with an SNR 8. The

total change in the SPB-SPB distance over the course of the movie is in the range of 100 nm, and is therefore statistically significant and clearly visible in the data.

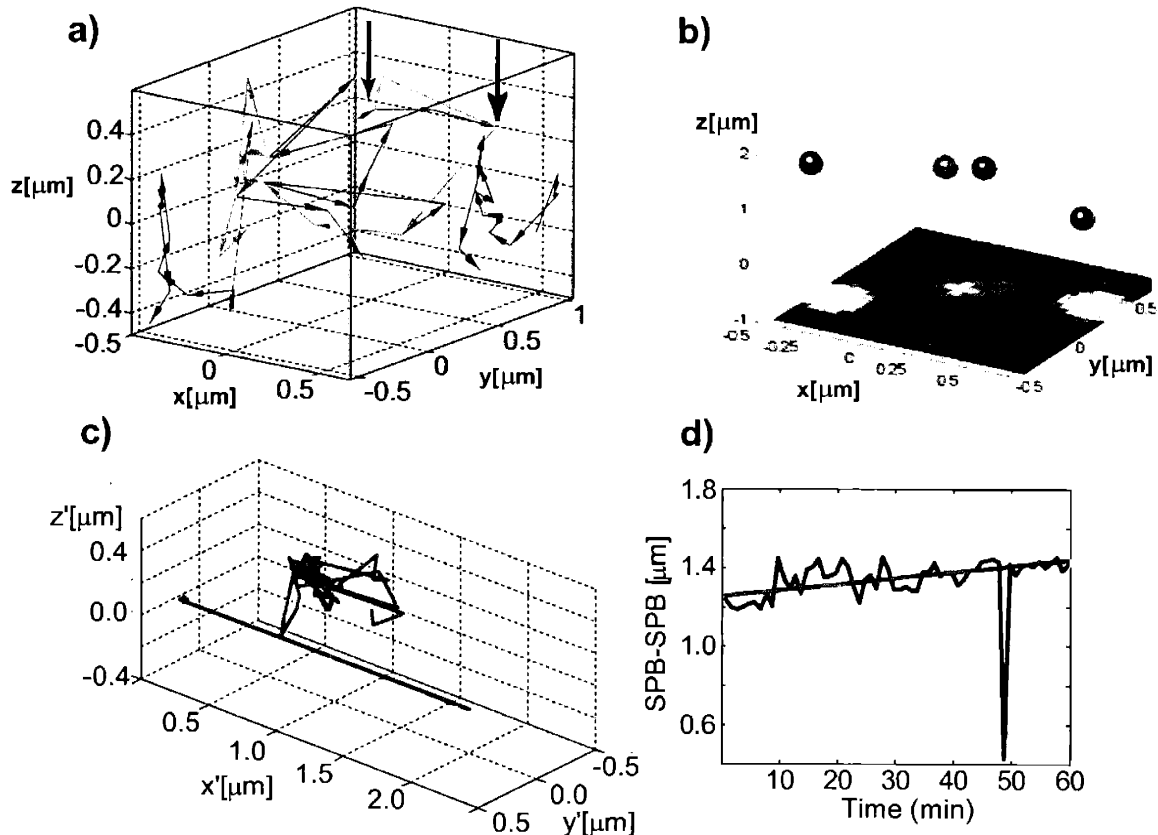


Figure 4-6. Kinetochores and SPB trajectories in 3D

Kinetochores (red, green) and SPB (blue) trajectories for a small part from a 60 frames movie. a) The trajectories are displayed in the microscope reference frame, where the movement is a superposition of i) drifts of the microscope stage; ii) whole-cell relocations in the buffer due to volume variation of the mounting gel; iii) spindle movements relative to the cell cortex and iv) kinetochores movements relative to the SPBs. The arrows indicate positions where the kinetochores separate before rejoining later again. Figure b) shows a typical example where the two kinetochores spots overlap (displayed in the maximum intensity projection). The algorithm can still estimate the positions of both tags. c) Trajectories of a different movie are shown in a reference system with a fixed SPB-SPB axis. The kinetochores remain in a small central region between the SPBs suggesting that the cell is still in metaphase. d) The SPB-SPB distance as a function of time. The SPBs move apart with a constant rate.

4.5.2 Performance on synthetic data

Before initiating large-scale biological studies in which protein function is linked to chromosome trajectories in wild-type and mutant cells, we investigated the performance of our algorithm using synthetic data. Synthetic spots mimicking the image of sub-resolution GFP tags were created using the Gibson-PSF-model (Gibson and Lanni, 1991). The parameters of the model were determined with a fit of the model to experimental data (see the “A practical 3D model for the point spread function” section). The spots were positioned in a virtual 3D image space filled with a constant background value and additive white noise was superimposed to obtain test data at a predefined SNR. To study the resolution performance and the interplay between resolution and localization accuracy we prepared model trajectories of two tags converging towards one another. For every SNR setting and point-to-point distance, 100 Monte Carlo simulations were run to accumulate statistical data on the detectability of spots and the accuracy with which they could be localized.

4.5.2.1 Resolution of tag separation

Figure 4-7a displays the resolution performance of the algorithm as a function of SNR and distance. Here, we define resolution as a statistical measure: Given a certain SNR, the resolution is determined as the tag-to-tag distance, d , at which the tag pairs can be separated with a predefined confidence. For our analysis, we chose a confidence level of 95%. For example, the graph in Figure 4-7a indicates that an SNR = 20 permits our algorithm to separate tags of a distance $d=1.9\sigma$ with 95% confidence. Consequently, the area above and to the right of the distance-SNR curve represents the ‘resolvable’ domain, while the area below

and to the left of the curve represents the ‘unresolvable’ domain. The boundary line between these domains is drawn for two cases:

- i) Equal brightness of tags, $I_1=I_2$ and
- ii) A brightness ratio 1:2, hence $I_1=2 I_2$.

As expected, the algorithm performs somewhat less well in the second case. There exists a limit below which the mixture model breaks down independent of the SNR for both cases. We did not explore this limit further and suspended our simulations for SNR values larger than 40, because values beyond this are irrelevant for biological fluorescence microscopy.

Figure 4-7b illustrates the result of the simulation for the Z-direction. Comparing the curves for XY and Z direction we find similar resolution factors (i.e. the ratio between the resolvable distance and the Gaussian parameter σ for the respective direction), this although the Gibson model includes aberration terms which mainly affect the axial (Z) direction and which are neglected by our Gaussian PSF representation. This confirms again that in practice the Gaussian PSF is sufficient to represent high-resolution and low SNR images of sub-resolution tags. Notice that the apparent difference between the simulations in a) and b) are not significant. The locus of the boundary line at a certain distance is found by adaptive adjustment of the SNR until 95 to 100% of the spots are correctly identified in 100 Monte Carlo runs. Therefore, the curve does not represent an absolute boundary but the mean position of algorithm breakdown within a certain tolerance band. The gray area underlain in Figure 4-7a) and b) indicates the width of this 5% variation band.

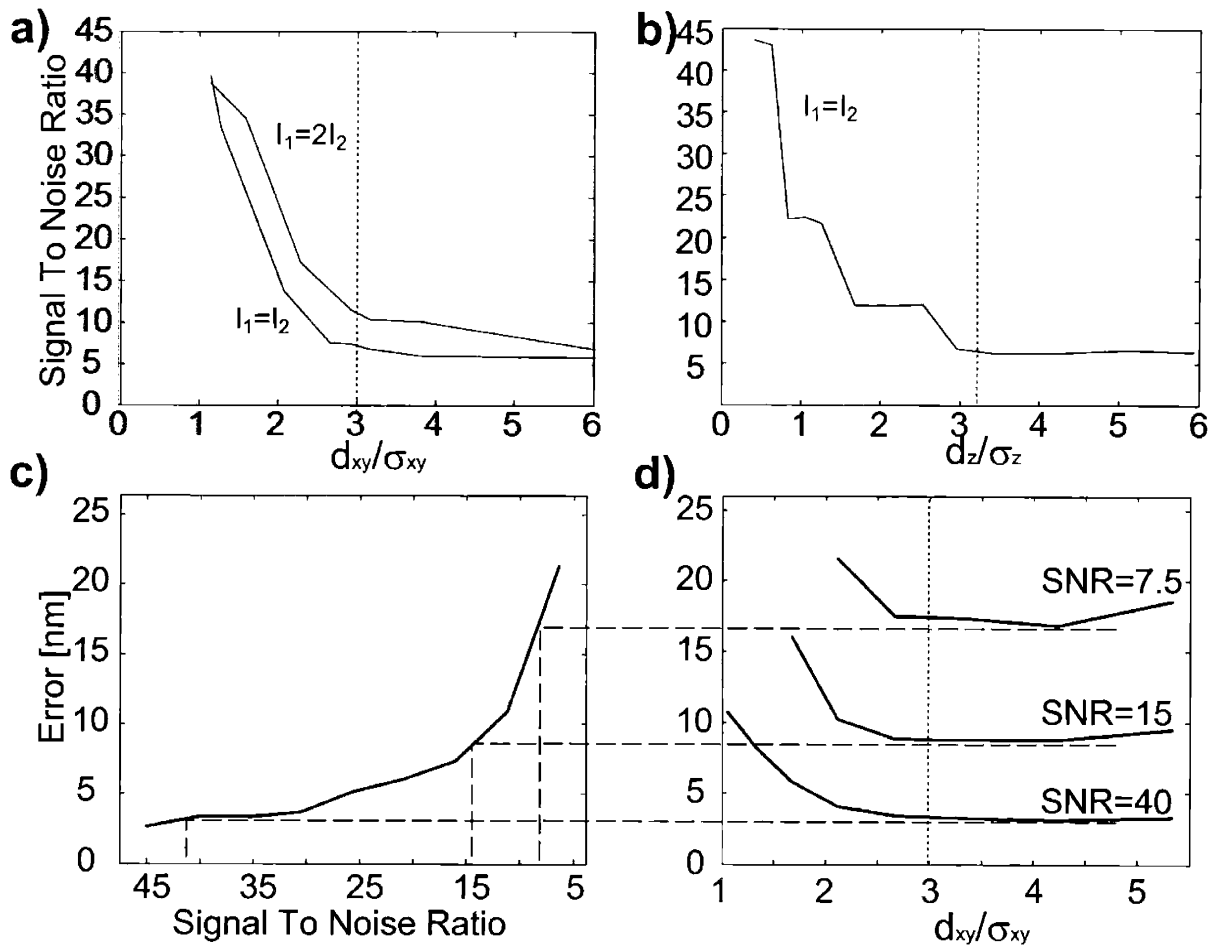


Figure 4-7. Evaluating the algorithm

Performance limits of the algorithm analyzed with synthetic data. a) Resolution as a function of SNR and the tag-to-tag distance, calculated for equally bright tags and tags with a brightness ratio 2:1. The distance is indicated as a factor of the parameter σ that characterizes the Gaussian PSF approximation. The curves display the boundary lines between the resolvable and unresolvable domains. Above the curve, spots are detected with a confidence of approx. 95%. The gray area gives an estimate for the range of confidence probability of 95-100%. b) Resolution in Z-direction for equally bright tags. The localization accuracy depends on two factors: i) The SNR. ii) The tag-to-tag distance. The accuracy is analyzed by calculating an error statistics (Equation 4-9) of 100 random experiments for each parameter setting. c) The localization error of a single spot as a function of the SNR. d) The localization error as a function of the point-to-point distance calculated for three different SNR values.

For both cases $I_1=I_2$ and $I_1=2 I_2$ we found that the algorithm can resolve tags at sub-Rayleigh distances (domain on the left side of the dashed line in Figure 4-7a). Recall that the inverse of the Rayleigh distance corresponds to approximately the cut-off frequency of the OTF. Thus, the ability to resolve sub-Rayleigh distances requires the recovery of frequencies beyond the OTF passband, indicating the super-resolution performance of the algorithm. Super-resolution is achievable for SNRs as low as 5. Interestingly, for SNR values below 5 the algorithm fails to detect the spots independent of distance. This lower limit for SNR is defined by the confidence limit controlling the switch from a single kernel to a two-kernel mixture model. Below a certain SNR, the test statistics in Equation 4-7 will never reach the quantile associated with the predefined confidence probability. Neither a single- nor a two-kernel model will accommodate the noisy signal and thus the improvement in the goodness of fit for the two-kernel model is marginal. Potentially, we could push this breakdown to lower SNR values, but only at the risk of accepting more false spots. For real data, we usually choose 90% instead of 95% confidence. The breakdown observed with real data was therefore a little lower than with the synthetic data, corresponding to an SNR of 4. For super-resolution factors larger than 2, SNR values larger than 30 are required. For the image data presented here, this is rarely achieved, yet the graph indicates the potential power of the algorithm in applications with brighter tags.

4.5.2.2 Accuracy in point localization

Not only the separation of tags but also the accuracy with which positions can be estimated is of practical interest. Positional accuracy is influenced by two factors, i) the SNR and ii) the point-to-point distance.

To address the influence of the SNR, we ran simulations on isolated spots. We define the statistical localization error as

$$err = \sqrt{\frac{1}{N} \sum_{i=1}^N |\hat{\mathbf{x}}_i - \mathbf{x}_0|^2}, \quad \text{(Equation 4-9)}$$

where $\hat{\mathbf{x}}$ is the estimated position of the tag, which is the center position of the Gaussian PSF approximation, and \mathbf{x}_0 represents the true tag position known from the simulation settings.

Figure 4-7c displays the localization error as a function of the SNR. Notice that the horizontal axis points from high to low SNR. The graph confirms the well known fact that center positions of features with a known intensity distribution, in our case the distribution of the PSF, can be determined with sub-20nm precision (Bobroff, 1986; Inoue, 1989). For $SNR > 15$ the precision even reaches the single nanometer range. Interestingly, this high precision can only be maintained for tags separated by at least the Rayleigh distance. With shorter separation distances the accuracy decreases, as suggested by the graph in Figure 4-7d (the Rayleigh limit is denoted by a dashed vertical line). An explanation for this may be found in the weaker determinability of the extent to which the two signals contribute to the super-position. Notice that in a 1D mixture model for distances larger than the Rayleigh distance, the rising edge of the mixture signal corresponds almost exclusively to the rising edge of the first kernel, while the falling edge coincides with the falling edge of the second kernel. Therefore, half of the intensity measurements in support of each kernel are uniquely associated with this kernel. Below the Rayleigh distance this is no longer true. The fitting algorithm needs to partition every intensity measurement into a contribution of the first and the second kernel. In the presence of noise, this is not unambiguous, leading to decreased accuracy in fitting.

To conclude, the performance tests on simulated data clearly demonstrate the super-resolution potential of mixture model fitting even in the case of low SNR. However, the results also show that high precision single-kernel fits cannot be maintained in the sub-Rayleigh domain. Although the spots are still separable by the algorithm, the localization accuracy drops remarkably. However, in no relevant case is there a crossover between resolution and accuracy: the minimal distance resolvable is always larger than the associated measurement error. In other words, once two tags are detected as separate, the uncertainty in the distance estimate is small enough to render the difference in the tag coordinates statistically significant. This represents a condition imperative for any further statistical analysis of tag positions.

4.6 Discussion

In this paper, we report a generic algorithm for automated fluorescent tag detection with super-resolution. Both the possibility of attaining resolution beyond the diffraction limited passband of a microscope as well as methods for efficient and unsupervised spot detection by computer vision have been discussed. The novelty of our contribution is in the rigorous extension of such methods to 3D, where manual measurements are especially cumbersome. Furthermore, we demonstrate the performance not only on synthetic data but also on a relevant set of biological data in which distance measurements below the conventional resolution limit are required.

4.6.1 Biological Applications

In the immediate future, the primary biological application of the methods described in this paper is automated motion analysis of GFP-tagged chromatids during yeast mitosis. We plan

to exploit our algorithm to perform systematic cell-based analysis of proteins involved in force generation by kinetochore-microtubule attachments. For every genetically modified yeast strain tens of movies, representing several GByte of image data, will be collected and processed automatically to generate information on chromosome trajectories. We aim then to extract principal motion components from the trajectories and compare trajectories among wild-type and 50 to 100 mutant yeast strains. To achieve the high-throughput necessary for this analysis, a large degree of automation is imperative, and the chromosome tracking software must perform reliably without the supervision of an operator. Furthermore, for robust principal component analysis by statistical means the generation of outliers must be reduced to an absolute minimum. Thus, the segmentation and tracking algorithms we have built are tuned with conservative thresholds and high confidence levels. Our philosophy is that it is better to miss some details of a trajectory than to introduce erroneous positional information on artifactual spots. Importantly, despite the conservative nature of our approach we show in this paper that sister chromatid separation can be detected at distances as small as 100nm laterally and 200nm vertically. This corresponds to a super-resolution factor of better than 2 in both directions.

4.6.2 Performance of the Algorithm

Using synthetic data, we have rigorously tested the performance of our algorithm. We can report the following findings (see also Sec. 4.5.2):

1. Tags of approximately equal brightness can be distinguished at a distance two times lower than the Rayleigh criterion. The actual limit of our algorithm is governed by the SNR. For $\text{SNR} > 20$ the resolution can be pushed to a factor 3. With biological samples such SNR is rarely obtained and a super-resolution factor of 2 is typical. For

SNR < 5 the algorithm breaks down completely. The breakdown level is governed by the confidence probability applied to statistical tests. In some cases with real data we have lowered the confidence to make it possible to process data with an SNR below 5. However, this can only be done at the risk of detecting a higher percentage of false spots. Also, the system is susceptible to differences in tag brightness. For a brightness ratio 2:1 one can lose up to 50% of the super-resolution performance.

2. The localization accuracy for isolated spots is in the single nanometer range for SNR > 20 and 10 – 20 nm for the range $5 < \text{SNR} < 20$. Interestingly, this accuracy cannot be maintained for tag pairs separated by less than the Rayleigh distance. This arises because of the intimate relationship between resolution and accuracy. The smaller the resolvable distance is the less accurate the estimate of position. However, for relevant SNR values there is no cross-over between resolution and accuracy, consequently the shortest distance resolvable will always be several times larger than the uncertainty of the distance estimate. This is a condition necessary for any further processing of point-to-point distances.

The central component of our algorithm is a routine that fits a mixture model with multiple PSF kernels to clusters of features potentially corresponding to overlapping spots. The exact number of kernels to use is determined in a statistical test. We weigh the significance of an improvement in the goodness of fit of a mixture model containing more kernels against the lower degree of freedom, and hence greater robustness, of a mixture model with fewer kernels. Ideally, the statistical test will pick a mixture model with the smallest number of kernels necessary to represent all significant components of the data. The test we apply in Equation 4-7 tends to lose sensitivity with an increasing number of kernels and with larger

sets of input data, i.e. larger image volumes treated with one mixture model. This behavior is in agreement with our paradigm of conservatism. For example, to add a fifth kernel to a four-kernel mixture model will require much more evidence in the data than to add a third kernel to a two-kernel model. The flipside of this behavior is the demand that the amount of input data is kept as small as possible. In principle, one could fit a mixture model to the entire 3D stack and simultaneously fit all significant local maxima plus potential partner spots, no matter if all kernels in the mixture model are mutually overlapped. This would simplify the algorithm in that there would be no need to group local maxima in clusters prior to mixture model fitting (see Sec. 3.4.). However, the chance that the software would correctly find multiple spots underneath one of the local maxima would be dramatically diminished. The χ^2 -statistics for testing an n -order model against an $(n+1)$ -order model would be extracted from the residuals in all voxels of the stack. Consequently, the majority of tested residuals would originate from data that is not affected at all by an increment in the order of the model. Local improvements in the model arising from the addition of a supplemental kernel would be considered insignificant compared to the overall fitting quality. To circumvent this problem, we apply mixture model fitting to small clusters of spots, where only kernels are embraced in one mixture model that do indeed overlap.

Despite the strengths of our current mixture model method, we believe that we have not yet arrived at the ultimate limit of resolution for spot detection problems. In a completely different application, we have recently shown in theory and in practice that dynamic processing can increase super-resolution performance (Danuser, 2001). Using the concept of information theory, we have proven that the simple assumption that two objects move relative to one another is sufficient prior knowledge to improve the resolution by a factor 2.

In the analysis of yeast chromosome dynamics we should be able to adopt this concept as follows: Starting with a frame in which 4 tags can be localized using the static data processing scheme described in the paper, spots will be tracked differentially forward and backward in time into frames of the movie in which only three spots can be detected. This differential tracking will be supplemented by the prior knowledge that the number of actual objects – and thus the number of tags – is preserved over time. Supposing this, one can seek the optimal parameters, including tag displacement and intensity changes, of a function that maps two of the originally four spots into one merged spot. Such differential tracking is not only expected to improve the resolution but carries the advantage of directly providing chromosome trajectories rather than generating a list of unconnected tag coordinates. In addition, differential tracking allows one to account for currently neglected, complex effects such as the mechanical deformation of tags between frames.

4.7 Acknowledgements

The authors acknowledge support from the Swiss National Science Foundation (grant No. 21-59452.99 to G.D.) and from NIH (grant No. GM51464 to P.K.S.)

4.8 References

- Bevington, P. R., and Robinson, D. K. (1992). *Data Reduction and Error Analysis for the Physical Sciences* (New York, McGraw-Hill).
- Bobroff, N. (1986). Position Measurement with a Resolution and Noise-Limited Instrument. *Review of Scientific Instruments* 57, 1152-1157.
- Bornfleth, S., Tzler, Eils, and Cremer (1998). High-precision distance measurements and volume-conserving segmentation of objects near and below the resolution limit in three-dimensional confocal fluorescence microscopy. *J Microsc* 189, 118-136.
- Bornfleth, H., Edelmann, P., Zink, D., Cremer, T., and Cremer, C. (1999). Quantitative motion analysis of subchromosomal foci in living cells using four-dimensional microscopy. *Biophys J* 77, 2871-2886.
- Bullitt, E., Rout, M. P., Kilmartin, J. V., and Akey, C. W. (1997). The yeast spindle pole body is assembled around a central crystal of Spc42p. *Cell* 89, 1077-1086.
- Carrington, W. A., Lynch, R. M., Moore, E. D., Isenberg, G., Fogarty, K. E., and Fay, F. S. (1995). Superresolution three-dimensional images of fluorescence in cells with minimal light exposure. *Science* 268, 1483-1487.
- Cheezum, M. K., Walker, W. F., and Guilford, W. H. (2001). Quantitative comparison of algorithms for tracking single fluorescent particles. *Biophys J* 81, 2378-2388.
- Coleman, T. F., and Li, Y. Y. (1994). On the Convergence of Reflective Newton Methods for Large-Scale Nonlinear Minimization Subject to Bounds. *Mathematical Programming* 67, 198-224.
- Coleman, T. F., and Li, Y. Y. (1996). An interior trust region approach for nonlinear minimization subject to bounds. *Siam Journal on Optimization* 6, 418-445.
- Danuser, G. (2001). Super-resolution microscopy using normal flow decoding and geometric constraints. *J Microsc* 204, 136-149.
- Gibson, S. F., and Lanni, F. (1991). Experimental Test of an Analytical Model of Aberration in an Oil-Immersion Objective Lens Used in 3-Dimensional Light-Microscopy. *Journal of the Optical Society of America* 8, 1601-1613.
- Goshima, G., and Yanagida, M. (2000). Establishing biorientation occurs with precocious separation of the sister kinetochores, but not the arms, in the early spindle of budding yeast. *Cell* 100, 619-633.

Gustafsson, M. G. (1999). Extended resolution fluorescence microscopy. *Curr Opin Struct Biol* 9, 627-634.

He, X., Asthana, S., and Sorger, P. K. (2000). Transient sister chromatid separation and elastic deformation of chromosomes during mitosis in budding yeast. *Cell* 101, 763-775.

He, X., Rines, D. R., Espelin, C. W., and Sorger, P. K. (2001). Molecular analysis of kinetochore-microtubule attachment in budding yeast. *Cell* 106, 195-206.

Inoue, S. (1989). *Method in Cell Biology*, Academic Press, Inc.).

Inoue, S. (1995). *Handbook of Optics*, McGraw-Hill, Inc.).

Klar, T. A., Jakobs, S., Dyba, M., Egner, A., and Hell, S. W. (2000). Fluorescence microscopy with diffraction resolution barrier broken by stimulated emission. *Proc Natl Acad Sci U S A* 97, 8206-8210.

Netten, H., Young, I. T., van Vliet, L. J., Tanke, H. J., Vrolijk, H., and Sloos, W. C. (1997). FISH and chips: automation of fluorescent dot counting in interphase cell nuclei. *Cytometry* 28, 1-10.

Pask, C. (1975). Simple optical theory of super-resolution. *Journal of the Optical Society of America* 66, 68-70.

Rines, D. R., He, X., and Sorger, P. K. (2002). Quantitative microscopy of green fluorescent protein-labeled yeast. *Methods Enzymol* 351, 16-34.

Santos, A., and Young, I. T. (2000). Model-based resolution: applying the theory in quantitative microscopy. *Applied Optics* 39, 2948-2958.

Sharp, D. J., Rogers, G. C., and Scholey, J. M. (2000). Microtubule motors in mitosis. *Nature* 407, 41-47.

Sullivan, K. F. (2001). A solid foundation: functional specialization of centromeric chromatin. *Curr Opin Genet Dev* 11, 182-188.

Tanaka, T., Fuchs, J., Loidl, J., and Nasmyth, K. (2000). Cohesin ensures bipolar attachment of microtubules to sister centromeres and resists their precocious separation. *Nat Cell Biol* 2, 492-499.

Thompson, R. E., Larson, D. R., and Webb, W. W. (2002). Precise nanometer localization analysis for individual fluorescent probes. *Biophys J* 82, 2775-2783.

Yang, Z. R., and Zwolinski, M. (2001). Mutual information theory for adaptive mixture models. *IEEE Transactions on Pattern Analysis and Machine Intelligence* 23, 396-403.

CHAPTER 5

The work presented in this chapter is now being completed and prepared for publication. These experiments have been performed in collaboration with a previous member of the Sorger lab, Rebecca Charnas. Spot tracking algorithms and spot identification tools were developed by Dominik Thomann and Jonas Dorn as part of an ongoing collaboration between the Danuser and Sorger labs. Their software tools were used for the distance analysis shown in Figure 5-1 and 5-2. Rebecca performed the initial kinetic experiments on G1 cells and Figures 5-1E, 5-3, 5-4 and 5-5 are reproduced from her Master's Thesis.

Analyzing the Role of Kinetochores Proteins on Monopolar Chromosome Dynamics in *S. cerevisiae*

5.1	Introduction.....	176
5.2	Methods.....	179
5.2.1	Strain preparation.....	179
5.2.2	Microscopy	180
5.2.3	Data analysis	181
5.3	Results.....	182
5.3.1	Comparing the kinetics of <i>ndc10-1</i> dependent chromosome-microtubule attachment in G1	182
5.3.2	Dam1p and Stu2p control kinetics of chromosome motion.....	187
5.3.3	Anaphase Chromosome Dynamics	192
5.3.4	Telophase Chromosome Dynamics	194
5.3.5	Chromosomes maintain kinetochore-MT attachment in G1 in <i>ndc80-1</i>	196
5.4	Discussion.....	199
5.4.1	The molecular basis of cell-cycle changes in kinetochore-microtubule attachment	199
5.4.2	Kinetochore MAPs regulate changes in chromosome dynamics.....	201
5.5	References.....	204

5.1 Introduction

Chromosome segregation involves a complex series of movements back and forth along the microtubules (MTs) of the mitotic spindle. The attachment of sister chromatids to MTs is mediated by kinetochores, specialized DNA-protein complexes that assemble on centromeric DNA (reviewed in McAinsh A, Tytell J and Sorger PK, 2003 *in press*). For chromosomes to be correctly segregated into two equal sets, it is essential that all kinetochores achieve bipolar attachment prior to the dissolution of sister cohesion at the onset of anaphase. Bipolar attachment occurs when one kinetochore binds to MTs emanating from one spindle pole and the sister kinetochore binds to MTs emanating from the opposite pole. The attachment of all kinetochores to MTs is a stochastic process that is monitored by a surveillance mechanism, known as the mitotic spindle assembly checkpoint (Hoyt et al., 1991; Li and Murray, 1991). Until attachment is made by all sister kinetochores, the checkpoint delays the onset of anaphase. Errors in kinetochore function or signaling during metaphase can lead to missegregation of sister chromatids and aneuploidy.

The spindle experiences an ordered series of structural changes during cell division. Budding yeast maintains a simple bipolar spindle and undergoes a closed mitosis in which the spindle pole bodies (SPBs) remain embedded in the nuclear envelope throughout the cell cycle. The SPBs are the yeast equivalent of the vertebrate microtubule organizing center (MTOC) and are responsible for nucleating all MTs. In G₁, a short linear array of MTs emanates from the unduplicated SPB. In late G₁/early S-phase, the spindle pole body undergoes duplication. The two SPBs, each with a complete set of microtubules, remain side-by-side, connected by a bridge structure (reviewed in Adams and Kilmartin, 2000). During prometaphase and metaphase the bipolar spindle elongates steadily, achieving a length of

approximately 2 μm prior to the onset of sister separation and the start of anaphase spindle elongation.

Budding yeast contain two classes of intranuclear MTs: those that bind to kinetochores (k-MTs) and those that project into the spindle midzone to overlap with MTs from the other pole (p-MTs). Each of the 16 centromeres in *S. cerevisiae* binds to a single MT so that the mature yeast spindle contains 32 k-MTs and 5–8 p-MTs (O'Toole et al., 1999). *S. cerevisiae* does not establish a traditional metaphase plate in which centromeres line up at the center of the spindle. Instead, centromeres are distributed on average in two lobes lying on either side of the spindle midzone (Goshima and Yanagida, 2000; He et al., 2000). The bilobed pattern arises from the overlap of 32 centromeres moving back and forth on the spindle and therefore changes subtly on a time scale of seconds. Proteins localized exclusively to kinetochores exhibit this fluctuating bilobed distribution (He et al., 2001).

Eukaryotic cells use two primary mechanisms to generate the force required to move chromosomes: the ATP-dependent sliding of molecular motor proteins along MTs (reviewed in McIntosh et al., 2002); and the GTP-dependent growth and shrinkage of microtubules regulated by microtubule associated proteins (MAPs). Forces can be generated at the plus-ends of k-MTs embedded in the kinetochore, at the minus ends of MTs anchored to the SPBs (microtubule flux) (Waters et al., 1996), or through the interaction of p-MTs with chromosome arms (polar ejection force) (Rieder and Salmon, 1994). The relative importance of these different mechanisms appears to vary considerably in different cell types. In the budding yeast, neither microtubule flux nor polar ejection force has been observed (Maddox et al., 2000; O'Toole et al., 1999); thus the interface between the kinetochore and the plus-ends of microtubules is likely to be the primary locus of force generation. However, we still

know very little about how kinetochores bind to microtubules or how the forces required for chromosome movement are generated.

It has recently been reported that centromeres in budding yeast cluster to a region near the SPB throughout interphase. Jin *et al.* used fluorescence *in situ* hybridization (FISH) and indirect immunofluorescence to show that centromeric clustering is reduced in the presence of the microtubule poison nocodazole and in a mutant that disrupts kinetochore structure (Jin *et al.*, 2000). This clustering during interphase suggests that, unlike animal cells, yeast kinetochores do not normally lose attachment to the MTs after mitosis. Moreover, the monopolar kinetochore-MT attachment creates a unique opportunity to study the role of kinetochore proteins in coupling MT force generation to chromosome motion. The absence of a second MT pulling in the opposite direction presents a more simplified mechanical system and reduces the number of competing forces on chromosomes.

To investigate the potential role of kinetochore proteins on the regulation of MT dependent force generation on chromosomes, we have used three-dimensional time-lapse microscopy combined with yeast strains possessing single fluorescent GFP chromosome tags (Ciosk *et al.*, 1998; Straight *et al.*, 1996). By comparing the kinetics of GFP-tagged chromosome motion in both wild-type and kinetochore mutant strains *in vivo*, we have examined the role of the Dam1p and Stu2p kinetochore proteins with respect to regulating directional instability. These proteins are known MAPs that have been previously demonstrated to interact with the kinetochore in budding yeast (Cheeseman *et al.*, 2001; He *et al.*, 2001). Additionally, our analysis of a conditional mutation in the essential kinetochore protein, *ndc80-1*, provides evidence that different subsets of kinetochore proteins are required for kinetochore-MT attachment at different phases of the cell cycle.

5.2 Methods

5.2.1 Strain preparation

All yeast strains used in this study were haploid and derived from S288C or W303. GFP tagged chromosome and SPBs were used to study chromosome dynamics in living yeast cells throughout the cell cycle. As described previously He et al., 2000, a tandem array of TetO repeats was integrated 2 kb away from CENIV in cells expressing GFP-tagged TetR and GFP-tagged Spc42p, a core SPB component. This generates cells in which CENIV proximal chromatin and the inner plaque of the SPB are marked by diffraction-limited fluorescent spots and allows chromosome motion to be tracked relative to the SPBs and the spindle axis.

Yeast cultures were prepared for live-cell microscopy using the methods described in Rines et al., 2002. In brief, cultures were grown at room temperature (RT) to mid-log phase in selective synthetic medium (SD-Ura) supplemented with 20 μ g/ml adenine and 2% glucose. The medium was refreshed prior to imaging. Synthetic media was used to minimize autofluorescence. Temperature sensitive mutants were shifted to 37°C 1 hour prior to imaging. The temperature shifts were done directly on the microscopy stage using a slide mount/objective color temperature control system (Bioptechs, Inc.). In the studies on the effects of nocodazole, cells were grown in YPD media at RT and 25 μ g/ml nocodazole was added 15 min prior to imaging. To arrest cells in α -factor, cultures were grown for 2 hrs at RT in media containing 5 μ g/ml α -factor.

5.2.2 *Microscopy*

Live-cell mounts were prepared essentially as described Rines et al., 2002. 1 ml of log phase cell culture was pelleted and resuspended in 0.05-0.10 ml of medium (a short spin of 8 sec appeared to minimize crushing of the cells). 2.1 μ l of the resuspended culture was spotted on a dust free slide, and covered with a cleaned 22x22 mm No 1.5 coverglass. A fine band of pure petroleum jelly was applied to the extreme edges of the coverglass to prevent the rapid evaporation of the media and create a better seal. Clear nail polish was used to seal the coverglass to the slide.

Live-cell imaging was performed using a Deltavision optical sectioning microscope (Applied Precision, Issaquah, WA) on a Nikon TE200 base with a 100 \times /1.4 NA objective and Roper RTE camera (Applied Precision, Inc. Issaquah, WA.) 3D image stacks consisting of 20 optical slices with exposures ranging from 0.02-0.08 milliseconds and separated by 0.25 μ m were recorded every 2-5 seconds to generate 3D movies. A neutral density filter of 0.3 or 0.5 OD units was used to minimize photobleaching and phototoxicity. 50-60 time points were collected for each movie. A custom build heated stage and a Bioptechs (Butler, PA) objective cooling/heating collar were used to maintain the temperature at 30 $^{\circ}$ C or 37 $^{\circ}$ C. The fluorescent filters used for live-cell imaging were EFP Chroma 41017 and Endow GFP Bandpass set.

Time-lapse images of live-cells were obtained by three-dimensional optical sectioning microscopy followed by 3D super-resolution spot detection on a Deltavision microscope (Thomann, et al., 2002). 5-7 minute movies were collected with sampling rates of 2-5 sec. The center of the fluorescent spots were located by automated spot detection of live-cell movies and allows chromosome motion to be tracked relative to the SPBs to within

75 nm in the X/Y-plane and 250 nm in the Z-direction (Rines et al., 2002; Thomann et al., 2002; Thomann, *et. al.*, 2003 *in press*); distances, velocities, and other parameters were calculated from the positional information.

To avoid factoring into our calculations non-kinetochore mediated motion caused by drift or rotational movement of the nucleus during interphase, we measured the distance between the Spc42p-GFP spot and CENIV-GFP spot and performed diffusional analysis based on the methods of Marshall et al., 1997. Metaphase and anaphase chromosome movements were measured quantitatively relative to the spindle, transforming the XYZ Cartesian coordinates of the microscope stage to a spindle centered coordinate system with the spindle axis as the reference frame (He et al., 2000).

5.2.3 Data analysis

All data analysis was performed using custom tools developed in the MATLAB programming environment. MATLAB analysis programs were written to automatically detect and transform the position of chromosome tag to a SPB-centered spherical reference frame (Thomann et al., 2002). The XYZ coordinates of the SPB were subtracted from the XYZ coordinates of the chromosome tag at each time point to generate the relative position of the chromosome tag; this relative position was converted to spherical coordinates, in which the radial distance (R) corresponds to the CENIV-SPB distance. MATLAB and Microsoft Excel graphing tools were used to create the CENIV-SPB distribution graphs with Gaussian curve overlays and the three-dimensional scatter plots.

5.3 Results

5.3.1 Comparing the kinetics of *ndc10-1* mutant dependent chromosome-microtubule attachment in G1

As a first step in our study of interphase chromosome dynamics, we wanted to confirm in live-cells that G1 chromosomes are attached to the SPB via the kinetochore. *In vivo* chromosome dynamics were evaluated during interphase in wild-type and cells containing *ndc10-1*, a temperature sensitive mutation in a core-kinetochore complex (Goh and Kilmartin, 1993). The linear distance between the fluorescent spots were compared in a time-dependent manner from 10 to 20 live cells of each genetic background (Figure 5-1). In normal cells, the average distance between the CEN-GFP spot and Spc42p-GFP, a core component of the inner SPB plaque, was 0.62 μm with $\sigma = 0.35 \mu\text{m}$ (Figure 5-1A). On closer inspection, it was also noted that the CEN-SPB distance in any one cell changed relatively little during the course of the movie. Based on 720 time-points the average velocity was determined to be 0.01 $\mu\text{m}/\text{sec}$ with a maximum velocity of 0.10 $\mu\text{m}/\text{sec}$. Wild-type cells demonstrate similar kinetics at both 30 °C and 37 °C. In *ndc10-1* cells, however, we observed that the average CEN-SPB distance increased to 1.48 μm with $\sigma = 0.43 \mu\text{m}$ (Figure 5-1B). The average velocity also increased to 0.04 $\mu\text{m}/\text{sec}$. and had a maximum velocity of 0.36 $\mu\text{m}/\text{sec}$. (n = 612 time-points).

To ascertain the diffusional properties of the centromeric DNA region in the nucleus at 37 °C, we calculated the mean squared distance between the two spots over time based on the methods described in Marshall et al., 1997. From the relationship between the average change in the SPB-CEN distance d and the length of the time interval Δt , we computed the mean squared change in $d(t)$ as $\langle \Delta d^2 \rangle = \langle [d(t) - d(t + \Delta t)]^2 \rangle$. For two unconstrained

particles undergoing 3D random walks, the distance between them should increase linearly ({von Smoluchowski, 1917}). However, in the case of the yeast nucleus, linear diffusion would only be anticipated initially. If two proximal objects are diffusing unconstrained in a large volume, on average, the two objects will continue to move away from each other in a linear fashion proportional to their diffusion constants. However, two proximal objects in an enclosed nucleus (e.g., CEN and SPB), can only reach a maximum distance up to the diameter of nucleus, thus maintaining an overall constraint on diffusion proportional to the size of the nucleus. Therefore the $\langle \Delta d^2 \rangle$ becomes independent of Δt and the plots will plateau, indicating a restriction on diffusion (e.g., nuclear envelope).

In the case of wild-type interphase cells, the chromosome GFP spot is closely constrained to the SPB-GFP spot. Conversely, the $\langle \Delta d^2 \rangle$ of the CEN-GFP spot in *ndc10-1*, shows a highly diffuse pattern and suggests that the spots are only constrained by the nuclear envelope and not by a tethering mechanism (Figure 5-1C). This phenomenon is easier to visualize when we compare 3D scatter plots of the time-dependent positions centered about the SPB (Figure 5-1D). In this way, the diffusion is represented by highly distributed pattern.

To provide independent confirmation that this attachment is mediated by microtubules, we investigated the effects of the microtubule depolymerizing drug nocodazole on centromere proximal chromosome motion. If kinetochores are not attached to microtubules, then nocodazole should not affect the motion of the chromosome tag. However, if the kinetochores are attached to microtubules, we would expect to see a change in chromosome dynamics in the presence of nocodazole. Two possible changes can be imagined. One possibility is that when microtubules depolymerize in the presence of nocodazole, kinetochores detach; in this case, chromosome dynamics in nocodazole-treated

cells should phenocopy *ndc10-1* cells. Alternatively, the kinetochore could remain attached to the destabilized microtubules, in which case nocodazole treatment should shorten the observed CEN-SPB distance.

We added nocodazole to asynchronous cultures growing in YPD and imaged G1 cells after 15 minutes incubation. The results were striking. In nearly 100% of the G1 cells, the chromosome tag collapsed next to the SPB. Based on 2-D projections of chromosome movement relative to the SPB suggests the average CEN-SPB distance in nocodazole treated cells was $0.26 \pm 0.15 \mu\text{m}$ (Figure 5-1E). These findings further support the conclusion that chromosomes remain attached to the SPB during G1 in an Ndc10p dependent manner as previously suggested by Jin et al., 2000. Furthermore, these results show that nocodazole-destabilized microtubules do not necessarily lose their attachment to kinetochores. On-going studies in our lab on the effects of nocodazole suggest that there may only be a small window during S-phase when nocodazole treatment causes kinetochores to detach from microtubules (data not shown).

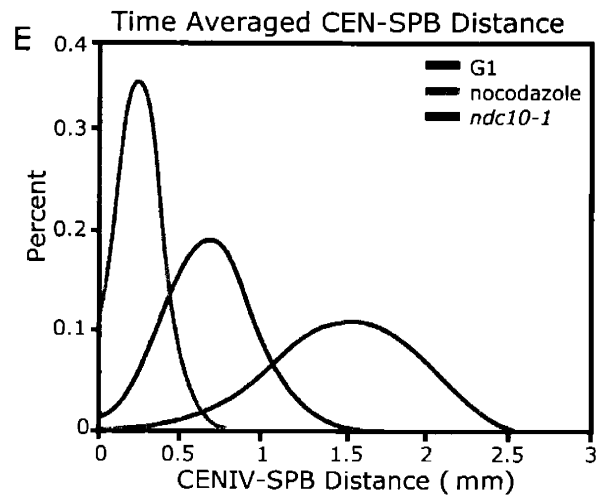
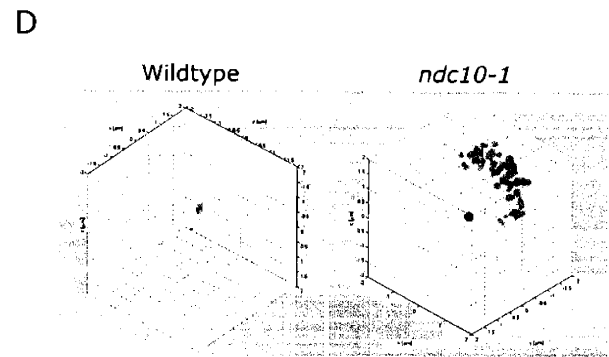
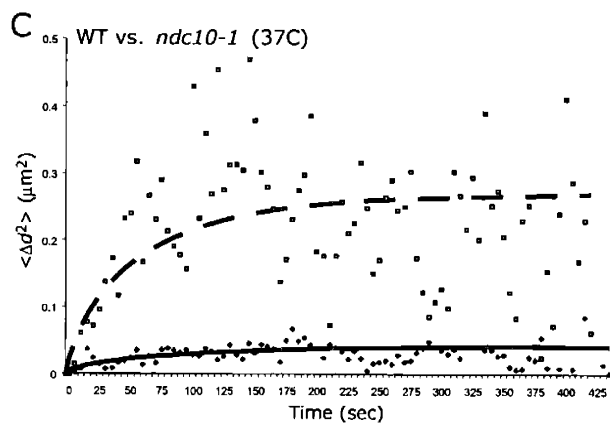
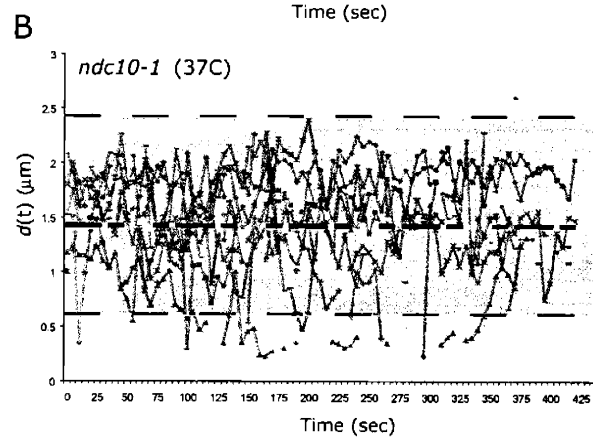
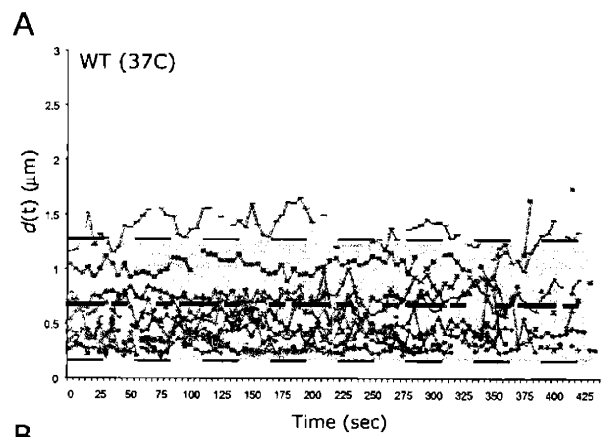


Figure 5-1. Analysis of chromosome motion in interphase cells.

Comparison of chromosome movement in living yeast cells. (A) Typical data record obtained by super-resolution spot tracking (Thomann et al., 2002), showing a plot of the distance $d(t)$ against t , between the GFP-tagged SPB and the GFP-tagged chromosome CEN. Over time the three-dimensional distance between the two spots increases and decreases, shown are the traces of 10 – 20 traces from wild-type cells maintained at 37 °C. The gray box represents a 2σ distribution of distances between spots with respect to time. The black dashed line in the middle of the gray box marks the average distance between spots for all timepoints in all cells. (B) Same as described in part (A), except data is recorded from *ndc10-1* at restrictive temperature (37 °C). Traces demonstrate large changes in displacement and higher velocities than seen in wild-type cells. (C) Overall mean-squared change in distance between GFP spot $\langle \Delta d^2 \rangle$ plotted against elapsed time interval Δt between distance measurements (5 seconds between each time point). Solid circles represent the average of all data collected for each time point from wild-type cells and *ndc10-1* cells (hollow boxes). The lines represent the best-fit curves of the data. Wild-type mean square change is small compared to *ndc10-1* suggesting that in *ndc10-1* cells chromosome diffuse in a much larger region. (D) The 3D distribution of CEN-SPB displacement for WT and *ndc10-1* G1 cells (green dots) centered about a single SPB (blue dot). (E) The distance between the chromosome tag and the SPB tag was calculated at every time point for multiple movies of each strain/condition. The distances were grouped into bins of $.1\mu\text{m}$ to generate the frequency distribution. The distributions were roughly Gaussian, and overlaid on the histograms are Gaussian models of the distributions, using the mean (μ) and standard deviation (σ) of the CEN-SPB distances as parameters. All XYZ coordinates were determined using automated tracking with super-resolution.

5.3.2 *Dam1p* and *Stu2p* control kinetics of chromosome motion

Having confirmed that chromosomes are monopolarly attached to the SPB in G1, we examined the role that known kinetochore-MAPs might play in regulating chromosome dynamics. In our current analysis, we concentrate on changes in the radial distance between the chromosome and the SPB (CEN-SPB distance). Under restrictive conditions for cells possessing either *dam1-1* or *stu2-277* temperature sensitive mutations, we see a significant change in the CEN-SPB length as compared to wild-type cells over time (Figure 5-2).

Dam1p, a MAP that localizes to kinetochores in an Ndc80 dependent manner (He et al., 2001; Jones et al., 1999), has recently been shown to be part of a multi-protein complex that plays a role in the establishment of bipolar attachment (Cheeseman et al., 2001; He et al., 2001; Hofmann et al., 1998; Jones et al., 1999; Li et al., 2002). At the restrictive temperature, *dam1-1* metaphase cells do not achieve proper bipolar attachment; instead, both sister chromatids remain associated with a single SPB (He et al., 2001). Based on CEN-SPB distance charts, cells placed under restrictive conditions for *dam1-1* (37 C) appeared to exhibit similar patterns of chromosome motion as compared with wild-type (Figure 5-1A). However, based on closer inspection we noticed that the average CEN-SPB distance increased from 0.70 μm up to 1.10 μm . Interestingly, the average velocity for the mutant only increased to 0.02 $\mu\text{m}/\text{sec}$, with a maximum velocity of 0.15 $\mu\text{m}/\text{sec}$. The increase in average length initially suggested that some of the kinetochores might have lost attachment and so we once again performed diffusion analysis to calculate $\langle \Delta d^2 \rangle$ (Figure 5-2C). The change in mean-squared displacement does not support this conclusion and instead suggests

that the average CEN-SPB distance is greater in the absence of *Dam1p*. Thus *Dam1p* may play a role in increasing the forces exerted on the sister chromatids.

Stu2p is a member of a conserved family of MT-binding proteins and an essential protein in yeast (Wang and Huffaker, 1997). Members of this family localize to the SPB (MTOC) and spindle during mitosis. Mutations in several of the members have demonstrated improper spindle formation and chromosome missegregation (Cullen et al., 1999; Matthews et al., 1998; Nabeshima et al., 1995). Under restrictive conditions for *stu2-277*, cells demonstrate a dramatic change in CEN-SPB distances as chromosomes become more closely associated with the SPB (Figure 5-2B & D). In fact, the average CEN-SPB distance decreased to 0.60 μm with smaller velocities (average velocity 0.01 $\mu\text{m}/\text{sec}$, maximum velocity 0.10 $\mu\text{m}/\text{sec}$). We have previously observed a similar phenotype during metaphase where mitotic spindles are much shorter and chromosomes move along the spindle at slower rates (He et al., 2001).

In about 20% of the *stu2-277* cells examined under restrictive conditions in G1, we also noticed that some chromosomes appeared to completely lose kinetochore-MT attachment. When we monitored the progress of these chromosomes, we found that they exhibited phenotypes similar to *ndc10-1* cells. By comparing the diffusional properties and kinetics to wild-type (Figure 5-2E), we see a much larger distribution in the $\langle \Delta d^2 \rangle$. In these cells the average CEN-SPB distance increased to 1.70 μm with an average velocity of 0.03 $\mu\text{m}/\text{sec}$ and a maximum velocity of 0.11 $\mu\text{m}/\text{sec}$.

In a preliminary set of experiments, we have also combined either *dam1-1* with *stu2-277* or *dam1-1* with *bik1 Δ* . *Bik1p* is a plus-end MT binding protein that colocalizes with

tubulin, kinetochores and cortical attachment sites (Berlin et al., 1990; He et al., 2001).

Initial results suggest that the chromosomes become much more dynamic in the *dam1-1/stu2-277* double mutant rapidly transitioning between growth and shrinkage similar to wild-type (data not currently shown). The deletion of *bik1Δ* in a *dam1-1* background, however, further accentuated the long CEN-SPB phenotype (Figure 5-2F) as no cells were found with CEN-SPB distances less than 0.70 μm. More analysis on both strains must be completed to confirm these observations and is currently underway.

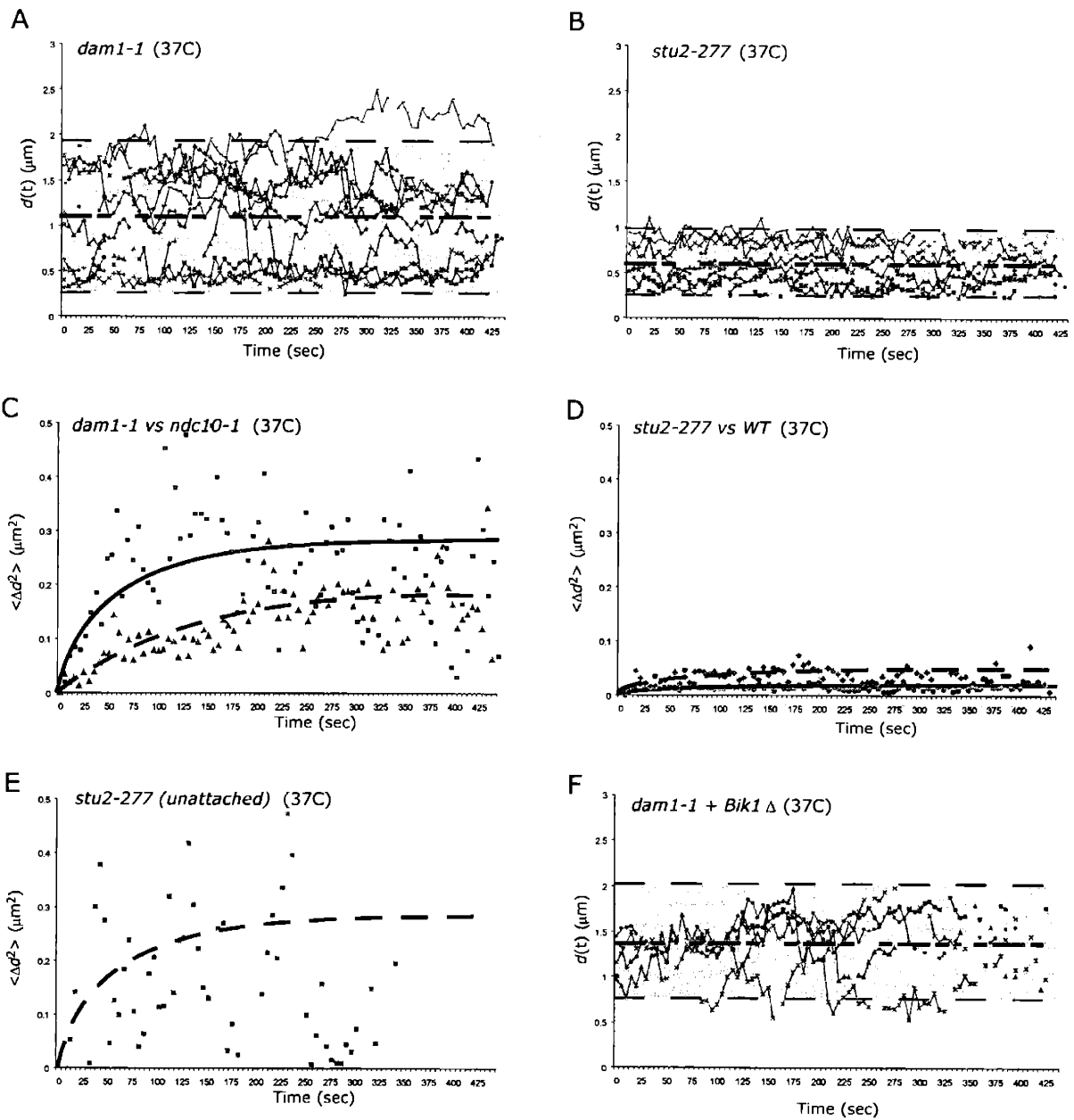


Figure 5-2. Analysis of chromosome motion in cells with mutant k-MAPs.

Similar analysis to that shown in Figure 5-1. (A) *dam1-1* temperature sensitive (ts) mutants were used to track distance between SPB-GFP and CEN-GFP tag over time. Time points were acquired every 5 sec for up to 7 mins in duration. Average distance between fluorescent tags is indicated by heavy dashed line in middle of gray box. (B) Same as part (A) except in *stu2-277* ts background. *dam1-1* cells have large distribution patterns and appear to possess both populations of large distances and a population of short distances. Conversely, *stu2-277* cells only exhibit short distance between spots suggesting a tight association between the CEN and SPB, even more so than seen in wild-type cells. (C) mean-squared displace analysis as described in Figure 5-1 comparing *dam1-1* and *stu2-277* effects on SPB-CEN behavior. As expected from data shown in (B) *stu2-277* chromosomes (circles) show very little diffusional motion. However, *dam1-1* chromosomes (triangles) demonstrate greater diffusion but to a lesser extent than seen in *ndc10-1* cells suggesting that chromosomes are more dynamic but still not detached. (D) comparing the diffusional motion of a *stu2-277* cell (squares) with what appears to be an unattached chromosome. When compared to wild-type cells (diamonds) the pattern is similar to that seen in *ndc10-1* cells and supports the possibility of loss-of-attachment in a certain number of *stu2-277* cells. (E) Preliminary comparison of *dam1-1/bik1*Δ cells.

5.3.3 *Anaphase Chromosome Dynamics*

There are several other distinct stages of the cell cycle besides G1 where chromatids are only associated with a single SPB (monopolar) including anaphase and telophase. In yeast, as in other organisms, anaphase is characterized by two types of movements: poleward movement of the kinetochores (anaphase A); and an increase in pole-to-pole distance (anaphase B). The spindle dynamics of anaphase B in yeast have been well characterized and have been shown to be biphasic. At the onset of anaphase, the metaphase spindle of approximately 2.0 μm increases rapidly to 4 - 6 μm . This rapid phase is followed by a slower growth phase in which the spindle reaches a final length of up to 11 μm (Kahana et al., 1995; Pellman et al., 1995). Using linear regression analysis of chromosome trajectory plots from 5 movies of anaphase cells, we calculated an average rapid phase spindle elongation rate of $0.01 \pm 0.01 \mu\text{m}/\text{sec}$ ($0.74 \pm 0.12 \mu\text{m}/\text{min}$) beginning at an average spindle length of $2.0 \pm 0.2 \mu\text{m}$ (Figure 5-3). These figures are in agreement with previously published data (Severin et al., 2001; Straight et al., 1998).

In contrast to anaphase B, the literature is inconsistent about the dynamics and existence of anaphase A in yeast (Guacci et al., 1997; Pearson et al., 2001; Straight et al., 1997). With our methods, we observe anaphase A movement beginning within 30 sec (-6 to +25 sec) of anaphase B (Figure 5-3). Intriguingly, in all cells observed, anaphase A movement was immediately preceded by the transient movement of the sister chromatids towards each other. In the cells we analyzed, the sisters were an average of $0.71 \pm 0.24 \mu\text{m}$ apart before anaphase A, while they were only $0.40 \pm 0.20 \mu\text{m}$ apart at the initiation of anaphase A (Table 5-1). This close association appears to be short-lived, usually lasting less than ten seconds. After briefly moving together, the sister chromatids separate rapidly

towards the poles. The rate we measured for anaphase A poleward movement of the chromosomes was quite variable ranging from 0.02 -0.10 $\mu\text{m}/\text{sec}$ (average 0.04 ± 0.03 $\mu\text{m}/\text{sec}$; 2.60 ± 1.80 $\mu\text{m}/\text{sec}$). The rapid poleward motion lasted on average only 16.0 ± 9.0 sec (5-30 sec), during which time the chromosomes traveled an average distance of 0.6 ± 0.3 μm . After this short burst of motion, the chromosomes moved at the same rate as the SPBs (0.01 ± 0.01 $\mu\text{m}/\text{sec}$) and no additional directed poleward movement could be observed; the chromosome tag remained an average of 0.33 ± 0.07 μm from its proximal SPB (Table 5-1). In contrast, during the minutes immediately preceding anaphase A, the chromosomes were on average 0.59 ± 0.16 μm from their SPB (Table 5-1).

Table 5-1. Anaphase Distances.

	pre- anaphase A [†] (μm)	at anaphase A initiation [‡] (μm)	post anaphase A [#] (μm)
CENIV-SPB	.59 \pm .16	.73 \pm .25	.33 \pm .07
CENIV-CENIV	.71 \pm .24	.40 \pm .20	--

[†] The average distance between chromosome tags or chromosome and SPB tags before the initiation of anaphase A in time-lapse movies during which cells went through anaphase. The calculations represent the averages from five movies, which began 30 sec to 5 minutes before anaphase A initiation.

[‡] The average distance between chromosome tags or chromosome and SPB tags at the initiation of anaphase A.

[#] The average distance between the chromosome and SPB tags after the conclusion of directed anaphase A motion in time-lapse movies during which cells went through anaphase. The five movies analyzed ended 3 to 5 minutes after anaphase A.

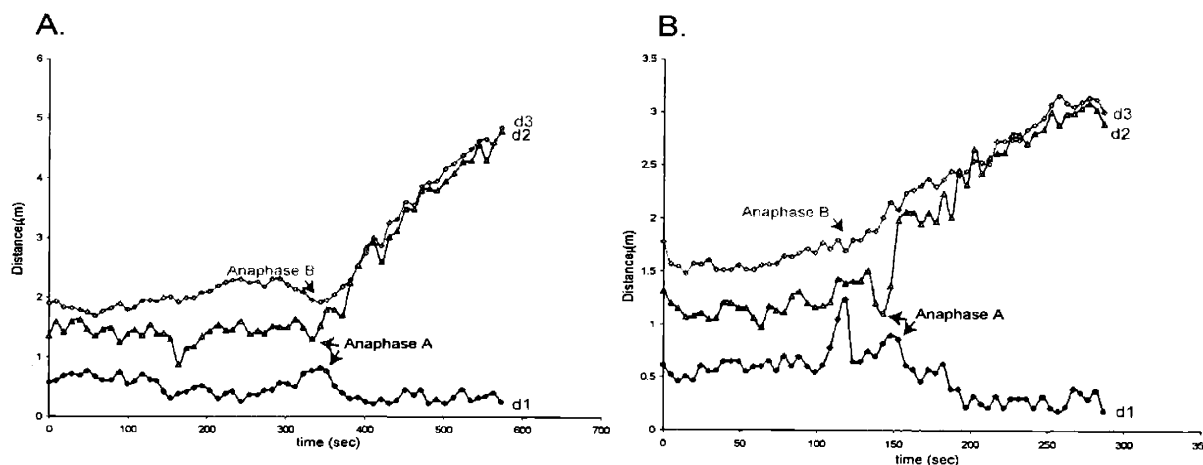


Figure 5-3. Kinetic analysis of chromosome separation during anaphase.

Anaphase chromosome dynamics. Chromosome trajectory plots of two representative anaphase cells are shown. Distance on Y-axis represent the linear distance between a reference SPB and either the other SPB (green line, spindle length) or the CEN tags on chromosome IV when paired sisters are physically pulled apart (red and blue lines). Arrows show the initiation of anaphase A and anaphase B.

5.3.4 Telophase Chromosome Dynamics

Next, we investigated chromosome dynamics during telophase. Large budded cells in which one spindle pole body and sister chromatid had moved into the daughter cell were considered to be telophase. Correctly distinguishing telophase cells from anaphase and G1 cells presented significant difficulty. To exclude late anaphase cells that had not broken down their spindle, cells in which the two chromosomes were no longer aligned with the spindle axis were chosen for analysis. Additionally, cells were sonicated immediately before being imaged. Sonication separates mother and daughter cells that have completed cytokinesis, which helped minimize classification of G1 cells as telophase. However, since we have probably incorrectly classified some G1 cells as telophase, we may be underestimating the differences between the chromosome dynamics in telophase and G1

cells. The chromosome tag was always found tightly associated with the SPB (Figure 5-4), with an average CENIV-SPB distance of $0.38 \pm 0.14 \mu\text{m}$.

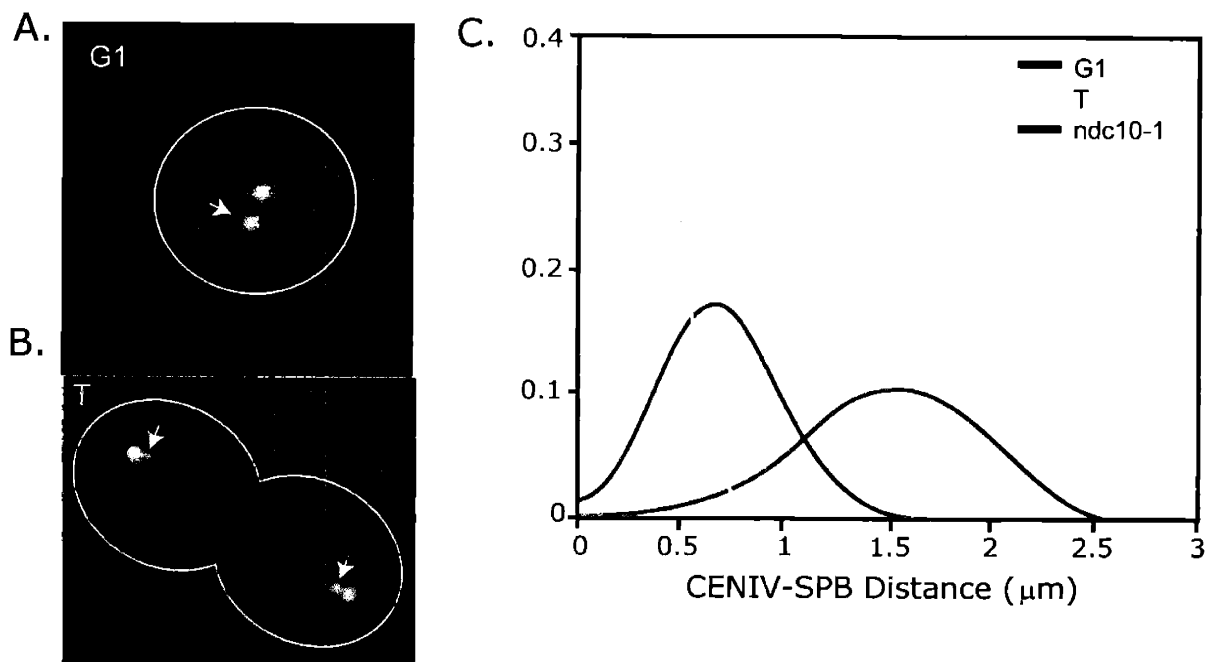


Figure 5-4. Kinetic analysis of chromosome motion during telophase.

Chromosome position during comparing G1 and Telophase. (A & B) Images of cells carrying SP42p-GFP, to mark the spindle pole bodies, and a CEN tag to mark the chromosomes at various phases of the cell cycle. Example maximum intensity projections from one time point of a time-lapse movie are shown. Arrows point to the chromosome tags. (A) G1 (B) Telophase. (C) The 2D distribution of CEN-SPB distances for wild-type G1 (blue line), and telophase (T) cells at 30°C (yellow line). The CEN-SPB distribution of G1 *ndc10-1* cells at 37°C (red line), in which the chromosome is unattached, is included as a control. The distance between the CEN tag and the SPB tag was calculated at every time point for 6-26 movies at each stage in the cell cycle. Each movie consisted of 50-60 time points, with 2-5 sec time lapses between each time point. The position of chromosome tag (colors) was determined as in Figure 5-1. The SPB (black) is at the origin.

5.3.5 Chromosomes maintain kinetochore-MT attachment in G1 in *ndc80-1*

We reasoned that the differences in chromosome behavior observed at different phases of the cell cycle likely reflected some change in MT dynamics and force generation during these stages. One especially interesting possibility is that different sets of kinetochore proteins mediate microtubule attachment at different stages of a cell cycle. Our studies of *ndc80-1* cells in G1 provide initial evidence that this is the case.

Ndc80p is a part of a conserved multi-protein complex that associates with the kinetochore. The essential complex is believed to be involved in linking DNA binding kinetochore components with microtubule binding components (He et al., 2001; Wigge and Kilmartin, 2001). Recent data suggests that the Ndc80 complex may also interact with checkpoint proteins (Gillett, E., Espelin C. and Sorger PK., personal communication). Previously, we showed that in *ndc80-1*, chromosomes become detached from microtubules during metaphase at the restrictive temperature (He et al., 2001). Initially, we planned to use an *ndc80-1* strain in our G1 studies as an additional control for unattached chromosomes. *ndc80-1* cells containing GFP tagged chromatids and SPBs were grown at a permissive temperature (23 °-25 °C), shifted to 37 °C for 1 hour prior to imaging, and imaged at 37 °C for an additional 1.5 hrs. To our surprise, in G1 cells the chromosome tag appeared to be closely associated with the SPB, while in early S-phase cells the chromosome tag was no longer preferentially associated with the SPBs.

In order to control for temperature, timing, and cell growth conditions that could affect the *ndc80-1* phenotype, G1 cells were imaged from the same slide. For every G1 cell that was imaged a S-phase cell was imaged immediately after. The experiment was also repeated on different days and with different isolates of the *ndc80-1* chromosome tagged

strain. Statistical analysis of CEN-SPB distances showed a striking difference between MT attachment during the two stages of the cell cycle. During early S phase, *ndc80-1* cells show chromosome dynamics nearly identical to those observed in *ndc10-1* cells (Figure 5-5). In contrast, *ndc80-1* cells the chromosome tag was on average 0.90 μm away from the SPB in G1, only slightly greater than the average distance observed in wild-type cells at 37 °C (Figure 5-5). In both wild-type and *ndc80-1* G1 cells the distribution of CEN-SPB lengths fit well to a Gaussian curve with a standard deviation of 0.40 μm . 3D scatter plots of chromosome position relative to the SPB confirm that, similarly to wild-type cells, the chromosome tag in *ndc80-1* cells is confined to a small region near the SPB throughout four minute movies of G1 cells (a representative scatter plot is shown in Figure 5-5). Additionally, the average relative velocity of the chromosome tag in *ndc80-1* strains during G1 was the same as for wild-type cells (Figure 5-1). From this data we conclude that chromosomes remain attached during G1 in *ndc80-1* cells. This data also suggest that Ndc80p is required for kinetochore-MT attachment during early S phase but not in G1. However, the longer CEN-SPB distance seen in *ndc80-1* cells compared to NDC80 cells suggests that although *ndc80-1* is not essential for attachment in G1 it is playing some role in regulating G1 directional instability. However, we must also investigate the *ndc80-1* allele inactivation rates during G1 to understand the role of Ndc80p in G1.

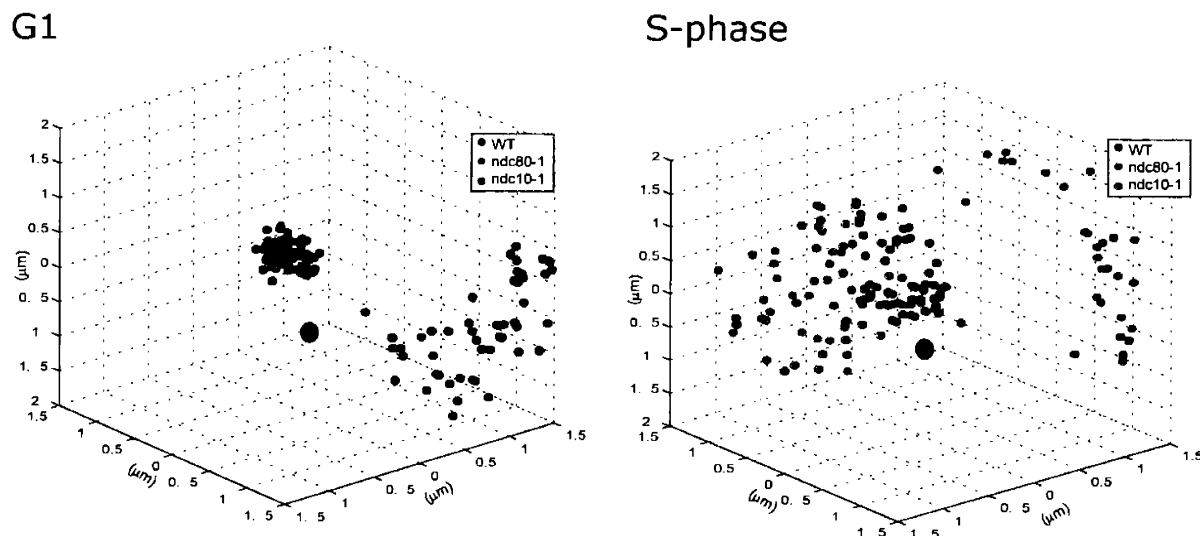


Figure 5-5. Positional analysis of chromosome motion in *ndc80-1* cells.

Three-dimensional scatter plot showing the position of CEN tag in SPB-centered reference frame with wild-type, *ndc10-1* and *ndc80-1* cells. G1 (left scatter plot) shows a tight distribution for chromosome tags in an *ndc80-1* background and shows similar properties to wild-type in contrast to *ndc10-1*. Conversely, the distribution pattern increases dramatically in S-phase and is more similar to *ndc10-1* than wild-type at this phase of the cell cycle. These data suggests that Ndc80p is not required to maintain kinetochore-MT attachment during G1 and becomes essential only after cells move into S-phase. For each strain, the range of motion over 4 minutes of a representative time-lapse movie (50 time points/movie) is shown. The position of chromosome tag (colors) in the SPB-centered reference frame was determined by subtracting the XYZ coordinates of the SPB from the XYZ coordinates of the chromosome tag at each time point. The SPB (black) is at the origin. All movies acquired at 37 °C.

5.4 Discussion

In this study, we have used rapid time-lapse imaging of budding yeast to investigate chromosome dynamics and kinetochore function at various stages of the cell cycle. By comparing the movement of a GFP-tagged chromosome in wild-type cells and mutants that lack a functional kinetochore (*ndc10-1*), we have confirmed that chromosomes remain attached to SPB during the G1 phase of the cell cycle. Improved microscopy techniques and acquisition rates ten times faster than those used in our prior studies (He et al., 2000; He et al., 2001) have allowed us to gain a more detailed and quantitative understanding of chromosome dynamics than was previously possible. We have found that significant movement can be observed in movies with 2-5 sec time lapses that has been overlooked in movies with slower sampling times. We have analyzed the chromosome dynamics of monopolar attached chromosomes at different stages of the cell cycle and in the presence of various mutant k-MAPs. Our observations suggest that Dam1p and Stu2p play opposite roles in regulating chromosome dynamics at the plus-end of k-MTs.

5.4.1 *The molecular basis of cell-cycle changes in kinetochore-microtubule attachment*

We found that Ndc80p is required for attachment in early S-phase but not in G1. This provides evidence that there is a molecular basis for the cell-cycle changes in chromosome position and dynamics. *ndc80-1* cells lack the proteins required to establish kinetochore-MT attachment during the S-phase and metaphase stages of the cell cycle. Conversely, *ndc80-1* cells still possess the ability to maintain kinetochore-MT attachment in G1. ChIP and microscopy studies of asynchronous *ndc80-1* cultures show that while the DNA binding layer remains intact, most of the known microtubule binding proteins are dissociated from the kinetochore (He et al., 2001). As would be expected, Ndc80p was previously found to be

essential for attachment in metaphase (He et al., 2001; Wigge and Kilmartin, 2001).

Therefore, the finding that Ndc80p is not required for attachment in G1 was very surprising. It raises the intriguing possibility that a much simpler kinetochore can mediate monopolar attachment in G1 than is required for bipolar attachment in metaphase. Alternatively, the *ndc80-1* allele may not be completely inactivated at 37C during G1 or the protein may only be essential for the establishment of attachment and not the maintenance of attachment.

Identifying which proteins are required for attachment in G1 will be a high priority for future studies. Of the known kinetochore microtubule binding proteins, Kip3p and Bik1p are possible candidates since they have not been shown to dissociate from the kinetochore in *ndc80-1* mutants. There may also be additional, not yet identified, kinetochore proteins or G1-specific proteins that mediate MT attachment in G1. It is also possible, however, that some of the proteins that appear to be dependent on Ndc80p in asynchronous cultures, actually remain at the kinetochore in *ndc80-1* cells during G1. Thus, it will be important to confirm the Ndc80 dependencies by CHIP or microscopy in synchronous G1 cultures.

It also remains to be determined what happens in early S-phase to cause *ndc80-1* cells to lose attachment. Although our data suggests that the chromosomes remain attached to the microtubules throughout the cell cycle, it is known that in wild-type cells the parent sister chromatid does not preferentially separate with the parent SPB (Neff and Burke, 1991). Therefore, the chromosomes must at least transiently separate from the SPBs. Most likely this transient loss of attachment occurs during centromeric replication, which happens in early S-phase (Winey and O'Toole, 2001). One explanation for our data is that Ndc80p dependent kinetochore proteins are required to reattach the sister chromatids to microtubules but not to maintain monopolar attachment. In this case, we might expect the early S-phase

loss of attachment in *ndc80-1* cells to be dependent on replication. To test this, we are currently looking at chromosome dynamics in *cdc6* mutants. *cdc6* cells are not able to replicate their DNA but nevertheless progress through the cell cycle (Zhou et al., 1989). We have recently determined that Bik1p depends on the presence of Mtw1p (McAinsh A., *personal communication*), an essential component of the kinetochore (Goshima and Yanagida, 2000), and suggests at the possibility multiple k-MAPs that function redundantly in kinetochore-MT attachment. Considering that *dam1p* mutant cells can't re-establish bipolar attachment in S-phase or metaphase and instead remain monopolarly attached, we might reason that Bik1p maintains kinetochore-MT attachment while Dam1p functions to establish new MT attachments. This line of investigation is currently being pursued more closely by comparing the chromosome-MT attachment status in *dam1-1/bik1Δ* and *ndc80-1/bik1Δ* cell lines.

5.4.2 Kinetochore MAPs regulate changes in chromosome dynamics

Our results suggest that different subsets of kinetochore proteins regulate the dynamic nature of directional instability differentially. Stu2p has previously been shown to localize to the kinetochore *in vivo* (He et al., 2001) and to localize to the end of the microtubules *in vitro* (Shirasu-Hiza et al., 2003; Van Breugel et al., 2003). Our data demonstrates that the majority of chromosomes in *stu2-277* cells demonstrate reduced chromosome dynamics where the centromere is held in close proximity to the SPB. This is in agreement with a recent study by Kosco *et. al.* showing that microtubules were fewer in number and less dynamic in G1 and pre-anaphase based on GFP-labeled tubulin (Kosco et al., 2001). The authors argue that Stu2p increases both the catastrophe and rescue frequency. When examined in light of the chromosome dynamics data we've observed, it is reasonable to argue that the chromosome

motion is coupled to MT dynamics. However, in our live-cell movies of chromosome motion, we only observe a decrease in CEN-SPB distance. Since we don't know how long it takes to inactivate *stu2-277*, it is possible that we are only observing the effects long after the proteins function has been removed. Moreover, there is also the possibility that other proteins function to destabilize the the microtubule *in vivo* and are independent of Stu2p, especially since our studies are conducted in the context of other functional MAPs. Further characterization of cells containing combinations of temperature sensitive alleles of multiple MAPs may help to elucidate this difference. Intriguingly, the presence of Stu2p at the plus-end of the MT suggests that it may play an important role in coupling MT dependent force production with chromosome segregation. This model fits well with our prior observations where during metaphase chromosomes experienced a reduction in transient separation in a *stu2-277* background under restrictive conditions.

When we examined the role of the Dam1p protein on chromosome dynamics, we observed a large difference in the CEN-SPB distances. However, when the CEN-SPB distances from *dam1-1* cells are statistically compared to wild-type CEN-SPB distances, we notice that *dam1-1* cells have a greater number of cells with large CEN-SPB distance (1.0 – 2.0 μm). Moreover when we delete the nonessential protein Bik1p from *dam1-1* cells, we notice the population of large CEN-SPB distances increases even more. The possibility that multiple k-MAPs have redundant functions in kinetochore-MT binding and polymerization regulation is an attractive concept and suggests that the relationship between multiple MT binding factors should be looked at more closely. It will be interesting to explore whether this similarity is indicative of functionally similar kinetochore proteins at different phases of the cell cycle. One possibility is that changes occur at early S-phase to make the kinetochore

competent for bipolar attachment and then persist until telophase. Why and how the kinetochore returns to its G1 state will be important questions for future studies examining potential upstream regulation of chromosome dynamics.

5.5 References

- Adams, I. R., and Kilmartin, J. V. (2000). Spindle pole body duplication: a model for centrosome duplication? *Trends Cell Biol* 10, 329-335.
- Berlin, V., Styles, C. A., and Fink, G. R. (1990). BIK1, a protein required for microtubule function during mating and mitosis in *Saccharomyces cerevisiae*, colocalizes with tubulin. *J Cell Biol* 111, 2573-2586.
- Cheeseman, I. M., Enquist-Newman, M., Muller-Reichert, T., Drubin, D. G., and Barnes, G. (2001). Mitotic spindle integrity and kinetochore function linked by the Duo1p/Dam1p complex. *J Cell Biol* 152, 197-212.
- Ciosk, R., Zachariae, W., Michaelis, C., Shevchenko, A., Mann, M., and Nasmyth, K. (1998). An ESP1/PDS1 complex regulates loss of sister chromatid cohesion at the metaphase to anaphase transition in yeast. *Cell* 93, 1067-1076.
- Cullen, C. F., Deak, P., Glover, D. M., and Ohkura, H. (1999). mini spindles: A gene encoding a conserved microtubule-associated protein required for the integrity of the mitotic spindle in *Drosophila*. *J Cell Biol* 146, 1005-1018.
- Goh, P. Y., and Kilmartin, J. V. (1993). NDC10: a gene involved in chromosome segregation in *Saccharomyces cerevisiae*. *J Cell Biol* 121, 503-512.
- Goshima, G., and Yanagida, M. (2000). Establishing biorientation occurs with precocious separation of the sister kinetochores, but not the arms, in the early spindle of budding yeast. *Cell* 100, 619-633.
- Guacci, V., Koshland, D., and Strunnikov, A. (1997). A direct link between sister chromatid cohesion and chromosome condensation revealed through the analysis of MCD1 in *S. cerevisiae*. *Cell* 91, 47-57.
- He, X., Asthana, S., and Sorger, P. K. (2000). Transient sister chromatid separation and elastic deformation of chromosomes during mitosis in budding yeast. *Cell* 101, 763-775.
- He, X., Rines, D. R., Espelin, C. W., and Sorger, P. K. (2001). Molecular analysis of kinetochore-microtubule attachment in budding yeast. *Cell* 106, 195-206.
- Hofmann, C., Cheeseman, I. M., Goode, B. L., McDonald, K. L., Barnes, G., and Drubin, D. G. (1998). *Saccharomyces cerevisiae* Duo1p and Dam1p, novel proteins involved in mitotic spindle function. *J Cell Biol* 143, 1029-1040.
- Hoyt, M. A., Totis, L., and Roberts, B. T. (1991). *S. cerevisiae* genes required for cell cycle arrest in response to loss of microtubule function. *Cell* 66, 507-517.

- Jin, Q. W., Fuchs, J., and Loidl, J. (2000). Centromere clustering is a major determinant of yeast interphase nuclear organization. *J Cell Sci* 113 (Pt 11), 1903-1912.
- Jones, M. H., Bachant, J. B., Castillo, A. R., Giddings, T. H., Jr., and Winey, M. (1999). Yeast Dam1p is required to maintain spindle integrity during mitosis and interacts with the Mps1p kinase. *Mol Biol Cell* 10, 2377-2391.
- Kahana, J. A., Schnapp, B. J., and Silver, P. A. (1995). Kinetics of spindle pole body separation in budding yeast. *Proc Natl Acad Sci U S A* 92, 9707-9711.
- Kirschner, M. W., and Mitchison, T. (1986). Microtubule dynamics. *Nature* 324, 621.
- Kosco, K. A., Pearson, C. G., Maddox, P. S., Wang, P. J., Adams, I. R., Salmon, E. D., Bloom, K., and Huffaker, T. C. (2001). Control of microtubule dynamics by Stu2p is essential for spindle orientation and metaphase chromosome alignment in yeast. *Mol Biol Cell* 12, 2870-2880.
- Li, R., and Murray, A. W. (1991). Feedback control of mitosis in budding yeast. *Cell* 66, 519-531.
- Li, Y., Bachant, J., Alcasabas, A. A., Wang, Y., Qin, J., and Elledge, S. J. (2002). The mitotic spindle is required for loading of the DASH complex onto the kinetochore. *Genes Dev* 16, 183-197.
- Lin, H., de Carvalho, P., Kho, D., Tai, C. Y., Pierre, P., Fink, G. R., and Pellman, D. (2001). Polyploids require Bik1 for kinetochore-microtubule attachment. *J Cell Biol* 155, 1173-1184.
- Maddox, P. S., Bloom, K. S., and Salmon, E. D. (2000). The polarity and dynamics of microtubule assembly in the budding yeast *Saccharomyces cerevisiae*. *Nat Cell Biol* 2, 36-41.
- Marshall, W. F., Straight, A., Marko, J. F., Swedlow, J., Dernburg, A., Belmont, A., Murray, A. W., Agard, D. A., and Sedat, J. W. (1997). Interphase chromosomes undergo constrained diffusional motion in living cells. *Curr Biol* 7, 930-939.
- Matthews, L. R., Carter, P., Thierry-Mieg, D., and Kemphues, K. (1998). ZYG-9, a *Caenorhabditis elegans* protein required for microtubule organization and function, is a component of meiotic and mitotic spindle poles. *J Cell Biol* 141, 1159-1168.
- McIntosh, J. R., Grishchuk, E. L., and West, R. R. (2002). Chromosome-microtubule interactions during mitosis. *Annu Rev Cell Dev Biol* 18, 193-219.
- Nabeshima, K., Kurooka, H., Takeuchi, M., Kinoshita, K., Nakaseko, Y., and Yanagida, M. (1995). p93dis1, which is required for sister chromatid separation, is a novel microtubule and spindle pole body-associating protein phosphorylated at the Cdc2 target sites. *Genes Dev* 9, 1572-1585.

Neff, M. W., and Burke, D. J. (1991). Random segregation of chromatids at mitosis in *Saccharomyces cerevisiae*. *Genetics* 127, 463-473.

O'Toole, E. T., Winey, M., and McIntosh, J. R. (1999). High-voltage electron tomography of spindle pole bodies and early mitotic spindles in the yeast *Saccharomyces cerevisiae*. *Mol Biol Cell* 10, 2017-2031.

Pearson, C. G., Maddox, P. S., Salmon, E. D., and Bloom, K. (2001). Budding yeast chromosome structure and dynamics during mitosis. *J Cell Biol* 152, 1255-1266.

Pellman, D., Bagget, M., Tu, Y. H., Fink, G. R., and Tu, H. (1995). Two microtubule-associated proteins required for anaphase spindle movement in *Saccharomyces cerevisiae*. *J Cell Biol* 130, 1373-1385.

Rieder, C. L., and Salmon, E. D. (1994). Motile kinetochores and polar ejection forces dictate chromosome position on the vertebrate mitotic spindle. *J Cell Biol* 124, 223-233.

Rines, D. R., He, X., and Sorger, P. K. (2002). Quantitative microscopy of green fluorescent protein-labeled yeast. *Methods Enzymol* 351, 16-34.

Severin, F., Habermann, B., Huffaker, T., and Hyman, T. (2001). Stu2 promotes mitotic spindle elongation in anaphase. *J Cell Biol* 153, 435-442.

Shirasu-Hiza, M., Coughlin, P., and Mitchison, T. (2003). Identification of XMAP215 as a microtubule-destabilizing factor in *Xenopus* egg extract by biochemical purification. *J Cell Biol* 161, 349-358.

Straight, A. F., Belmont, A. S., Robinett, C. C., and Murray, A. W. (1996). GFP tagging of budding yeast chromosomes reveals that protein-protein interactions can mediate sister chromatid cohesion. *Curr Biol* 6, 1599-1608.

Straight, A. F., Marshall, W. F., Sedat, J. W., and Murray, A. W. (1997). Mitosis in living budding yeast: anaphase A but no metaphase plate. *Science* 277, 574-578.

Straight, A. F., Sedat, J. W., and Murray, A. W. (1998). Time-lapse microscopy reveals unique roles for kinesins during anaphase in budding yeast. *J Cell Biol* 143, 687-694.

Thomann, D., Rines, D. R., Sorger, P. K., and Danuser, G. (2002). Automatic fluorescent tag detection in 3D with super-resolution: application to the analysis of chromosome movement. *J Microsc* 208, 49-64.

Van Breugel, M., Drechsel, D., and Hyman, A. (2003). Stu2p, the budding yeast member of the conserved Dis1/XMAP215 family of microtubule-associated proteins is a plus end-binding microtubule destabilizer. *J Cell Biol* 161, 359-369.

Wang, P. J., and Huffaker, T. C. (1997). Stu2p: A microtubule-binding protein that is an essential component of the yeast spindle pole body. *J Cell Biol* 139, 1271-1280.

Waters, J. C., Skibbens, R. V., and Salmon, E. D. (1996). Oscillating mitotic newt lung cell kinetochores are, on average, under tension and rarely push. *J Cell Sci* 109 (Pt 12), 2823-2831.

Wigge, P. A., and Kilmartin, J. V. (2001). The Ndc80p complex from *Saccharomyces cerevisiae* contains conserved centromere components and has a function in chromosome segregation. *J Cell Biol* 152, 349-360.

Winey, M., and O'Toole, E. T. (2001). The spindle cycle in budding yeast. *Nat Cell Biol* 3, E23-27.

Zhou, C., Huang, S. H., and Jong, A. Y. (1989). Molecular cloning of *Saccharomyces cerevisiae* CDC6 gene. Isolation, identification, and sequence analysis. *J Biol Chem* 264, 9022-9029.

CHAPTER 6

Conclusions and Future Directions

6.1	Introduction.....	210
6.2	Conclusions.....	211
6.2.1	Characterizing kinetochore-microtubule attachment.....	211
6.2.1.1	Loss of attachment.....	212
6.2.1.2	Monopolar attachment.....	213
6.2.1.3	Non-functional bipolar attachment.....	214
6.2.2	Computational analysis of spindle geometry.....	215
6.2.3	Enhanced in vivo microscopy techniques for budding yeast.....	218
6.2.4	Molecular basis of cell-cycle changes in chromosome dynamics.....	224
6.3	Future Directions.....	225
6.3.1	Further biochemical purification of subcomplexes.....	226
6.3.2	Investigating redundant kinetochore-microtubule attachment.....	227
6.3.3	Mechanical modeling of chromosome segregation mechanisms.....	228
6.4	Summary.....	228
6.5	References.....	230

6.1 Introduction

When I first began working with Xiangwei He to further identify yeast kinetochore components very little was known about the composition, structure or functional role of the kinetochore in budding yeast. Our molecular understanding of the kinetochore-microtubule attachment in *S. cerevisiae* was limited to the recognition that attachment depended on a well defined centromeric DNA sequence, a small centromere binding complex, CBF3 (Cai and Davis, 1990; Clarke and Carbon, 1980; Espelin et al., 1997; Lechner and Carbon, 1991; Sorger et al., 1994), and a handful of other proteins such as Cse4p (Fitzgerald-Hayes et al., 1982; Stoler et al., 1995). In fact, most of the kinetochore proteins were either not known or suspected of having alternative functions (Wigge et al., 1998). Based on genetic screens, many other genes had been implicated in increasing the fidelity of genetic transmission (Hyland et al., 1999; Kitagawa et al., 1999; Ortiz et al., 1999), but the field lacked direct assays for kinetochore involvement. Progress was hindered by the absence of an assay to monitor kinetochore-microtubule interactions.

Three important breakthroughs lead to further identification of kinetochore components and opened the door for rapid advancement. First, the insight that kinetochore proteins localized into a bilobed pattern during metaphase (He et al., 2001); second, the establishment of chromatin immunoprecipitation (ChIP) to assay for direct centromeric DNA interactions; and lastly, the introduction of fluorescent single chromosome tagging for *in vivo* microscopy (Ciosk et al., 1998; He et al., 2000; Straight et al., 1996). In the past three years alone, more than 30 new proteins have been shown to either localize, co-precipitate, or function in kinetochore-microtubule attachment (Cheeseman et al., 2001; Euskirchen, 2002;

Goshima and Yanagida, 2000; He et al., 2001; Janke et al., 2002; Li et al., 2002; Tanaka et al., 2002; Wigge and Kilmartin, 2001).

My research has contributed to understanding the role of several kinetochore complexes in establishing proper bipolar attachment, characterizing kinetics of chromosome dynamics, and enhancing *in vivo* fluorescent microscopy techniques for performing chromosome motion studies at resolutions better than the Rayleigh limit (Thomann et al., 2002). This chapter presents the results of my research in the context of the field of kinetochore exploration, and follows with suggestions for approaches and directions for future investigation of the budding yeast kinetochore.

6.2 Conclusions

6.2.1 Characterizing kinetochore-microtubule attachment

Observations of transient sister separation using a single fluorescently tagged chromosome were the first direct evidence for the formation of opposing tensile force on sister chromatids in yeast (Goshima and Yanagida, 2000; He et al., 2000). Experiments with budding yeast strains containing a single GFP-tagged chromosome suggested that prior to the onset of anaphase, sister chromatids experienced sufficient tensile force to physically separate ~10 kb of centromere proximal DNA (Goshima and Yanagida, 2000; He et al., 2000). In addition, the development of tension depended on the presence of the DNA cohesion molecule, Scc1p (Mcd1p) (Ciosk et al., 1998; Michaelis et al., 1997), to resist early sister separation. The formation of tension was also shown to be dynamic and transient in nature (He et al., 2000). By combining GFP-tagged chromosomes with temperature sensitive mutants, I was able to develop a classification system for defects in chromosome-MT

attachment using *in vivo* fluorescence microscopy. By exploiting the tension assay for bipolar attachment this approach demonstrated that mutations in kinetochore proteins can result in distinctly different types of attachment and differences in chromosome movement. The chromosome tracking data presented in Chapter 2, along with the localization and ChIP experiments quickly lead us to realize that the kinetochore contained multiple layers and that redundant attachment factors were dependent on core components for their centromere association (He et al., 2001). Clearly, the kinetochore-MT attachment is more complex than originally thought and these results now constitute a proof-of-principle that chromosome dynamics can be dissected genetically as described in the following sections.

6.2.1.1 Loss of attachment

CBF3 and the Ndc80 complex are essential for the establishment of kinetochore-MT attachment. Initial genetic studies with *ndc10-1* and *ndc80-1* demonstrated severe rates of chromosome loss (Goh and Kilmartin, 1993; Wigge and Kilmartin, 2001). Based on tubulin staining in these mutants it was also observed that the mitotic spindle matured throughout the cell cycle and segregated spindle pole bodies with normal kinetics. Despite the appearance of a normal spindle, chromosomes failed to segregate normally and cell division led to high rates of aneuploidy. By combining these mutations with the GFP labeled chromosome and with a GFP-tagged SPB, it became possible to observe the time-dependent motion and SPB-CEN association (He et al., 2000). After the onset of S-phase, cells shifted to the restrictive temperature demonstrated random patterns of chromosome motion and failed to associate directly with either SPB.

6.2.1.2 Monopolar attachment

Temperature sensitive mutations in *dam1* lead to monopolar attachment. The *DAM1* gene was originally identified in a screen for mutants that enhanced the defects of mutations in *MPS1* (Jones et al., 1999), a kinase involved in SPB duplication and the spindle checkpoint (Weiss and Winey, 1996; Winey et al., 1991). Immunofluorescence experiments demonstrated MT localization and electron micrographs showed that *dam1* mutations result in bent, broken and hyper-elongated spindles (Hofmann et al., 1998). Based on GFP localization and CHIP, Dam1p was shown to interact with kinetochores and MTs, suggesting that Dam1p may play a role in linking chromosomes directly to the spindle (Cheeseman et al., 2001; He et al., 2001). However, it was not known what role the protein may play in this linkage. My chromosome dynamics studies quickly demonstrated that defects in *dam1p* resulted in monopolar attachments, that is, sisters bound to MTs from only one SPB (He et al., 2001).

The yeast homologue of the human Aurora-kinase, Ipl1p, also demonstrates a monopolar phenotype in cells possessing the temperature sensitive mutation, *ipl1-321*. The similarity of phenotype in both *dam1p* and *ipl1p* cells suggested that the kinase plays an upstream role in regulating Dam1p activity (Cheeseman et al., 2002; Tanaka et al., 2002). However, recent chromosome motion analysis in yeast suggests that while Ipl1p may act upstream of the Dam1p complex, defects in the two proteins do not actually phenocopy (Rines *et. al.*, unpublished results). Cells with mutant *dam1p* demonstrate monotelic attachment and appear to lack the capacity for a second attachment whereas *ipl1p* chromosomes appear to have syntelic attachment. This difference in phenotype suggests that the Dam1p complex may only play a role in establishing the second MT attachment site and

that a redundant MT binding complex may be needed to maintain the attachment from the previous round of cell division. Clouding the picture further, there is conflicting evidence from mutations in another component of the Dam1 complex, *spc34-3*, that do not support this model (Janke et al., 2002). Nonetheless, the combination of these results suggests further at the complex differences between establishing MT attachment and the maintenance of attachment. This line of investigation has recently been extended in higher organisms where Aurora B has been shown to be involved in correcting syntelic attachment, a state where both sister chromatids are attached to MTs from the same pole (Hauf et al., 2003). Further investigation will be needed.

6.2.1.3 Non-functional bipolar attachment

A third set of mutants appear to demonstrate proper bipolar attachment yet lack normal chromosome dynamics. Stu2p is a MT binding protein that has recently been localized to the extreme plus-ends of MTs (Van Breugel, Dreschel & Hyman, *personal communication*). Based on the results presented, Stu2p acts to induce catastrophes by destabilizing rather than stabilizing MTs *in vitro* and may sterically block tubulin addition to the MT plus-end. These findings are consistent with my *in vivo* data showing attached chromosomes are less dynamic in *stu2* mutants compared to wild-type cells (He et al., 2001) and suggest that kinetochores in *stu2* cells have a reduced ability to depolymerize MTs and generate force.

The importance of nonmotor MAPs in kinetochore-MT binding and force generation is intriguing and suggests at redundant attachment factors. Based on the relatively large number of kinetochore components, one can speculate that there might be separate functions in establishing the attachment and maintaining the attachment. Indeed, it has been proposed

previously that MT depolymerization is required to mature the kinetochore attachment (Peskin and Oster, 1995). Thus these kinetochore-MAPs may play antagonistic roles in regulating polymerization and depolymerization, where some proteins function to stabilize the MT during the establishment of attachment, and others function to destabilize the polymer in an effort to mature or strengthen the attachment. Whatever the functional importance, their role in attachment and force generation is still not well understood and will require more investigation.

6.2.2 Computational analysis of spindle geometry

The results described above were based largely on qualitative observations. While the human eye can observe XY-distances in micrographs easily enough, depth information is much more difficult to interpret (Z-direction). In addition, observations relating chromosome motion from one cell to the next were impossible to analyze in a consistent manner. To overcome these issues, I developed a computational approach to analyzing three-dimensional (3D) spindle geometry. Using a cylindrical coordinate system with an axis centered on the two SPBs, centromere position could be related in a time dependent manner. In addition, since the SPBs remain within the nuclear envelope throughout the cell cycle, positional errors from non-kinetochore mediated motion caused by nuclear rotation or drift were automatically subtracted away (Figure 6-1) (He et al., 2001). Once coordinate data was obtained through manual tracking, 3D distance were calculated, stored in a relational database and graphed in an easy to understand manner.

The development of this system (Lab Assistant) is part of an ongoing open-source project known as the open microscopy environment (OME), and involves both academic and industry contributors (www.openmicroscopy.com). Although Lab Assistant is not currently

available to the general academic community, it should become available as part of the future software releases.

Accurate geometric spindle calculation depends heavily on the precision of the coordinate data entered and initially relied on inaccurate manual detection. By establishing a collaboration with an applied mathematics group at the ETH in Zurich, headed by Gaundez Danuser, our two labs have developed an automated approach to spot detection and tracking (Thomann et al., 2002). Diffraction limited resolution of chromosome spots in light microscopy typically resides around 230 nm in the XY-plane and 600 nm in the Z-direction (see Chapter 4 for more detailed information on resolution limits). Using the algorithms developed by the Danuser group has improved XY-resolution to ~50 nm and Z-resolution to ~200 nm (Thomann *et al.*, 2003 *in press*).

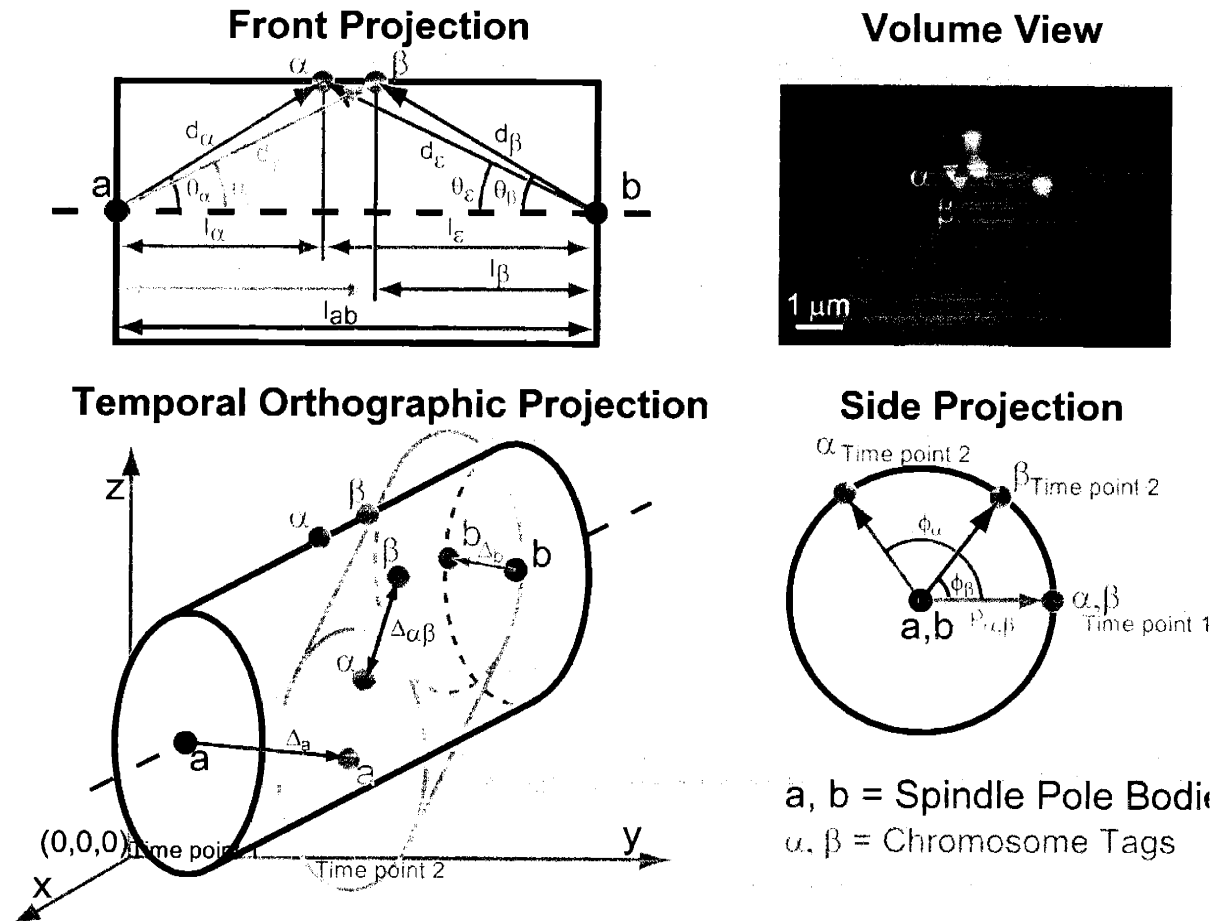


Figure 6-1. Parameters for assaying time-dependent chromosome motion

Chromosome position is determined based on a cylindrical coordinate system centered about the axis of a yeast spindle as determined by the position of the two SPBs. **Front Projection:** The relative measurements made with respect to chromosome position. The two red spots (a & b) represent the SPBs, while the two green spots (α & β) represent the position of the GFP tagged sister chromatids. Linear distance determinations are represented by the arrows in the figure. **Volume View:** A fluorescent micrograph imaged from formaldehyde fixed and DAPI stained yeast. The GFP spots represent the position of SPB (marked in red) and the CEN tags (marked in green). Image was generated from a volume view projection off a Deltavision deconvolution microscope. **Temporal Orthographic Projection:** As the nuclear envelope rotates and shifts in position, time-dependent changes are measured with respect to the cylindrical coordinate system. **Side Projection:** The radial distance of the chromosome tag from the spindle axis is calculated.

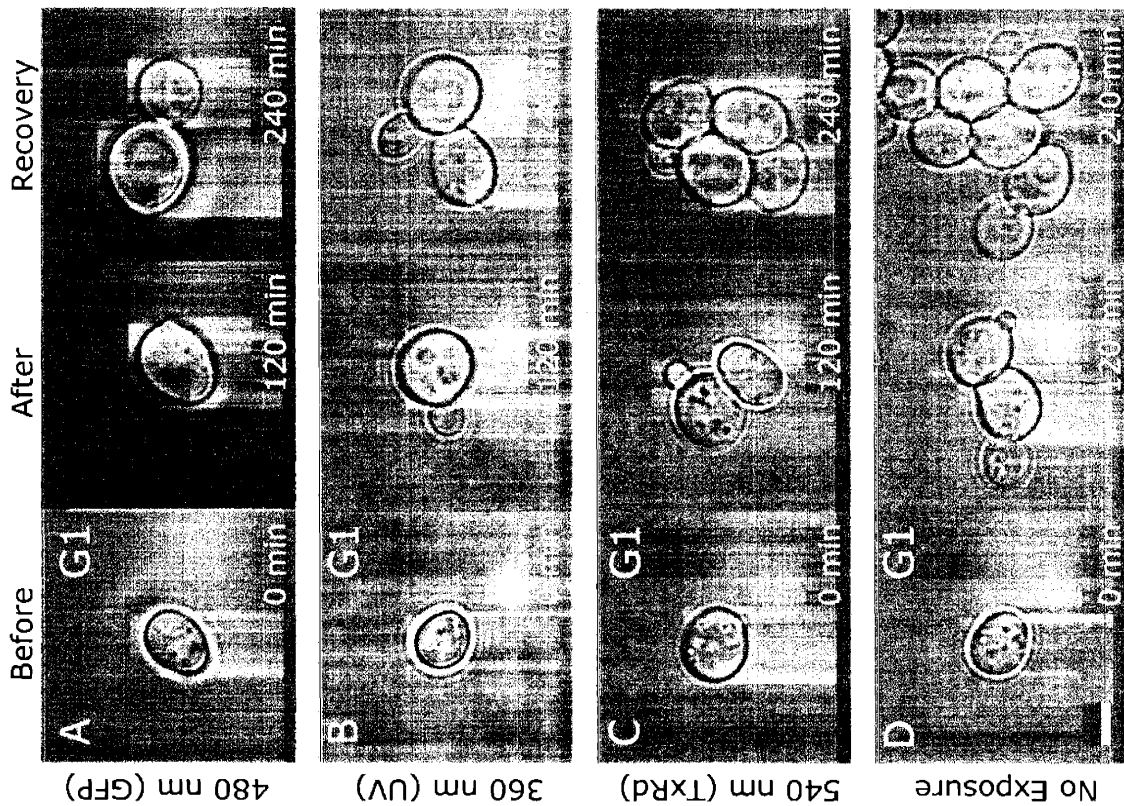
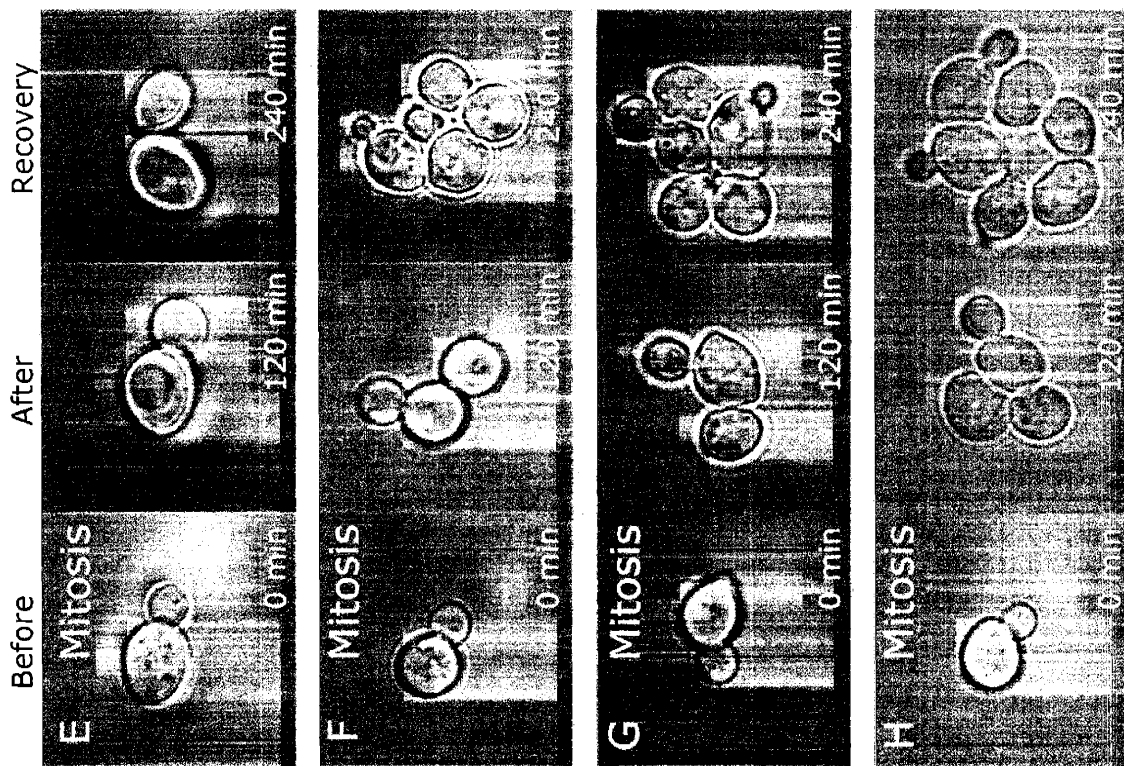
6.2.3 *Enhanced in vivo microscopy techniques for budding yeast*

Improved microscopy techniques and acquisition rates ten times faster than those used in prior studies have also allowed us to gain a more detailed and quantitative understanding of chromosome dynamics with greater temporal precision than was previously possible. By comparing the movement of a GFP-tagged chromosome in wild-type cells and mutant cells that lack a functional kinetochore (*ndc10-1*), I have confirmed that chromosomes remain attached to SPBs throughout the cell cycle in a kinetochore/MT dependent manner. My work also demonstrated both short, rapid oscillations and longer periods of directed movement in G1 cells. As would be expected if the movement reflects underlying MT dynamics, we found that during periods of directed movement, centromeres moved towards the SPBs more rapidly than they moved away (Rines et. al., *see Chapter 5*). The speeds measured for directed movement away from the chromosome during G1 are very similar to growth rates measured *in vitro* for MTs attached to mammalian kinetochores, although the rates we observed for movement towards the SPB were not as fast as MT shrinkage rates measured by Hunt and McIntosh, 1998.

Despite the confirmation of similar kinetics between yeast and mammals, recent experimentation has demonstrated a side effect where excessive long-term imaging with GFP specific light (480 nm) on yeast cells has negative physiological effects on growth (Figure 6-2 and 6-3). My research on imaging *in vivo* chromosome dynamics throughout an entire cell cycle has recently revealed phototoxicity and photobleaching results in yeast.

Photobleaching and phototoxicity impose a tradeoff between the exposure time of each image and the total number of images that can be acquired. Photobleaching directly affects the emission capabilities of a fluorophore and is readily apparent as a reduction in

signal strength. Phototoxicity indirectly describes a general class of harmful effects on live-cells based on repeated or short but extreme exposures to a light source. The exposure typically has a negative effect on a cells ability to grow in a normal manner. Phototoxicity is much more difficult to discern than photobleaching since it is harder to measure directly and can be a consequence of DNA damage (ultra-violet light) or protein damage (infra-red light). To avoid unpredicted effects during live-cell acquisition with budding yeast, I have determined that it is important to incorporate interference filters that block damaging rays into the microscope system. Quite often multiple filters can be piggybacked on top of one another. Providing cells with longer relaxation periods between each time-point may limit the effects. However, in preliminary studies we have found that even providing a 3 minute relaxation period between time-points causes cells to grow at less than half the normal rate (Figure 6-2)



480 nm (GFP)

360 nm (UV)

540 nm (TxRd)

No Exposure

Figure 6-2. Phototoxic effects at different wavelengths on yeast growth

Wild-type cells were imaged on a Deltavision deconvolution microscopy system using various wavelengths of light to determine effects on growth and cell cycle progression during a long-term imaging session (2 hours) based on cell morphology. Cells lacking any exogenous fluorophores were grown to mid-log phase and placed on an agarose depression slide (refer to Chapter 3 for more details). 20 optical Z-sections were acquired using 50 millisecond exposures were taken per Z-section for a total of 2 – 3 seconds of exposure. Time points were acquired every three minutes. After the 2 hour imaging session, cells were allowed to recover for an additional 2 hours in the absence of any fluorescent exposure. Phase contrast images were taken before imaging ('Before' column), immediately after the two hour imaging session ('After' column), and immediately after the 2 hour recovery period ('Recovery' column). Non-imaging control cells on the same slide were used as a comparison for growth under the same condition minus direct fluorescent exposure (Figure 6-2D & H). Cells on the left were all imaged starting at some point in G1 while cells on the right were imaged starting at some point in late S-phase or early metaphase based on cell morphology. (A & E) demonstrates that cells repeatedly exposed to 480 nm light (the same wavelengths used for GFP activation) experienced drastic reduction in growth although they didn't appear to arrest as compared to the non-imaging controls (D & H). The imaging did not appear to kill the cells as they continued to grow and divide during the recovery period. (B & F) Cells were imaged using the same experimental setup except with 360 nm light (UV). Surprisingly, the cells were much less susceptible to the effects of the light and grew only slightly slower than the control cells. (C & G) Again cells were imaged, except with light closer to the IR spectrum or 540 nm light (TexRd) and also appear to be relatively unaffected by the fluorescent light. This data suggests that 480 nm light is highly toxic to cell growth although the physiological effects are not obvious.

The exact mechanism of GFP photobleaching has not been elucidated. It is known that the fluorescent molecule is not destroyed or degraded; rather continuous or long-term repeated exposure to excitation wavelengths will irreversibly alter the GFP molecule so that it can no longer fluoresce. Photobleaching can be minimized by using neutral density filters to reduce the excitation intensity in combination with the shortest exposures possible. Reductions in fluorescent exposure negatively affect the contrast of an image and reduce the signal-to-noise ratio. Conversely, the tradeoff in signal strength is repaid with longer duration time course movies. We have found that 50 milliseconds and a 1.0 neutral density filter (10% transmission) works best for rapid acquisition movies where 14-20 optical Z-sections are taken every 5 seconds (Figure 6-3). This combination allows us to acquire movie with 180 time-points up to 15 minutes long using EGFP labeled spindle pole bodies and single chromosome tags.

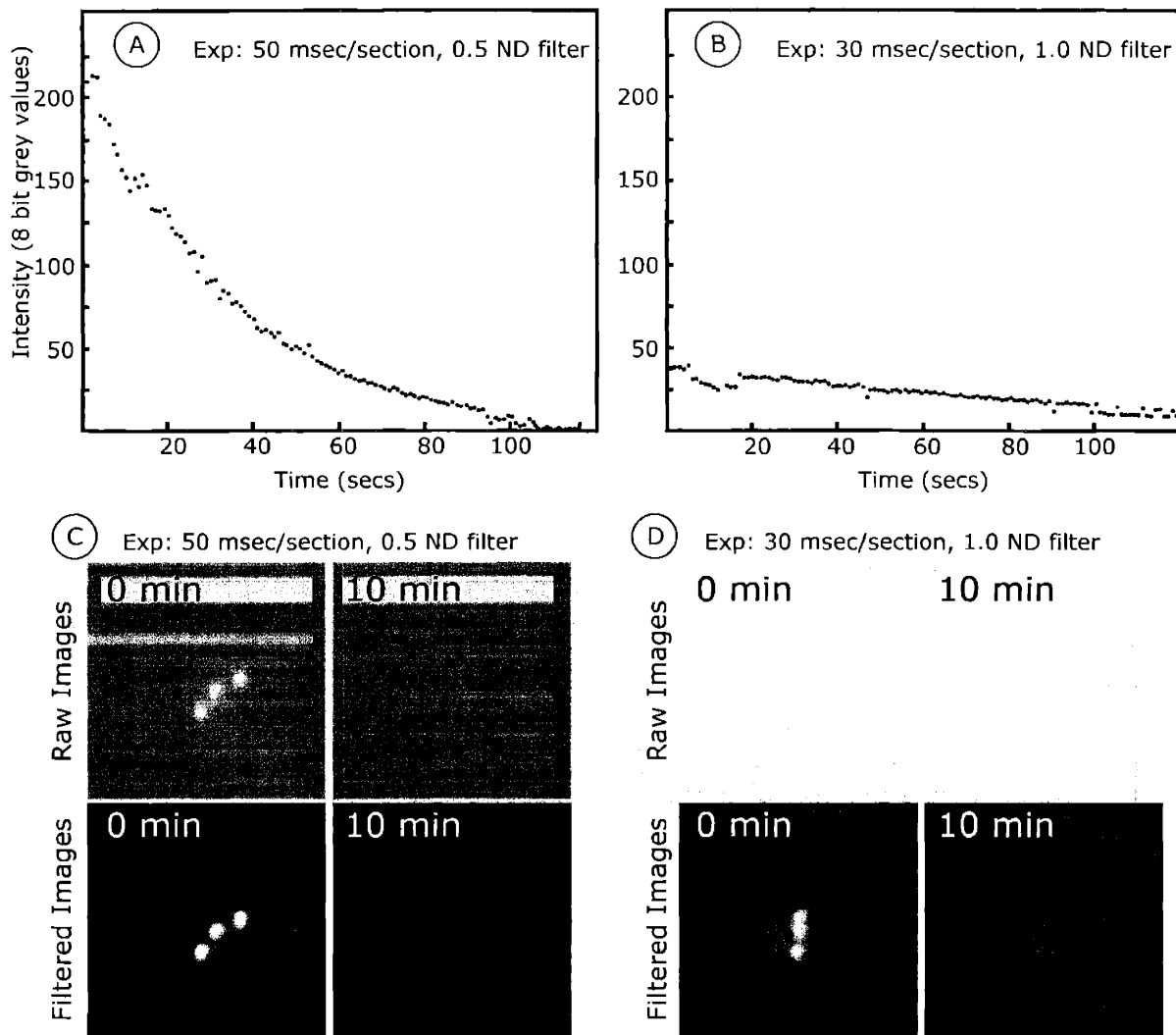


Figure 6-3. Photobleaching rates of EGFP in yeast

Using automated spot detection and tracking, photobleaching of GFP spots are compared to evaluate rates of bleaching and under different imaging conditions. (A) Cells are imaged every 5 seconds by taking 20 optical Z-sections with 75 msec/section exposures and a 0.5 neutral density filter. Rates of photobleach are graphed and appear to bleach exponentially. (B) Cells imaged using 25 msec/section and a 1.0 ND filter. The lower intensity light and shorter exposure times have much less effects on the change in emission intensity over time. However, the signal to noise also decreases drastically. (C & D) Show maximum intensity projections of the images used for (A & B). The top set of images are raw data while those on the bottom are filtered using the automated spot detection and tracking software (see Chapter 4 for more information). Although the signal is much weaker in the righthand set of images, the spot tracking software is still capable of resolving the fluorescent spots under more favorable physiological conditions.

6.2.4 Molecular basis of cell-cycle changes in chromosome dynamics

Determining how chromosome movement is coupled to ATP-dependent sliding of motors along MTs and GTP-coupled MT dynamics is among the most important issues in the study of chromosome segregation. In higher eukaryotes, the force-generating processes responsible for chromosome movement arise in at least three spindle locations: the plus-ends of MTs embedded in kinetochores, the minus-ends of kinetochore-MTs embedded in spindle poles (Hays and Salmon, 1990), and along chromosome arms via interactions with non-kinetochore MTs (Rieder et al., 1986). The importance of these processes varies among different cell types. In yeast, spindle MTs are highly dynamic in mitosis, but photobleaching studies in live cells and EM analysis of plus-ends suggest that the poleward flux of MTs is unlikely to make a major contribution to chromosome movement (Maddox et al., 2000). In addition, yeast spindles appear to lack MTs that might interact with chromosome arms to generate polar ejection forces (O'Toole et al., 1999). Thus, it is reasonable to question whether chromosome movement in yeast is powered only by kinetochores. I began investigating this question by examining the kinetics of chromosome motion at phases in the cell cycle with monopolar and bipolar spindles and in cells containing mutations in specific kinetochore MAP functionality.

The research presented in the later half of this thesis demonstrates that Ndc80p is required for attachment in early S-phase but not in G1, which provides evidence that there is a molecular basis for the cell-cycle changes in chromosome position and dynamics. Cells possessing the *ndc80-1* mutation lack outer kinetochore complexes (e.g., Dam1p complex). CHIP and microscopy studies of asynchronous *ndc80-1* cultures show that while the DNA

binding components (Ndc10p) remains intact, most of the known MT binding proteins are dissociated from the kinetochore (He et al., 2001). As would be expected, Ndc80p was previously found to be essential for attachment in metaphase (He et al., 2001). Therefore, the finding that Ndc80p is not required for attachment in G1 was surprising. It raises the intriguing possibility that a different branch of the kinetochore can mediate monopolar attachment in G1 that is distinct from proteins required for bipolar attachment in metaphase. Moreover, it is possible that maturation of attachment may occur in two steps. Chromosomes may first establish interactions with the MT by one set of components. The attachment is then strengthened by an additional set of proteins. This hypothesis is further supported in higher organisms where studies have demonstrated that in prometaphase, chromosomes bind to the sides of MTs and move rapidly toward a pole (Alexander and Rieder, 1991; Rieder and Alexander, 1990). Kinetochore-MT attachments capture and embed the extreme plus-ends of MTs when bipolarity is established. As we learn more about the cell cycle dependent role of the yeast kinetochore, a better understanding of this branching should develop.

6.3 Future Directions

While the presence of mitotic spindle fibers and their functional role in chromosome segregation has been known since the late 1960's (Inoue and Sato, 1967), discovery of kinetochore genes only began in the last decade (reviewed in McAinsh A, Tytell J and Sorger PK, 2003 *in press*). Identification of these genes has facilitated genetic experiments revealing their importance in chromosome segregation. Although informative and occasionally surprising, these analyses so far have largely only confirmed our expectations of centromere-MT function. A complete molecular description of how cells link centromeric DNA to MTs

has yet to be answered. We also have a preliminary understanding of the events that take place to ensure proper chromosome segregation and a basic description of the components necessary to mechanically separate the sisters, yet the details remain unclear. Despite knowledge of what is now a large number of kinetochore proteins and sub-complex interactions in yeast, we still are unsure how the kinetochore physically holds onto the MT. While additional purifications and further identification of more components will undoubtedly prove informative, significant progress in describing the molecular events necessary for kinetochore-MT attachment in both yeast and higher organisms will require the development of new techniques for studying kinetochore function *in vivo* and *in vitro* (see below).

6.3.1 Further biochemical purification of subcomplexes

Understanding the kinetochore structure will ultimately require knowledge of how the proteins interact *in vivo*. Although several interactions have been previously identified, we know very little about their physiological relevance, when the individual protein complexes are recruited to the kinetochore, and how these complexes are modified or regulated. Recent identification of the 'bilobed' localization pattern of kinetochore proteins provided the real first evidence for distinct differences in kinetochore proteins and SPB proteins (He et al., 2001). Biochemical purification of the epitope tagged proteins in yeast has not only confirmed their presence at the kinetochore but also identified additional components. But it appears that some of the kinetochore-MT associated proteins are still missing. It will continue to be informative as the purification of kinetochore complexes gets closer to the kinetochore-MT interface. This approach should both reveal physiological relevant protein-protein interactions and also be useful for identifying novel MT associated protein genes.

6.3.2 Investigating redundant kinetochore-microtubule attachment

Despite the utility of a biochemical approach, the kinetochore-MT linkage does not appear to be a single linear chain of proteins from the centromeric DNA to MT. The attachment utilizes redundant factors in a cell-cycle dependent manner (Rines *et. al.*, Chapter 5). Identifying the proteins required for attachment in G1 will be a high priority for future studies. Of the known kinetochore MT binding proteins, Bik1p or Stu2p are possible candidates since they have been shown to interact with the kinetochore. However, a failure to lose attachment in *dam1p/bik1Δ* or *dam1p/stu2p* double mutants suggests that other components are involved in the maintenance of kinetochore-MT attachment in G1 (Rines *et. al.*, Chapter 5). There may also be additional, not yet identified, kinetochore proteins or even cell cycle-specific kinetochore proteins that mediate MT attachment in G1. It is also possible, however, that some of the proteins that appear to be dependent on Ndc80p in asynchronous cultures, actually remain at the kinetochore in *ndc80-1* cells during G1. Thus, it will be important to confirm the Ndc80 dependencies by ChIP or microscopy in synchronous G1 cultures.

It also remains to be determined what happens in early S-phase to cause *ndc80-1* cells to lose attachment. Although our data suggest that the chromosomes remain attached to the MTs throughout the cell cycle, it is known that in wild-type cells the parent sister chromatid does not preferentially separate with the parent SPB (Neff and Burke, 1991). Therefore, the chromosomes must at least transiently separate from the SPBs. Most likely this transient loss of attachment occurs during centromeric replication, which happens in early S-phase (Winey and O'Toole, 2001). One explanation for our data is that Ndc80p dependent kinetochore proteins are required to reattach the sister chromatids to MTs but not to maintain monopolar

attachment. In this case, we might expect the early S-phase loss of attachment in *ndc80-1* cells to be dependent on replication. To examine this closer, chromosome dynamics in *cdc6* mutants, which are not able to replicate their DNA but nevertheless progress through the cell cycle, could be combined with *ndc80-1*.

6.3.3 Mechanical modeling of chromosome segregation mechanisms

A fundamental problem in the study of chromosome segregation is developing a spatial and temporal description in which the roles of multiple redundant components are more important. To gain further understanding into the force production on the sister chromatids a data driven mathematical model will be of critical importance and serve as a source of simulated results that will help to guide future experimental work. The challenge will be to develop models that can capture the mitotic spindle's stochastic behavior and mechanical force generation (Cytrynbaum et al., 2003). Force-balance equations will need to integrate MT dynamic instability, MT-motor properties, and DNA cohesive molecules to gain insight into the mechanical nature of the spindle. Since redundancy appears to be an important factor in the kinetochore-MT attachment, a major goal will be to combine data from molecular genetics to effectively dissect the complexity. Specific mutants in yeast and RNAi in mammalian cells will be of great value in determining the role of the redundant components in the process of kinetochore-MT attachment.

6.4 Summary

The work presented in this thesis describes a significant contribution to the understanding of yeast biology. The reclassification of previously identified proteins as having a role in kinetochore function represents a large step forward. Analysis of mutations

in these proteins on chromosome dynamics has established the steps necessary to mature bipolar attachment in yeast. Additionally, the role of kinetochore microtubule associated proteins on chromosome dynamics demonstrates the first *in vivo* study at kinetochore regulation of MT generated forces inside the nucleus. Despite the value of these results, this work also reveals the limitations of this approach. The recognition that temperature sensitive mutations in kinetochore proteins may be hypomorphic in nature suggests that total disruption of proteins will be essential for proper functional determinations. Furthermore, the redundant nature of kinetochore-MT attachment means that many different combinations of mutants and gene disruptions will be necessary for complete understanding. I believe that the next phase of kinetochore research in yeast and humans should focus on approaches for identifying the remaining additional factors involved and investigating the complexities of mechanical force production through data driven models. The motion studies based on fluorescently tagged chromosomes with semi-permissive kinetochore mutants will serve as an initial step towards a comprehensive mechanical model. As we obtain a more complete molecular description from the biochemical studies computational models enhanced to include finer details and will help us to arrive at a better understanding of the functional role of kinetochore-MT attachments.

6.5 References

- Alexander, S. P., and Rieder, C. L. (1991). Chromosome motion during attachment to the vertebrate spindle: initial saltatory-like behavior of chromosomes and quantitative analysis of force production by nascent kinetochore fibers. *J Cell Biol* 113, 805-815.
- Cai, M., and Davis, R. W. (1990). Yeast centromere binding protein CBF1, of the helix-loop-helix protein family, is required for chromosome stability and methionine prototrophy. *Cell* 61, 437-446.
- Cheeseman, I. M., Anderson, S., Jwa, M., Green, E. M., Kang, J., Yates, J. R., 3rd, Chan, C. S., Drubin, D. G., and Barnes, G. (2002). Phospho-regulation of kinetochore-microtubule attachments by the Aurora kinase Ipl1p. *Cell* 111, 163-172.
- Cheeseman, I. M., Enquist-Newman, M., Muller-Reichert, T., Drubin, D. G., and Barnes, G. (2001). Mitotic spindle integrity and kinetochore function linked by the Duo1p/Dam1p complex. *J Cell Biol* 152, 197-212.
- Ciosk, R., Zachariae, W., Michaelis, C., Shevchenko, A., Mann, M., and Nasmyth, K. (1998). An ESP1/PDS1 complex regulates loss of sister chromatid cohesion at the metaphase to anaphase transition in yeast. *Cell* 93, 1067-1076.
- Clarke, L., and Carbon, J. (1980). Isolation of a yeast centromere and construction of functional small circular chromosomes. *Nature* 287, 504-509.
- Cytrynbaum, E. N., Scholey, J. M., and Mogilner, A. (2003). A force balance model of early spindle pole separation in *Drosophila* embryos. *Biophys J* 84, 757-769.
- Espelin, C. W., Kaplan, K. B., and Sorger, P. K. (1997). Probing the architecture of a simple kinetochore using DNA-protein crosslinking. *J Cell Biol* 139, 1383-1396.
- Euskirchen, G. M. (2002). Nnf1p, Dsn1p, Mtw1p, and Nsl1p: a new group of proteins important for chromosome segregation in *Saccharomyces cerevisiae*. *Eukaryot Cell* 1, 229-240.
- Fitzgerald-Hayes, M., Clarke, L., and Carbon, J. (1982). Nucleotide sequence comparisons and functional analysis of yeast centromere DNAs. *Cell* 29, 235-244.
- Goh, P. Y., and Kilmartin, J. V. (1993). NDC10: a gene involved in chromosome segregation in *Saccharomyces cerevisiae*. *J Cell Biol* 121, 503-512.
- Goshima, G., and Yanagida, M. (2000). Establishing biorientation occurs with precocious separation of the sister kinetochores, but not the arms, in the early spindle of budding yeast. *Cell* 100, 619-633.

- Hauf, S., Cole, R. W., LaTerra, S., Zimmer, C., Schnapp, G., Walter, R., Heckel, A., Van Meel, J., Rieder, C. L., and Peters, J. M. (2003). The small molecule Hesperadin reveals a role for Aurora B in correcting kinetochore-microtubule attachment and in maintaining the spindle assembly checkpoint. *J Cell Biol*.
- Hays, T. S., and Salmon, E. D. (1990). Poleward force at the kinetochore in metaphase depends on the number of kinetochore microtubules. *J Cell Biol* 110, 391-404.
- He, X., Asthana, S., and Sorger, P. K. (2000). Transient sister chromatid separation and elastic deformation of chromosomes during mitosis in budding yeast. *Cell* 101, 763-775.
- He, X., Rines, D. R., Espelin, C. W., and Sorger, P. K. (2001). Molecular analysis of kinetochore-microtubule attachment in budding yeast. *Cell* 106, 195-206.
- Hofmann, C., Cheeseman, I. M., Goode, B. L., McDonald, K. L., Barnes, G., and Drubin, D. G. (1998). Saccharomyces cerevisiae Duo1p and Dam1p, novel proteins involved in mitotic spindle function. *J Cell Biol* 143, 1029-1040.
- Hunt, A. J., and McIntosh, J. R. (1998). The dynamic behavior of individual microtubules associated with chromosomes in vitro. *Mol Biol Cell* 9, 2857-2871.
- Hyland, K. M., Kingsbury, J., Koshland, D., and Hieter, P. (1999). Ctf19p: A novel kinetochore protein in Saccharomyces cerevisiae and a potential link between the kinetochore and mitotic spindle. *J Cell Biol* 145, 15-28.
- Inoue, S., and Sato, H. (1967). Cell motility by labile association of molecules. The nature of mitotic spindle fibers and their role in chromosome movement. *J Gen Physiol* 50, Suppl:259-292.
- Janke, C., Ortiz, J., Tanaka, T. U., Lechner, J., and Schiebel, E. (2002). Four new subunits of the Dam1-Duo1 complex reveal novel functions in sister kinetochore biorientation. *Embo J* 21, 181-193.
- Jones, M. H., Bachant, J. B., Castillo, A. R., Giddings, T. H., Jr., and Winey, M. (1999). Yeast Dam1p is required to maintain spindle integrity during mitosis and interacts with the Mps1p kinase. *Mol Biol Cell* 10, 2377-2391.
- Kitagawa, K., Skowyra, D., Elledge, S. J., Harper, J. W., and Hieter, P. (1999). SGT1 encodes an essential component of the yeast kinetochore assembly pathway and a novel subunit of the SCF ubiquitin ligase complex. *Mol Cell* 4, 21-33.
- Lechner, J., and Carbon, J. (1991). A 240 kd multisubunit protein complex, CBF3, is a major component of the budding yeast centromere. *Cell* 64, 717-725.

- Li, Y., Bachant, J., Alcasabas, A. A., Wang, Y., Qin, J., and Elledge, S. J. (2002). The mitotic spindle is required for loading of the DASH complex onto the kinetochore. *Genes Dev* 16, 183-197.
- Maddox, P. S., Bloom, K. S., and Salmon, E. D. (2000). The polarity and dynamics of microtubule assembly in the budding yeast *Saccharomyces cerevisiae*. *Nat Cell Biol* 2, 36-41.
- Michaelis, C., Ciosk, R., and Nasmyth, K. (1997). Cohesins: chromosomal proteins that prevent premature separation of sister chromatids. *Cell* 91, 35-45.
- Neff, M. W., and Burke, D. J. (1991). Random segregation of chromatids at mitosis in *Saccharomyces cerevisiae*. *Genetics* 127, 463-473.
- Ortiz, J., Stemmann, O., Rank, S., and Lechner, J. (1999). A putative protein complex consisting of Ctf19, Mcm21, and Okp1 represents a missing link in the budding yeast kinetochore. *Genes Dev* 13, 1140-1155.
- O'Toole, E. T., Winey, M., and McIntosh, J. R. (1999). High-voltage electron tomography of spindle pole bodies and early mitotic spindles in the yeast *Saccharomyces cerevisiae*. *Mol Biol Cell* 10, 2017-2031.
- Peskin, C. S., and Oster, G. F. (1995). Force production by depolymerizing microtubules: load-velocity curves and run-pause statistics. *Biophys J* 69, 2268-2276.
- Rieder, C. L., and Alexander, S. P. (1990). Kinetochores are transported poleward along a single astral microtubule during chromosome attachment to the spindle in newt lung cells. *J Cell Biol* 110, 81-95.
- Rieder, C. L., Davison, E. A., Jensen, L. C., Cassimeris, L., and Salmon, E. D. (1986). Oscillatory movements of monooriented chromosomes and their position relative to the spindle pole result from the ejection properties of the aster and half-spindle. *J Cell Biol* 103, 581-591.
- Sorger, P. K., Severin, F. F., and Hyman, A. A. (1994). Factors required for the binding of reassembled yeast kinetochores to microtubules in vitro. *J Cell Biol* 127, 995-1008.
- Stoler, S., Keith, K. C., Curnick, K. E., and Fitzgerald-Hayes, M. (1995). A mutation in CSE4, an essential gene encoding a novel chromatin-associated protein in yeast, causes chromosome nondisjunction and cell cycle arrest at mitosis. *Genes Dev* 9, 573-586.
- Straight, A. F., Belmont, A. S., Robinett, C. C., and Murray, A. W. (1996). GFP tagging of budding yeast chromosomes reveals that protein-protein interactions can mediate sister chromatid cohesion. *Curr Biol* 6, 1599-1608.
- Tanaka, T. U., Rachidi, N., Janke, C., Pereira, G., Galova, M., Schiebel, E., Stark, M. J., and Nasmyth, K. (2002). Evidence that the Ipl1-Sli15 (Aurora kinase-INCENP) complex

promotes chromosome bi-orientation by altering kinetochore-spindle pole connections. *Cell* 108, 317-329.

Thomann, D., Rines, D. R., Sorger, P. K., and Danuser, G. (2002). Automatic fluorescent tag detection in 3D with super-resolution: application to the analysis of chromosome movement. *J Microsc* 208, 49-64.

Weiss, E., and Winey, M. (1996). The *Saccharomyces cerevisiae* spindle pole body duplication gene MPS1 is part of a mitotic checkpoint. *J Cell Biol* 132, 111-123.

Wigge, P. A., Jensen, O. N., Holmes, S., Soues, S., Mann, M., and Kilmartin, J. V. (1998). Analysis of the *Saccharomyces* spindle pole by matrix-assisted laser desorption/ionization (MALDI) mass spectrometry. *J Cell Biol* 141, 967-977.

Wigge, P. A., and Kilmartin, J. V. (2001). The Ndc80p complex from *Saccharomyces cerevisiae* contains conserved centromere components and has a function in chromosome segregation. *J Cell Biol* 152, 349-360.

Winey, M., Goetsch, L., Baum, P., and Byers, B. (1991). MPS1 and MPS2: novel yeast genes defining distinct steps of spindle pole body duplication. *J Cell Biol* 114, 745-754.

Winey, M., and O'Toole, E. T. (2001). The spindle cycle in budding yeast. *Nat Cell Biol* 3, E23-27.